Experimental and Theoretical Studies of Phloem Transport with the Inclusion of Lateral Solute Exchange and Apoplastic Conditions

Inaugural-Dissertation zur Erlangung des Doktorgrades der Naturwissenschaften (Dr. rer. nat.)

beim Fachbereich Biologie und Chemie

der Justus-Liebig-Universität Gießen

vorgelegt von

M.Sc. Paulo Cabrita

aus Algoz / Portugal

Gutachter: Dr. Jens B. Hafke

Prof. Dr. Volker Wissemann

Dekan: Prof. Dr. Volkmar Wolters

Gießen 2011

to my mother

Acknowledgements

Without direct and indirect involvement of the following persons, this work would have not been made possible. I would like therefore to convey my most deeply and sincere gratitude and thankfulness to:

My supervisor and dearest friend Dr. Michael Thorpe for educating me on the exciting world that is plant physiology and phloem transport. He has accompanied all my work from the beginning and I am deeply grateful for all his support, enthusiasm and friendship.

Dr. Peter Minchin, from the New Zealand Institute for Plant and Food Research Ltd, at Te Puke, New Zealand, for all the support and careful reading and commenting on this work.

Professor Dr. Ulrich Schurr for giving me the chance of being involved in plant sciences research at the Institute of Bio- and GeoSciences: Plant Sciences (IBG-2), Research Centre Jülich, and for his continuous support, encouragement, and expertise.

Dr. Jens Hafke, at the Botany Institute, Justus-Liebig-Universität Gießen, for all the support and careful reading of this work.

Dr. Siegfried Jahnke and Dr. Heike Schneider, for all their support and encouragement, and Dr. Gregor Huber for all the support and valuable discussions on mathematical modelling.

Dr. Gerhard Roeb and Marco Dautzenberg for all the help and support with ^{11}C labeling and plant growth.

Dr. Hinrich Lühring and van-Dy Nguyen for the friendship and useful discussions.

Thomas Hombach for the support and assistance with ^{11}C labeling and experimental setup.

Dr. Walter Schröder, with his humor and expertise, very sincere and honest thanks for his friendship and support on microscopy.

Dr. Helmut Soltner, at the Central Technology Division (ZAT), Research Centre Jülich, for introducing me to the world of Mathcad modelling.

All colleagues and co-workers from the Institute of Bio- and GeoSciences: Plant Sciences (IBG-2).

Julie Thorpe for the careful reading of this work and friendship and for the lovely memories of our enlightening "*gerundizing*" sessions.

Liti and César for all the support and friendship and simply for being there.

A great and heartfelt thank goes to my brother Nuno and to my mother Maria Emília for all the inestimable support.

Gießen, 2011

Contents

Abstract 1

Zusammenfassung 2

1 Introduction

1.1 Main Objectives 3

1.1.1 Theoretical Approach 4

1.1.2 Experimental Approach 4

1.2 Plant Species 5

2 Mathematical Modelling of Phloem Transport: A Review

2.1 Translocation of Tracers 6

2.2 Münch Pressure Flow Hypothesis 8

2.2.1 Steady State Models 8

2.2.1.1 Laminar Flow 8

2.2.1.2 Radial Water Exchange 11

2.2.1.3 Phloem Anatomy and Physiology 13

2.2.1.4 Loading and Unloading Processes 21

2.2.1.5 Radial Water Potential Equilibrium 25

2.2.1.6 Plasmodesmatal Flux 26

2.2.1.7 Stokes Flow 29

2.2.1.7.1 Radial Water Exchange Revised 30

2.2.1.7.2 Diffusion-like Behaviour of Phloem Transport 34

2.2.1.7.3 Pressure Differences Caused by Sieve Plates 35

2.2.2 Time-dependent Laminar Flow 36

2.2.2.1 Changes in the Pathway Resistance 36

2.2.2.2 Bidirectional Movement 37

2.2.2.3 Time-dependent Loading and Unloading Processes 37

2.2.2.4 Sieve Tube Structure and Cell Wall Elasticity 38

2.2.2.5 Radial Water Potential Equilibrium Reexamined 41

2.2.2.6 Concentration-Pressure Waves and Information Transmission 43

2.2.2.7 Osmoregulatory Flow 47

2.2.2.8 Phloem Relays 48

2.2.3 Coupled Xylem and Phloem Flows Models 51

2.2.3.1 The Effect of Transpiration on Phloem Transport 54

2.2.3.2 Münch Counterflow 58

2.2.4 Transport Resistance Models 59

2.2.4.1 Temperature 60

2.2.4.2 Plant Architecture 61

3 Hydrodynamics of Phloem Transport: Steady State Flow in Sieve Tubes with Radial Convection and Solute Exchange

3.1 The Model 65

3.2 Fundamental Equations and Boundary Conditions 67

3.3 The Hydrodynamic Problem - Perturbation Theory 77

3.3.1 Zeroth Order Approximation 78

3.3.2 First Order Approximation 81

3.3.3 Velocity and Turgor Pressure Profiles 86

3.4 Solute Movement 89

3.4.1 Zeroth Order Approximation 89

3.4.2 First Order Approximation 90

3.5 Non-selective Membrane 95

3.6 Physiological Parameters 98

3.6.1 Sieve Tube Structure 98

3.6.2 Sap Viscosity 99
3.6.3 Turgor Pressure 100
3.6.4 Sieve Tube Membrane Hydraulic Conductivity, L_p 101
3.6.5 Solute Permeability, P_s, and Reflection Coefficient, σ 102
3.6.6 Apoplastic Environment 103
3.7 Results 103
3.7.1 Semipermeable Membrane - The Effect of Radial Water Exchange 105
3.7.2 Permeable Membrane - The Effect of Radial Solute Exchange 108
3.7.3 Apoplastic Water Potential 116
4 Material & Methods
4.1 Chemicals 120
4.2 Plants and Growth Conditions 120
4.3 ^{11}C Labelling 121
4.4 Stem Perfusion 122
4.5 Chilling Experiments 124
4.6 Wheat Root Water Uptake 124
4.7 Humidity Control in the Squash Leaf Chamber 124
4.8 Solution Osmolality 125
4.9 Light Microscopy 125
4.10 ^{11}C Data Analysis 126
4.10.1 Input-output Analysis 126
4.10.2 Translocation Speed 129
4.10.3 Tracer Influx Rate 129
5 Results
5.1 Solute Penetration into Vascular Bundles through Perfusion 130
5.1.1 Wheat 130

5.1.2 Squash 131

5.2 Typical ^{11}C Data for Control Experiments 134

5.3 Influx of Tracer and Tracer Transport Speed 134

5.4 Tracer Loss 139

5.5 Effect of Sucrose and Mannitol Perfusion on Tracer Loss in Wheat 142

5.6 Effect of Sucrose, Mannitol, Raffinose and PEG Perfusion on Tracer Loss in Squash 145

5.7 Solutions Osmolality 157

5.8 Effect of Sucrose and Mannitol Perfusion on Water Exchange in Wheat Peduncle and Root 159

5.9 Effect of Sucrose, Mannitol, Raffinose and PEG Perfusion on Water Exchange in Squash Internodes 161

5.10 PCMBS Effects on Tracer Loss 162

5.10.1 Wheat 164

5.10.2 Squash 164

5.11 PCMBS Effects on Water Uptake in Squash 168

5.12 Chilling Effects on ^{11}C Transport in Squash 169

6 Compartmental Model of Phloem Transport

6.1 Compartmental System 171

6.2 Model Equations 173

6.2.1 Volume Conservation 173

6.2.2 Solute Conservation 176

6.2.3 Tracer Conservation 180

6.2.4 Translocation Time Delay, θ 183

6.3 Model Parameters 184

6.3.1 Sugar Concentration 184

6.3.2 Sap Viscosity 185

6.3.3 Anatomy and Structure 185
6.3.4 Membrane Hydraulic Conductivities 186
6.3.5 Sieve Tube Axial Conductivity 188
6.3.6 Model Evaluation and Transfer Coefficients 189
6.4 Model Results 190
6.4.1 Control Runs 191
6.4.2 Effects of PEG on ^{11}C Translocation in Squash 200
6.4.3 Effects of Sucrose on ^{11}C Translocation in Squash 205
6.4.4 Effects of Mannitol on ^{11}C Translocation in Squash 210
7 Discussion
7.1 Effect of Radial Water Exchange 216
7.2 Effect of Sieve Plates and Other Intracellular Structures 221
7.3 Effect of Radial Solute Exchange 222
7.4 Sieve Tubes are in Water Potential Equilibrium with the Apoplast 224
7.5 Translocation Speed 225
7.6 Perfusion by ABS does not Affect Phloem Transport 228
7.7 Tracer Loss 231
7.8 Effects of Phloem/Apoplast Water Exchange on Phloem Translocation 232
7.9 Raffinose is not Loaded into the Phloem 235
7.10 Sucrose Uptake into the SECC in Squash Internodes 235
7.11 Sucrose Uptake into SECC in Squash Internodes May Involve an Apoplastic Step 239
7.12 Mannitol Uptake into the SECC in Squash Internodes 242
7.13 Changes in the Pathway Resistance Explain Phloem Stoppage Caused by Mannitol Perfusion 244
7.13.1 Mannitol Catabolism 246
7.13.2 Ca^{2+}-dependent P-protein Gelation 247

7.14 Differences in the Physiological State in Wheat Explain Phloem Transport Results Diversity 249

7.15 Compartmental Model Analysis of Phloem Transport 252

7.16 Future Work 255

8 Conclusions 256

Bibliography 258

Abbreviations & Definitions 295

Appendix 300

Abstract

It has been shown that long-distance transport of solutes through the phloem within plants is driven by an osmotically generated pressure gradient, with associated radial exchange of water in the source and sink regions. However, there is also water and solute exchanges along the long-distance pathway, but their magnitudes are poorly known and their physiological role has rarely been investigated, especially in mathematical models of phloem transport. Therefore, this study investigated the magnitude of these fluxes in stems, and what can regulate them, by both theory and experiment. A steady state model of phloem transport developed using Navier-Stokes and convection-diffusion equations with allowance for water and solute exchange along the pathway showed that radial water exchange affects the pressure gradient. Solute exchange, dependent on the phloem cells permeability, also affects the pressure gradient by modifying water exchange. This result is significantly different from Hagen-Poiseuille flow which has been used so far in most mechanistic descriptions of phloem transport, not considering solute radial exchange. The experimental approach to investigate the importance of radial exchange of water and solutes on phloem transport made use of ^{11}C to non-invasively trace sugars, and transfer-function analysis to calculate tracer transport and unloading in squash and wheat plants, in response to treatments of the stem apoplast by perfusion with test solutions. In squash, effects of treatments with sucrose or mannitol on tracer unloading were similar at concentrations up to 300 mM. At 500 mM mannitol caused a transient stoppage of phloem transport, unlike sucrose. Application of mannitol may have caused a more abrupt osmotic shock than sucrose because of a higher permeability into the tissue, corresponding to its lower molecular size. In squash, the loss of tracer increased in the presence of PCMBS, which inhibits membrane transport, suggesting that there was phloem reloading of sugar via membrane transport from the apoplast. The observed response to apoplastic treatments was interpreted with a simple compartmental model: changes in the apoplast water potential and solute exchange greatly affected phloem transport, in agreement with the experimental work. Both the theoretical and experimental approaches showed that radial solute and water exchange in pathway regions between sources and sinks have to be recognised for a better understanding of phloem transport to be possible.

Zusammenfassung

Seit langem ist bekannt, dass der Langstreckentransport gelöster Stoffe im Phloem der Pflanzen durch einen osmotisch getriebenen Druckgradienten bewirkt wird, der mit dem radialen Austausch von Wasser in den Belade- und Speicherorganen verknüpft ist. Allerdings gibt es auch Austauschvorgänge von Wasser und gelösten Stoffen entlang der Transportstrecke, über deren Größenordnung aber wenig bekannt ist und deren physiologische Rolle selten untersucht wurde, insbesondere in mathematischen Modellen des Phloemtransports. In der vorliegenden Studie wurden daher die Größe dieser Flüsse in Sprossachsen und ihre Regulation sowohl theoretisch als auch experimentell untersucht. Auf der Grundlage der Navier-Stokes-Gleichungen und Konvektions-Diffusionsgleichungen wurde ein stationäres Modell für den Phloemtransport entwickelt, das radialen Austausch von Wasser und gelösten Stoffen entlang des Transportweges zulässt und zeigte, dass lateraler Wasseraustausch den Druckgradienten beeinflusst. Auch der Austausch gelöster Stoffe, der von der Permeabilität der Phloemzellen abhängt, beeinflusst den Druckgradienten durch Änderung des Wasseraustauschs. Dieses Ergebnis unterscheidet sich deutlich vom Hagen-Poiseuille-Fluss, der bisher für die meisten mechanistischen Beschreibungen des Phloemtransportes benutzt wurde, aber keinen radialen Austausch gelöster Stoffe berücksichtigt. Experimentall wurde in Weizen und Kürbispflanzen der Einfluss des radialen Austausches von gelösten Stoffen und Wasser auf den Phloemtransport untersucht durch nicht-invasive Messung von ^{11}C als Tracer für Zucker, wobei der Apoplast der Sprossachsen mittels Perfusion mit verschiedenen Testlösungen behandelt wurde. Zur Bestimmung des Transportes und Austauschs des Tracers wurde eine Transfer-Funktions-Analyse verwendet. Bei Kürbispflanzen gab es zwischen Behandlungen mit Saccharose und Mannit bei Konzentrationen bis zu 300 mM keine signifikant unterschiedlichen Auswirkungen auf die Tracerentladung. Bei 500 mM Mannit kam es jedoch, anders als bei Saccharose, zu einem vorübergehenden Stoppen des Phloemtransportes. Dies ist möglicherweise auf einen im Vergleich zu Saccharose abrupteren osmotischen Schock zurückzuführen, da Mannit aufgrund seiner geringeren Molekülgröße eine höhere Permeabilität in das Gewebe hat. Bei Kürbispflanzen erhöhte sich der Tracerverlust in der Gegenwart des von PCMBS, was damit erklärt werden kann, dass die Phloemrückbeladung gelöster Teilchen aus dem Apoplasten durch diesen Membrantransporthemmstoff blockiert wurde. Die beobachteten Reaktionen auf die Behandlung des Apoplasten wurden mit Hilfe eines einfachen Kompartimentmodells interpretiert: in Übereinstimmung mit den experimentellen Resultaten ergab sich, dass Änderungen im apoplastischen Wasserpotential und Austausch der gelösten Stoffe einen großen Einfluss auf den Phloemtransport haben. Sowohl die theoretischen als auch experimentellen Ansätze zeigen, dass der radiale Austausch von gelösten Stoffen und Wasser auf der Transportstrecke zwischen Quellen und Senken für ein besseres Verständnis des Phloemtransportes berücksichtigt werden muss.

1. Introduction

Phloem transport denotes long-distance transport, mainly of assimilates arising from photosynthesis, and is the movement of a solution in a continuum of interconnected cells, the so-called sieve tubes, within the phloem of the vascular tissues in plants. It is currently accepted that solutes enter and exit the sieve tubes at sources and sinks, water enters and exits osmotically, and the solution moves in these sieve tubes due to the consequent osmotically generated pressure gradient: the theory of Münch pressure flow (1927, 1930). However, there is also a considerable radial exchange of solutes between the sieve tubes and the adjacent cells along the long-distance pathway between source and sink regions, associated with storage of resources and growth of tissues (Minchin & Thorpe, 1984). The regulation of these radial exchanges has rarely been studied, nor has their role been addressed in mechanistic modelling of phloem transport. This omission is not only a major gap in the description of phloem transport, but it also makes the mathematical modelling an unsatisfactory tool for better understanding the vast amount of experimental data concerning phloem physiology.

1.1 Main Objectives

This study concerns solute and water exchanges between the long-distance phloem pathway and its surroundings in plant stems, which includes the apoplast, the free diffusional space outside plasma membranes, and what can regulate them, making use of both theoretical and experimental approaches. The aim was to construct a mechanistic model that, complemented with experiments, would tell us about the importance of unloading/reloading processes along the sieve tubes for long-distance transport in the phloem pathway regions. The magnitude of the radial fluxes in stems, and what can regulate them, was studied experimentally, and the implications for the theory of phloem transport were investigated.

1.1.1 Theoretical Approach

First, an extensive review of the literature on mathematical modeling of phloem transport, and the extent to which it included the increasing knowledge of phloem physiology is given. From the physical point of view, phloem sap may be seen as a viscous water solution in which sugars make the largest fraction of solutes, flowing slowly through highly specialized sieve tube elements. Therefore, the Navier–Stokes equations were chosen since they rigorously describe the motion of fluids, and used to construct a steady state model of phloem transport. Previous models had been based on approximations. In addition, so as to assess the importance of water and solute exchanges on phloem transport in plant stems, the convection–diffusion equation was applied to describe solute movement within the phloem, with specific boundary conditions for the radial exchanges of solute and water at the sieve tube membrane. These exchange processes were described using the formalism of irreversible thermodynamics for transport across membranes (Kedem & Katchalsky, 1958). In this way, a more realistic mechanistic model of phloem transport as a leaky system was constructed. The main focus of this model was to study the influence of solute permeability of the sieve tube membrane, and the physiological conditions in the surrounding tissue, on phloem transport.

1.1.2 Experimental Approach

Non-invasive measurements were made in order to investigate the dependence of phloem transport on the physiological conditions of the surrounding tissue. Phloem transport was observed by the use of $^{11}CO_2$ to label photoassimilates. A solution perfusion method was developed to allow the surrounding environment of the phloem cells to be modified while observing long-distance transport. Different osmolytes and chemicals were perfused to change the water status and solute content of the tissues. A compartmental model of water and solute exchanges in the stem perfused internode was developed to interpret the experimental results.

1.2 Plant Species

The plant species wheat (*Triticum aestivum*) and squash (*Cucurbita maxima*), both with hollow stems, were chosen because perfusion of solutions was possible. Both of these species have been extensively studied, giving a wide literature on their phloem transport physiology. Wheat is an annual grass with a hollow stem around which the vascular bundles are distributed symmetrically, although the bundles are some distance away from the internode pith cavity (Patrick, 1972). Sucrose is the only sugar transported and the stem internodes serve as the main storage organ (Hayashi & Chino, 1986; Gebbling, 2003). Squash is a climbing plant with long internodes having bicollateral vascular bundles, i.e. there is phloem on either side of the xylem. The phloem is located very close to the internode pith cavity so that penetration of solutions into the cavity is very likely and allowing experimental modification of the apoplastic environment of phloem. The phloem in squash, like other species of the *Cucurbitaceae* family, transports mainly oligosaccharides such as stachyose, raffinose (Webb & Gorham, 1964; Hendrix, 1968, Hsiang Bush, 1992) and verbascose (Hendrix, 1982). The oligosaccharides are translocated throughout the sieve tubes and seem not to leave the phloem system (Schaffer *et al*. 1996; Webb & Gorham, 1964, 1965).

2. Mathematical Modelling of Phloem Transport: A Review

2.1 Translocation of Tracers

Since radioactive tracers have been used to study biological systems, plant physiologists have seen it as valuable way of studying vascular transport. Monitoring tracer movement within the plant body not only shows the pathways where transport occurs but also allows quantitative measurements on speed and concentration of tracer. The first mathematical analysis and description of translocation through the phloem was made by Horwitz (1958) who derived several mathematical models in order to explain the transport of radioactivity within a plant (^{14}C, ^{32}P, ^{42}K and ^{137}Cs). Typically, $^{14}CO_2$ is applied to a leaf for a period of time and translocation is allowed to proceed down the stem. At various times after the start of the labelling, plants are removed and the stems are cut up into segments of known length. The total ^{14}C activity is extracted and measured in each segment and in some cases the chemical composition of the radioactive material is also determined. By repeating the experiment for various translocation periods, a spatial and temporal picture of the kinetics of tracer distribution is built up. Vernon & Aronoff (1952) and Biddulph & Cory (1957) found that if the logarithm of the ^{14}C activity was plotted as a function of distance down the stem, the profiles were linear during the early stages of translocation; whereas later the profile either proceeded down the stem as an undistorted straight line or developed into a convex curvilinear function of distance. Horwitz's (1958) main intention was to investigate whether the several theories of translocation proposed up to that time could explain the short term translocation patterns of isotopically labelled materials in plants. In Horwitz's simple models, "translocation is visualized simply as involving unidirectional mass flow of the fluid contents of a pipe (the sieve tube column) regardless of the actuating mechanism". Solutes may diffuse through the pipe walls, but convection of solutes through the water exchange between the pipe and the surrounding medium is neglected. The system dimensions are small enough so that diffusion gives sufficient mixing and the concentration of solutes is radially uni-

form at any position in the tube, a regime termed "idealized slug movement". Horwitz considered two possible modes of passive solute exchange with the surrounding medium: irreversible and reversible losses. Irreversible loss of observable solutes can be assumed when the unloaded solute is immediately bound or is diluted into such a large external pool that the specific radioactivity[1] remains very low in the time of the experiment. In reversible loss, unloaded tracer can re-enter the sieve tube. In both cases the tracer efflux rate is linear with the concentration of tracer in the sieve tube C_i, and the influx rate is linear with the external tracer concentration C_{out} so that, from mass conservation, the sieve tube tracer concentration gradient as given by Horwitz (1958) is:

$$\frac{dC_i}{dx} = \frac{P_s}{Av}\left(C_{out} - C_i\right) \tag{2.1}$$

in which A is the sieve tube cross sectional area, P_s is the sieve tube membrane permeability to solutes and v is the phloem flow speed. Basically, the irreversible loss model is a special limiting case of this model. Horwitz (1958) found better agreement with experimental data from Biddulph & Cory (1957) with irreversible loss of tracer only. It was often shown experimentally that tracer profiles suggest reversible loss, with tracer accumulating in the surrounding tissues (Clauss *et al*., 1964; Evans *et al*., 1963; Moorby *et al*., 1963; Spanner & Prebble, 1962; Webb & Gorham, 1964; Whittle, 1970). Tyree (1975) included irreversible loss of tracer by Michaelis–Menton kinetics in which the lateral solute flux, j_{ls}, is determined by:

$$j_{ls} = \frac{R}{2}\frac{dC_i}{dt} = \frac{j_{smax}C_i}{K_m + C_i} \tag{2.2}$$

Where R is the sieve tube radius, j_{smax} is the maximum rate of solute flux when all catalytic membrane sites are filled and K_m is the Michaelis–Menten constant – the solute concentration at which the flux reaches half of its maximum value. Tyree (1975) also found good agreement with experimental data from Canny & Phillips (1963). Benefitting from more available experimental data at the time, Tyree (1975) also extended Horwitz's model of reversible loss of tracer and found a very good agreement with experimental

[1] the amount of radioactivity per unit amount of substance.

data from several plant species labelled with $^{14}CO_2$ and THO (Canny, 1973). Horwitz (1958) also studied the case of non-steady state of tracer concentration in the source region, where sugars are loaded into the phloem, and concluded that the change of the loading rate with time in the source region influences the spatial distribution of tracer in the plant dramatically. This was an important finding since experimentalists at that time considered, as many still consider today, that the tracer concentration at the source region is constant in time. Tyree (1975) confirmed Horwitz's findings.

Following the work of Horwitz, Evans *et al*. (1963) made use of Horwitz's (1958) bulk flow description of phloem translocation to interpret their measurements of tracer observation using $^{11}CO_2$ labelling on soybean (*Glycine max*) (Moorby *et al*., 1963). This included lateral irreversible loss of sugar at a constant rate which was linear with the local sugar concentration. Their model brought no improvement over Horwitz's ideas, since it was only based on mass conservation equations for the tracer, and did not consider any physiological process or mechanism. Nonetheless, it used experimental evidence to estimate the translocation velocity of 1 $cm.min^{-1}$ (up to that time only possible to determine very indirectly from ^{14}C labelling), and the irreversible leakage of tracer along the pathway (the stem) into the surrounding tissue at a rate of 0.8 $\%.cm^{-1}$.

2.2 Münch Pressure Flow Hypothesis

2.2.1 Steady State Models

2.2.1.1 Laminar Flow

The first mathematical and quantitative physical analysis of the Münch hypothesis (Münch, 1926, 1927, 1930) for transport in the phloem – osmotic pressure flow theory – was presented by Horwitz (1958). Horwitz's model (Fig. 2.1) consisted of two pipes with rigid walls. The phloem pipe is composed of an upper region where sugar is produced by photosynthesis, an intermediate region analogous to the sieve tube, and a lower consuming region where sugar is transformed into an osmotically less active form – sink region. There is an adjacent second pipe, which is analogous to the xylem, containing only water, separated from the sieve tube by a rigid membrane, and permeable to water but not to

sugar. This second tube is connected to a water supply that is assumed to be limitless. In Horwitz's model, sugar produced in the photosynthetic region causes an osmotic influx of water which raises the pressure at the head of the sieve tube column. Sugar solution flows down the column, with water moving out of the sink region into the adjacent xylem pipe the end of the column. Thus, both phloem and xylem compose an open system in which water circulates throughout the plant body. If the photosynthetic and sugar consuming rates are held constant, a steady state distribution of sugar concentration, pressure, and flow velocity will be eventually achieved in the pipe simulating the sieve tube.

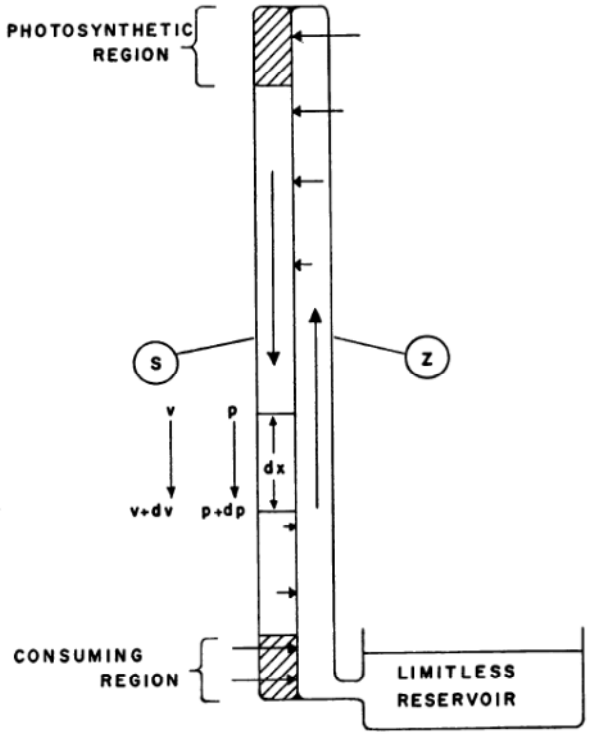

Figure 2.1 – Horwitz's model of osmotic pressure flow theory. S – Sieve tube; Z – Xylem; v – velocity; p – turgor pressure; x – spatial coordinate (in Horwitz, 1958)

Horwitz (1958) showed that the Hagen–Poiseuille equation (2.3) cannot be applied; nevertheless it has been used in phloem translocation studies for estimating turgor pressure gradients and translocation speed (Aikman & Anderson, 1971; Amin, 1983; Crafts, 1931; Fensom & Spanner, 1969; Nonweiler, 1975; Preston, 1963; Sheehy *et. al*., 1995; Tammes *et al*., 1971; Weatherley, 1972; Weatherley & Johnson, 1968; Zimmerman & Brown, 1971). Hagen–Poiseuille equation:

$$\mathrm{j} = -\frac{R^2}{8\mu}\frac{d\mathrm{p}}{dx} \tag{2.3}$$

which describes the pressure drop, $\frac{d\mathrm{p}}{dx}$, in the direction of flow in a laminar regime[2] of an incompressible viscous fluid, of viscosity μ, flowing with an average volume flux j ($m.s^{-1}$) through a long cylindrical pipe, which is significantly longer than its diameter, with rigid impermeable walls of constant circular cross section of radius R. Hence, it cannot be applied to a tube in which water is entering or leaving through the walls causing momentum changes. Using some structural and anatomical data from *Cucurbita pepo* (Crafts, 1931) and translocation speeds measured by Biddulph & Cory (1957), Horwitz (1958) estimated that the Reynolds number[3] for translocation of a 10% (m/v) sucrose solution would be in order of 10^{-3} for both sieve tube lumen and sieve plate pores. This is well below the lower critical Reynolds number that defines laminar pipe flow regime (≤ 2000) (Streeter *et al.*, 1998). Therefore, Horwitz (1958) concluded that flow in sieve tubes would be certainly laminar, and suggested that with such a small Reynolds number the effects of viscosity should far outweigh accelerative effects. In this particular case, for sieve tubes with radial water exchange and even when undergo marked changes in form, e.g. sieve plate, Horwitz (1958) found that the dissipation of pressure is given by:

$$\frac{d\mathrm{p}}{dx} = -\varsigma \mathrm{v} - 2\rho \mathrm{v}\frac{d\mathrm{v}}{dx} \tag{2.4}$$

ignoring gravity, assuming a linear relation between viscous forces and translocation speed through a coefficient ς proportional to the solution viscosity μ and ρ is the phloem sap density. If one approximates the viscous resistance term, the first term of the right hand side of equation (2.4), using Hagen-Poiseuille equation (2.3), and compares it with the second term, referring to contribution of the inertial effects due to entrance and exit of water through the pipe walls, determined from known rates of translocation, the viscous

[2] sometimes known as streamline flow, occurs when a fluid flows in parallel layers, with no disruption between the layers.

[3] is a dimensionless number that gives a measure of the ratio of inertial forces to viscous forces and consequently quantifies the relative importance of these two types of forces for given flow conditions.

resistance term dominates. In this respect, the second term on the right hand side can be dropped and the sieve tube pressure gradient can be written as proportional to the first power of the average flow velocity:

$$\frac{d\mathrm{p}}{dx} = -\varsigma \mathrm{v} \tag{2.5}$$

Thereby, equation (2.5) should be a reasonable representation of the pressure gradient in the sieve tube. Even though Horwitz (1958) points out that his model was too simple, which may limit its use, for his purposes he concludes that the Münch hypothesis agrees with the spatial and temporal radioisotope profiles obtained. He considers that along the phloem pathway there is unloading of radioactive tracer together with simultaneous water exchange between the phloem and the surrounding tissue. Unfortunately, Horwitz does not justify his conclusions regarding the Münch hypothesis nor does he show as much detail as he did with his other proposed models for tracer loss.

2.2.1.2 Radial Water Exchange

Because of the difficulty to observe functional sieve tubes and to measure turgor pressure gradients along the phloem pathway, Young *et al*. (1973) proposed a mathematical analysis of the Münch pressure flow hypothesis. Their model was based on the experimental setup made of dialysis tubing constructed by Eschrich *et al*. (1972). Eschrich *et al*. (1972) and Young *et al*. (1973) firmly argued against the use of Hagen–Poiseuille equation to such flow regime because of the radial water exchange between sieve tubes and the surrounding tissue. However, Eschrich *et al*. (1972) used a misleading experimental setup with too large tubing and consequently too large membrane surface to volume ratio, unlikely to be found in plants. They also erred in pointing to the difference in water chemical potential between sources and sinks as being the driving force for solution flow in the phloem, opposed to the turgor pressure difference. Weatherley (1972) and Lang (1973) strongly criticised the work of Eschrich *et al*. (1972) considering the experimental setup of Eschrich *et al*. (1972) to be doubtful for several reasons. First, they considered the movement of discontinuous concentrations fronts that do not happen in plants. Second, they neglected any physiological relevance of sieve plates and other anatomical pa-

rameters. Finally, and most significantly, Eschrich *et al*. (1972) disregarded turgor pressure gradients, believing them to be too small and thus negligible. Notwithstanding the misconceptions of both Eschrich *et al*. (1972) and Young *et al*. (1973) regarding fluid dynamics, their studies were the first to emphasize the importance of membrane transport (of water) in phloem transport. As they noted, the non-equilibrium thermodynamics formalism, pioneered by the work of Kedem & Katchalsky (1958) on membrane transport, is what best describes solution movement across cell membranes. Accordingly, the volume flux, j, through an ideal differentially permeable membrane that limits the tube is given by Starling's equation (Katchalsky & Curran, 1965):

$$j = -L_p\left[p_i - p_o - R_g T\left(C_i - C_{out}\right)\right] \tag{2.6}$$

where L_p is the membrane hydraulic conductivity, R_g denotes the universal gas constant (8.314 $J.mol^{-2}.K^{-1}$), T the absolute temperature and p_i and p_o is the pressure inside and outside the tube respectively. Note that although Horwitz (1958) suggested that the Münch pressure flow hypothesis could be used to explain tracer data, he failed to say how. Thus, the work of Eschrich *et al*. (1972) and Young *et al*. (1973) constituted an advance.

Lang (1973) developed an experimental model similar to Eschrich *et al*. (1972), made from dialysis tubing rendered semi-permeable, but interconnected by capillary resistances at regular intervals. Thereby it was possible to measure pressure and to extract samples of solution. A sucrose solution was pumped, at a fixed rate, into one end and collected at the other while the whole system was submerged in water at constant temperature. With this system Lang followed the spatial and temporal profiles of pressure and solution concentration along the setup and the approach to steady state. He also used ^{14}C–sucrose and compared the model predictions with his experimental results of ^{137}Cs movement in *Nymphoides peltata* petioles. ^{137}Cs was applied directly to the phloem of the petiole, near to the lamina, and its downwards movement was followed. Compared to the model of Eschrich *et al*. (1972), the model of Lang (1973) was much more realistic as it had a much higher resistance, provided discontinuously but not unrealistically by a series of capillaries. However, like its predecessor, it was mainly focused on the pathway region, linking source and sink regions, and ignoring any processes of phloem loading and unloading, or any solute exchange along the pathway. In addition, Lang's model, having

the pressure gradient as the source for driving bulk flow throughout the system, was able to show a clear agreement between the model ^{14}C–sucrose labelling steady state and the ^{137}Cs labelling on *Nymphoides peltata* data. In both cases, there is a gradient of tracer concentration in the direction of flow. In the case of the experimental model, Lang (1973) pointed out that this concentration gradient down the direction of flow is explained by lateral intake of water, which has the effect of reducing the concentration of the sugar solution as it travels along the tube (Fig. 2.2B). In the steady state, a convex pressure gradient with distance (Fig. 2.2A) was also observed, which agrees with lateral influx of water. Lang (1973) noted that the increasing pressure gradient along the pathway must be accompanied by an increasing volume flow, and a concomitant increase in flow velocity, dictated by the linear relationship between pressure gradient and velocity described by Hagen–Poiseuille equation (2.3). Lang's data illustrated that linear relationship very well, as can be expected for the pressure flow hypothesis, and indeed in any mass flow theory. Lang (1973) also emphasized the limitations of his model, specifically that the surface area to volume ratio in the model did not represent sieve tubes, and that there was no solute exchange with the bathing medium at constant water potential (which was pure water at atmospheric pressure). Therefore, these facts make the velocity measurement not comparable with real measurements on plants, but qualitatively they gave a very good agreement with the predictions of Horwitz (1958) about tracer distribution, flow velocity (Huber, 1941; Spanner & Prebble, 1962) and the influence of radial water exchange.

2.2.1.3 Phloem Anatomy and Physiology

The first mathematical model of phloem transport to include information on phloem anatomy and physiology as input data explicitly was proposed by Christy & Ferrier (1973). They proposed a numerical steady state model based on irreversible thermodynamics (Kedem & Katchalsky, 1958) to evaluate the Münch pressure flow hypothesis of phloem translocation, with two different modes of phloem loading and unloading processes. First, they considered both loading and unloading processes to happen through active transport directly into and from the sieve tube. Second, they assumed a symplastic pathway[4]. The symplast consists of the entire network of cell cytoplasm interconnected

[4] Those same processes would occur primarily in specialized parenchyma cells surrounding source and sink regions and from there sugars would move passively to sieve tubes.

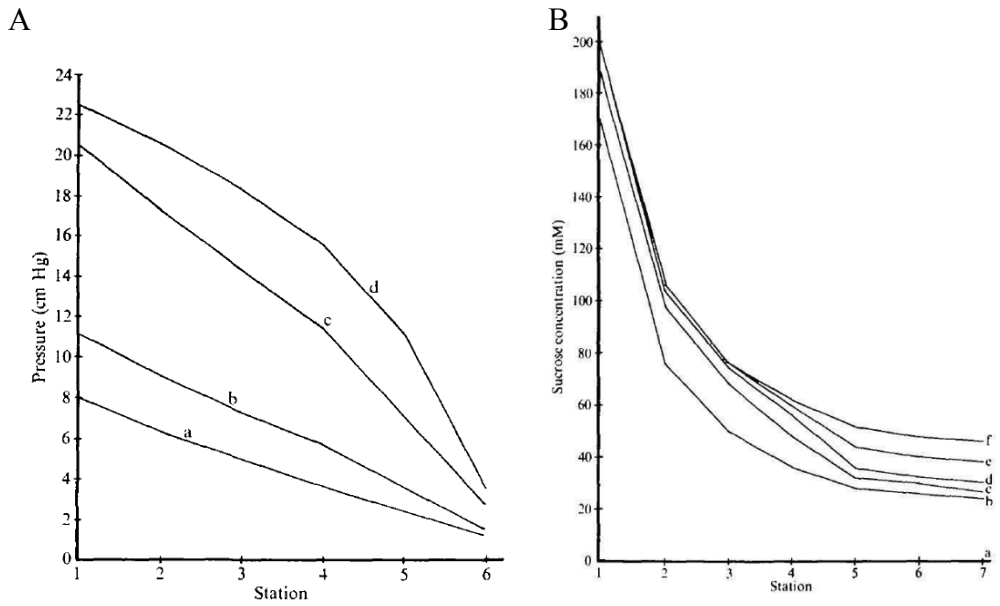

Figure 2.2 – A – Pressure measured in Lang's (1973) experimental model at different times after loading of 0.2 M sucrose: (a) immediately after; (b) 7 hours; (c) 30 hours and (d) steady state reached after 90 hours. B – sucrose concentration for the experiment in A: (a) 0 hours; (b) 10 hours; (c) 20 hours; (d) 30 hours; (e) 60 hours and (f) steady state reached after 90 hours (in Lang, 1973).

by plasmodesmata, tubular extensions of the plasma membrane traversing the cell wall. In this second scenario, each sieve tube element in the path region is surrounded by a companion cell. In both cases the specified loading und unloading rates are constant. The phloem system has three regions: the source, the sink and the pathway between the other two, with their consequent physiological implications, and surrounded by a reservoir at constant water potential. Although it would refer to a single sieve tube composed as an array of sieve tube elements, separated by sieve plates with radial exchange of water only, as described in Starling's equation (2.6), it was a much more anatomically and physiologically accurate model than its predecessors[5] (i.e. Eschrich *et al*., 1972; Evans *et al*., 1963; Horwitz, 1958; Young *et al*., 1973). The model of Christy & Ferrier (1973) was intended to simulate translocation from a mature source leaf to an expanding sink leaf located at some distance away. It assumed that the proportionality between turgor pres-

[5] It considered anatomy and experimental data from sugar beet for cell dimensions in the pathway and in both source and sink regions with tapered sieve tube elements and used the loading rate determined from ^{14}C labelling (Fisher, 1970; Geiger & Cataldo, 1969).

sure gradient down the sieve tube, from source to sink, and the average flow velocity would be given by Hagen–Poiseuille equation (2.3), unlike previous models (Eschrich *et al*., 1972; Horwitz, 1958; Young *et al*., 1973). However, being aware of that error, and acknowledging Horwitz's arguments against the use of Hagen–Poiseuille equation (2.3), Christy & Ferrier (1973) agreed that there are additional rapid changes of momentum at the pores. From this, they also concluded that any estimate of the hydraulic conductivity of sieve tube elements, L_s, derived from Hagen–Poiseuille equation (2.3) is likely to be high, although, it takes into account the dimensions of cell lumen and sieve plate pores:

$$L_s = \frac{\left(l + l_p\right) R^2 r_p^2}{8\mu\left(r_p^2 l + \frac{R^2 l_p}{\alpha}\right)} \tag{2.7}$$

μ being the sap of viscosity, l and R the sieve tube element length and radius, with N_p pores of radius r_p per sieve plate of length l_p, and α is the fractional area occupied by all sieve plate pores relative to sieve tube lumen cross sectional area. The model of Christy & Ferrier (1973) was the first to account for the volumetric contribution of solutes (in this case sucrose). They specified the solution flow as the sum of water and solutes flows, separately permeant to the system membranes.

Christy & Ferrier (1973) model confirmed that in the source region the volume flow rate along the sieve tube would increase, as more sugar and water enter the sieve tube (as predicted by the Münch model). This flow increase is also very likely to occur in a plant. On the other hand, in the sink region the flow rate decreases as water and solute leave the sieve tube. But, due to the different cell cross sectional area in the different sieve tube regions, combined with the radial water exchange with the surrounding medium, there is a continuous increase in the translocation velocity along the sieve tube in the direction of flow. Their model neglects any specific connections between the specialized parenchyma cells surrounding sieve tube elements, and considers the hydraulic conductivity connecting both types of cells as infinite, i.e. the cells have the same turgor pressure and concentration. Basically, the main differences between the two different ways of phloem loading are the site of loading and the path of water from the xylem to the sieve tube only. Consequently, there is a bigger lateral area presented to the surrounding medium for all regions in the second case, thus causing more water to enter the sieve

tube. This, in turn, creates a higher velocity and a higher rate of increase in velocity with distance, as compared to the first case. Considering the experimental difficulties in determining the hydraulic conductivity of cell membranes and tissues and the assumptions made, the Christy & Ferrier (1973) model results were consistent with experimental findings. They were also in fairly good agreement with experimental data for sugar beet. It is also worthy of notice that the additional resistance to water flow offered by the lateral membranes had not been considered in previous estimates of the resistance to water movement in the translocation system. The Christy & Ferrier (1973) model adequately describes translocation and supports the Münch pressure flow hypothesis as a plausible mechanism. It also demonstrates that the turgor pressure gradient required to drive solution flow in sieve tubes can be produced by the water potential difference between the sieve tube and surrounding tissue. However, Christy & Ferrier (1973) were aware of the limitations of their model. Their model established the importance of membrane conductivity to a pressure flow mechanism, and demonstrated that the turgor pressure that can be generated by a given osmotic pressure may be much less than the osmotic pressure, rather than equal to it, as it was previously and conventionally assumed. But as Christy & Ferrier (1973) recognized, it was difficult to explain translocation over long distances such as occurs in trees.

Not so long after, Christy & Ferrier improved their numerical method and established a more concise system of equations for a steady state that allows for a clearer qualitative understanding of Münch pressure flow and for application on the study of very long translocation paths (up to 50 m) as it occurs in trees (Tyree, Christy & Ferrier, 1974). Structurally their model remained the same, but as opposed to their first work, they considered a water potential gradient with distance in the surrounding medium, with increasing water potential values in the direction of flow (from source to sink regions). This tends to be a more likely situation to occur in big plants such as trees. However, despite the distances considered Tyree, Christy & Ferrier (1974) totally ignored the contribution of gravity to turgor pressure drop, and to external water potential gradient, as pointed out by Weir (1981). Tyree, Christy & Ferrier concluded that a better agreement with the Münch pressure flow would be attained if the pathway region was considered as a very long weak sink; inasmuch as growth, metabolism and storage processes occur throughout the stem of trees. According to their model, Tyree, Christy & Ferrier (1974) concluded that for the osmotically generated pressure flow to work over such lengths the sap concentrations must remain relatively high and the velocities must remain relatively low.

Tyree, Christy & Ferrier (1974) based on Hagen–Poiseuille equation (2.3) used the same formula that Christy & Ferrier (1973) derived for total sieve tube element conductivity (2.7). From their model predictions and comparing with the very few data available at the time on phloem transport rates and specific mass transfer rates from different species, Tyree, Christy & Ferrier (1974) suggested that axial sieve tube conductivity, if there were functional unoccluded sieve plate pores, would have to be higher than the values found for transport at shorter distances. In order to avoid sieve tube element plasmolysis anywhere, Tyree, Christy & Ferrier (1974) concluded that the hydraulic conductivity of the membrane would have to be higher than 5×10^{-14} m $s^{-1}.Pa^{-1}$. Their predictions for the flow speed fell well within the range of velocities reported for *Fraxinus americana* (Zimmermann, 1958). Sheehy *et al*. (1995) extended the formula of Tyree, Christy & Ferrier (1974) for sieve tube conductivity for use in crop growth modelling. They compared phloem anatomy data of three species with different types of phloem anatomy: elm (*Ulmus americana*), with shorter sieve tube elements with transverse sieve plates; a non-specified tree species with longer and narrower sieve tube elements with steep oblique sieve plates (considered more primitive) and a grass, fescue (*Festuca arundinacea*). Sheehy *et al*. (1995) showed that the range of sieve tube conductivity would vary greatly solely on sieve tube elements and sieve plate dimensions. Consequently, the analysis of phloem transport by using Hagen–Poiseuille equation (2.3) is also affected. In this way, Sheehy *et al*. (1995) showed how critical the data for phloem anatomy are for mathematical modelling phloem transport.

Despite the improvement over previous attempts to mathematically describe the Münch pressure flow mechanism, Tyree, Christy & Ferrier (1974) pointed out that their model was still oversimplified. It was only referring to a single sieve tube and did not take into consideration the real branching and interconnecting of the plants vascular system. It was focusing only on one single solute when the phloem sap, as it was already well known at the time, is a complex liquid phase of many different solutes with sugars being the major mass fraction of all solutes present. Even with this oversimplification, Tyree, Christy & Ferrier (1974) approach is also particularly useful. It established clear evidence that their mathematical description of the Münch pressure flow was able to predict the diffusion analogue transport that Mason & Maskel (1928a, b) proposed to explain their experimental linear relation between solution mass flow and the concentration gra-

dient observed down the stem[6]. Ross & Tyree (1979) also concluded that this linear relationship was in its turn linear with the axial hydraulic conductivity of the sieve tube, and rather independent of the hydraulic conductivity of the sieve tube membrane.

Taking his experimental model results Lang (1978) presented a mathematical steady state description of phloem transport but focusing on the pathway region only, thus excluding any loading or unloading processes in source and sink regions. Lang (1978) used typical sieve tube element dimensions (Weatherley & Johnson, 1968) and like the models before, it also did not consider any solute exchange between the pathway region and the surrounding medium. Lang's (1978) model lacked a sucrose volumetric term, as predicted by non-equilibrium thermodynamics formalism, in order to describe solution flow across membranes as used by Christy & Ferrier (1973) and subsequent models. Lang used Hagen–Poiseuille equation (2.3) because his previous experimental model showed a linear relationship between pressure gradient and flow velocity (Lang, 1973). Lang's model (1978) adds nothing new to previous mathematical descriptions of phloem transport it is mainly another confirmation of the plausibility of the Münch pressure flow hypothesis, but with the help of experimental support. In this case, Lang (1978) predicted his experimental results (Lang, 1973), although, as he pointed out his previous experimental model probably relates to a very extreme situation, not fully met in nature. Using what he called extreme situations of phloem transport, he tested the relative contributions of radial vs. axial flow resistance to the dynamics of the system. In addition, although Lang (1978) was not the first to consider viscosity changes due to changes in solute content, he used an empirical formula different from Ferrier & Christy (1975). Lang (1978) considered an empirical function of viscosity of water solutions dependent on sucrose concentration, that led to the ideal limit of the concentration value for which the pressure gradient to drive flow would be minimum, at a given steady state flux. He confirmed what Passioura (1976) had previously suggested, that a Münch translocating system, transporting sucrose, is at its most efficient state in the concentration range measured in sieve tubes. It is thus worthy of notice that an optimum sucrose concentration, found both by Lang (1978) and Passioura (1976) so as to minimize the pressure gradient, and consequently less energy costs, agrees very well with the values of sucrose concentration measured in the phloem from 0.3 to 1 M (Fisher, 2002; Salisbury & Ross, 1992). Lang (1978) also explored the importance of the relative osmotic strength of various carbohy-

[6] In this case, it refers to cotton plant (*Gossypium barbadense* L.).

drates with respect to the solution viscosity to determine for each solute the ‘‘ideal’’ concentration that would cost less to drive a laminar flow regime. He suggests a clear advantage of sucrose over sugar alcohols (mannitol, sorbitol), raffinose and reducing sugars most commonly found in plants. However, in this case, some care must be taken on analysing his conclusions. Lang (1978) used an empirical formula for sucrose water solutions for comparison between the different sugars, and only corrected it based on the different molecular weights of the possible sugars expected in the phloem, neglecting the interactions between solvent and solute molecules which reflect the different solubilities of sugars in water, e.g. raffinose is far less soluble than sucrose.

Weir (1981) extended the theoretical results of Christy & Ferrier (1973) and Tyree, Christy & Ferrier (1974) for the steady state Münch pressure flow hypothesis. He used their model and non-equilibrium thermodynamics formalism of a single sieve tube limited by a rigid semipermeable membrane with tapered ends. Both loading and unloading processes were described by constant rates with passive water exchange through the lateral wall (Starling’s equation, 2.6). Radial solute exchange was ignored along the region between source and sink, as in Christy & Ferrier (1973) and Tyree, Christy & Ferrier (1974). Weir (1981) generalized the equations derived by Christy & Ferrier and used a differential approach, as opposed to the integral approach used by Christy & Ferrier (1973) and Tyree, Christy & Ferrier (1974). He derived a more general expression for the pressure change along the sieve tube, applying Newton’s second law of dynamics:

$$\mathrm{f}_s - \frac{\partial \mathrm{p}}{\partial x} - \frac{\mathrm{v}}{\mathrm{L_s}} - \rho \mathrm{g} \frac{\partial \mathrm{h}}{\partial x} = \frac{1}{R^2} \frac{\partial}{\partial t} \left(\rho R^2 \mathrm{v} \right) + \mathrm{v} \frac{\partial}{\partial x} \left(\rho R^2 \mathrm{v} \right) \tag{2.8}$$

That is, the sum of metabolic, pressure, viscous and gravitational forces applied to any fluid volume element equals the rate of change of fluid momentum along the sieve tube. Here f_s is the local force per unit volume of sieve tube developed by active metabolic processes; L_s the axial hydraulic conductivity of the sieve tube; ρ the sieve tube sap density flowing at velocity v; g the gravitational acceleration; h the height above some suitable horizontal reference plane; R the sieve tube radius. However, Weir (1981) ignored the momentum of fluid entering the sieve tube from the lateral walls, due to water exchange, arguing that the force needed to accelerate the inflowing fluid to the velocity found on phloem flow is very small compared with the gravitational force. Weir (1981)

also considered the pressure gradient caused by the viscous drag force proportional with velocity, v, in which the coefficient ς shown in equation (2.5) is taken as L_s^{-1}, the sieve tube resistivity. However, contrary most models, he did not use the famous Hagen–Poiseuille equation (2.3) to describe it. Instead, in Weir's model the axial sieve tube resistivity is another constant parameter with no explicit dependence on any sieve tube anatomical features and on solution viscosity as it is usually described from Hagen–Poiseuille equation (2.3). Also, Weir (1981) considered the effect of sieve plates as an extra contribution to viscous drag, and simply included in the sieve tube axial resistivity ς. For the same reasons pointed out by Christy & Ferrier (1973) and Tyree, Christy & Ferrier (1974), Weir (1981) also considered that there is instantaneous mixing of fluid occurring within sieve tubes so that sieve tube sucrose concentration (the only solute present) can only vary due to convective flux, trapping and loading or unloading processes. In the approach of Weir on evaluating the steady state translocation, he derived an "energy-type" conservation law for sieve-tube motion using sugar beet data from Christy & Ferrier (1973). Weir (1981) concluded that the loading region has a finite extent, and consequently the flux of sucrose along the sieve tube has an upper limit. Otherwise the sieve tube pressure would become negative, in contradiction of experimental evidence. Another consequence is that upper and lower limits were obtained for both the velocity and the distance over which translocation could proceed in the pathway region. Weir (1981) also confirmed Tyree, Christy & Ferrier (1974) that velocity increases with distance, but in this case up to an upper limit. Although qualitative arguments, these findings are not new since Christy & Ferrier (1973) and Tyree, Christy & Ferrier (1974) had already mentioned them, but the approach used by Weir (1981) gives much stronger physical and mathematical basis for the physiological and anatomical factors that impose these limits. Perhaps, the most important contribution of Weir's work was his confirmation of the conclusions of Tyree, Christy & Ferrier (1974), that higher values of sieve tube axial hydraulic conductivity, L_s, should be expected in bigger plant species for which translocation occurs up to or over 100 m, considering the order of magnitude of the transport velocity (10^{-4} m.s^{-1}) and the turgor pressure expected to occur in sieve tube elements (10^6 Pa). At those distances, the effect of gravity on vertical transport is comparable to the pressure change caused by viscous drag. Thus, if 10^{-4} m.s^{-1} velocities occur in high trees, then it is essential that the gravitational force be included in long-distance Münch-type translocation calculations.

2.2.1.4 Loading und Unloading Processes

Goeschl *et al.* (1976) pointed out that the models of Christy & Ferrier do not provide unique, closed form solutions since there were more variables than independent equations. This would require specifying the solute concentration at the very beginning of the system and the unloading rate arbitrarily so that many steady state solutions could be obtained, giving the same specific mass transfer rate of sucrose, depending on the choices made. Following the same line, Magnuson *et al*. (1979) using an empirical relation of viscosity with sugar concentration noted that there could be modelling artefacts for some solute concentrations and unloading rate chosen *a priori* at the origin of the system, $C_i(0)$. Tyree *et al.* (1974) had already pointed out that for such models the calculated profiles of concentration, turgor pressure, velocity and water exchange under any given loading and unloading conditions would depend on the previous history of the system, represented by the choice of $C_i(0)$. Based on mathematical more than physiological reasons, as an alternative to previous models of Christy & Ferrier, Goeschl *et al.* (1976) suggested that to obtain a closed form solution of solute transport in the phloem, it is necessary to provide explicit concentration-dependent functions of phloem unloading, although the same proposal could be made for phloem loading. But as the authors noted, solutes are loaded into the phloem against a concentration gradient by active transport. Thus, the rate of loading is more likely to be a function of the solute concentration in mesophyll cells, in specialized loading cells, such as transfer cells, and/or companion cells, and depend on their metabolic energy level (e.g. ATP/ADP ratio). Consequently, the rate of loading would be relatively independent of solute concentration within the sieve tube elements *per se*. So, in response to the non-uniqueness problem, Goeschl *et al*. (1976) suggested two different processes for sucrose concentration dependent unloading: a linear function, similar to what Horwitz (1958) and Tyree (1975) had suggested for radioactive labelling (2.1), and a Michaelis–Menten saturable kinetics (2.2), also previously studied by Tyree (1975). Essentially, the model of Goeschl *et al*. (1976) is an extension of the Christy & Ferrier (1973) model for sugar beet, but with concentration-dependent unloading processes. Qualitatively, the Goeschl *et al*. (1976) model made no advance from Christy& Ferrier (1973), other than showing that concentration-dependent unloading functions could also be incorporated. In that view, it could serve as a good way of providing a better link be-

tween experimental and theoretical work. But, as Ferrier & Christy (1977) pointed out, the undesirable number of possible solutions raised by Goeschl *et al.* (1976) was also possible to achieve in their own approach. As for finding those same unique closed form solutions, as Goeschl *et al.* (1976) recommended, one would have to choose the constant parameters that best characterize the concentration-dependent unloading functions. In this case, those parameters would be the proportionality constant for the linear function (2.1) and the j_{smax} and K_m parameters for the Michaelis–Menten kinetics (2.2). Even though one obtains for each set of parameters a unique solution for the set of model equations, there is a great number of possible solutions depending on the choice of the concentration-dependent unloading functions parameters, as pointed out by Lang (1978). As an advantage and to more strongly prove their statement, Ferrier & Christy (1977) used their previous model for phloem loading over long distances (in a 15 m tree) (Ferrier, Tyree & Christy, 1974) but with viscosity corrections as previously used (Ferrier & Christy, 1975) and an empirical relation for determining osmotic pressure. This empirical relation was obtained by Michel (1972) and simulates better the non-linear relation between osmotic pressure and solute concentration observed for higher concentration sugar solutions. Thus it describes better phloem sap osmotic pressure than the usual van't Hoff linear relation previously used in other models (Christy & Ferrier, 1973; Ferrier, 1976; Ferrier & Christy, 1975; Ferrier, Tyree & Christy, 1974; Tyree, Christy & Ferrier, 1974). Although Ferrier & Christy (1977) only presented the case for a linear concentration-dependent function, the same aspects can be raised for a Michaelis–Menton function (2.2) or any concentration dependent unloading function. As Ferrier & Christy (1977) noted "such models can be useful, but physiological considerations rather than mathematical ones should lead the way on mathematical modelling of phloem transport". According to Lang (1978), in nature, velocity, sugar concentration and sieve tube turgor pressure are probably changing continuously with changes in temperature, light and other environmental factors which will affect growth, photosynthetic and translocation rates. In other words, the solute fluxes and concentration in the sieve tubes are probably determined outside the phloem by the interplay of supply and demand in the various sources and sinks. This has to do with their metabolic activity and not simply with a concentration dependent unloading rate. Thus, it seems more reasonable to choose the input values on the basis of physiological data rather than finding a single closed form set of parameters as proposed in the model of Goeschl *et al*. (1976).

Goeschl & Magnuson (1986) analysed the possible effects of loading rate on unloading processes described by linear, non-linear (Michaelis–Menten kinetics) and a combination of both kinetics. Their main hypothesis was that phloem loading would be an active transport process, requiring the expenditure of metabolic energy, and controlled primarily by the concentration of solutes outside the sieve tube (Giaquinta, 1983). Hence, the loading rate in their model is an independent parameter. For a linear unloading process in the Goeschl & Magnuson (1986) model, an increased rate of loading increases both transport velocity and solute concentration, along with increased turgor pressure and influx and efflux of water. However, for small values of the linear unloading coefficient, transport velocity saturates at very low loading rates, and the primary effect of increased loading rates is an increased concentration. With a greater unloading coefficient, the overall speed is higher and concentration is lower than with smaller values of the unloading coefficient, but both velocity and concentration increase similarly with increasing loading rates (Fig. 2.3).

This type of response was not observed for saturable Michaelis–Menten unloading kinetics (2.2). Changing one of the parameters K_m and j_{smax}, but keeping the other constant, produced the same type of response characterized by an increase followed by a decrease in the transport velocity for increasing loading rates. This suggests that there will be a loading rate range that maximizes transport velocity while concentration rises steeply upward with increased loading rate. The authors recognized that the values of K_m and j_{smax} used are higher than those normally found for most enzyme kinetics. However, those values were chosen to illustrate enzymatic effect at sucrose concentrations likely to occur in the phloem, and the same behaviour was also observed considering real values of the loading rate obtained by Zimmerman & Brown (1971). Taking unloading processes of both linear and saturable kinetics running in parallel simultaneously, Goeschl & Magnuson (1986) observed that speed increases toward an asymptotic maximum, while concentration increases smoothly. Changing the values of the unloading coefficient, K_m and j_{smax} tends to produce scenarios closer to one or the other of the previous cases discussed, showing the dominance of one process over the other. The relative contribution of the linear and saturable mechanisms can be expected to vary. Thus, one might expect any one of the patterns predicted by the models depending on the species and physiological condition of the test plants.

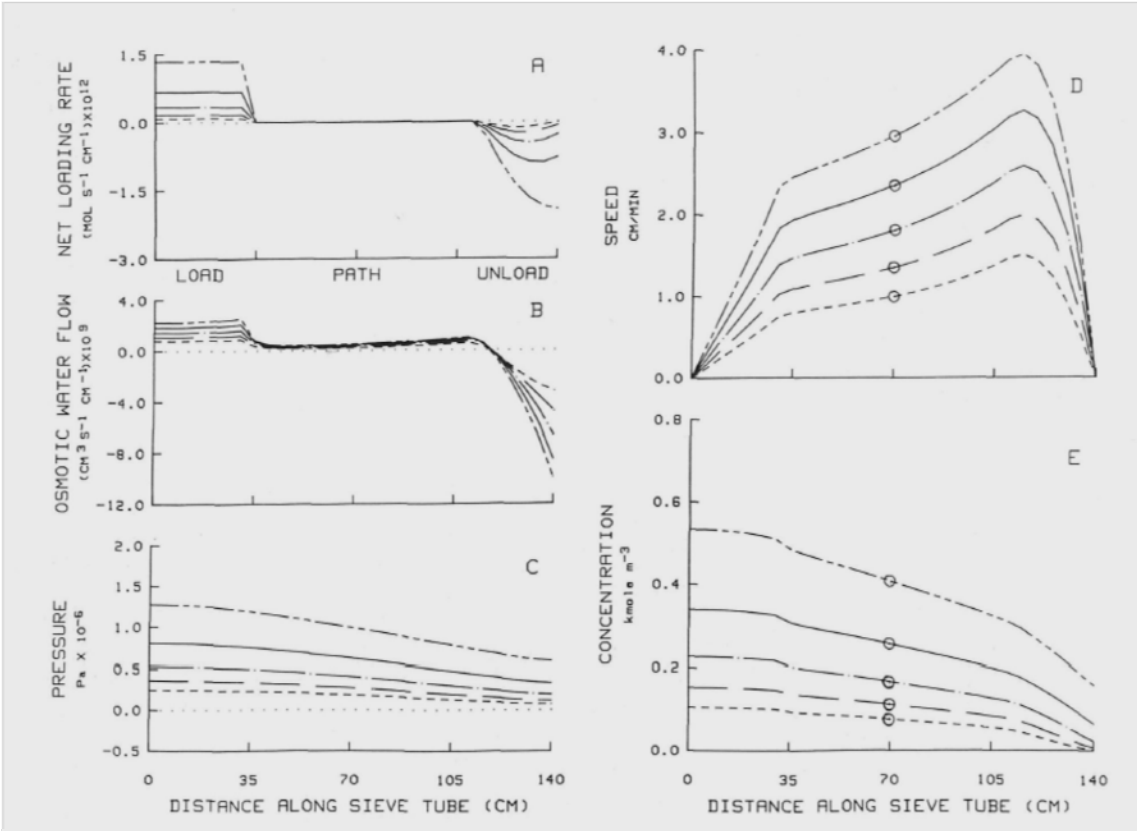

Figure 2.3 – Effect of loading rate on turgor pressure, lateral water flux, concentration and speed for a steady state model of phloem transport with linear concentration-dependent unloading in the sink region. Loading rates: 0.25, 0.5, 1, 2.2 and 4×10^{-11} mol.s^{-1} (in Goeschl & Magnuson, 1986).

Goeschl & Magnuson (1986) noted that the most straightforward prediction of the model (with any given set of sieve tube dimensions and properties) is that increasing the loading rate should always cause an increase in velocity and the concentration of translocates, in contrast with the Tyree, Christy & Ferrier (1974) model, in which the concentration was arbitrarily held constant at the top of the hypothetical sieve tube. Increased loading resulted in increased velocity, pressure gradient and radial water exchange, but decreased the concentration and turgor pressure in the remainder of the sieve tube. However, care must be taken when comparing both models, since Tyree, Christy & Ferrier (1974) considered a 25 m long sieve tube in which the sink region comprised 99.5 % of total sieve tube length, submitted to a water potential gradient, and the loading and the unloading rates were fixed parameters. Although a direct comparison is hard to make, contrary to what Goeschl & Magnuson (1986) suggest, they propose that a constant concentration at the top of such a Münch pressure flow sieve tube, and its decrease along the

axis, could occur only if the increased loading rates were accompanied by substantial and independent increases in sink conductance.

Following the Goeschl & Magnuson (1986) theoretical work, Magnuson *et al*. (1986) tested some of the hypothetical effects of loading rates on transport speed and concentration, using $^{11}CO_2$ labelling. They measured the rate of photosynthate export from leaves, transport speed, and tracer activity) in the phloem of live, intact plants of 6 different species. In order to have different loading rates Magnuson *et al*. (1986) changed the CO_2 concentration, manipulating photosynthesis, and labelled the plants both shortly after the beginning of the photoperiod and close to its end. In this way, Magnuson *et al*. (1986) took advantage of the endogenous diurnal changes in photosynthetic activity, storage and export rate which tend to produce diurnally increased phloem loading rates. Magnuson *et al*. (1986) observed that increased loading rates resulted in increased levels of ^{11}C activity of translocates in the phloem of all specimens tested. Increased loading also resulted in increased transport speed on 4 species, decreased on one species, and on the other one it showed a behaviour which they attributed to non-linear saturable unloading kinetics. These results convinced the authors of their model predictions and the importance of concentration dependent unloading processes on mathematical description of phloem transport. However, Magnuson *et al*. (1986) results were contradicted by other authors. Vreugdenhil & Koot-Gronsveld (1989) studying phloem exudation on castor bean cotyledons confirmed Tyree, Christy & Ferrier (1974) model results, observing a negative correlation between sucrose loading and the sucrose concentration in the phloem, contrary to what Goeschl & Magnuson (1986) and Magnuson *et al*. (1986) had observed.

2.2.1.5 Radial Water Potential Equilibrium

In general, translocating sieve elements are not in water flux equilibrium, thus sieve tube turgor pressure, p, can be determined from the water potential difference between sieve tubes and their surrounding apoplast, the continuous system of cell walls, xylem vessels lumen and intercellular air spaces in plant tissues:

$$p = \Psi_{out} + \Pi - \Delta\Psi \tag{2.9}$$

where Ψ_{out} is the external water potential; Π is the sieve tube osmotic pressure and $\Delta\Psi$ is the water potential difference between sieve tubes and their surrounding apoplast. Commonly, to infer phloem turgor pressures from eq (2.9) and evaluate the Münch pressure flow hypothesis it is assumed that sieve tubes are close to water flux equilibrium with their surroundings (Kaufman & Kramer, 1967; Sovonick-Dunford *et al*., 1981; Wright & Fisher, 1980), thus $\Delta\Psi \approx 0$. Lang (1974) justified this approximation for measuring turgor pressure in stems. Using the estimations of Weatherley & Johnson (1968), Lang (1974) concluded a water potential difference between sieve tubes and their surrounding apoplast $\Delta\Psi \approx 200$ Pa; thus much smaller than the normal values expected for sieve tube turgor pressure. Hence, according to equation (2.9), turgor pressure gradients can be simply given by the sum of the external water potential gradient and the osmotic pressure gradient within sieve tubes, i.e.:

$$\frac{dp}{dx} = \frac{d\Psi_{out}}{dx} + \frac{d\Pi}{dx} \tag{2.10}$$

Murphy (1989b) extended the analysis of Lang (1974) of phloem transport to show that ignoring $\Delta\Psi$ in equation (2.9) should yield good estimates of phloem turgor pressure and turgor pressure gradients in tree trunks. Murphy (1989b) showed that turgor pressure gradients will be in the range –2.5 to 0.5 $MPa.m^{-1}$ while the water potential difference across the sieve tube membrane, between sieve tubes and the apoplast, $\Delta\Psi$, should vary from 5 to 30 kPa having 0 or 100 % plasmodesmata blocked.

2.2.1.6 Plasmodesmatal Flux

The theoretical implications of solution transport through plasmodesmata on the mathematical modelling of phloem transport were first addressed by Murphy (1989a). Murphy (1989a-d) investigated the accuracy of the common approximation of radial water potential equilibrium in the phloem on determining phloem turgor pressure and turgor pressure gradients. He presented a mathematical model of water and sucrose transport across the sieve tube boundary, considering the role of plasmodesmata connecting sieve tube elements with their neighbouring companion cells. Based on conservation of matter and on the phenomenological equations for plasmodesmatal transport with the more gen-

eral view of the Münch pressure flow hypothesis of phloem transport, he envisaged axial volume flux, j, driven by a gradient of gravity-corrected turgor pressure:

$$\mathrm{j} = -\mathrm{L_s}\left(\frac{d\mathrm{p}}{dx} + \rho \mathrm{g}\frac{d\mathrm{h}}{dx}\right) \tag{2.11}$$

This inclusion of phloem associated cells is not new; Christy & Ferrier (1973) had already considered sieve tube association with specialized parenchyma cells and companion cells but without giving any particular significance to their intercellular connections. In Murphy's model, the sieve tube is connected via simple (unbranched) plasmodesmata to an adjacent symplastic compartment, comprised of many associated cells with the same membrane hydraulic conductivity. For simplicity, solute concentration and turgor pressure are regarded as uniform within this compartment, at least in the direction of plasmodesmatal transport. Murphy (1989a) also considered that sucrose flux across the sieve tube element plasmalemma is identical to that across the plasmalemmata of the cells comprising the adjacent compartment. Murphy used the same integral approach as Christy & Ferrier (1973), with finite loading and unloading regions occurring in sinks and sources in which the sieve tube system terminates, and designated them as primary sinks and primary sources respectively. Murphy (1989a) considered the possibility of a symplastic step in the loading/ unloading processes of water and solutes together with a gradient of external water potential. Therefore, the solute and water fluxes across the sieve tube boundary represent the sum of a membrane component and a plasmodesmatal component. Following Tyree (1970) and Anderson (1976), in Murphy's model plasmodesmatal solute transport is a combination of convection and diffusion through axially uniform pores (unconstricted cytoplasmic annulus) filled with a free flowing solution. Levitt (1975) has shown that plasmodesmatal transport can be described by the phenomenological equations for the transport of volume and uncharged solutes across membranes as developed by Kedem & Katchalsky (1958). These equations were then later applied to symplastic transport described by Tyree (1970). Murphy (1989a) recognized that considering simple unbranched plasmodesmata resulted in some underestimation of plasmodesmata hydraulic conductivity and solute permeability for branched plasmodesmata, which occurs often connecting sieve tube elements and companion cells such as in stems of bean (*Phaseolus vulgaris* L.) (Hayes *et al*., 1985). Perhaps a more physiologically significant advance over previous models was Murphy's inclusion of solution viscosity

changes with concentration which in turn will be important especially in such flow dimensions as the plasmodesmata annulus. In this respect, Murphy (1989a) considered that the fluid flowing through plasmodesmata is similar to that of the sieve tube sap, for which its viscosity was taken as the viscosity of a sucrose solution used for the range of 0.3 to 2.5 M (Weast, 1982).

Murphy also determined that the magnitude of the sucrose unloading rate in tree trunks must be less than 50 $nmol.m^{-2}.s^{-1}$ while shorter plants could afford higher rates of unloading, as would seem to be the case in stems of bean (*Phaseoulus vulgaris* L.) (Hayes *et al*., 1985). Similarly, osmotic pressure gradients may be higher than those found in trees. As suggested by Milburn (1974), steeper osmotic pressure gradients in small plants may mean steeper turgor pressure gradients. Murphy (1989b) noted that these effects would mean larger errors in small plants and one should be more cautious when estimating turgor pressure gradients in these plants. However, if the concentration gradients and unloading rates do not change markedly in the stem interval under consideration, and/or if the sieve tubes are connected to adjacent cells via unconstricted plasmodesmata, then sieve tube water flux equilibrium should still yield reasonable estimates of turgor pressure gradients in small plants. Nevertheless, this will depend on the gradients of external water potential, the estimation of which is always difficult. Murphy (1989b) also suggested that in the absence of changes in phloem anatomy, variations in the transport speed associated with sucrose unloading and transmembrane water fluxes would be small, in the order of $\mu m.s^{-2.}$ Accordingly apoplastic loading of sucrose is more likely than loading via plasmodesmata. If the plasmodesmata unloading of sucrose occurs via an unconstricted cytoplasmic annulus, then the sieve elements and their associated cells will sustain very similar turgor and osmotic pressures, even in the case where 99% of the plasmodesmata are blocked. Both convection and diffusion can contribute significantly to the plasmodesmatal sucrose flux, although their relative contributions will vary widely. Similarly, pressure flow and osmosis can both contribute to the plasmodesmatal volume flux. Murphy's (1989a-d) approach was analytical and steady state, showing that the pressure flow of solution between the sieve elements and companion cells must be accounted for when calculating sieve tube pressure gradients from measurements. By observing the behaviour of some water relations variable (e.g. turgor pressure) following the perturbation of external and internal sieve tube water potential, it may be possible to assess the extent to which sieve elements are hydraulically coupled to adjacent cells via plasmodesmata. The major contribution of Murphy's (1989a-d) work was the relationship of phloem transport theory

to experimental measurement of sieve turgor pressure considering the presence of plasmodesmata.

2.2.1.7 Stokes Flow

A number of qualitative experimental observations have been thought to be in conflict with existing mathematical models of the Münch pressure flow hypothesis. The most important were the radial water exchange associated with concentration and movement of carbohydrates (Minchin & Thorpe, 1982; van Bel, 1990) and the diffusion-like behaviour firstly observed by Mason & Maskel (1928a, b). Considering these facts, and acknowledging previous remarks on the use of Hagen–Poiseuille equation (2.3) (e.g. Horwitz, 1958), several authors considered better to apply the Navier–Stokes equation to phloem flow. The Navier–Stokes equation (momentum balance equation) describes fluid dynamics by the momentum change for a volume element of fluid resulting from the pressure, gravitational and viscous forces acting on it:

$$\rho\left[\frac{\partial \vec{v}}{\partial t}+\left(\vec{v}.\nabla\right)\vec{v}\right]= -\vec{\nabla}p+\rho\vec{g}+\mu\nabla^2\vec{v} \qquad (2.12)$$

Due to the specific conditions in which phloem flow is thought to occur, namely its low speed, sieve tube dimensions and its apparent steady state condition, it has been common to assume that advective inertial forces are small compared with viscous forces, so that the second term in the left hand side is neglected. As already noted (§ 2.2.1.1), the Reynolds number is low (<< 1) because of both the very small sieve tube radius and low flow speed. Hence, under these conditions, the Navier–Stokes equation reduces to Stokes equation:

$$\vec{\nabla}p = \rho\vec{g} +\mu\nabla^2\vec{v} \qquad (2.13)$$

for what it is named creeping flow, low Reynolds number flow or Stokes flow (Happel & Brenner, 1965).

2.2.1.7.1 Radial Water Exchange Revised

The effects of radial water exchange through the sieve tube membrane on phloem transport, for the pathway only, were addressed in two ways by applying Stokes equation (2.13). First, following Lang (1974) and Murphy (1989a), Henton *et al*. (2002) assumed the typical situation where the turgor pressure inside the sieve tube is always maintained at an osmotic equilibrium with respect to the external medium, neglecting gravity. This results in a dynamic equilibrium where a local pressure difference exists across the tube walls and so the turgor pressure inside the tube can be given by Stokes equation (2.13). The radial component of the velocity is neglected in comparison with the longitudinal component. As a consequence the wall resistance to the radial water flux is also neglected (meaning infinite hydraulic conductivity). Henton *et al*. (2002) argued that this last assumption also simplifies the mathematics of the model, consequently its interpretation, and it eliminates concerns about membrane hydraulic conductivity as a parameter. With viscosity chosen to be constant for mathematical convenience, Henton *et al*. (2002) used the van't Hoff equation for the solution osmotic pressure, as is mostly done in phloem transport mathematical modelling. A curious and questionable feature of the Henton *et al*. (2002) mathematical model is their assumption of "no large, localized variations in the solution velocity along the tube, which means that the longitudinal solute velocity profile is regarded as smooth". This, together with fixed concentration values at both system ends led to nonlinear velocity profiles different from Phillips & Dungan (1993). Although it shows an increasing velocity down the direction of flow, the assumption of Henton *et al.* is highly questionable since they neither prove it nor justify it physiologically and physically, giving the impression that it is another mathematical advantageous argument instead. Henton *et al*. (2002) did not place particular importance on sieve tube internal structure but acknowledged the existence of sieve plates. Taking their uniform and regular distribution along the sieve tube, they suggested that an empirical coefficient should multiply the solution viscosity, equivalent to having a more viscous solution. Although it may seem strange, since they obtain that same coefficient by comparing the sieve tube axial conductivity predicted by their model with the value suggested by Goeschl *et al*. (1976), physically the sieve plates behave as an extra factor opposing solution flow in the same way as viscous forces.

Second, Phillips & Dungan (1993) presented an analytical steady state model to evaluate the effects of semipermeable walls on osmotically driven flow through cylindrical tubes, and also allowing the possibility of radial variations in sugar concentration. They considered a 5 m long narrow tube enclosed by a semipermeable wall (2.6) and with a radius to length ratio $R/L << 1$. The system of typical sieve tube dimensions[7] used by Phillips & Dungan (1993) was surrounded by pure water, representing a region between and far away from source and sink regions. Pressure, velocity and concentration are set up at $x = 0$. Phillips & Dungan (1993) used perturbation expansion theory (van Dyke, 1964) to solve Stokes' equation (2.13) under the particular conditions of phloem flow. As with most models, Phillips & Dungan (1993) ignored external water potential changes, since they considered a system surrounded by pure water at constant pressure and temperature and no solute radial exchange. They also used the non-equilibrium thermodynamics formalism to describe radial water exchange across the semi permeable wall, i.e. Starling's equation (2.6). They considered three possible scenarios: i) dominant osmotic effects over viscous forces; ii) negligible osmotic effects with viscous effects dominant and finally iii) comparable effects of osmotic pressure and viscous forces, and compared each case with the Hagen–Poiseuille solution (2.3). For the case where osmotic effects are dominant, a very extreme situation, Phillips & Dungan (1993) model reproduced qualitatively very well the Münch pressure flow mechanism. Pressure decreases down the tube and is affected in two ways by the entry of water due to the osmotic difference with the external medium, first by diluting the sugar solution, and second by the increased viscous losses due to the increase of the average axial velocity. In this case, flow through the tube wall is not affected by the pressure in the tube. Phillips & Dungan (1993) also noted the qualitative good agreement of the shape of the velocity profile with the profiles obtained by Tyree, Christy & Ferrier (1974) and Goeschl *et al*. (1976) for the region where no solute radial exchange processes occur. In the second case, where viscous force effects are dominant and osmotic effects negligible, the same trends are qualitatively observed. Phillips & Dungan (1993) noted this scenario as not realistic for plants, since osmotic effects drive water exchange in both sinks and sources which ultimately drives phloem flow. Their results showed increasing average velocity and decreasing concentration and pressure down the direction of flow, but the shapes of the profiles were different compared with dominant osmotic effects. With viscous effects being dominant, concentration, pres-

[7] Kursanov (1984) and Smith *et al*. (1980)

sure and velocity changed more rapidly down the end of the tube, exhibiting a more pronounced nonlinear change of their respective gradients with distance (Fig. 2.4). According to Phillips & Dungan (1993), viscous dissipation causes pressure to drop below the surroundings and thus water flows into the tube through the semipermeable walls. As water flows, the fluid accelerates in the tube and the pressure drops increasingly with distance. Increasing velocity and decreasing concentration due to water entrance tend to make viscous forces more dominant. Phillips & Dungan (1993) results showed progressively nonlinear higher slopes, similar to what Tyree, Christy & Ferrier (1974) obtained for sugar beet. Having viscous effects dominant, all profiles are dependent on the inlet conditions, and specifically the initial pressure. In the third case, having both effects equally contributing, and comparing with the previous limiting cases, Phillips & Dungan (1993) concluded that the viscous forces are responsible for the concave upward shape of the velocity profile. Consequently, they are also responsible for the convex shape of the pressure profile with axial distance, showing a clear deviation from the Hagen–Poiseuille regime (2.3) in which there is a constant gradient of pressure with distance. Phillips & Dungan (1993) emphasized that viscous losses in real sieve tubes are likely to be higher than in their model (straight tubes with no internal structures) which may therefore overemphasize the importance of osmotic effects. In order to validate their model predictions, Phillips & Dungan (1993) compared their results with the experimental data from Lang (1973), Spanner & Prebble (1962)[8] and from Qureshi & Spanner (1973)[9]. They found good agreement for the concentration profile predicted when both osmotic and viscous forces are equally important so that the concentration gradient decreases in magnitude with the axial distance. They pointed out it is difficult to compare their model with Lang's (1973) experimental model, but nevertheless the profiles from Lang's model are in good agreement with their case where osmotic effects are dominant, as expected since pressure decreases more rapidly in Lang's experimental set up with semipermeable walls than would be the case if the tube walls were impermeable. Phillips & Dungan also noted the exclusion of time-dependent effects and the effects of loading and unloading processes happening in real plants. Oddly given their focus on viscous effects, Phillips & Dungan (1993) did not consider the effect of solute concentration on viscosity. However, their main intention was to study the physical mechanisms that cause phloem flow and that sol-

[8] on ^{137}Cs movement in *Nymphoides peltata* stems

[9] on ^{14}C-sucrose movement along the stolons of *Saxifraga stolonifera*

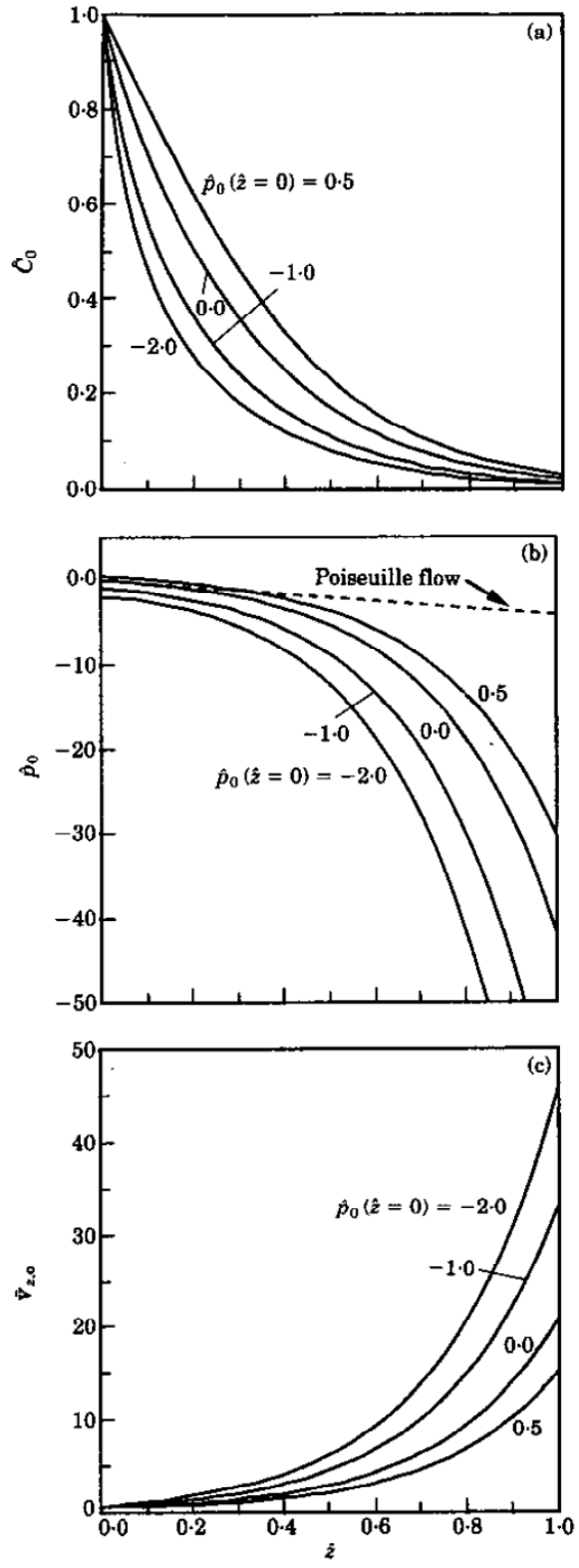

Figure 2.4 – Concentration (a), pressure (b) and average axial velocity (c) plotted versus axial position with both osmotic and viscous effects present for different initial pressures (in Phillips & Dungan, 1993).

vent will be forced into the tube lumen by both the osmotic and the viscous mechanisms operating in any tube with semipermeable walls. These effects of semipermeability become more important as the flow rate increases, diluting the sugar concentration in a way that is in qualitative agreement with data obtained from living plants (Hammel, 1968; Hocking, P. J., 1980; Milburn, 1974; Zimmermann, 1957). Phillips & Dungan (1993) also confirmed Lang's (1973) assertion that a decrease in sugar concentration in the direction of flow need not to be caused by lateral leakage of sugar out of the tube.

2.2.1.7.2 Diffusion-like Behaviour of Phloem Transport

Henton *et al*. (2002) showed how there is a diffusion-like behaviour of the steady state flux of solute inside sieve tubes, observed firstly by Mason & Maskell (1928a, b) and later confirmed by the Tyree, Christy & Ferrier (1974) and Ross & Tyree (1979) mathematical description of the Münch pressure flow mechanism. Henton *et al*. (2002) obtained an expression that is similar to Fick's 1st law of molecular diffusion which is also implicit in several other phloem transport models (Thornley & Johnson, 2000; Minchin *et al*., 1993; Sheehy *et al*., 1995). In this case the apparent diffusivity coefficient is proportional to the local solute concentration and also depends on the radius of the tube and on a set of physical constants. Henton *et al*. showed that the apparent diffusivity coefficient is around seven orders of magnitude greater than the diffusivity coefficient for sucrose in stationary water ($\approx 10^{-10}$ $m^2.s^{-1}$), showing the impossibility of diffusion *per se* to drive phloem flow. Without explicitly acknowledging it, Kizilova & Posdniak (2005) used the Henton *et al*. (2002) model, also applying Navier-Stokes equation but including diffusion of solute (described by Fick's 1st law). They used dimensionless parameter analysis and perturbation theory after Regirer (1960), similar to Phillips & Dungan (1993), in a steady state model of phloem transport. Kizilova & Posdniak (2005) findings add little to Henton *et al*. (2002) but do confirm their conclusions and prove that their simplification was correct. The Kizilova & Posdniak (2005) method although more mathematically rigorous, confirms the diffusion-like solute movement, with a radially-parabolic velocity profile[10] and a nonlinear concentration gradient along the sieve tube for a steady state phloem flow.

[10] Kizilova& Posdniak (2005) called a Poiseuille-like flow.

2.2.1.7.3 Pressure Differences Caused by Sieve Plates

It is important to consider the presence of sieve plates. Rand & Cooke (1978) compared the sieve tube resistance formula derived from Hagen–Poiseuille equation (2.7) for flow in both lumen and sieve plate pores, as commonly used by plant physiologists to describe phloem transport (e.g. Christy & Ferrier (1973), with resistance obtained from the pressure profile for Stokes' equation (2.13). Their approach represents a more realistic situation by considering the sieve tube as a pipe with constrictions spaced at regular distances, intended to simulate the presence of sieve plates. Thus, in their model, Rand & Cooke (1978) determined the pressure drop necessary to drive flow over a model sieve tube element. As they stated, their focus was the fluid mechanics of the phloem pathway, without considering the physiological factors which drive that same flow. For better comparison with the Hagen–Poiseuille equation (2.3), their model had no water flow through the lateral wall. They also justified their approach, as did Horwitz (1958), Christy & Ferrier (1973) and Tyree, Christy & Ferrier (1974)[11], acknowledging the fact that Hagen–Poiseuille equation (2.3) also neglects the effects on the pressure drop that occur as the streamlines in the sieve tube bend to pass through the pores in the sieve plate, of much smaller radius than sieve tube lumen. In this respect, Rand & Cooke (1978) applied the Stokes equation (2.13) for the axisymmetric[12] steady creeping[13] motion of an incompressible viscous fluid in a single sieve tube element with a single circular pore. From sieve tube element dimensions (Weatherley & Johnson, 1968), giving sieve tube element radius to length ratio of the order of 0.1, Rand & Cooke (1978) found that the sieve tube resistance derived from Hagen–Poiseuille equation (2.3) was about 2 times smaller than the value obtained from their formula. This means that according to their predictions, the resistance of a sieve tube element with a single narrower sieve plate pore would double the resistance predicted by the Hagen–Poiseuille equation (2.3) for the same system. The factor increased for longer and narrower sieve tube elements, and the discrepancy will be larger in the more realistic situation of more than one sieve plate pore.

[11] in this last case for using Hagen–Poiseuille equation

[12] cylindrical symmetry around the direction of flow

[13] fluid flow in which the velocity of flow is very small and the Reynolds number is << 1

Rand, Upadhyaya & Cooke (1980) supplemented the Rand & Cooke (1978) model by considering the bending of the streamlines as they pass through the sieve plate as a region of creeping conical flow. In this way they argued to build a compromise between the mathematically difficult Stokes' equation (2.13) (Rand & Cooke, 1978) and the more unrealistic flow regime associated with the Hagen–Poiseuille equation (2.3), considering the actual number of sieve plate pores instead of their previous idealization of one sieve plate pore only. As they previously predicted (Rand & Cooke, 1978), the Hagen–Poiseuille equation (2.3) gives smaller pressure drop values across a sieve tube element with N pores per sieve plate which varies, not surprisingly, according to the structural and anatomical parameters. According to the survey of Rand, Upadhyaya & Cooke (1980) on 6 species, most commonly used in phloem transport studies at the time, the pressure drop predicted by Hagen–Poiseuille equation varied between 15 and 75 % less than the pressure drop determined by the conical flow equations they obtained. This suggests that some care must be taken and their approximate equation provides a significant improvement for quantitative studies requiring greater precision, specifically when using anatomy data as input.

2.2.2 Time-dependent Laminar Flow

2.2.2.1 Changes in the Pathway Resistance

The first non-steady state model of the Münch pressure flow hypothesis published was from Ferrier & Christy (1975). They developed from Christy & Ferrier (1973) with loading and unloading of the phloem through companion cells and studied the time-dependent behaviour of a Münch translocation system following application of a cold block. Ferrier & Christy (1975) simulated the responses observed in sugar beet where phloem transport was temporarily reduced by chilling, if not inhibited. They interpreted the effect of chilling at a region in the pathway as a local resistance increase (as postulated by Geiger & Sovonick, 1970; Giaquinta & Geiger, 1973). Ferrier & Christry (1975) concluded that the resistance factor required to produce translocation inhibition indicates that even moderate inhibition is primarily due to sieve plate pore blockage rather than solution viscosity increase. The time for recovery from cold inhibition determined by Ferrier & Christry (1975) and the shape of the translocation recovery curve agreed with

experimental results. In addition, the time for translocation recovery and the level of velocity recovery depended on the rate of sucrose unloading in the sink; on the sucrose concentration in the sieve tube; on the position, length, and resistance factor of the cold block; and on the axial hydraulic conductivities. Thus, their work not only provided some insights into this mechanism but also supported its validity.

2.2.2.2 Bidirectional Movement

One of the most important features of the Henton *et al*. (2002) model is that it is the first time-dependent application of the Navier–Stokes equation to phloem transport. Although very simplified, as they rightfully state, and referring to a 30 cm tube, nevertheless it has its own merit. Henton *et al*. (2002) showed that the time-dependent model evolves to the steady state depending on the boundary conditions fixed at system ends. The time that it would require for that to happen also depends on structural and physiological parameters such as viscosity. It was also demonstrated that solute and water can simultaneously travel in opposite directions at different locations along the model tube at a given time, which could be arising from competing sources and sinks (Eschrich *et al*., 1972; Minchin *et al*., 1993). On the other hand, solute and water flow direction at a given location along the tube can change over time, which Henton *et al*. (2002) interpreted as being compatible with physiological changes such as sink/source transition (Geiger, 1987; Turgeon, 1989). Thus, Henton *et al*. (2002) showed that bidirectional movement within sieve tubes is consistent with the original Münch pressure flow hypothesis.

2.2.2.3 Time-dependent Loading and Unloading Processes

Smith *et al*. (1980) developed a non-steady-state model of phloem transport from the model of Goeschl *et al*. (1976), with the same set of equations and approximations. The model considered a single non-tapered sieve tube divided in source, pathway and sink regions with water exchange between the pathway and the surrounding apoplast. The time-dependent unloading process was considered linearly dependent on concentration, described by an unloading coefficient depending both on time and position. Smith *et al*. (1980) also used a constant averaged sieve tube element axial hydraulic conductivity be-

tween cell lumen and sieve plates, ultimately based on the Hagen–Poiseuille equation (2.3), and developed by Tyree, Christy & Ferrier (1974). Like all its predecessor models, it considered only sucrose as solute. Using a Newton–Raphson time–stepping method, Smith *et al*. (1980) improved the non-steady state phloem modelling over that of Ferrier, Tyree & Christy (1974) and Ferrier (1978), but given the limited computing power available at the time, the spatial and temporal resolution of their non-steady state approximation was low. Thus a thorough analysis of phloem long distance transport was difficult. The steady state results of their non-steady state model agreed well with the results of Goeschl *et al*. (1976), on whose equations their model was based, but bring no qualitative improvement over the Christy & Ferrier (1973) and Tyree, Christy & Ferrier (1974) models.

2.2.2.4 Sieve Tube Structure and Cell Wall Elasticity

Thompson & Holbrook (2003a) presented a time dependent model of Münch's pressure flow over long distances, including sieve tube wall elasticity, nonlinear functions of viscosity (Bouchard & Grandjean, 1995) and solute potential, and a more detailed calculation of sieve pore resistance than in previous models. The Thompson & Holbrook (2003a) model is similar to previous models (Christy & Ferrier, 1973; Goeschl *et al*., 1976; Murphy, 1989a, b; Tyree, Christy & Ferrier, 1974) by considering the phloem divided in three zones: loading and unloading regions of equal length and a pathway region between the two, all surrounded by a semi-permeable plasma membrane immersed in a medium at constant water potential representing the apoplast. Like most preceding models it has a constant loading rate and a linear concentration-dependent unloading rate in the sink region but no solute loading and unloading processes in the pathway region. The anatomy for sieve plates was used in a much more detailed manner than previous works. Sieve plates are simple (containing only one sieve area) with circular pores of equal size and length, distributed homogeneously over the sieve plate. Although based on an expected very small Reynolds number, Thompson & Holbrook (2003a) assumed that, contrary to Horwitz (1958), Hagen–Poiseuille equation (2.3) accounts, to a very good approximation, for what they call the "local conductivity" of the sieve tube, although water radial transport (2.6) was explicitly included. However, given their intention of showing the role of sieve plates with more precise and anatomy data input, their argument "Not

only can the inertial components of the Navier–Stokes equation be neglected, but relative to viscous forces, radial flow will transfer very little momentum – and very little volume – to the sieve tube sap" is more than enough for applying the more appropriate Stokes equation, given the system space dimensions. Hagen–Poiseuille equation (2.3) is not the only way of expressing a linear relationship between pressure drop and flow velocity as Rand & Cooke (1978) and Horwitz (1958) suggested, and as shown by Phillips & Dungan (1993).

Assuming that "Flow through the sieve pores is a linear function of the pressure difference across the sieve plate…" and using the work of Dagan *et al*. (1982) on Hagen–Poiseuille flow in a pore of finite length, Thompson & Holbrook (2003a) suggested that an additional term, given by Sampson (1891), should be included into Hagen–Poiseuille equation (2.3) for the total pressure across the sieve plate. Consequently, the pressure drop does not fall to zero as the pore length becomes infinitesimally small compared to sieve tube lumen, as is the case with the expression used by Lang (1978), Sheehy *et al*. (1995) and Tyree, Christy & Ferrier (1974) (2.7), derived strictly from Hagen–Poiseuille equation (2.3) and applied to both sieve tube lumen and sieve plate pores. Thompson & Holbrook (2003a) showed that for the sieve plate geometry that they used, taken from Lang (1978), the sieve tube axial conductivity, L_s, is 13.2% of its value in the absence of sieve plates and is given by:

$$L_s = \frac{\alpha R^4 r_p^2 l}{\mu\left[\alpha 8R^2 r_p^2\left(l - l_p\right) + R^4\left(8l_p + 3\pi r_p\right)\right]} \tag{2.14}$$

where the symbols used are the same as in equation (2.7). In this way, Thompson & Holbrook (2003a) showed a much more realistic way of using anatomical information regarding the role of such sieve tube structures which were for so long an obstacle to Münch's pressure flow acceptance.

Another very questionable argument is presented by Thompson & Holbrook (2003a) for neglecting gravitational effects on the basis that "…the standing pressure gradient in the xylem will cancel the standing gradient in the phloem (Milburn, 1975)." If one were only interested in phloem-xylem flow, which is normal to both phloem and xylem flows direction, that would be the case, but it is not correct, as pointed out by Murphy (1989a) and Weir (1981), especially for exploring the plausibility of Münch pressure flow

for long distances, a major goal of their work, and for the case when both xylem and phloem flow are in the same direction. It would make more sense to neglect gravitational effects, as most authors did, and as Thompson & Holbrook (2003a) admitted "…because typical pressure gradients in the phloem (~ 0.4 $MPa.m^{-1}$) are much greater than the 0.01 $MPa.m^{-1}$ standing gradient imposed by gravity". Thompson & Holbrook (2003a) assumed, like others, that radial diffusion is rapid relative to axial convection such that the radial sucrose concentration gradient is effectively zero. As well, axial molecular diffusion and dispersion are small, relative to axial solute convection, and thus can also be ignored.

Together with the new way of including the role of sieve plates, Thompson & Holbrook (2003a) also brought for discussion the elasticity of sieve tube walls, based on the work of Lee (1981a) and Sovonick-Dunford *et al*. (1982). Thompson & Holbrook (2003a) assumed that the sieve tube cross-sectional area expands linearly and elastically with pressure, and that sieve plates do not expand. Similarly to previous models and using irreversible thermodynamics formalism for describing radial water exchange (2.6), Thompson & Holbrook (2003a) made use of the solute potential given by Michel (1972) in the same way as Ferrier & Christy (1977). Qualitatively, Thompson & Holbrook (2003a) obtained similar steady state results to other authors (Christy & Ferrier, 1973; Goeschl *et al*., 1976; Phillips & Dungan, 1993; Tyree *et al*., 1974;), specifically non-linear spatial profiles of decreasing concentration and turgor pressure, with a turgor pressure gradient varying from –0.68 to –0.75 $MPa.m^{-1}$, and an increasing velocity. Lee (1981a) and Sovonick-Dunford *et al*. (1982) measured the volumetric elastic modulus of bulk phloem tissue, assuming that sieve tubes expanded with the same elastic coefficient as the phloem tissue. They suggested that expansion could act to locally increase sieve tube conductance and increase the rate of flow in periods of transiently high pressure. However, with sieve plates, which dominate in determining conductance, there is almost no increase at all in the sieve tube conductivity due to cell lumen expansion. An increase in sieve tube lumen radius though significantly increasing the conductance of the lumen itself will have little effect on the overall conductivity of the sieve tube element, since the sieve plate resistance can be as much as 90% of the total sieve tube axial resistance (e.g. sugar beet (*Beta vulgaris*), Thomspson & Holbrook, 2003b). Thompson & Holbrook (2003a) also determined that energy dissipation in axial flow due to sieve plates and lumen resistance is over 40 times greater than the loss due to lateral wall flow, and the decline in sucrose chemical potential during transport is negligible as a dissipative loss.

Thus, it would be fair to assume that transport under the considered cylindrical sieve tube geometry is limited predominantly by axial resistance to flow, and that resistance to the membrane transport of water plays only a minor role.

2.2.2.5 Radial Water Potential Equilibrium Re-examined

Thompson & Holbrook (2003b) examined the common assumption that phloem sap is in water potential equilibrium with the surrounding apoplast more rigorously than Lang (17978) and Murphy (1989a). They used dimensional analysis for the steady state of their previous model (Thompson & Holbrook, 2003a) and focused only in the behaviour of the intermediate (pathway) region. The solute loading and unloading were reduced to boundary conditions at its ends, but the linearly concentration-dependent unloading at the sink end was maintained. Because geometry and membrane properties of the pathway are important, Thompson & Holbrook (2003b) used a thorough survey of phloem anatomy from the literature, even including gymnosperms. Due to their findings of sieve plates dominance in axial flow resistance, Thompson & Holbrook (2003b) considered the sieve tube as having rigid walls, and sieve tube axial resistance as a function of length and structure only. Phloem sap was also considered of constant viscosity. The osmotic potential taken according to the van't Hoff equation and the volumetric contribution of sucrose was set to zero, such that the transport of solution was volumetrically equivalent to the transport of water. Regarding their previous effort, namely the emphasis put on using nonlinear functions of viscosity and solute potential and in being more rigorous in simulating phloem sap composition and behaviour, these last assumptions seem somehow in conflict. This is especially so, if the mathematical argument is the only one presented. Also, as in their previous work, Thompson & Holbrook (2003b) assumed that the static gravitational component of phloem transport is negligible just as axial diffusion and radial diffusion is sufficiently fast to cause radial homogeneity (Thompson & Holbrook, 2003a).

Through dimension analysis Thompson & Holbrook (2003b) built up a model of phloem translocation that scales with just two dimensionless parameters, both depending strongly on sieve plate geometry, sieve tube radius and sieve tube length and membrane permeability. This emphasizes the necessity of good measurements of anatomy for any phloem study. The parameters are equivalent to the dimensionless parameters obtained by Phillips & Dungan (1993): first, the ratio of axial resistance to membrane resistance; sec-

ond, the ratio of phloem sap osmotic strength to turgor pressure drop (between the systems ends).

First, Thompson & Holbrook (2003b) showed that the assumption of water potential equilibrium is satisfied only for very high values of the product of those two dimensionless parameters. In physiological terms this is equivalent to the product of osmotic strength, time scale, membrane permeability and the ratio of surface area to volume. Hence, for water potential equilibrium, the total turgor pressure drop for the pathway must be very small compared with the sieve tube sap osmotic strength, and the sieve tube axial resistance must be much greater than the lateral membrane resistance. Consequently, for equilibrium we must have a leaky system (given the high value of resistance ratio) submitted to small turgor pressure gradients, as suggested by Hammel (1968). This in its turn favours parietal membrane water flux and consequently water potential in closer equilibrium with the apoplast along the whole length of the sieve tube. A very large turgor drop would indicate that the sieve tube transports solute inefficiently.

Second, Thompson & Holbrook (2003b) constrained the range of possible values of the two dimensionless parameters (or 'geometry limited' range), setting reasonable bounds on sieve tube length and on the axial conductivity of sieve plates using a survey of available sieve tube geometries across different species including trees, grasses, succulents and crop species, in a total of 15 species. They found that the axial sieve plate conductivity ratio seldom falls outside the range of 0.05 – 0.5, meaning the sieve plates reduce from 5 to 50 % the sieve tube axial conductivity and they also constrain the range of dimensionless parameters values more than the sieve tube length. From their survey Thompson & Holbrook (2003b) concluded that sieve tubes operate in water potential equilibrium. However, for very long narrow sieve tubes with low sieve plates axial conductivity ratio, the transit time will become longer. Sieve tube behaviour depends very strongly on length and radius in a way that is problematic for very long sieve tubes, as transit time is an approximate index of how fast the sieve tube can recover from perturbation (Thompson & Holbrook 2003a). Using anatomical data from black locust (*Robinia pseudoacacia*), Thompson & Holbrook (2003b) concluded that the axial sieve tube turgor pressure drop is nearly independent of changes in the apoplast water potential, and the concentration gradient adjusts to those changes.

2.2.2.6 Concentration–Pressure Waves and Information Transmission

A big leap forward in the mathematical description of the pressure flow hypothesis was made by Ferrier, Tyree & Christy (1975) and Ferrier (1976) on working out the time-dependent behaviour of the Münch pressure flow system. Any time-variation of loading produces a corresponding variation of osmotic pressure (solute concentration). Both studies considered a 15 m tree and sinusoidal time variations of sucrose loading and water potential, with a period of one day. This idea is based on the fact that in real plants two important factors can prevent translocation from attaining a steady state. The problems are more severe in large specimens like trees; one being the diurnal fluctuation in water potential throughout the tree; the other is diurnal fluctuations in sugar loading rate in the leaves, perhaps caused by the growth of the leaf sugar pool during the day and the decline of the pool through the night. Concentration waves had been detected to propagate in trees (Huber *et al*., 1937; Ziegler, 1956; Zimmermann, 1969; Zimmermann & Brown, 1971). The model of Ferrier, Tyree & Christy (1975) was an extension of Christy & Ferrier (1973) to a single sieve tube of a 15 m tree, within an apoplast water potential gradient in the direction of flow. They found that a time variation of the loading rate and of the apoplast water potential with a period of one day produces concentration waves propagating down the sieve tube. These waves are superimposed on a concentration gradient in which the amplitude of the concentration waves decreases down the tree. This is similar to what Huber *et al*. (1937) have reported in northern red oak (*Quercus borealis* L.). However, Huber *et al*. (1937) detected concentration and pressure waves from bark cuts at various heights in *Quercus borealis*, but incorrectly interpreted the data as flux of the bulk solution. Concentration varied diurnally at all heights measured, but with an increasingly large phase shift with distance from the crown. Zimmermann (1969) correctly interpreted the phase shift as the propagation of concentration waves. Ferrier, Tyree & Christy (1975) also predicted that a concentration maximum occurs some time after the maximum loading rate. Their model also shows that the waves move with a phase velocity 4 to 8 times higher than the solution velocity. Unlike the concentration dynamic profile, the phase velocity is not affected for a phase difference between loading rate and surrounding water potential up to 6 hours. This is in agreement with Huber *et al*. (1937) who sug-

gested a maximum concentration at night time, which in turn agrees with the common situation in nature of having a minimum water potential surrounding the phloem at about the middle of the day followed by a maximum peak on the loading rate at sunset or evening. However, the same concentration waves resulting from time dependent loading rate and apoplast water potential gradient can equally well be generated from periodic time dependent unloading rates at a sink region and travel from sink to source as shown by Ferrier (1978). In fact, such waves can originate anywhere in the phloem transport system at which a time-dependent variation of sugar concentration (or other solute concentration) is imposed by a time-dependent loading or unloading rate. As Ferrier (1978) speculated, these waves may carry information that could provide feedback linking source and sink regions, and more quickly than changes in the concentration gradient or hormone transport. The propagation of these waves can be thought of as "information transmission" about local changes, both as a whole sieve tube signal of disturbance (such as a change in apoplastic water potential or mechanical damage) and as a feedback signal for photosynthesis and allocation of solutes. Thus, it can be seen as a way of whole plant level regulation of sugar loading and unloading in response to changes in turgor or osmotic pressure in the sieve tube as first suggested by Ferrier *et al*. (1975). Ferrier (1978) proposed the term concentration-pressure-flux waves, CPJ[14], due to the complex interactions between solute concentration, turgor pressure and the solute and water fluxes. Ferrier (1978) showed that changes in concentration (or pressure) leads those in lateral water exchange by a phase angle equivalent to 6 hours for a diurnal variation.

Any time variation of loading or unloading produces a corresponding variation of osmotic pressure (solute concentration), which then results in a time-dependent water exchange across the sieve tube membrane, and causes a time-dependent variation of turgor pressure at the point of loading. The pressure propagates axially. This moving fluctuation in turgor pressure affects the water flux across the sieve tube membrane, and therefore the concentration. The concentration and turgor pressure variations tend to have counteracting effects on the water influx. These complex interactions between concentration, turgor pressure, and water exchange constitute the CPJ wave. The main parameters governing the wave speed are frequency, axial hydraulic conductivity of the tube, and average osmotic pressure. If a time-dependent variation of osmotic pressure is imposed at some point within any semipermeable tube of small radius in an aqueous environment

[14] stands for fluxes, usually represented by J

then a CPJ wave will occur. For the normal physiological conditions of functional sieve tubes, CPJ waves are virtually certain to occur.

Following Henton *et al*. (2002) model, Kizilova & Posdniak (2005) also solved Navier–Stokes equations (2.12) for the time-dependent case of phloem transport, with both concentration and velocity submitted to periodic perturbations. Their objective was to show that wave propagation, already observed in plants, is a "possible biophysical mechanism of long-distance signalling in higher plants". However, although more rigorous than previous models (Ferrier, Tyree & Christy, 1975; Ferrier, 1976), their predictions of wave velocity were very unrealistic for phloem transport, not only being far greater (20 to 60 $m.s^{-1}$!) than the average 10^{-4} $m.s^{-1}$ speed expected for phloem transport, but also still much bigger than the experimentally consistent values predicted by Ferrier, Tyree & Christy (1975) and Ferrier (1976). The problem may be the periodic functions Kizilova & Posdniak (2005) used, since they obtained a different formula from Ferrier (1976) relating wave velocity with the phloem physiological parameters. They clearly state their model to be based on both experimental and theoretical work of Karmanov & Meleshchenko (1982) on "auto-oscillations of the processes of water exchange" on xylem water transport. Thus, it seems that Kizilova & Posdniak (2005) considered wave propagation origins and behaviour as being the same for both xylem and phloem tissues, which may not be always the case.

Based on their theoretical findings, that the steady state sieve tube axial turgor pressure drop is independent of the apoplastic water potential gradient, unlike the axial concentration drop (Thompson & Holbrook, 2003b), and seeing that as an indication of a fast transmission of turgor pressure changes throughout the entire sieve tube, Thompson & Holbrook (2004) used their previous model and dimensional analysis (Thompson & Holbrook, 2003b) to investigate the speed with which turgor pressure and solute concentration are transmitted throughout the sieve tube. The most plausible explanation for rapid propagation of concentration waves requires that the water potentials of the sieve tube sap and apoplast be tightly coupled. These waves drive membrane water flux elsewhere in the sieve tube, either diluting or concentrating the solution until the sieve tube sap comes again into water potential equilibrium with the apoplast. If the pressure waves propagate quickly, so will the concentration waves, as long as the sieve tube sap can readily return to water potential equilibrium. This in turn depends on the local elastic and membrane properties of the sieve tube (Dainty 1976; Kallarackal & Milburn 1985) or at the very least is affected by it (Lee, 1981a; Sovonick-Dunford, 1986; Sovonick-Dunford *et al*.,

1982). An increase in local solute concentration will lead to an influx of water that will raise the pressure until the balance is restored. Furthermore, a propagating pressure wave will be accompanied by a concentration wave as the increased pressure drives water out of the sieve tube, concentrating the solute already present. Thompson & Holbrook (2003b) demonstrated that the relevant phloem transport equations greatly simplify in water potential equilibrium. This makes sieve tube dynamics solely dependent on the value of the dimensionless parameter defined as the ratio of the sieve tube sap osmotic pressure to turgor pressure drop between the intermediate phloem ends, dependent on the flow rate and sieve tube geometry. Thompson & Holbrook (2004) called this ratio "phloem transport scale". Conceptually, this ratio reflects whether a local perturbation in sieve tube state is more likely to propagate axially (when having a greater osmotic strength) or to accumulate locally (when the turgor pressure drop is greater than the osmotic strength). Thompson & Holbrook (2004) used a sinusoidal time dependent loading process, with a 24 hour period, similar to what Ferrier, Tyree & Christy (1975) and Ferrier (1976) did, as a local perturbation in sieve tube concentration, and consequently in pressure[15]. Sieve tube sap is osmotically coupled to the apoplast through a semipermeable membrane. As we know, pressure is rapidly transmitted in a steel pipe totally full of fluid, but solutes move only as fast as the flow of solution. In the phloem, the two are coupled. Kallarackal & Milburn (1985) argued that the primary limitation to the movement of pressure waves was the sieve tube elastic and membrane properties, for changes in cell volume, following small perturbations in concentration or apoplastic water potential. But, local perturbations in sieve tube solute concentration and pressure can be rapidly transmitted over long distances in response to any physicochemical perturbation that locally alters the water potential of the sap or the surrounding apoplast. The rate of transmission depends mainly on the value of the phloem transport scale, being faster for higher values and is inversely proportional to the sieve tube length, i.e. the velocity of the wave increases as the sieve tube becomes shorter (Thompson & Holbrook, 2004). Hence, local perturbations in concentration and turgor pressure are more rapidly transmitted throughout the entire sieve tube when the sieve tube axial turgor pressure gradient is relatively small compared with the sap osmotic strength. These wave fronts can move several orders of magnitude faster than the solution itself, in both upstream and downstream directions,

[15] from data for black locust (*Robinia pseudoacacia*), a leguminous tree, and castor bean (*Ricinus communis*), which has high axial sieve tube conductivity, for different sieve tube lengths submitted to an apoplastic water potential gradient.

i.e. for castor bean (*Ricinus communis*) it can be 100 times de sap speed (Thompson & Holbrook, 2006). Hölttä *et al*. (2006) determined a concentration wave speed of about 1 $m.h^{-1}$ and a pressure front propagating at a rate of approximately 25 $m.h^{-1}$, similar to Ferrier, Tyree & Christy (1975). These findings agree with previous measurements of diameter variation that have also indicated very rapid propagation of pressure along the xylem and with a small time lag in the phloem (Perämäki *et al*., 2001; Sevanto *et al*., 2003).

Thompson (2005) extended the analysis of previous contributions to the problem of concentration-pressure waves (Ferrier, 1976; Thompson & Holbrook, 2004) by determining the effect of non-rigid walls on the wave rate of propagation. He used the same dimensional analysis and phloem transport model of previous studies (Thompson & Holbrook, 2003b, 2004), but this time with elastic terms included. As Thompson and Holbrook (2004) predicted, the observed effect was that the speed of pressure wave propagation depends predominantly on phloem transport scale, ultimately on the sieve tube sap osmotic strength, with cell wall elasticity being only a minor factor. Hence, Thompson (2005) concluded that elastic terms are not of enough importance to include in basic models of phloem transport.

2.2.2.7 Osmoregulatory Flow

For situations where osmotic strength is much higher than the turgor pressure drop along a pathway, the results of Thompson & Holbrook (2003b) show that sieve tube turgor pressure becomes almost the same everywhere in the sieve tube, irrespective of local variation in solute content or apoplastic water potential. In this manner, any turgor pressure changes occurring in some part of the sieve tube, due to some osmotic activity, are readily transmitted throughout the entire sieve tube. So, if, as an example, solute unloading increases then the whole sieve tube turgor pressure will drop. This will lead in its turn to a concerted increase in the rate of solute loading from all (or some) sieve tube elements to recover that lost in turgor, perhaps due to enhanced or diminished activity of proton pumps and membrane transporters (Lalonde *et al*., 2003; Patrick *et al*., 2001). Consequently, such a system would be extremely convenient from a control perspective: all sieve tube elements in a sieve tube could react the same way because they all receive the same stimulus. Direction of transport would then be determined by the relative position and density of solute loaders and unloaders, but rates of solute loading would be partially

governed by the need to globally regulate turgor. Thompson & Holbrook (2003b) called this mode of transport "osmoregulatory flow". Their findings are similar to Lang's (1983) proposal of turgor regulated translocation in which individual sieve tube elements maintain a graded series of turgor pressures. This will give rise to a stable turgor pressure gradient, and therefore flow rate, in the whole sieve tube. Thompson & Holbrook (2003b) point out in contrast that if osmoregulatory control operated along the length of the sieve tube in the presence of a large turgor pressure drop, as it is commonly assumed as prerequisite for Münch pressure flow, a set point turgor would have to be programmed. This would be a function of distance along the sieve tube depending on the turgor pressure drop necessary to maintain a certain axial flow. But if the flow rate changed, the programmed gradient would have to be reprogrammed, making it unclear, on the basis of its decentralized body plan, how the plant would accomplish this more complicated mode of control. Moreover, such a system would place the flow control in the intermediate region between sources and sinks, instead of where the solutes are actually produced and consumed. On the other hand, low turgor pressure drop (or high osmotic strength) osmoregulatory flow is compatible with recent suggestions by Patrick *et al*. (2001) and Lalonde *et al*. (2003) that information regarding sink demand or plant water status could be transmitted throughout the phloem as a change in turgor pressure, in agreement with Ferrier (1978). Under this concept, the phloem intermediate region is conceptually better viewed as a turgor regulating unit as proposed by Lang (1983) than as a simple conduit for transport. This distinction highlights turgor regulation as the primary means of controlling translocation, rather than turgor pressure gradient regulation, and greatly simplifies the demands placed on membrane solute transport.

2.2.2.8 Phloem Relays

For Münch pressure flow over long distances Thompson & Holbrook (2003a) showed that the transit time to travel the whole system length, L, is proportional to L^2, thus confirming the idea of Tyree, Christy & Ferrier (1974) that phloem transport will take far longer at greater distances and that taller plants could be "expected to have" lower sieve plate resistance, or shorter sieve tubes linked in series, or both. Hence, Thompson & Holbrook (2003a) suggested that instead of relying on a single osmotically isolated path from source to sink, the plant may rely on a set of such paths arranged in

series – a composite or ‘‘relay’’ system (Lang, 1979; Aikman, 1980; Murphy & Aikman, 1989), in which between two adjoining relays there is an intermediate apoplastic step of both unloading/loading processes. Consequently, there are energy costs associated with active loading of solutes at each relay, which obviously increase with the number of relays. In this scenario, lengths of sieve tube are hydrostatically isolated and relays expend energy transporting assimilates from one length to the next. Consequently, with transit time being linear with L^2, halving the transport distance would reduce the transit time. Thus, it is not difficult to see how two concatenated 10 m sieve tubes would have a composite transit time of only 1/2 that of a single 20 m sieve tube, and four 5 m sieve tubes only ¼ that of a 20 m tube. For different lengths Thompson & Holbrook (2003a) applied a small sinusoidal diurnal impulse wave function in the unloading zone as a perturbation to the steady state simulations. They determined that not only are longer sieve tubes slow at delivering their assimilates to distant points in the plant, but they are also considerably less sensitive to changes in supply or demand at one or the other end of the tube. At very small lengths sieve tube concentration is extremely sensitive to small differentials between the loading and unloading rates. This evokes the heavy dependence of the sieve tube element on the cell activity of its associated companion cells (van Bel & Knoblauch, 2000) or Strabusger cells[16], nowadays considered as a single physiological unit – the sieve element companion cell complex, SE/CC. In this way, another disadvantage of the relay mechanism (Lang, 1979), aside from the cost of active loading, is that in short sieve tubes sucrose concentration is very sensitive to differentials between loading and unloading rates. A very low value of the transit time could mean that transport through the system is rapid relative to storage. Intermediate active transport is at least circumstantially supported by the presence of sucrose and water membrane transporters throughout the plant body (Patrick *et al*., 2001). Passive loss and active loading of sucrose are known to occur everywhere (Komor *et al*., 1996). Perhaps the ‘‘leak pump’’ behaviour of phloem tissue is not simply a matter of storage, or supply to stem tissue, but additionally transports sucrose from one sieve tube to the next. Unfortunately, as Thompson & Holbrook (2003a) point out, the relay hypothesis is difficult to test directly, since little is known about the fine-scale anatomy of the phloem in different taxa. Rates of loading and unloading in the stem are poorly known, and even less is known on marrying the two types of information.

[16] in the case of gymnosperms

The efficiency of osmoregulatory flow, and the conditions in which it occurs presented by Thompson & Holbrook (2003a, b), seems to require that sieve tubes be shorter than the plant axial length. The idea of multiple, concatenated sieve tube modules, with solute loading and unloading between them, although not new (Lang, 1979), has only been tested once by Murphy & Aikman (1989), who looked for relays in castor bean (*Ricinus communis*), using an analysis of phloem bleeding in stems and petioles. Their data suggested that there is hydrodynamic continuity between stem and petiole, and did not point to solute relays. However, such evidence does not count against relays in general, since the osmotic strength to turgor pressure drop ratio is large enough to consider castor bean a good example of osmoregulatory flow and thus making relays unnecessary (Smith & Milburn, 1980). Milburn (1974) showed that a concentration drop is present, perhaps to oppose the gradient in apoplastic water potential, but no big turgor pressure drop (Milburn, 1972). But, on the other hand, if a plant phloem translocation system is organized in modules, as in many large trees given the complexity of their vasculature, then the coordination of different sources and sinks would occur through intermediate nodes, being either vascular nodes or petiole insertions. There is some circumstantial evidence that would allow relays to operate: the prevalence and orientation of transfer cells in vascular insertions (Gunning & Pate, 1974); the rapid solute leakage and retrieval processes throughout the phloem in the stem (Aloni *et. al*., 1986; Minchin & Thorpe, 1987a); sieve tube solute content is known to vary considerably between sieve tubes of different vascular bundles (Milburn 1974), as is turgor pressure (Hammel, 1968; Lee, 1981b; Wright & Fisher, 1980), and the axial turgor pressure drop is found to vary between 0.05 and 0.2 $MPa.m^{-1}$, even in trees. Furthermore, as Thompson & Holbrook (2003b) show, a large gradient in concentration does not necessarily indicate a large gradient in turgor pressure. Hence, the large quantity of solute known to be leaked and retrieved along the translocation pathway could represent more than just lateral exchange with stem storage pools; it could represent transport from one module to the next, a process that would be difficult to distinguish from "retrieval" given the small distances involved.

Hölttä *et al*. (2009) using a simplified version of their previous model (Hölttä *et al*., 2006) basically considering only phloem and xylem systems, investigated the influence of phloem morphology and potassium on the phloem transport capacity to distribute carbohydrates in a tree. Hölttä *et al*. (2009) maintained all their previous model assumptions (Hölttä *et al*., 2006) and presented a steady state model in which both phloem and

xylem axial conductivity are taken from Hagen–Poiseiulle equation (2.3) with a geometric factor[17]. In this way, phloem conductivity implicitly depends on concentration, as viscosity depends on sugar concentration (Hölttä *et al*., 2006), as in many models. The main convenience is that it can relate with anatomical and physiological features and validate model assumptions. However, as stated by several authors its validity is highly questionable in the presence of lateral water fluxes; like all the models before this one. Hölttä *et al*. (2009) model highlights the advantages of the solute relays (Lang, 1979), specifically in big plants where axis length is a problem for efficient transport. Hölttä *et al*. (2009) showed that with solute relays the same amount of sugar can be transported with fewer parallel tubes compared with the case of continuous sieve tubes, and the number of required parallel tubes (and solution speed) were approximately inversely proportional to the number of tubes in series. Both pressure and concentration propagated at a speed inversely related to the number of relays. Hölttä *et al*. (2009) also observed that the turgor pressure difference between the source and sink regions dropped considerably when having solute relays, thus achieving a more uniform turgor pressure in the phloem. The Hölttä *et al*. (2009) model showed the advantageous osmotic role of potassium. If it is actively loaded and unloaded against concentration gradients, it merely increases the turgor pressure and its gradient by drawing in water to the phloem without increasing the solution viscosity in the same way as sugars. Their results agree with the actual physiological role of potassium in the phloem and with earlier measurements of phloem potassium gradients in the same direction as carbohydrates gradients (Vreugdenhil, 1985).

2.2.3 Coupled Xylem and Phloem Flows Models

The vast majority of phloem transport models published does not consider xylem-phloem interactions, despite the close proximity of the two vascular systems and the well known water exchange between the two. Probably the main reason for not treating both systems simultaneously is the complication of increasing the number of transport equations that would have to be solved. Thus, it is not surprising that the first model of coupled xylem and phloem flows used "state-of-the-art numerical methods solved on digital computer" (McKinion & Weaver, 1979). They presented a compartmental model (Fig

[17] multiplied by the number of parallel running elements and by a dimensionless factor accounting for the effect of the intervascular pits and sieve plate pores for both xylem and phloem respectively.

2.5) of coupled xylem and phloem flows simulating a cotton plant seedling (*Gossypium barbadense* L.) consisting of four different compartments in which water circulates from leaves to phloem, to roots, to xylem and back again to leaves. Between these last two compartments there is a semipermeable membrane separating xylem from the rest of the leaves tissue. McKinion & Weaver (1979) emphasized that in both xylem and phloem pathways, water moves down a pressure gradient circulating throughout the plant body, being taken up from the soil by the roots and being lost through evapotranspiration in leaves. In this manner, both root and leaf compartments change their respective volumes due to differences in both incoming and outgoing flows together with water uptake in the roots and water loss in the leaves respectively. The root compartment was regarded as limited by a barrier separating it from the soil through which the hydrostatic and osmotic pressure differences developed would cause water to be taken up by the root. On the other extreme, water loss from the leaf through evapotranspiration is considered as a linear function of the differences in the water vapour pressure in the leaf and surrounding air. McKinion & Weaver (1979) were mainly concerned with stress caused by carbohydrate and water shortages in the cotton plant. They used the main biochemical rate equations for describing carbohydrate concentration changes both in leaves and roots, together with the Hagen–Poiseiulle laminar flow description of vascular transport (2.3). McKinion & Weaver (1979) also showed that changes of the biochemical rate parameters describing carbohydrate production and consumption also affected both xylem and phloem flow rates. Similarly the sucrose levels in both leaves and roots were also affected. Although very simplified, specifically in terms of spatial and physical limiting of the different compartments, the McKinion & Weaver model has the merit of showing how informative and important integrative models of xylem and phloem flows can be, and opened the way to more complete and realistic models.

Boersma *et al*. (1991) extended the McKinion & Weaver (1979) compartmental approach for a better understanding of how water stress affects transport rates in both xylem and phloem and source/sink relationships. The main improvement was not only the more realistic physical dimensioning of plant vascular architecture but also to link fluid flow between the two transport systems. Boersma *et al*. (1991) considered both phloem and xylem systems as series of interconnected compartments or discrete units describing the transport pathway from the soil, through roots, stems, leaves and into the atmosphere, including the water vapour flow from intercellular spaces to the atmosphere. They also considered the control of water vapour loss and CO_2 uptake through stomata including al-

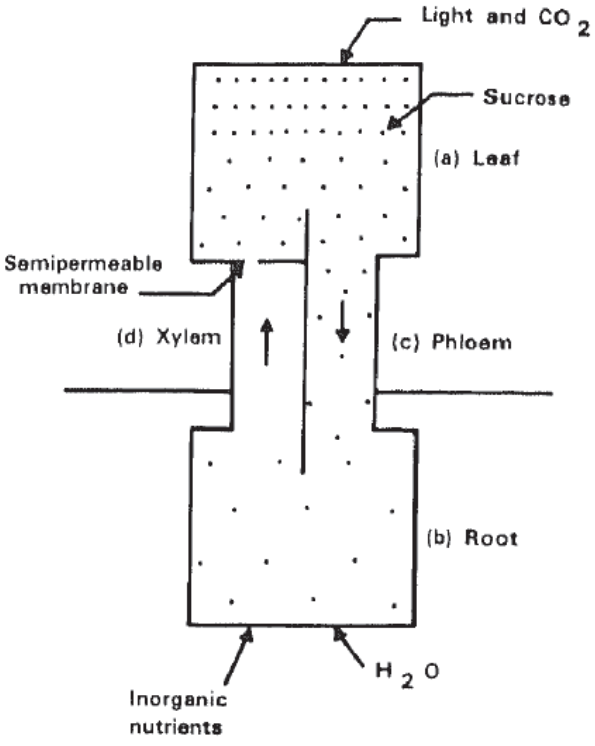

Figure 2.5 – McKinion & Weaver compartmental model (in McKinion & Weaver, 1979).

so some structural detail never studied before in mathematical modelling of phloem transport (Fig. 2.6). The coupling of both xylem and phloem flows was only considered in both source (leaves) and sink (roots) regions where Boersma *et al*. (1991) examined lateral water transfer between xylem and the phloem driven by water potential gradients that are affected by the sugar concentration in the sieve elements. The Boersma *et al*. (1991) model, like its predecessor from McKinion & Weaver (1979), is a steady state model making constant the concentration of sugars in both source and sink compartments. But, unlike the model of McKinion & Weaver it does not include photosynthesis described by biochemical rate equations. Even though it only refers to transport between one sink and one source, the Boersma *et al*. (1991) model is useful in showing that xylem water potential affects phloem transport, mimicking experimental observations of xylem and phloem transport rates, and sugar concentration in the source and in the sink. It also shows how both xylem and phloem flows are sensitive to environmental changes.

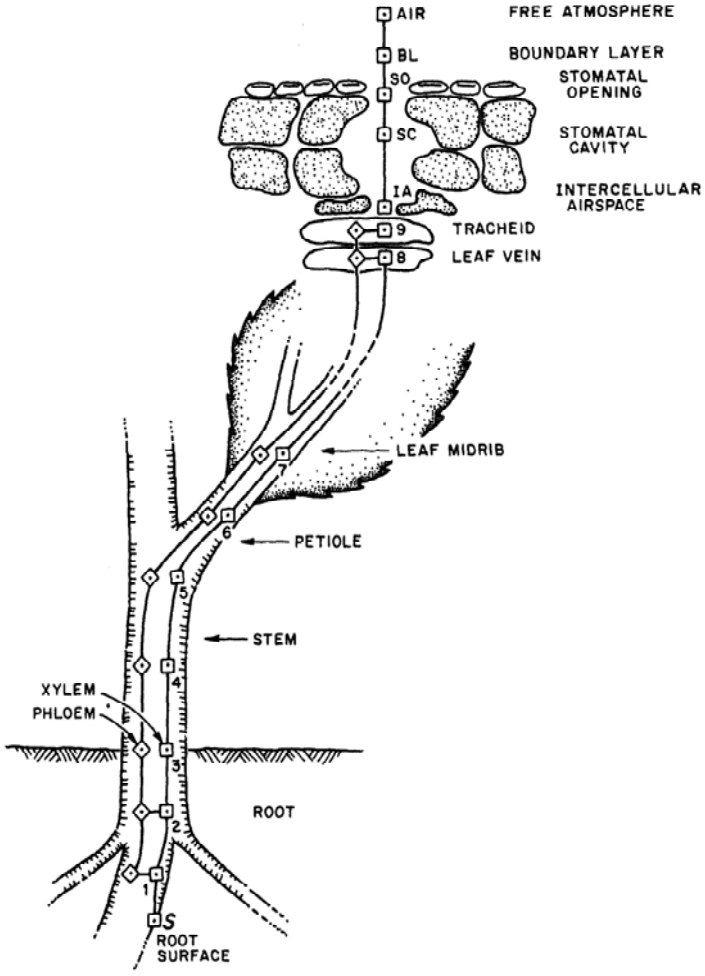

Figure 2.6 – Compartmental model of xylem and phloem transport pathways (in Boersma *et al*., 1991).

2.2.3.1 The Effect of Transpiration on Phloem Transport

Hölttä *et al*. (2006) did "modelling of xylem and phloem water flows in trees according to cohesion theory and Münch's hypothesis" to simulate phloem transport in Scots pine (*Pinus sylvestris* L.). Although not the first phloem transport model to consider tree dimensions, their model has the merit of including coupled xylem and phloem flows in which the transpiration stream is the main cause of changes in the apoplastic water potential. Thus, it gives a much more realistic picture of the water circulation in trees when compared with the previous works of Ferrier, Tyree &Christy (1975) and Ferrier (1976). Interestingly, physiology and anatomy data of a gymnosperm species are included

as well as for angiosperms; which is unusual for phloem modelling. No particular emphasis on anatomical or structural features of xylem or phloem is given. Also, sieve plates, xylem pith membranes, or any other particular cell structures are ignored, considering that any effect of such cell structures may be implicitly included in the axial conductivity at the macroscopic level, assuming it as constant. As in most mathematical models of phloem transport, radial solute exchange along the phloem pathway is also not considered. The focus of the Hölttä *et al*. (2006) model is on the flow in the pathway between sources and sinks. For that reason the model considers transpiration, a constant phloem loading rate, and a linearly concentration-dependent unloading rate. Root is also not considered, and water absorption from the soil at the bottom end of the xylem pathway is given as input as is soil water tension. In this particular respect it represents a disadvantage when compared with the models of Boersma *et al*. (1991) and McKinion & Weaver (1979). Sugar loading rate is taken from the measured CO_2 daily uptake in leaves according to Sevanto *et al*. (2003), assuming that the entire CO_2 intake into the tree is converted into sucrose which is then loaded into the phloem. Given its dimensions and in order to best simulate water and solute movement in trees, the gravitational hydrostatic pressure gradient is included. The model of Hölttä *et al*. (2006) is strongly based on the Perämäki *et al*. (2000) model of water flow based on the cohesion theory of xylem water movement. Anatomically, the Hölttä *et al*. (2006) model is more advanced than its coupled xylem-phloem flows model predecessors (Boersma *et al*., 1991; McKinion & Weaver, 1979). It offers a more realistic picture as it divides the model tree into four different functional components in the radial direction: xylem, cambium, phloem and "other living bark tissue", excluding ray cells for geometry simplicity, thus making each component with a homogeneous radial distribution of water pressure. Both axial xylem and phloem flows are determined using Darcy's law, which describes the flow of a fluid through a porous medium:

$$\mathrm{j} = -\frac{k}{\mu}\frac{d\mathrm{p}}{dx} \tag{2.15}$$

in which the flux, j, of a fluid of viscosity μ, is linear with the pressure gradient in some segment of length (e.g. xylem vessel or sieve tube element) of axial conductivity k dependent of sieve tube structure only. The radial water exchange between the adjacent components is given by Starling's equation (2.6). The changes in the diameter of each

component relate to changes in water pressure through the bulk modulus K definition from the elastic properties of plant cell accompanying cell expansion due to water movement (Dainty, 1976; Nobel, 1999; Wright & Fisher, 1983):

$$\frac{d\mathrm{p}}{dt} = \frac{K}{\mathrm{V}}\frac{d\mathrm{V}}{dt} \tag{2.16}$$

Any effects on xylem hydraulic conductivity caused by embolism and refilling of xylem vessels are not included. Interestingly and not explicitly justified by the authors, they consider that phloem sap viscosity changes with sugar concentration following Morison (2002); in a very conflicting and highly questionable decision they chose van't Hoff's equation to express phloem sap osmotic pressure. Thus it is really hard to think how viscosity can change with sugar concentration, which they claim as being important to explain phloem transport speed changes, and at the same time the linear relationship between osmotic pressure and concentration is still maintained. Hölttä *et al*. (2006) give no justification and seem to follow uncritically the common use of van't Hoff equation in plant physiology.

With a polemic choice of sugar concentration-dependent viscosity yet a simultaneous linearly concentration-dependent osmotic pressure, Hölttä *et al*. (2006) observed that the system was sensitive to the sugar loading rate. A too high sugar concentration (of approximately 7 MPa osmotic pressure) would cause phloem translocation to be irreversibly hindered, and soon totally blocked, due to accumulation of sugar at the top of the phloem and the consequent rise in the viscosity of the phloem sap that would change sieve tube resistance, according to Darcy's equation (2.15). On the other hand, a too low sugar loading rate would not induce a sufficient axial pressure gradient to cause any flow at all. The sugar flux decreases uniformly as the sugar concentration and osmotic pressure at the unloading zone are increased. At the same time axial pressure gradient in the sieve tubes decreases and sap viscosity increases. Common to all models, which presented an explicit dependence of viscosity on phloem sap sugar concentration, changes in viscosity have severe effects on the phloem translocation capacity of the phloem sap as viscosity also varies substantially with distance as a consequence of the sieve tube concentration gradient. Hölttä *et al*. (2006) found that the viscosity of the phloem sap can be over 10 times higher than the viscosity of pure water at the same temperature. There is an "optimal value" for the sugar loading rate for maximum sugar translocation to balance be-

tween the two scenarios of drop in turgor pressure and the dilution of the sap solution, and the rise in viscosity. This optimal value was evidently dependent on the structure of the transport system and environmental conditions. This optimal value was about 5×10^{-5} $mol.s^{-1}$, resulting in an osmotic pressure of 6 MPa at the source region which is equivalent to a total sugar concentration of 2 M, about two times the normal expected values found (Salisbury & Ross, 1991; Sevanto *et al*., 2003).

Of interest and specifically due to their success in showing coupled xylem and phloem flows, Hölttä *et al*. (2006) were also able to show the noticeable impact of transpiration on the amount of sugar loading that can be sustained. Sufficiently low water tensions must be maintained in the leaf to avoid excess embolism. However, very high tensions could also prevent water crossing to phloem, inducing limitation on stomatal conductivity. Water tension build-up would reverse the direction of the phloem flow, with water being "sucked" to the xylem during the daily peak transpiration, if transpiration was raised to more than five times the normal transpiration rate they measured for Scots pine(*Pinus sylvestris* L.). Hölttä *et al*. (2006) suggest that the water tension in leaf might be controlled by stomatal conductivity, facilitating the Münch pressure flow in agreement with Schultze (1991), who pointed out that the requirements of regulating the xylem and phloem flows could be the driving reason for stomatal control of transpiration (and photosynthesis) in leaves.

Ferrier, Tyree & Christy (1976) and Ferrier (1976) were the first to explicitly consider time-dependent changes on the apoplastic water potential surrounding sieve tubes, but Hölttä *et al*. (2006) presented a more integrative way of considering transpiration as the main driver of apoplastic water potential changes, along with the radial water exchange between xylem and phloem tissues. Using field measurements from Sevanto *et al*., 2002, Hölttä *et al*. (2006) showed coupling of radial phloem and xylem flows with transpiration. This confirmed the Sovonick-Dunford *et al*. (1981) measurements of phloem turgor pressure in white ash (*Fraxinus americana* L.) trunk and Buttery & Boatman (1964) measurements of turgor pressure in the laticiferous phloem tissue of Pará rubber tree (*Hevea brasiliensis*). Thus, during high transpiration xylem pulls water from the sieve elements and their turgor pressure is reduced. The turgor pressure drop is greater at the top of the tree during diurnal transpiration peaks, which reduces the axial turgor pressure gradient and raises the viscosity of the sap as sugars accumulate. When transpiration is lowered, water and sugar flows in the phloem are enhanced.

It is well known that stem diameter changes and water status in trees are closely related. Hölttä *et al*. (2006) showed that the diameter change of the whole stem depends on both xylem and phloem pressure. The whole stem diameter variation has the same basic pattern as the xylem diameter variation. At the top of the tree (source of transpiration) the change in stem diameter lags behind the xylem change diameter, leading the xylem diameter change at the bottom, with both changes following transpiration. This same pattern has also been observed in field measurements (Sevanto *et al*. 2002, 2003). Comparing the relative amplitudes of the xylem and stem diameter variations Hölttä *et al*. (2006) found that one third of the whole stem diameter change was due to changes in xylem and two thirds to the living tissue outside the xylem, i.e. almost exclusively the phloem, agreeing with the field measurements from Sevanto *et al*. (2002).

2.2.3.2 Münch Counterflow

As strange as it may seem the model predictions of McKinion & Weaver (1979) are more interesting than what they presented. Whether intentional or not, McKinion & Weaver (1979) presented the first published evidence, although theoretical, of what is called today the Münch counterflow – in which due to the continuous sugar loading and unloading during the absence of transpiration there is a transpiration-independent water flow in the xylem during the night. The axial xylem pressure gradient is thus induced by withdrawal of water from the xylem into the phloem at the source region, and the efflux of water from the phloem to the xylem at the bottom of the stem, promoting a continuous circulation of water in the plant body. Unfortunately, in a lost opportunity, McKinion & Weaver (1979) did not highlight this situation. They do, however, present results in which xylem flow rate at night-time is reduced to the same value as phloem flow rate. This is about 5 % of the maximum xylem flow rate as shown by Hölttä *et al*. (2006), Pedersen & Sand-Jensen (1997) and Tanner & Beevers (2001). Phloem flow is fairly constant throughout the day, while the xylem flow lags behind the transpiration, confirming McKinion & Weaver (1979) experimental data. Experimental evidence of the Münch counterflow has only been shown recently by Kockenberger *et al*. (1997) and Tanner & Beevers (2001), confirming Tanner & Beevers (1990) previous investigations. It may be important especially for large trees, since it provides a transport mechanism for nutrients from roots to canopy even in low transpiration conditions.

2.2.4 Transport Resistance Models

Thornley (1976) proposed that the Münch osmotically generated pressure flow could be explained by considering a "one source-one sink model". In such a model, source and sink reservoirs are limited by semipermeable membranes and connected by a non-permeable tube representing the transport phloem region so that solution flow through this tube between source and sink is governed by Hagen–Poiseuille equation (2.3). The low resistance return pathway for the solvent (water) represents the xylem (Fig. 2.7). The water flow into the source region and out of the sink region is not restricted by the semipermeable membrane so that the turgor pressures in both source and sink are maintained. Source region concentration is constant. Hence, from Hagen–Poiseuille equation (2.3) the driving force Δp is proportional to the volume flow rate times a resistance, Φ, that is given by:

$$\Phi = \frac{8\mu L}{\pi R^4} \tag{2.17}$$

which is the pathway resistance for a pathway of length L. If the system is in water potential equilibrium and at atmospheric pressure, the solute flow, J_s, is given by:

$$J_s = = \frac{R_g T}{\Phi} C_1 \left(C_1 - C_2 \right) \tag{2.18}$$

where C_1 and C_2 are the solute concentrations in source and sink, respectively. The term:

$$\Gamma = \frac{R_g T}{\Phi} \tag{2.19}$$

can be considered as the resistance to a concentration-driven solute flow while Φ, given by equation (2.16), is the resistance to a pressure-driven volume flow. Considering gravity, specifically in big specimens like trees, an extra resistance term can be added to resistance Φ in equation (2.16). But for smaller species, Thornley (1976) showed that gravity

contributes about 0.1 %, for distances up to 1 m. However, for longer distances, e.g. 50 m, gravity can account for up to 7 % of the total pathway resistance between source and sink regions. Thus some caution must be taken when deciding to neglect gravity effects on phloem transport, as pointed out by Weir (1981).

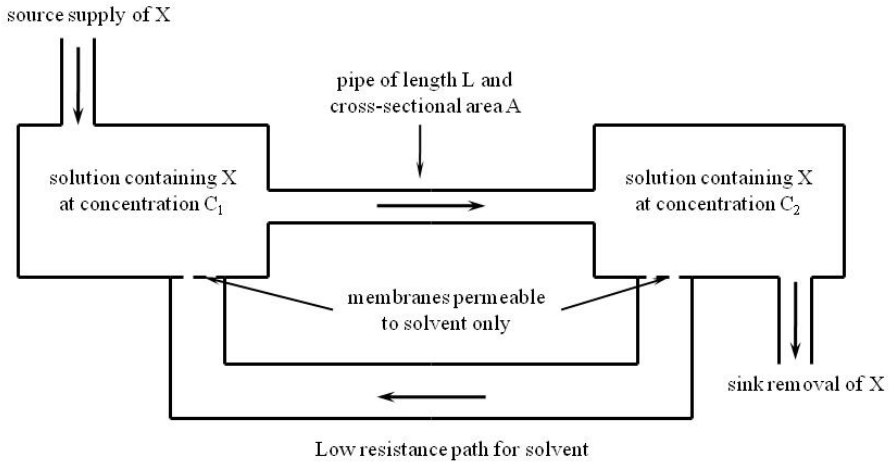

Figure 2.7 – One source–one sink Münch flow model of xylem and phloem transport pathways (adapted from Thornley, 1976).

2.2.4.1 Temperature

The influence of temperature differences within a plant on phloem transport was also investigated by Thornley (1987). This may arise, for instance, from the effects of sunlight and shade causing horizontal temperature gradients, or from air and soil temperature differences, made effective by the Benard-Rayleigh convection[18]. The mechanism occurs in temperature-driven convection, and it is also dependent upon gravity and the effect of temperature on density and on viscosity. This may be important when distinguishing the different types of solutes in phloem sap (e.g. proteins) because phloem sap density depends on temperature in the same way as water, but neglecting the effects of temperature on viscosity. Thornley concluded that a temperature difference of 1 K would cause a translocation speed in the order of 10^{-6} $m.s^{-1}$, about 100 times smaller than observed speeds in the phloem. Even for a 10 K temperature difference the speed would still

[18] Movement of fluid between two plates at different temperatures in which there is an upwelling movement of warmer fluid from the heated bottom layer.

be very small, and such a temperature difference is hard to find naturally between parts of a plant, especially on smaller specimens. However, Thornley (1987) also points out that temperature-driven contribution to transport within plants may be significant, depending upon the relative magnitude of other contributions, e.g. viscosity.

2.2.4.2 Plant Architecture

Minchin *et al*. (1993) presented the first Münch-based model of phloem transport of more than one sink, by extending the Thornley (1976) transport resistance model. Two competing sinks are connected to one source by a non-permeable tube with a Y-branch (Fig. 2.8) with unloading in each sink described by saturable Michaelis–Menten kinetics (2.2); no loading mechanism was specified. This combination of the Münch pressure flow with Michaelis–Menten kinetics, although not new (e.g. Magnuson *et al*., 1979), made a considerable advance in the understanding of how solutes are distributed amongst sinks, by focussing on local properties of the sink compartments. This model, for example, was able to explain observations where one-half of the barley root system was removed by means of a steam girdle, but photosynthate import into the other half was not appreciably affected (Farrar & Minchin 1991); and, when an ovule of a pea fruit was removed, there was no change in import into the untouched ovules (Thorpe *et al*., 1993). The explanation is that the sinks were functioning at or near saturation, so when one sink was removed, the others were not able to utilize the extra photosynthate that became available. In this saturation state the Minchin *et al*. (1993) model also predicted that a change in the flow resistance of the translocation pathway did not exert control over sink growth normally. On the other hand the changes in carbon partitioning to two developing leaves of sugar beet in response to a slow cooling of the petiole of a labelled source leaf, reported by Grusak & Lucas (1985), could be explained by Minchin *et al*. (1993) as the changes in partitioning between alternative sinks predicted by when there is a change in the pathway resistance of the common pathway which is in this case the petiole of the labelled source leaf. These pathway resistance changes may well be due to partial blockage of the phloem pathway due to the well known phloem sensitivity to low temperatures. Changing the source solute concentration, Minchin *et al*. (1993) observed a change in carbon partitioning between two inequivalent sinks, thus predicting a hierarchy of sinks based upon their ability to “attract” photosynthate when the supply is changed (Wardlaw, 1990). This hier-

archy was determined by the parameters describing the sink function and is referred to as sink priority. The main significance of the Minchin *et al*. (1993) study was that it established how intra-plant competition can be explained without any reference to hormones or any other signal (except through their regulating the kinetic properties of sinks).

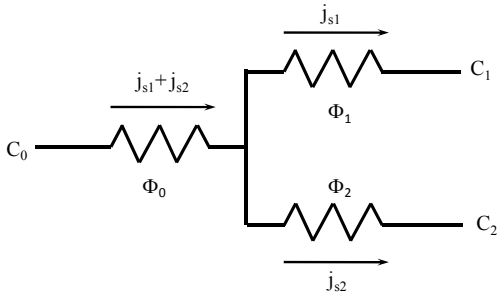

Figure 2.8 – One source–two sinks Münch flow model of phloem transport: C –solute concentration; Φ – pathway pressure-driven flow resistance and j_s – solute fluxes. Subscripts 0 refer to source and 1 and 2 to sinks (adapted from Minchin *et al*, 1976).

Bancal & Soltani (2002) pointed out that a major limitation of the Minchin *et al*. (1993) model was the constant concentration at the source, whereas it is most likely to vary. A "revised version" included the effect of temperature and concentration upon viscosity, and considered source and sinks as activities rather than compartments (Bancal & Soltani, 2002). The main argument favouring this interpretation is that compartment concentrations, as suggested by most mathematical models of phloem transport, are in fact difficult to measure. But, organ activities are much easier to obtain and thus to compare with model predictions. On the other hand mass conservation constrains source and sink activities, thus invalidating source and sink-limiting concepts (Minchin *et al*., 1993). Bancal & Soltani (2002) took the temperature dependence of phloem sap viscosity to be the same as the one observed with water viscosity; for the concentration dependence of viscosity Bancal & Soltani (2002) used the approach taken by Magnuson *et al*. (1979) to quantify the concentration dependence of sucrose solutions viscosity. Bancal & Soltani (2002) argued that for the physiological range of sugar concentrations found, viscosity can change several orders of magnitude, thus affecting pathway resistances dramatically. Bancal & Soltani (2002) also pointed out that the pathway resistance is not in fact constant as equation (2.17) suggests. Instead, the pathway resistivity will dramatically increase at each sieve plate. In this way, Bancal & Soltani (2002) used a 2.5 multiplying

factor on equation (2.17) (Sheehy *et al*., 1995) to account for these anatomical factors which are difficult for a simple mathematical description due mainly to its complex nature. Bancal & Soltani (2002) confirmed the Minchin *et al*. (1993) predictions of sinks operating normally in saturation conditions at which they are not affected by changes in the phloem pathway resistance. Most notably, in choosing a specific system – wheat grain filling – Bancal & Soltani (2002) showed that pathway resistances can be excluded if one wants to describe source/sink relations, which would be helpful due the difficulty to determine resistances from anatomy and physiology data. In their specific example, Bancal & Soltani (2002) demonstrated that source/sink relations in the wheat grain filling process could easily be explained using Michaelis–Menten kinetics only.

Daudet *et al*. (2002) extended the Minchin *et al*. (1993) model to a comprehensive model of carbohydrate and water fluxes, incorporating xylem water flow and phloem-xylem interactions and their involvement in growth limitations on competing sinks. They considered the pathway as a series of segments with terminal sources and sinks, with each unit described by a set of water and solute flow equations (cf. Christy and Ferrier, 1973). Daudet *et al*. (2002) used walnut (*Juglans regia*) as the model species from which anatomy and physiology experimental data were used as model inputs. However, a strong limitation was the lack of solute radial exchange in both vascular systems. Lacointe & Minchin (2008) extended the modular approach of Daudet *et al*. (2002), demonstrating that it can model interactions between phloem and xylem transport with a two-sink system. Each element includes a xylem and a phloem flow pathway, with lateral flows between these, and is connected to the neighbouring elements by the 2 longitudinal pathways. Further, attached to the phloem is a parenchyma compartment incorporating metabolism and lateral solute exchanges (unloading/reloading), and the associated xylem flow. Lateral solute leakage and reloading occur along the long-distance pathway, together with lateral water flow determined by water potential gradients and the sieve tube membrane water permeability. Both xylem and phloem flows are given by Darcy's equation (2.15) in which the phloem resistance is proportional to the phloem sap viscosity, depending on both temperature and concentration, as suggested by Bancal & Soltani (2002). Lacointe & Minchin (2008) also accounted for the nonlinear relationship between osmotic pressure and solute concentration, cf. Michel (1972) and considered both symplastic and apoplastic loading/unloading processes. Following the suggestion by Bancal & Soltani (2002) that the source is better described by a constant flux of solute that is a constant rate of photosynthesis, rather than its solute concentration, Lacointe & Minchin's

model predicted sink priority behaviour as in the simplified version of Minchin *et al*. (1993). They showed that xylem flow can affect phloem distribution, as changes in leaf transpiration from the source can lead to changes in relative phloem unloading rates at both sinks. Both of these phenomena have been debated and predicted based upon qualitative argument, but Lacointe & Minchin (2008) presented the first simulations of phloem-xylem interaction in a branched architecture.

3. Hydrodynamics of Phloem Transport: Steady State Flow in Sieve Tubes with Radial Convection and Solute Exchange

3.1 The Model

The previous chapter concluded that the importance and physiological role of radial water and solute exchanges along the phloem pathway have rarely been investigated in mathematical models of phloem transport. Here we propose a steady state two-dimensional flow model of phloem transport, according to the Münch pressure flow hypothesis, of a single solute with allowance for water and solute exchange along the pathway (Fig. 3.1).The model is developed using the Navier–Stokes and convection-diffusion equations. The following assumptions are made:

1. The sieve tube is considered as a right circular cylinder of length L and radius R, such that $R << L$, limited by a membrane through which water and solutes fluxes occur.
2. The end effects caused by the entry and exit of sap in the sieve tube are negligible.
3. The flow is axisymmetrical.
4. The system is at steady state.
5. The sap enters the sieve tube with an average speed U, with an average solute concentration C_i and at average turgor pressure p_i.
6. The membrane is porous. Solute exchange across the membrane is regarded as a passive process in which there is: i) diffusion of solutes that is linear with the concentration difference between the sieve tube and the surrounding apoplast, and dependent on the sieve tube membrane solute permeability, P_s; ii) convection of solutes with water movement through the membrane pores.

7. The apoplast solute concentration, C_{out}, is not affected by solute or water exchange with the sieve tube.
8. There is a constant water potential gradient $\frac{d\Psi_{out}}{dz}$ surrounding the sieve tube.
9. The sieve tube membrane hydraulic conductivity, L_p, is constant.
10. The sieve tube sap is regarded as a homogeneous water solution, i. e. an incompressible Newtonian fluid (of constant density, ρ) in which the shear stress exerted by the fluid, the drag, τ:

$$\tau = \mu \frac{\partial v}{\partial r}$$

is linear with the velocity gradient perpendicular to the direction of shear, with μ, the constant of proportionality, being the fluid viscosity – known as Newton's viscosity law.

11. Sieve tube sap viscosity, μ, is constant.
12. The diffusion of solutes within sieve tube sap is isotropic and obeys Fick's law of diffusion with a constant diffusion coefficient D, solute-specific.
13. There is no slip at the sieve tube membrane.
14. No chemical reactions are considered.
15. For simplicity, the osmotic pressure is given by van't Hoff equation: $\Pi = CR_gT$, where R_g is the universal gas constant and T the absolute temperature.
16. Sieve plates are transverse and spaced at regular intervals. The effect of sieve plates on the overall sieve tube conductance is described by an impedance factor β which is related to sieve tube element structure and given by:

$$\beta = \frac{\frac{8l_p}{8l_p + 3\pi r_p} \alpha r_p^2 l}{R^2 l_p + \frac{8l_p}{8l_p + 3\pi r_p} \alpha r_p^2 \left(l - l_p\right)}, \qquad r_p < R \tag{3.1}$$

and

$$\alpha = N_p \frac{\pi r_p^2}{\pi R^2} = N_p \left(\frac{r_p}{R} \right)^2 \tag{3.2}$$

is the fraction of sieve plate area composed of sieve pore area with N_p pores; R and l are the sieve tube elements radius and length, while r_p and l_p define the sieve plate pore dimensions: radius and length respectively (Thompson & Holbrook, 2003a). As $l > l_p$ and $R > r_p$ we have always $\beta < 1$. For the special case of $r_p = R$, then $N_p = 1$ and $\alpha = 1$, the impedance factor is $\beta = 1$, there is no sieve plate.

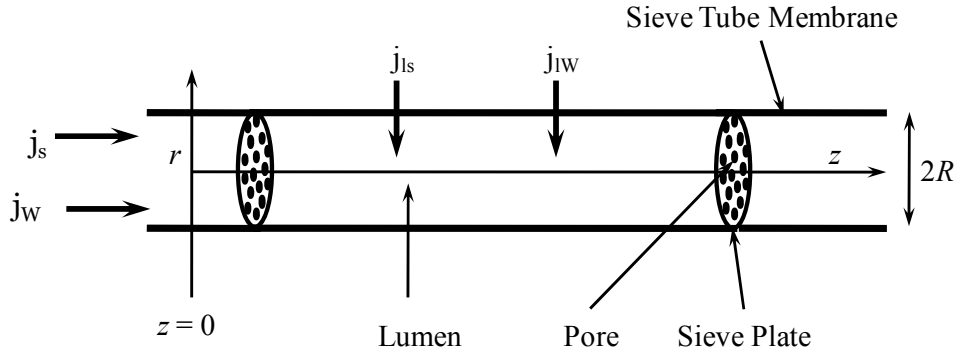

Figure 3.1 – Sieve tube model: R – Sieve tube radius; j_w – water flux; j_s – solute flux; j_{lw} – radial water flux; j_{ls} – radial solute flux; r – direction of radial flow; z – direction of axial flow.

3.2 Fundamental Equations and Boundary Conditions

With these assumptions the hydrodynamics of the system is completely described by the Navier–Stokes equation (momentum balance equation) (3.3) and the continuity equation (3.4). The Navier–Stokes equation describes the momentum change for a volume element of fluid resulting from the pressure and viscous forces acting on it. That is:

$$\frac{\partial \vec{\mathrm{v}}}{\partial t} + \left(\vec{\mathrm{v}}.\vec{\nabla} \right) \vec{\mathrm{v}} = -\frac{1}{\rho} \vec{\nabla} \mathrm{p} + \nu \nabla^2 \vec{\mathrm{v}} \tag{3.3}$$

where $\frac{\partial \vec{v}}{\partial t} = 0$ for the steady state flow; $v = \mu/\rho$ is the kinematic viscosity. The effect of sieve plates is described by multiplying the viscous term of the Navier–Stokes equation (second term of the right hand side) by $1/\beta$ and is equivalent to having a more viscous fluid since $\beta < 1$. This approach treats the sieve tube as a conduit of essentially uniform resistivity, a close approximation to reality in view of the distribution of the sieve plates within sieve tubes (Weir, 1981; Henton *et al*., 2002). The pressure p includes the gravitational effect, i.e. $p = p' + \rho gh$; where p' is termed the hydrodynamic pressure inside the sieve tube, g the local acceleration of gravity and *h* is the vertical coordinate above a standard reference plane. The continuity equation for an incompressible fluid:

$$\vec{\nabla}.\vec{v} = 0 \tag{3.4}$$

is the mass balance equation for the solution. These two equations together describe the solution movement inside the sieve tube.

The solute transport in the sieve tube is governed by the convection–diffusion equation:

$$\frac{\partial C}{\partial t} = D\nabla^2 C - \left(\vec{v}.\vec{\nabla}\right)C \tag{3.5}$$

which is the mass balance equation for the solute. For the steady state flow $\frac{\partial C}{\partial t} = 0$. Equation (3.5) describes the transport of solutes within sieve tube sap as the sum of terms describing diffusion and convection respectively. D is the solute diffusion coefficient, its diffusivity. Thus, the solute flux, $\vec{j}_s$, inside the sieve tube is:

$$\vec{j}_s = -D\vec{\nabla}C + \vec{v}C \tag{3.6}$$

A cylindrical coordinate system is the most suited to the sieve tube geometry, with the *z* axis direction being the system axis (Fig. 3.1), and with r and φ specifying radial coordinate and azimuth respectively. Radial fluxes are negative for influx and positive for efflux. According to the model assumption of axisymmetric flow, the dependent variables:

velocity $\vec{v}$, turgor pressure p (from now on just called pressure) and concentration C are all independent of the azimuth φ. This means that:

$$v_{\varphi} = 0 \tag{3.7}$$

and

$$\frac{\partial v_r}{\partial \varphi} = \frac{\partial v_z}{\partial \varphi} = 0 \tag{3.8}$$

together with

$$\frac{\partial C}{\partial \varphi} = \frac{\partial p}{\partial \varphi} = 0 \tag{3.9}$$

Hence, the Navier–Stokes equation (3.3) can be split in the radial and axial components, giving:

$$v_r \frac{\partial v_r}{\partial r} + v_z \frac{\partial v_r}{\partial z} = -\frac{1}{\rho}\frac{\partial p}{\partial r} + \frac{\nu}{\beta}\left[\frac{\partial}{\partial r}\left(\frac{1}{r}\frac{\partial (r v_r)}{\partial r}\right) + \frac{\partial^2 v_r}{\partial z^2}\right] \tag{3.10}$$

$$v_r \frac{\partial v_z}{\partial r} + v_z \frac{\partial v_z}{\partial z} = -\frac{1}{\rho}\frac{\partial p}{\partial z} + \frac{\nu}{\beta}\left[\frac{1}{r}\frac{\partial}{\partial r}\left(r\frac{\partial v_z}{\partial r}\right) + \frac{\partial^2 v_z}{\partial z^2}\right] \tag{3.11}$$

The continuity equation (3.4) simplifies to:

$$\frac{1}{r}\frac{\partial (r v_r)}{\partial r} + \frac{\partial v_z}{\partial z} = 0 \tag{3.12}$$

The convection–diffusion equation (3.5) is:

$$v_r \frac{\partial C}{\partial r} + v_z \frac{\partial C}{\partial z} = D\left[\frac{1}{r}\frac{\partial}{\partial r}\left(r\frac{\partial C}{\partial r}\right) + \frac{\partial^2 C}{\partial z^2}\right] \tag{3.13}$$

and the sieve tube solute flux is:

$$j_{sr} = -D\frac{\partial C}{\partial r} + v_r C \tag{3.14}$$

$$j_{sz} = -D\frac{\partial C}{\partial z} + v_z C \tag{3.15}$$

By definition, the apoplastic water potential gradient surrounding the sieve tube is given by:

$$\frac{d\Psi_{out}}{dz} = \frac{dp_{out}}{dz} - \frac{d\Pi_{out}}{dz} \tag{3.16}$$

where $\frac{dp_{out}}{dz}$ and $\frac{d\Pi_{out}}{dz}$ are assumed as constant. Π_{out} is the osmotic pressure in the apoplast given by the van't Hoff equation and p_{out} is the apoplastic pressure outside the sieve tube. From the van't Hoff equation, the apoplastic concentration gradient is given by:

$$\frac{dC_{out}}{dz} = \frac{1}{R_g T}\frac{d\Pi_{out}}{dz} \tag{3.17}$$

The following boundary conditions are proposed:

i.) At the sieve tube membrane, $r = R$:

The radial volume flux through the membrane is given by Starling's equation (2.6):

$$v_r(R,z) = L_p\left[p(R,z) - p_{out}(0) - \frac{dp_{out}}{dz}z - \sigma R_g T\left(C(R,z) - C_{out}(0) - \frac{dC_{out}}{dz}z\right)\right] \tag{3.18}$$

where σ is the solute reflection coefficient of the sieve tube membrane, varying between 0 (totally permeable membrane) and 1 (impermeable membrane). The reflection coefficient describes how much the sieve tube membrane can reflect solute particles from passing through – ultrafiltration. A value of 0 results in all particles passing through and a value of 1 is such that no particle can pass. Pressure, p_{out}, and solute concentration, C_{out}, in the apoplast are considered as varying linearly with distance according to (3.16), i. e:

$$p_{out}(z) = p_{out}(0) + \frac{dp_{out}}{dz} z \tag{3.19}$$

an

$$C_{out}(z) = C_{out}(0) + \frac{dC_{out}}{dz} z \tag{3.20}$$

The no-slip condition implies that:

$$v_z(R,z) = 0 \tag{3.21}$$

which means that at the boundary the fluid velocity will be in the radial direction only; it "sticks" to the sieve tube membrane. Conceptually, one can think of the outermost molecules as stuck to the surface past which the fluid flows.

The radial passive flux of solutes through the sieve tube membrane is considered as the sum of convective flux (solvent drag effect), that is linear with the average solute concentration in the membrane $C_m(z)$, plus the diffusive flux described by P_s and proportional to the concentration difference across the membrane (Benedek & Villars, 2000; Kedem & Katchalsky, 1958). That is:

$$\begin{aligned} v_r(R,z)C(R,z) - D\frac{\partial C}{\partial r}(R,z) &= (1-\sigma)v_r(R,z)C_m(z) + \\ &+ P_s\left(C(R,z) - C_{out}(0) - \frac{dC_{out}}{dz} z\right) \end{aligned} \tag{3.22}$$

The concentration of solute, $\mathrm{C_m}(z)$, in the sieve tube membrane is given by:

$$\mathrm{C_m}(z) = \frac{\mathrm{C_{out}}(0) + \frac{d\mathrm{C_{out}}}{dz} z + \mathrm{C}(R,z)}{2} \tag{3.23}$$

ii.) Symmetry at the centre of the sieve tube, $r = 0$, implies that:

$$\mathrm{v_r}(0,z) = 0 \tag{3.24}$$

$$\frac{\partial \mathrm{v_z}}{\partial r}(0,z) = 0 \tag{3.25}$$

$$\frac{\partial \mathrm{C}}{\partial r}(0,z) = 0 \tag{3.26}$$

iii.) At the origin, $z = 0$, and according to (3.18) and model assumptions we have that:

$$\mathrm{v_r}(r,0) = \mathrm{L_p}\left[\mathrm{p}(r,0) - \mathrm{p_{out}}(0) - \sigma \mathrm{R_g T}\left(\mathrm{C}(r,0) - \mathrm{C_{out}}(0)\right)\right] \tag{3.27}$$

$$\bar{\mathrm{v}}_z(0) = \frac{1}{\pi R^2}\int_0^R 2\pi \mathrm{v_z}(r,0)\, r dr = U \tag{3.28}$$

$$\bar{\mathrm{C}}(0) = \frac{1}{\pi R^2}\int_0^R 2\pi \mathrm{C}(r,0)\, r dr = \mathrm{C_i} \tag{3.29}$$

$$\bar{\mathrm{p}}(0) = \frac{1}{\pi R^2}\int_0^R 2\pi \mathrm{p}(r,0)\, r dr = \mathrm{p_i} \tag{3.30}$$

where the subscript i stands for initial values at the origin.

Note that the hydrodynamics problem described by equations (3.3) and (3.4) does not depend on the solute concentration explicitly, and viscosity is concentration independent. The dependence on concentration is only through the boundary condition (3.18). Thus we can treat independently the hydrodynamics problem that describes how pressure and velocity change and the solute transport equation (3.13) which is solved once the velocity field is determined (§ 3.4). As with many problems in fluid dynamics and especially when applying Navier–Stokes equation (3.3), the problem becomes more simple to solve using dimensional analysis (Kundu & Cohen, 2008). Whit this method, it is possible to predict physical parameters that influence the sap flow and determine the relationships between several variables (pressure, velocity and concentration) when an exact functional relationship is unknown. This is not possible with a direct numerical solution of the governing equations (3.3) to (3.5). Following Regirer (1960) and Phillips & Dungan (1993), we consider a set of dimensionless variables defined in such way that the spatial coordinates, the velocity components and the concentration are of order of 1 on average. This gives:

$$\hat{r} = \frac{r}{R}, \quad \hat{z} = \frac{z}{L}, \quad \hat{\mathrm{v}}_z = \frac{\mathrm{v}_z}{U}, \quad \hat{\mathrm{v}}_r = \frac{\mathrm{v}_r}{\varepsilon U} \text{ and } \hat{\mathrm{C}} = \frac{\mathrm{C}}{\mathrm{C}_i} \tag{3.31}$$

Where parameter ε is the ratio of the sieve tube radius R and length L,

$$\varepsilon = \frac{R}{L} \tag{3.32}$$

$\varepsilon << 1$, as $R << L$. Therefore the dimensionless pressure $\hat{\mathrm{p}}$ is given by:

$$\hat{\mathrm{p}} = \mathrm{p}\frac{R^2}{\mu L U} \tag{3.33}$$

and its values are not in the order of unity as with the other variables (3.31). Equation (3.33) is important because it shows that the magnitude of pressure inside sieve tubes is in

the order of $\frac{\mu LU}{R^2}$. Substituting the dimensionless variables into the governing equations, the dimensionless Navier–Stokes equations (3.10) and (3.11) become:

$$\mathcal{Re}\varepsilon^3\left(\hat{\mathrm{v}}_\mathrm{r}\frac{\partial\hat{\mathrm{v}}_\mathrm{r}}{\partial\hat{r}}+\hat{\mathrm{v}}_\mathrm{z}\frac{\partial\hat{\mathrm{v}}_\mathrm{r}}{\partial\hat{z}}\right)=-\frac{\partial\hat{\mathrm{p}}}{\partial\hat{r}}+\frac{\varepsilon^2}{\beta}\left[\frac{\partial}{\partial\hat{r}}\left(\frac{1}{\hat{r}}\frac{\partial\left(\hat{r}\hat{\mathrm{v}}_\mathrm{r}\right)}{\partial\hat{r}}\right)+\varepsilon^2\frac{\partial^2\hat{\mathrm{v}}_\mathrm{r}}{\partial\hat{z}^2}\right] \tag{3.34}$$

$$\mathcal{Re}\varepsilon\left(\hat{\mathrm{v}}_\mathrm{r}\frac{\partial\hat{\mathrm{v}}_\mathrm{z}}{\partial\hat{r}}+\hat{\mathrm{v}}_\mathrm{z}\frac{\partial\hat{\mathrm{v}}_\mathrm{z}}{\partial\hat{z}}\right)=-\frac{\partial\hat{\mathrm{p}}}{\partial\hat{z}}+\frac{1}{\beta\hat{r}}\frac{\partial}{\partial\hat{r}}\left(\hat{r}\frac{\partial\hat{\mathrm{v}}_\mathrm{z}}{\partial\hat{r}}\right)+\frac{\varepsilon^2}{\beta}\frac{\partial^2\hat{\mathrm{v}}_\mathrm{z}}{\partial\hat{z}^2} \tag{3.35}$$

The continuity equation becomes:

$$\frac{1}{\hat{r}}\frac{\partial\left(\hat{r}\hat{\mathrm{v}}_\mathrm{r}\right)}{\partial\hat{r}}+\frac{\partial\hat{\mathrm{v}}_\mathrm{z}}{\partial\hat{z}}=0 \tag{3.36}$$

The convection diffusion equation is:

$$\varepsilon\left(\hat{\mathrm{v}}_\mathrm{r}\frac{\partial\hat{\mathrm{C}}}{\partial\hat{r}}+\hat{\mathrm{v}}_\mathrm{z}\frac{\partial\hat{\mathrm{C}}}{\partial\hat{z}}\right)=\frac{1}{\mathcal{Pe}_r}\left[\frac{1}{\hat{r}}\frac{\partial}{\partial\hat{r}}\left(\hat{r}\frac{\partial\hat{\mathrm{C}}}{\partial\hat{r}}\right)+\varepsilon^2\frac{\partial^2\hat{\mathrm{C}}}{\partial\hat{z}^2}\right] \tag{3.37}$$

and the components of the sieve tube solute flux are given by:

$$\hat{\mathrm{j}}_\mathrm{sr}=\frac{\mathrm{j}_\mathrm{r}}{\varepsilon U\mathrm{C}_\mathrm{i}}=-\frac{1}{\mathcal{Pe}_r}\frac{\partial\hat{\mathrm{C}}}{\partial\hat{r}}+\varepsilon\hat{\mathrm{v}}_\mathrm{r}\hat{\mathrm{C}} \tag{3.38}$$

$$\hat{\mathrm{j}}_\mathrm{sz}=\frac{\mathrm{j}_z}{U\mathrm{C}_\mathrm{i}}=-\frac{1}{\mathcal{Pe}_z}\frac{\partial\hat{\mathrm{C}}}{\partial\hat{z}}+\hat{\mathrm{v}}_z\hat{\mathrm{C}} \tag{3.39}$$

where

$$\mathcal{Re}=\frac{RU}{\nu} \tag{3.40}$$

$$\mathcal{P}e_r = \frac{RU}{D} \quad \text{and} \quad \mathcal{P}e_z = \frac{LU}{D} \tag{3.41}$$

$\mathcal{R}e$ and $\mathcal{P}e_r$ are the Reynolds and Péclet numbers for the radial flows while $\mathcal{P}e_z$ is the Péclet number for axial flow. The Reynolds number is the ratio of inertial forces to viscous forces. The Péclet number gives the ratio of the rate of convection of the solute, by the flow of sap, to the rate of diffusion of that solute driven by a concentration gradient. In our model, we compare both flows in the radial direction, in which water and solute exchanges occur. With equations (3.31) to (3.33), the dimensionless boundary conditions (3.18) to (3.30) become:

i.) At the sieve tube membrane, $\hat{r} = 1$:

$$\hat{\mathrm{v}}_\mathrm{r}\left(1,\hat{z}\right) = \hat{\mathrm{L}}_\mathrm{p}\left[\hat{\mathrm{p}}\left(1,\hat{z}\right) - \hat{\mathrm{p}}_\mathrm{out}\left(0\right) - \frac{d\hat{\mathrm{p}}_\mathrm{out}}{d\hat{z}}\hat{z} - \sigma\hat{\mathrm{H}}\left(\hat{\mathrm{C}}\left(1,\hat{z}\right) - \hat{\mathrm{C}}_\mathrm{out}\left(0\right) - \frac{d\hat{\mathrm{C}}_\mathrm{out}}{d\hat{z}}\hat{z}\right)\right] \tag{3.42}$$

$$\hat{\mathrm{v}}_\mathrm{z}\left(1,\hat{z}\right) = 0 \tag{3.43}$$

$$\begin{aligned}\varepsilon\hat{\mathrm{v}}_\mathrm{r}\left(1,\hat{z}\right)\hat{\mathrm{C}}\left(1,\hat{z}\right) - \frac{1}{\mathcal{P}e_r}\frac{\partial\hat{\mathrm{C}}}{\partial\hat{r}}\left(1,\hat{z}\right) &= \varepsilon\left(1-\sigma\right)\hat{\mathrm{v}}_\mathrm{r}\left(1,\hat{z}\right)\hat{\mathrm{C}}_\mathrm{m}\left(\hat{z}\right) + \\ &+\varepsilon\hat{\mathrm{P}}_\mathrm{s}\left(\hat{\mathrm{C}}\left(1,\hat{z}\right) - \hat{\mathrm{C}}_\mathrm{out}\left(0\right) - \frac{d\hat{\mathrm{C}}_\mathrm{out}}{d\hat{z}}\hat{z}\right)\end{aligned} \tag{3.44}$$

and

$$\hat{\mathrm{C}}_\mathrm{m}\left(\hat{z}\right) = \frac{\hat{\mathrm{C}}_\mathrm{out}\left(0\right) - \frac{d\hat{\mathrm{C}}_\mathrm{out}}{d\hat{z}}\hat{z} + \hat{\mathrm{C}}\left(1,\hat{z}\right)}{2} \tag{3.45}$$

ii.) At the sieve tube centre, $\hat{r} = 0$:

$$\hat{v}_r\left(0,\hat{z}\right)=0 \tag{3.46}$$

$$\frac{\partial \hat{v}_z}{\partial \hat{r}}\left(0,\hat{z}\right)=0 \tag{3.47}$$

$$\frac{\partial \hat{C}}{\partial \hat{r}}\left(0,\hat{z}\right)=0 \tag{3.48}$$

iii.) At the origin, $\hat{z}=0$:

$$\hat{v}_r\left(\hat{r},0\right)=\hat{L}_p\left[\hat{p}\left(\hat{r},0\right)-\hat{p}_{out}\left(0\right)-\sigma\hat{H}\left(\hat{C}\left(\hat{r},0\right)-\hat{C}_{out}\left(0\right)\right)\right] \tag{3.49}$$

$$\overline{\hat{v}_z}\left(0\right)=1 \tag{3.50}$$

$$\overline{\hat{C}}\left(0\right)=1 \tag{3.51}$$

$$\overline{\hat{p}}\left(0\right)=\hat{p}_i \tag{3.52}$$

where

$$\hat{L}_p=\frac{L_p\mu}{\varepsilon^2 R} \tag{3.53}$$

$$\hat{H}=\frac{R_g T C_i \varepsilon R}{\mu U} \tag{3.54}$$

$$\hat{P}_s=\frac{P_s}{\varepsilon U} \tag{3.55}$$

$\hat{L}_p$ and $\hat{P}_s$ are the dimensionless sieve tube membrane hydraulic conductivity, and the dimensionless sieve tube membrane permeability to the solute, respectively. $\hat{H}$ is the dimensionless parameter that gives the ratio of osmotic forces to viscous forces occurring for a flow with a characteristic velocity U (Phillips & Dungan, 1993).

3.3 The Hydrodynamic Problem – Perturbation Theory

The small value of the Reynolds number, $\mathcal{Re}$, for phloem transport ($\approx 10^{-4}$ to 10^{-3}) suggests that the system operates in the slow flow regime (Horwitz, 1958; Phillips & Dungan, 1993). This fact combined with the very small value of parameter ε (3.30) for the geometry of sieve tubes, allows us to use perturbation theory (Van Dyke, 1964) to find an approximate solution of the governing equations (3.34) to (3.37) that cannot be solved exactly. This method allows a relatively complicated mathematical problem to be simplified into a hierarchy of simpler problems that yield solutions accurate to progressively higher powers of a small parameter, in this case we chose this parameter to be ε. Expanding the dependent variables $\hat{v}_r$, $\hat{v}_z$, $\hat{C}$ and $\hat{p}$ as power series of the small dimensionless parameter ε (3.32) one obtains:

$$\hat{v}_r = \sum_{j=0}^{\infty} \varepsilon^j \hat{v}_{rj} \tag{3.56}$$

$$\hat{v}_z = \sum_{j=0}^{\infty} \varepsilon^j \hat{v}_{zj} \tag{3.57}$$

$$\hat{p} = \sum_{j=0}^{\infty} \varepsilon^j \hat{p}_j \tag{3.58}$$

$$\hat{C} = \sum_{j=0}^{\infty} \varepsilon^j \hat{C}_j \tag{3.59}$$

The accuracy of the expansions, i.e. the number of terms to include will depend on the value of ε. In each of these series the ratio of a following term to a preceding one is of the

order of magnitude of ε. The smaller ε is the more significant are the first terms compared to higher order terms. In the case of phloem transport, and as ε was defined on the sieve tube dimensions (3.32), we have that ε will be less than 10^{-3} for typical sieve tube dimensions (Esau, 1969). For this reason we will only take the first two terms of the expansion which are thus sufficient to describe flow in a sieve tube.

3.3.1 Zeroth Order Approximation

In the zeroth approximation, of terms linear with ε^0 only, we have that: $\hat{v}_r = \hat{v}_{r0}$, $\hat{v}_z = \hat{v}_{z0}$, $\hat{C} = \hat{C}_0$ and $\hat{p} = \hat{p}_0$. Substituting the corresponding variables into the Navier–Stokes equations (3.34) and (3.35) and taking the terms linear with ε^0 only, those reduce to:

$$\frac{\partial \hat{p}_0}{\partial \hat{r}} = 0 \tag{3.60}$$

$$-\frac{\partial \hat{p}_0}{\partial \hat{z}} + \frac{1}{\beta \hat{r}} \frac{\partial}{\partial \hat{r}} \left(\hat{r} \frac{\partial \hat{v}_{z0}}{\partial \hat{r}} \right) = 0 \tag{3.61}$$

from which we conclude that pressure $\hat{p}_0$ is a function of $\hat{z}$ only, being constant in any plane normal to the direction of flow. In this way, $\frac{d\hat{p}_0}{d\hat{z}}$ is also constant over $\hat{r}$, which allows us to integrate equation (3.61) twice over $\hat{r}$. Using the boundary conditions (3.43) and (3.47) we obtain:

$$\hat{v}_{z0}\left(\hat{r}, \hat{z}\right) = \frac{\beta}{4} \frac{d\hat{p}_0}{d\hat{z}} \left(\hat{r}^2 - 1 \right) \tag{3.62}$$

Determining the average value of the axial component of the velocity $\overline{\hat{v}_{z0}}$ at a given position $\hat{z}$ yields:

$$\overline{\hat{v}_{z0}}\left(\hat{z}\right)=-\frac{\beta}{8}\frac{d\hat{p}_0}{d\hat{z}}\left(\hat{z}\right) \tag{3.63}$$

from which, using our boundary condition for flow at $\hat{z}=0$ (3.50), we conclude that:

$$\frac{d\hat{p}_0}{d\hat{z}}(0)=-\frac{8}{\beta} \tag{3.64}$$

Substituting $\hat{v}_{z0}\left(\hat{r},\hat{z}\right)$ into the continuity equation (3.36) leads to:

$$\frac{\partial\left(\hat{r}\hat{v}_{r0}\right)}{\partial\hat{r}}=-\frac{\beta}{4}\frac{d^2\hat{p}_0}{d\hat{z}^2}\left(\hat{r}^3-\hat{r}\right)$$

After integration over $\hat{r}$ and considering the symmetry condition (3.46) we obtain:

$$\hat{v}_{r0}\left(\hat{r},\hat{z}\right)=-\frac{\beta}{16}\frac{d^2\hat{p}_0}{d\hat{z}^2}\left(\hat{r}^3-2\hat{r}\right) \tag{3.65}$$

From the boundary conditions at the sieve tube membrane, we can consider the right hand side of equation (3.42) as a function $\hat{z}$ only. Thus we define:

$$\boldsymbol{v}\left(\hat{z}\right)=\hat{v}_{r0}\left(1,\hat{z}\right)=\hat{L}_p\left[\hat{p}_0\left(\hat{z}\right)-\hat{p}_{out}(0)-\frac{d\hat{p}_{out}}{d\hat{z}}\hat{z}-\sigma\hat{H}\left(\hat{C}_0\left(1,\hat{z}\right)-\hat{C}_{out}(0)-\frac{d\hat{C}_{out}}{d\hat{z}}\hat{z}\right)\right] \tag{3.66}$$

and, as with the radial velocity component, $\hat{v}_r$. (3.31) we have that:

$$\boldsymbol{v}\left(\hat{z}\right)=\frac{\boldsymbol{v}(z)}{\varepsilon U} \tag{3.67}$$

At the sieve tube membrane, $\hat{r}=1$, we have from equations (3.65) and (3.66) that:

$$\frac{d^2\hat{\mathrm{p}}_0}{d\hat{z}^2}\left(\hat{z}\right)=\frac{16}{\beta}\boldsymbol{v}\left(\hat{z}\right) \tag{3.68}$$

Integrating over $\hat{z}$ and incorporating the result from equation (3.64), we get:

$$\frac{d\hat{\mathrm{p}}_0}{d\hat{z}}\left(\hat{z}\right)=\frac{16\int_0^{\hat{z}}\boldsymbol{v}\left(\hat{z}'\right)d\hat{z}'-8}{\beta} \tag{3.69}$$

Integrating one more time over $\hat{z}$ and using the boundary condition (3.52) we obtain:

$$\hat{\mathrm{p}}_0\left(\hat{z}\right)=\hat{\mathrm{p}}_\mathrm{i}+\frac{16\int_0^{\hat{z}}\int_0^{\hat{z}''}\boldsymbol{v}\left(\hat{z}'\right)d\hat{z}'d\hat{z}''-8\hat{z}}{\beta} \tag{3.70}$$

Defining the function $\boldsymbol{q}\left(\hat{z}\right)$ as:

$$\boldsymbol{q}\left(\hat{z}\right)=\int_0^{\hat{z}}\int_0^{\hat{z}''}\boldsymbol{v}\left(\hat{z}'\right)d\hat{z}'d\hat{z}'' \tag{3.71}$$

where

$$\boldsymbol{q}\left(\hat{z}\right)=\frac{\boldsymbol{q}\left(z\right)}{LRU} \tag{3.72}$$

we can write (3.70) as:

$$\hat{\mathrm{p}}_0\left(\hat{z}\right)=\hat{\mathrm{p}}_\mathrm{i}+\frac{16\boldsymbol{q}\left(\hat{z}\right)-8\hat{z}}{\beta} \tag{3.73}$$

In this way, the axial and radial velocity components, given respectively by equations (3.62) and (3.65), can be written as:

$$\hat{\mathrm{v}}_{\mathrm{z0}}\left(\hat{r},\hat{z}\right)=2\left(2\frac{d\boldsymbol{q}}{d\hat{z}}-1\right)\left(\hat{r}^{2}-1\right) \tag{3.74}$$

$$\hat{\mathrm{v}}_{\mathrm{r0}}\left(\hat{r},\hat{z}\right)=-\boldsymbol{\mathcal{V}}\left(\hat{z}\right)\left(\hat{r}^{3}-2\hat{r}\right) \tag{3.75}$$

Equations (3.73) to (3.75) are the zeroth order expressions for pressure and velocity describing fluid flow, where functions $\boldsymbol{q}$ ($\hat{z}$) and $\boldsymbol{\mathcal{V}}$ ($\hat{z}$) depend on the specific boundary conditions set for $\mathrm{p_{out}}$ (3.19) and $\mathrm{C_{out}}$ (3.20).

3.3.2 First Order Approximation

In the first order approximation, where only terms up to ε^{1} are retained, the Navier–Stokes equations (3.34) and (3.35) reduce to:

$$\frac{\partial\hat{\mathrm{p}}_{1}}{\partial\hat{r}}=0 \tag{3.76}$$

$$\boldsymbol{\mathcal{R}e}\left(\hat{\mathrm{v}}_{\mathrm{r0}}\frac{\partial\hat{\mathrm{v}}_{\mathrm{z0}}}{\partial\hat{r}}+\hat{\mathrm{v}}_{\mathrm{z0}}\frac{\partial\hat{\mathrm{v}}_{\mathrm{z0}}}{\partial\hat{z}}\right)=-\frac{\partial\hat{\mathrm{p}}_{1}}{\partial\hat{z}}+\frac{1}{\beta\hat{r}}\frac{\partial}{\partial\hat{r}}\left(\hat{r}\frac{\partial\hat{\mathrm{v}}_{\mathrm{z1}}}{\partial\hat{r}}\right) \tag{3.77}$$

from which we conclude that pressure $\hat{\mathrm{p}}_{1}$ is also a function of $\hat{z}$ only, in the same way as $\hat{\mathrm{p}}_{0}$. The boundary conditions (3.42) to (3.52) now change to:

i.) At the sieve tube membrane, $\hat{r}$ = 1:

$$\hat{\mathrm{v}}_{\mathrm{r1}}\left(1,\hat{z}\right)=\hat{\mathrm{L}}_{\mathrm{p}}\left(\hat{\mathrm{p}}_{1}\left(\hat{z}\right)-\sigma\hat{\mathrm{H}}\hat{\mathrm{C}}_{1}\left(1,\hat{z}\right)\right) \tag{3.78}$$

$$\hat{v}_{z1}\left(1,\hat{z}\right)=0 \tag{3.79}$$

$$\hat{v}_{r0}\left(1,\hat{z}\right)\hat{C}_0\left(\hat{z}\right)-\frac{1}{\mathcal{P}e_r}\frac{\partial\hat{C}_1}{\partial\hat{r}}\left(1,\hat{z}\right)=\left(1-\sigma\right)\hat{v}_{r0}\left(1,\hat{z}\right)\hat{C}_{m0}\left(\hat{z}\right)+$$
$$+\hat{P}_s\left(\hat{C}_0\left(\hat{z}\right)-\hat{C}_{out}\left(0\right)-\frac{d\hat{C}_{out}}{d\hat{z}}\hat{z}\right) \tag{3.80}$$

ii.) At the sieve tube centre, $\hat{r}=0$:

$$\hat{v}_{r1}\left(0,\hat{z}\right)=0 \tag{3.81}$$

$$\frac{\partial\hat{v}_{z1}}{\partial\hat{r}}\left(0,\hat{z}\right)=0 \tag{3.82}$$

$$\frac{\partial\hat{C}_1}{\partial\hat{r}}\left(0,\hat{z}\right)=0 \tag{3.83}$$

iii.) At the origin, $\hat{z}=0$:

$$\hat{v}_{r1}\left(\hat{r},0\right)=-\hat{L}_p\sigma\hat{H}\hat{C}_1\left(1,0\right) \tag{3.84}$$

$$\overline{\hat{v}_{z1}}\left(0\right)=0 \tag{3.85}$$

$$\overline{\hat{C}_1}\left(0\right)=0 \tag{3.86}$$

$$\overline{\hat{p}_1}\left(0\right)=0 \tag{3.87}$$

Substituting $\hat{v}_{z0}$ and $\hat{v}_{r0}$, given by equations (3.62) and (3.65), into equation (3.77), one obtains:

$$\frac{\mathcal{Re}\beta^2}{32}\frac{d^2\hat{\mathrm{p}}_0}{d\hat{z}^2}\frac{d\hat{\mathrm{p}}_0}{d\hat{z}}\left(\hat{r}^4-2\hat{r}^2+2\right)=-\frac{d\hat{\mathrm{p}}_1}{d\hat{z}}+\frac{1}{\beta\hat{r}}\frac{\partial}{\partial\hat{r}}\left(\hat{r}\frac{\partial\hat{\mathrm{v}}_{z1}}{\partial\hat{r}}\right) \tag{3.88}$$

Integrating (3.88) twice over $\hat{r}$ and considering the boundary conditions (3.79) and (3.82), yields:

$$\hat{\mathrm{v}}_{z1}\left(\hat{r},\hat{z}\right)=\frac{\beta}{4}\frac{d\hat{\mathrm{p}}_1}{d\hat{z}}\left(\hat{r}^2-1\right)+\frac{\mathcal{Re}\beta^3}{32}\frac{d^2\hat{\mathrm{p}}_0}{d\hat{z}^2}\frac{d\hat{\mathrm{p}}_0}{d\hat{z}}\frac{\left(2\hat{r}^6-9\hat{r}^4+36\hat{r}^2-29\right)}{72} \tag{3.89}$$

Thus, the average value of the axial component of the velocity $\overline{\hat{\mathrm{v}}_{z1}}\left(\hat{z}\right)$ at a given position $\hat{z}$ is:

$$\overline{\hat{\mathrm{v}}_{z1}}\left(\hat{z}\right)=-\frac{\beta}{8}\frac{d\hat{\mathrm{p}}_1}{d\hat{z}}-\frac{3\mathcal{Re}\beta^3}{512}\frac{d^2\hat{\mathrm{p}}_0}{d\hat{z}^2}\frac{d\hat{\mathrm{p}}_0}{d\hat{z}} \tag{3.90}$$

and using equation (3.68) we can write:

$$\overline{\hat{\mathrm{v}}_{z1}}\left(\hat{z}\right)=-\frac{\beta}{8}\frac{d\hat{\mathrm{p}}_1}{d\hat{z}}-\frac{3\mathcal{Re}\beta^2}{32}\boldsymbol{\mathcal{V}}\left(\hat{z}\right)\frac{d\hat{\mathrm{p}}_0}{d\hat{z}} \tag{3.91}$$

From which, considering the boundary condition at $\hat{z}=0$ (3.85), as well as equations (3.64) and (3.68), we have that:

$$\frac{d\hat{\mathrm{p}}_1}{d\hat{z}}(0)=6\mathcal{Re}\boldsymbol{\mathcal{V}}(0) \tag{3.92}$$

From the equation of continuity (3.36) one has that:

$$\frac{\partial}{\partial \hat{r}}\left(\hat{r}\hat{\mathrm{v}}_{\mathrm{r1}}\right)=-\frac{\beta}{4}\frac{d^2\hat{\mathrm{p}}_1}{d\hat{z}^2}\left(\hat{r}^3-\hat{r}\right)-\frac{\mathcal{Re}\beta^3}{32}\frac{d}{d\hat{z}}\left(\frac{d^2\hat{\mathrm{p}}_0}{d\hat{z}^2}\frac{d\hat{\mathrm{p}}_0}{d\hat{z}}\right)\frac{\left(2\hat{r}^7-9\hat{r}^5+36\hat{r}^3-29\hat{r}\right)}{72} \tag{3.93}$$

Integrating over $\hat{r}$ and considering the boundary condition (3.81) leads to:

$$\hat{\mathrm{v}}_{\mathrm{r1}}\left(\hat{r},\hat{z}\right)=-\frac{\beta}{16}\frac{d^2\hat{\mathrm{p}}_1}{d\hat{z}^2}\left(\hat{r}^3-2\hat{r}\right)-\frac{\mathcal{Re}\beta^3}{32}\frac{d}{d\hat{z}}\left(\frac{d^2\hat{\mathrm{p}}_0}{d\hat{z}^2}\frac{d\hat{\mathrm{p}}_0}{d\hat{z}}\right)\frac{\left(\hat{r}^7-6\hat{r}^5+36\hat{r}^3-58\hat{r}\right)}{288} \tag{3.94}$$

Together with the boundary condition (3.78), this gives:

$$\frac{d^2\hat{\mathrm{p}}_1}{d\hat{z}^2}\left(\hat{z}\right)=-\frac{3\mathcal{Re}\beta^2}{64}\frac{d}{d\hat{z}}\left(\frac{d^2\hat{\mathrm{p}}_0}{d\hat{z}^2}\frac{d\hat{\mathrm{p}}_0}{d\hat{z}}\right)+\frac{16}{\beta}\hat{\mathrm{L}}_{\mathrm{p}}\left(\hat{\mathrm{p}}_1\left(\hat{z}\right)-\sigma\hat{\mathrm{H}}\hat{\mathrm{C}}_1\left(1,z\right)\right) \tag{3.95}$$

But, from equations (3.68), (3.69) and (3.71) one obtains:

$$\frac{d^2\hat{\mathrm{p}}_0}{d\hat{z}^2}\frac{d\hat{\mathrm{p}}_0}{d\hat{z}}=\frac{128}{\beta^2}\boldsymbol{\mathcal{V}}\left(\hat{z}\right)\left(2\frac{d\boldsymbol{q}}{d\hat{z}}-1\right) \tag{3.96}$$

Hence, considering equations (3.66), (3.71), (3.96), together with the boundary condition (3.87), we obtain from (3.95) that:

$$\frac{d^2\hat{\mathrm{p}}_1}{d\hat{z}^2}\left(0\right)=6\mathcal{Re}\left[\frac{d\boldsymbol{\mathcal{V}}}{d\hat{z}}\left(0\right)-2\boldsymbol{\mathcal{V}}^2\left(0\right)\right]-\frac{16\sigma\hat{\mathrm{L}}_{\mathrm{p}}\hat{\mathrm{H}}}{\beta}\hat{\mathrm{C}}_1\left(1,0\right) \tag{3.97}$$

Substituting $\frac{d^2\hat{\mathrm{p}}_0}{d\hat{z}^2}\frac{d\hat{\mathrm{p}}_0}{d\hat{z}}$ (3.96) into equation (3.95) and observing that the second term of the right hand side of equation (3.95) is also a function of $\hat{z}$ only, in the same way as the boundary condition (3.78), we can write (3.95) as:

$$\frac{d^2\hat{\mathrm{p}}_1}{d\hat{z}^2}\left(\hat{z}\right)=-6\mathcal{Re}\frac{d}{d\hat{z}}\left[\boldsymbol{\upsilon}\left(\hat{z}\right)\left(2\frac{d\boldsymbol{q}}{d\hat{z}}-1\right)\right]+\frac{16}{\beta}\boldsymbol{u}\left(\hat{z}\right) \tag{3.98}$$

with function $\boldsymbol{u}\left(\hat{z}\right)$ defined as:

$$\boldsymbol{u}\left(\hat{z}\right)=\hat{\mathrm{L}}_{\mathrm{p}}\left(\hat{\mathrm{p}}_1\left(\hat{z}\right)-\sigma\hat{\mathrm{H}}\hat{\mathrm{C}}_1\left(1,\hat{z}\right)\right) \tag{3.99}$$

Similarly to $\boldsymbol{\upsilon}\left(\hat{z}\right)$ (3.67) we have that:

$$\boldsymbol{u}\left(\hat{z}\right)=\frac{\boldsymbol{u}(z)}{\varepsilon U} \tag{3.100}$$

Substituting the result for $\frac{d^2\hat{\mathrm{p}}_1}{d\hat{z}^2}$ (3.98) together with $\frac{d^2\hat{\mathrm{p}}_0}{d\hat{z}^2}\frac{d\hat{\mathrm{p}}_0}{d\hat{z}}$ (3.96) into equation (3.94) one obtains:

$$\hat{\mathrm{v}}_{\mathrm{r1}}\left(\hat{r},\hat{z}\right)=-\frac{\beta\mathcal{Re}}{72}\frac{d}{d\hat{z}}\left[\boldsymbol{\upsilon}\left(\hat{z}\right)\left(2\frac{d\boldsymbol{q}}{d\hat{z}}-1\right)\right]\left(\hat{r}^7-6\hat{r}^5+9\hat{r}^3-4\hat{r}\right)-\boldsymbol{u}\left(\hat{z}\right)\left(\hat{r}^3-2\hat{r}\right) \tag{3.101}$$

Integrating (3.98) over $\hat{z}$ and considering the result (3.92) yields:

$$\frac{d\hat{\mathrm{p}}_1}{d\hat{z}}\left(\hat{z}\right)=-6\mathcal{Re}\boldsymbol{\upsilon}\left(\hat{z}\right)\left(2\frac{d\boldsymbol{q}}{d\hat{z}}-1\right)+\frac{16}{\beta}\int_0^{\hat{z}}\boldsymbol{u}\left(\hat{z}'\right)d\hat{z}'+12\mathcal{Re}\boldsymbol{\upsilon}(0) \tag{3.102}$$

Integrating (3.102) over $\hat{z}$ and considering the boundary conditions (3.87) one obtains:

$$\hat{\mathrm{p}}_1\left(\hat{z}\right)=6\mathcal{Re}\left[\frac{d\boldsymbol{q}}{d\hat{z}}-\left(\frac{d\boldsymbol{q}}{d\hat{z}}\right)^2\right]+\frac{16}{\beta}\int_0^{\hat{z}}\int_0^{\hat{z}''}\boldsymbol{u}\left(\hat{z}'\right)d\hat{z}'d\hat{z}''+12\mathcal{Re}\boldsymbol{\upsilon}(0)\hat{z} \tag{3.103}$$

Defining function $\boldsymbol{s}\left(\hat{z}\right)$ as:

$$\mathcal{s}\left(\hat{z}\right)=\int_0^{\hat{z}}\int_0^{\hat{z}''}\mathcal{U}\left(\hat{z}'\right)d\hat{z}'d\hat{z}'' \tag{3.104}$$

where, similarly to $\boldsymbol{q}\left(\hat{z}\right)$ (3.72) we have that:

$$\mathcal{s}\left(\hat{z}\right)=\frac{\mathcal{s}\left(z\right)}{LRU} \tag{3.105}$$

we can write (3.103) as:

$$\hat{\mathrm{p}}_1\left(\hat{z}\right)=6\mathcal{Re}\left[\frac{d\boldsymbol{q}}{d\hat{z}}-\left(\frac{d\boldsymbol{q}}{d\hat{z}}\right)^2\right]+\frac{16}{\beta}\mathcal{s}\left(\hat{z}\right)+12\mathcal{Re}\mathcal{V}\left(0\right)\hat{z} \tag{3.106}$$

Thus, considering (3.96), (3.102) and (3.104), we can write (3.89) as:

$$\begin{aligned}\hat{\mathrm{v}}_{z1}\left(\hat{r},\hat{z}\right)=&\frac{\mathcal{Re}\beta}{18}\mathcal{V}\left(\hat{z}\right)\left(2\frac{d\boldsymbol{q}}{d\hat{z}}-1\right)\left(2\hat{r}^6-9\hat{r}^4+9\hat{r}^2-2\right)+\\&+4\left(\frac{d\mathcal{s}}{d\hat{z}}+\frac{3\beta\mathcal{Re}\mathcal{V}\left(0\right)}{4}\right)\left(\hat{r}^2-1\right)\end{aligned} \tag{3.107}$$

Equations (3.106), (3.101) and (3.107) are the first order expressions for pressure and velocity describing fluid flow in the modelled sieve tube.

3.3.3 Velocity and Turgor Pressure Profiles

Bringing together the results from zeroth and first order approximations, according to equations (3.56) and (3.57) and considering equations (3.74) and (3.75) together with equations (3.101) and (3.107), the velocity components $\hat{\mathrm{v}}_z$ and $\hat{\mathrm{v}}_r$ are given up to the first order by:

$$\hat{\mathrm{v}}_z\left(\hat{r},\hat{z}\right)=\left(2\frac{d\boldsymbol{q}}{d\hat{z}}-1\right)\left\{2\left(\hat{r}^2-1\right)+\frac{\varepsilon\beta\boldsymbol{Re}}{18}\boldsymbol{v}\left(\hat{z}\right)\left(2\hat{r}^6-9\hat{r}^4+9\hat{r}^2-2\right)\right\}+$$
$$+4\varepsilon\left(\frac{d\boldsymbol{s}}{d\hat{z}}+\frac{3\beta\boldsymbol{Re}\boldsymbol{V}(0)}{4}\right)\left(\hat{r}^2-1\right) \tag{3.108}$$

and

$$\hat{\mathrm{v}}_r\left(\hat{r},\hat{z}\right)=\left(\boldsymbol{v}\left(\hat{z}\right)-\varepsilon\boldsymbol{u}\left(\hat{z}\right)\right)\left(2\hat{r}-\hat{r}^3\right)-$$
$$-\frac{\varepsilon\beta\boldsymbol{Re}}{72}\frac{d}{d\hat{z}}\left[\boldsymbol{v}\left(\hat{z}\right)\left(2\frac{d\boldsymbol{q}}{d\hat{z}}-1\right)\right]\left(\hat{r}^7-6\hat{r}^5+9\hat{r}^3-4\hat{r}\right) \tag{3.109}$$

The average velocity, $\overline{\hat{\mathrm{v}}_z}$, in the direction of flow is:

$$\overline{\hat{\mathrm{v}}_z}\left(\hat{z}\right)=1-2\frac{d\boldsymbol{q}}{d\hat{z}}-2\varepsilon\left(\frac{d\boldsymbol{s}}{d\hat{z}}+\frac{3\beta\boldsymbol{Re}\boldsymbol{V}(0)}{4}\right) \tag{3.110}$$

According to equation (3.58), from equations (3.73) and (3.106), the pressure $\hat{\mathrm{p}}$ is given by:

$$\hat{\mathrm{p}}\left(\hat{z}\right)=\hat{\mathrm{p}}_{\mathrm{i}}+\frac{16\boldsymbol{q}\left(\hat{z}\right)-8\hat{z}}{\beta}+6\boldsymbol{Re}\varepsilon\left[\frac{d\boldsymbol{q}}{d\hat{z}}-\left(\frac{d\boldsymbol{q}}{d\hat{z}}\right)^2\right]+\frac{16\varepsilon}{\beta}\boldsymbol{s}\left(\hat{z}\right)+12\varepsilon\boldsymbol{Re}\boldsymbol{V}(0)\hat{z} \tag{3.111}$$

Thus, the pressure gradient is:

$$\frac{d\hat{\mathrm{p}}}{d\hat{z}}\left(\hat{z}\right)=\frac{8}{\beta}\left(2\frac{d\boldsymbol{q}}{d\hat{z}}-1\right)+6\boldsymbol{Re}\varepsilon\frac{d}{d\hat{z}}\left[\frac{d\boldsymbol{q}}{d\hat{z}}-\left(\frac{d\boldsymbol{q}}{d\hat{z}}\right)^2\right]+\frac{16\varepsilon}{\beta}\frac{d\boldsymbol{s}}{d\hat{z}}+12\varepsilon\boldsymbol{Re}\boldsymbol{V}(0) \tag{3.112}$$

Considering (3.71) and (3.110) the pressure gradient relates to the average axial velocity, $\overline{\hat{\mathrm{v}}_z}$:

$$\frac{d\hat{\mathrm{p}}}{d\hat{z}}\left(\hat{z}\right)=-\frac{8}{\beta}\overline{\hat{\mathrm{v}}_{\mathrm{z}}}\left(\hat{z}\right)-6\mathcal{Re}\varepsilon\boldsymbol{\mathcal{V}}\left(\hat{z}\right)\left(2\frac{d\boldsymbol{q}}{d\hat{z}}-1\right) \tag{3.113}$$

In the dimensional form the velocity component $\mathrm{v_z}$ is given by:

$$\mathrm{v_z}\left(r,z\right)=\left(2\frac{d\boldsymbol{q}}{dz}-UR\right)\left\{\frac{2}{R^3}\left(r^2-R^2\right)+\frac{\beta\boldsymbol{\mathcal{V}}\left(z\right)}{18\nu R^6}\left(2r^6-9R^2r^4+9R^4r^2+2R^6\right)\right\}+$$

$$+\frac{4}{LR^2}\left(\frac{d\boldsymbol{s}}{dz}+\frac{3ULR\beta\boldsymbol{\mathcal{V}}\left(0\right)}{4\nu}\right)\left(r^2-R^2\right) \tag{3.114}$$

and the average velocity in the direction of flow is:

$$\overline{\mathrm{v}_{\mathrm{z}}}\left(z\right)=U-\frac{2}{R}\frac{d\boldsymbol{q}}{dz}-\frac{2}{L}\frac{d\boldsymbol{s}}{dz}-\frac{3UR\beta\boldsymbol{\mathcal{V}}\left(0\right)}{2\nu} \tag{3.115}$$

The dimensional form of the radial component, $\mathrm{v_r}$, is given by:

$$\mathrm{v_r}\left(r,z\right)=\left(\boldsymbol{\mathcal{V}}\left(z\right)-\varepsilon\boldsymbol{\mathcal{U}}\left(z\right)\right)\frac{\left(2R^2r-r^3\right)}{R^3}-$$

$$-\frac{\beta}{72\nu R^6}\frac{d}{dz}\left[\boldsymbol{\mathcal{V}}\left(z\right)\left(2\frac{d\boldsymbol{q}}{dz}-UR\right)\right]\left(r^7-6R^2r^5+9R^4r^3-4rR^6\right) \tag{3.116}$$

The pressure is given by:

$$\mathrm{p}\left(z\right)=\mathrm{p_i}+\frac{8\mu}{\beta R^3}\left(2\boldsymbol{q}\left(z\right)-URz\right)+\frac{6\rho}{R^2}\left[RU\frac{d\boldsymbol{q}}{dz}-\left(\frac{d\boldsymbol{q}}{dz}\right)^2\right]+$$

$$+\frac{16\mu}{\beta LR^2}\boldsymbol{s}\left(z\right)+\frac{12\rho U\boldsymbol{\mathcal{V}}\left(0\right)}{R}z \tag{3.117}$$

and the pressure gradient is:

$$\frac{d\mathrm{p}}{dz}(z)=\frac{8\mu}{\beta R^3}\left(2\frac{d\boldsymbol{q}}{dz}(z)-UR\right)-\frac{6\rho}{R^2}\boldsymbol{v}(z)\left[2\frac{d\boldsymbol{q}}{dz}(z)-UR\right]+$$
$$+\frac{16\mu}{\beta LR^2}\frac{d\boldsymbol{s}}{dz}(z)+\frac{12\rho U\boldsymbol{v}(0)}{R} \tag{3.118}$$

where functions $\boldsymbol{q}$ (*z*) (3.72) and $\boldsymbol{v}$ (*z*) (3.67) relate to the zeroth order and $\boldsymbol{s}$(*z*) (3.105) and $\boldsymbol{u}$(*z*) (3.100) relate to first order terms, that describe radial water exchange. Finally, the relation between the pressure gradient and the average axial velocity (3.113) in the dimensional form is:

$$\frac{d\mathrm{p}}{dz}(z)=-\frac{8\mu}{\beta R^2}\overline{\mathrm{v}_z}(z)-\frac{6\rho}{R^2}\boldsymbol{v}(z)\left(2\int_0^{z'}\boldsymbol{v}(z)\,dz'-UR\right) \tag{3.119}$$

that is linear with the average axial velocity, $\overline{\mathrm{v}_z}$, but dependent on the zeroth order expression that describe radial flux of water, $\boldsymbol{v}$ (z) (3.66).

3.4 Solute Movement

3.4.1 Zeroth Order Approximation

As mentioned before, the equations that describe solvent flow (hydrodynamics) as defined by (3.3), (3.4) and solute flow (3.5) (convection–diffusion equation) are coupled by the boundary condition (3.18) that governs solute flux through the sieve tube membrane. In the zeroth approximation, the dimensionless form of the convection–diffusion equation (3.37) reduces to:

$$\frac{1}{\boldsymbol{P}e_r}\frac{1}{\hat{r}}\frac{\partial}{\partial\hat{r}}\left(\hat{r}\frac{\partial\hat{\mathrm{C}}_0}{\partial\hat{r}}\right)=0 \tag{3.120}$$

which integrating it over $\hat{r}$ gives:

$$\frac{\partial \hat{C}_0}{\partial \hat{r}} = \frac{a}{\hat{r}} \tag{3.121}$$

a being some constant. The boundary conditions (3.44), (3.48) and (3.51) are given by:

$$\frac{1}{\mathcal{P}e_r}\frac{\partial \hat{C}_0}{\partial \hat{r}}\left(1,\hat{z}\right) = 0 \tag{3.122}$$

$$\frac{\partial \hat{C}_0}{\partial \hat{r}}\left(0,\hat{z}\right) = 0 \tag{3.123}$$

$$\overline{\hat{C}_0}\left(0\right) = 1 \tag{3.124}$$

Hence, from equation (3.121) together with the boundary condition (3.122), one concludes that $a = 0$ and $\hat{C}_0$ is constant over $\hat{r}$ and a function of $\hat{z}$ only, and $\hat{C}_0\left(\hat{r},0\right) = \hat{C}_i = 1$.

3.4.2 First Order Approximation

In the first order approximation and considering the previous result, $\frac{\partial \hat{C}_0}{\partial \hat{r}} = 0$, the convection diffusion equation (3.37) reduces to:

$$\hat{v}_{z0}\frac{d\hat{C}_0}{d\hat{z}} = \frac{1}{\mathcal{P}e_r}\frac{1}{\hat{r}}\frac{\partial}{\partial \hat{r}}\left(\hat{r}\frac{\partial \hat{C}_1}{\partial \hat{r}}\right) \tag{3.125}$$

Substituting $\hat{v}_{z0}$ given by equation (3.62) into equation (3.125) and integrating it once over $\hat{r}$, one obtains:

$$\frac{\partial \hat{\mathrm{C}}_1}{\partial \hat{r}}\left(\hat{r},\hat{z}\right)=\frac{\beta \mathcal{P}\boldsymbol{e}_r}{16}\frac{d\hat{\mathrm{C}}_0}{d\hat{z}}\frac{d\hat{\mathrm{p}}_0}{d\hat{z}}\left(\hat{r}^3-2\hat{r}\right) \tag{3.126}$$

As already mentioned, the boundary conditions (3.44), (3.48), and (3.51) reduce to equations (3.80), (3.83) and (3.86) respectively. Thus, in this scenario, and considering (3.45), the first order approximation of the boundary condition (3.80) can be written as:

$$-\frac{1}{\mathcal{P}\boldsymbol{e}_r}\frac{\partial \hat{\mathrm{C}}_1}{\partial \hat{r}}\left(1,\hat{z}\right)=\frac{\boldsymbol{v}\left(\hat{z}\right)}{2}\left[-\left(1+\sigma\right)\hat{\mathrm{C}}_0\left(\hat{z}\right)+\left(1-\sigma\right)\left(\hat{\mathrm{C}}_{\mathrm{out}}\left(0\right)+\frac{d\hat{\mathrm{C}}_{\mathrm{out}}}{d\hat{z}}\hat{z}\right)\right]+$$
$$+\hat{\mathrm{P}}_{\mathrm{s}}\left(\hat{\mathrm{C}}_0\left(\hat{z}\right)-\hat{\mathrm{C}}_{\mathrm{out}}\left(0\right)-\frac{d\hat{\mathrm{C}}_{\mathrm{out}}}{d\hat{z}}\hat{z}\right) \tag{3.127}$$

Together with equation (3.126) this leads to:

$$\frac{\beta}{16}\frac{d\hat{\mathrm{C}}_0}{d\hat{z}}\frac{d\hat{\mathrm{p}}_0}{d\hat{z}}=\frac{\boldsymbol{v}\left(\hat{z}\right)}{2}\left[-\left(1+\sigma\right)\hat{\mathrm{C}}_0\left(\hat{z}\right)+\left(1-\sigma\right)\left(\hat{\mathrm{C}}_{\mathrm{out}}\left(0\right)+\frac{d\hat{\mathrm{C}}_{\mathrm{out}}}{d\hat{z}}\hat{z}\right)\right]+$$
$$+\hat{\mathrm{P}}_{\mathrm{s}}\left(\hat{\mathrm{C}}_0\left(\hat{z}\right)-\hat{\mathrm{C}}_{\mathrm{out}}\left(0\right)-\frac{d\hat{\mathrm{C}}_{\mathrm{out}}}{d\hat{z}}\hat{z}\right) \tag{3.128}$$

From which we obtain, considering equations (3.64), (3.66) and the boundary conditions (3.51):

$$\frac{d\hat{\mathrm{C}}_0}{d\hat{z}}\left(0\right)=-\boldsymbol{v}\left(0\right)\left[-1-\sigma+\left(1-\sigma\right)\hat{\mathrm{C}}_{\mathrm{out}}\left(0\right)\right]-2\hat{\mathrm{P}}_{\mathrm{s}}\left(1-\hat{\mathrm{C}}_{\mathrm{out}}\left(0\right)\right) \tag{3.129}$$

Equations (3.128) and (3.68), now in the form:

$$\frac{d^2\hat{\mathrm{p}}_0}{d\hat{z}^2}\left(\hat{z}\right)=\frac{16\hat{\mathrm{L}}_{\mathrm{p}}}{\beta}\left[\hat{\mathrm{p}}_0\left(\hat{z}\right)-\hat{\mathrm{p}}_{\mathrm{out}}\left(0\right)-\frac{d\hat{\mathrm{p}}_{\mathrm{out}}}{d\hat{z}}\hat{z}-\sigma\hat{\mathrm{H}}\left(\hat{\mathrm{C}}_0\left(\hat{z}\right)-\hat{\mathrm{C}}_{\mathrm{out}}\left(0\right)-\frac{d\hat{\mathrm{C}}_{\mathrm{out}}}{d\hat{z}}\hat{z}\right)\right] \tag{3.130}$$

compose a system of two coupled equations that we need to solve in order to obtain the velocity and pressure profiles given by equations (3.74), (3.75) and (3.73) where $\boldsymbol{v}\left(\hat{z}\right)$ is a function of $\hat{\mathrm{C}}_0$ and $\hat{\mathrm{p}}_0$ (3.66). Substituting $\frac{d\hat{\mathrm{C}}_0}{d\hat{z}}$ given by equation (3.127) into equation (3.126) we have that:

$$\frac{\partial\hat{\mathrm{C}}_1}{\partial\hat{r}}\left(\hat{r},\hat{z}\right)=\boldsymbol{\mathcal{P}e}_r\left(\hat{r}^3-2\hat{r}\right)\times$$

$$\times\left\{\frac{\boldsymbol{v}\left(\hat{z}\right)}{2}\left[-\left(1+\sigma\right)\hat{\mathrm{C}}_0\left(\hat{z}\right)+\left(1-\sigma\right)\left(\hat{\mathrm{C}}_{\mathrm{out}}\left(0\right)+\frac{d\hat{\mathrm{C}}_{\mathrm{out}}}{d\hat{z}}\hat{z}\right)\right]+\hat{\mathrm{P}}_{\mathrm{s}}\left(\hat{\mathrm{C}}_0\left(\hat{z}\right)-\hat{\mathrm{C}}_{\mathrm{out}}\left(0\right)-\frac{d\hat{\mathrm{C}}_{\mathrm{out}}}{d\hat{z}}\hat{z}\right)\right\}$$

(3.131)

Integrating it over $\hat{r}$, considering the boundary condition (3.86) and equation (3.129), one obtains:

$$\hat{\mathrm{C}}_1\left(\hat{r},\hat{z}\right)=\frac{\boldsymbol{\mathcal{P}e}_r}{4}\left(\hat{r}^4-4\hat{r}^2\right)\times$$

$$\times\left\{\frac{\boldsymbol{v}\left(\hat{z}\right)}{2}\left[-\left(1+\sigma\right)\hat{\mathrm{C}}_0\left(\hat{z}\right)+\left(1-\sigma\right)\left(\hat{\mathrm{C}}_{\mathrm{out}}\left(0\right)+\frac{d\hat{\mathrm{C}}_{\mathrm{out}}}{d\hat{z}}\hat{z}\right)\right]+\hat{\mathrm{P}}_{\mathrm{s}}\left(\hat{\mathrm{C}}_0\left(\hat{z}\right)-\hat{\mathrm{C}}_{\mathrm{out}}\left(0\right)-\frac{d\hat{\mathrm{C}}_{\mathrm{out}}}{d\hat{z}}\hat{z}\right)\right\}-$$

$$-\frac{5\boldsymbol{\mathcal{P}e}_r}{24}\frac{d\hat{\mathrm{C}}_0}{d\hat{z}}\left(0\right)$$

(3.132)

Hence, the average concentration $\overline{\hat{\mathrm{C}}_1}\left(\hat{z}\right)$ over a plane normal to the direction of flow, at a given position $\hat{z}$, is:

$$\overline{\hat{C}_1}\left(\hat{z}\right)=-\frac{5\mathcal{P}e_r}{12}\left\{\frac{v\left(\hat{z}\right)}{2}\left[-\left(1+\sigma\right)\hat{C}_0\left(\hat{z}\right)+\left(1-\sigma\right)\left(\hat{C}_{out}\left(0\right)+\frac{d\hat{C}_{out}}{d\hat{z}}\hat{z}\right)\right]+\right.$$

$$\left.+\hat{P}_s\left(\hat{C}_0\left(\hat{z}\right)-\hat{C}_{out}\left(0\right)-\frac{d\hat{C}_{out}}{d\hat{z}}\hat{z}\right)\right\}-\frac{5\mathcal{P}e_r}{24}\frac{d\hat{C}_0}{d\hat{z}}\left(0\right) \tag{3.133}$$

which together with $\hat{C}_0\left(\hat{z}\right)$, obtained from solving simultaneously equations (3.128) and (3.130) will give the concentration profile, taking only terms up to the first order perturbation in the expansion of $\hat{C}$ (3.59). The concentration gradient in the direction of flow can thus be written as:

$$\frac{d\overline{\hat{C}_1}}{d\hat{z}}\left(\hat{z}\right)=-\frac{5\mathcal{P}e_r}{12}\left\{\frac{v\left(\hat{z}\right)}{2}\left[-\left(1+\sigma\right)\frac{d\hat{C}_0}{d\hat{z}}+\left(1-\sigma\right)\frac{d\hat{C}_{out}}{d\hat{z}}\right]+\right.$$

$$\left.+\left[-\left(1+\sigma\right)\hat{C}_0\left(\hat{z}\right)+\left(1-\sigma\right)\left(\hat{C}_{out}\left(0\right)+\frac{d\hat{C}_{out}}{d\hat{z}}\hat{z}\right)\right]\frac{dv}{d\hat{z}}\left(\hat{z}\right)+\hat{P}_s\left(\frac{d\hat{C}_0}{d\hat{z}}-\frac{d\hat{C}_{out}}{d\hat{z}}\right)\right\}$$

But, using equation (3.68) we can write:

$$\frac{d\overline{\hat{C}_1}}{d\hat{z}}\left(\hat{z}\right)=-\frac{5\mathcal{P}e_r}{12}\left\{\frac{v\left(\hat{z}\right)}{2}\left[-\left(1+\sigma\right)\frac{d\hat{C}_0}{d\hat{z}}+\left(1-\sigma\right)\frac{d\hat{C}_{out}}{d\hat{z}}\right]+\right.$$

$$\left.+\left[-\left(1+\sigma\right)\hat{C}_0\left(\hat{z}\right)+\left(1-\sigma\right)\left(\hat{C}_{out}\left(0\right)+\frac{d\hat{C}_{out}}{d\hat{z}}\hat{z}\right)\right]\frac{\beta}{16}\frac{d^3\hat{p}_0}{d\hat{z}^3}+\hat{P}_s\left(\frac{d\hat{C}_0}{d\hat{z}}-\frac{d\hat{C}_{out}}{d\hat{z}}\right)\right\} \tag{3.134}$$

where $\frac{d^3\hat{p}_0}{d\hat{z}^3}$ is easily determined from (3.130) as:

$$\frac{d^3\hat{\mathrm{p}}_0}{d\hat{z}^3}\left(\hat{z}\right)=\frac{16\hat{\mathrm{L}}_\mathrm{p}}{\beta}\left[\frac{d\hat{\mathrm{p}}_0}{d\hat{z}}\left(\hat{z}\right)-\frac{d\hat{\mathrm{p}}_{\mathrm{out}}}{d\hat{z}}\hat{z}-\sigma\hat{\mathrm{H}}\left(\frac{d\hat{\mathrm{C}}_0}{d\hat{z}}\left(\hat{z}\right)-\frac{d\hat{\mathrm{C}}_{\mathrm{out}}}{d\hat{z}}\hat{z}\right)\right] \tag{3.135}$$

At the sieve tube membrane, we have from equation (3.132) that:

$$\begin{aligned}\hat{\mathrm{C}}_1\left(1,\hat{z}\right)=&-\frac{3\boldsymbol{\mathcal{P}e}_r}{4}\left\{\frac{\boldsymbol{v}\left(\hat{z}\right)}{2}\left[-\left(1+\sigma\right)\hat{\mathrm{C}}_0\left(\hat{z}\right)+\left(1-\sigma\right)\left(\hat{\mathrm{C}}_{\mathrm{out}}\left(0\right)+\frac{d\hat{\mathrm{C}}_{\mathrm{out}}}{d\hat{z}}\hat{z}\right)\right]\right.\\&\left.+\hat{\mathrm{P}}_\mathrm{s}\left(\hat{\mathrm{C}}_0\left(\hat{z}\right)-\hat{\mathrm{C}}_{\mathrm{out}}\left(0\right)-\frac{d\hat{\mathrm{C}}_{\mathrm{out}}}{d\hat{z}}\hat{z}\right)\right\}-\frac{5\boldsymbol{\mathcal{P}e}_r}{24}\frac{d\hat{\mathrm{C}}_0}{d\hat{z}}\left(0\right)\end{aligned} \tag{3.136}$$

thus substituting $\hat{\mathrm{C}}_1\left(1,\hat{z}\right)$ into equation (3.95) yields the expression for $\frac{d^2\hat{p}_1}{d\hat{z}^2}$ as a function of variables $\hat{\mathrm{p}}_0$ and $\hat{\mathrm{C}}_0$ only:

$$\begin{aligned}\frac{d^2\hat{\mathrm{p}}_1}{d\hat{z}^2}=&-\frac{3\boldsymbol{\mathcal{R}e}\beta^2}{64}\frac{d}{d\hat{z}}\left(\frac{d^2\hat{\mathrm{p}}_0}{d\hat{z}^2}\frac{d\hat{\mathrm{p}}_0}{d\hat{z}}\right)+\frac{16\hat{\mathrm{L}}_\mathrm{p}}{\beta}\left\{\hat{\mathrm{p}}_1\left(\hat{z}\right)+\right.\\&+\frac{3\sigma\hat{\mathrm{H}}\boldsymbol{\mathcal{P}e}_r}{4}\left\{\frac{\boldsymbol{v}\left(\hat{z}\right)}{2}\left[-\left(1+\sigma\right)\hat{\mathrm{C}}_0\left(\hat{z}\right)+\left(1-\sigma\right)\left(\hat{\mathrm{C}}_{\mathrm{out}}\left(0\right)+\frac{d\hat{\mathrm{C}}_{\mathrm{out}}}{d\hat{z}}\hat{z}\right)\right]+\right.\\&\left.\left.+\hat{\mathrm{P}}_\mathrm{s}\left(\hat{\mathrm{C}}_0\left(\hat{z}\right)-\hat{\mathrm{C}}_{\mathrm{out}}\left(0\right)-\frac{d\hat{\mathrm{C}}_{\mathrm{out}}}{d\hat{z}}\hat{z}\right)\right\}+\frac{5\sigma\hat{\mathrm{H}}\boldsymbol{\mathcal{P}e}_r}{24}\frac{d\hat{\mathrm{C}}_0}{d\hat{z}}\left(0\right)\right\}\end{aligned} \tag{3.137}$$

from which we obtain $\hat{\mathrm{p}}_1$ that together with $\hat{\mathrm{p}}_0$ will be used to determine the pressure profile taking terms up to the first order (3.58).

From equations (3.133) and (3.136) we note also that $\hat{\mathrm{C}}_1\left(1,\hat{z}\right)$ and $\overline{\hat{\mathrm{C}}_1}\left(\hat{z}\right)$ are related as:

$$\hat{\mathrm{C}}_1\left(1,\hat{z}\right)=\frac{9}{5}\overline{\hat{\mathrm{C}}_1}\left(\hat{z}\right)+\frac{\boldsymbol{\mathcal{P}e}_r}{6}\frac{d\hat{\mathrm{C}}_0}{d\hat{z}}\left(0\right) \tag{3.138}$$

3.5 Non-selective Membrane

There is a very special case $\sigma = 0$ in which the sieve tube membrane is totally non-selective; there is no distinction between water (the solvent) and solutes. Thus the osmotic effects that drive water exchange do not occur, and exchange is driven solely by the pressure difference across the membrane (3.140). Pressure being higher inside the sieve tube causes water efflux. In this situation, solute exchange across the sieve tube membrane is driven both by convection and by diffusion that occurs due to the concentration difference between the sieve tube and its surroundings. Putting the sieve tube surroundings at a constant water potential and using equation (3.68) the coupled transport equations (3.128) and (3.130) can be solved analytically and thus provide a way to check the result of the numerical method. They become respectively:

$$\frac{d\hat{C}_0}{d\hat{z}}\frac{d\hat{p}_0}{d\hat{z}} = \frac{1}{2}\frac{d^2\hat{p}_0}{d\hat{z}^2}\left(-\hat{C}_0\left(\hat{z}\right)+\hat{C}_{out}\right)+\frac{16\hat{P}_s}{\beta}\left(\hat{C}_0\left(\hat{z}\right)-\hat{C}_{out}\right) \tag{3.139}$$

and

$$\frac{d^2\hat{p}_0}{d\hat{z}^2}\left(\hat{z}\right) = \frac{16\hat{L}_p}{\beta}\left(\hat{p}_0\left(\hat{z}\right)-\hat{p}_{out}\right) \tag{3.140}$$

The solution of equation (3.140) is:

$$\hat{p}_0\left(\hat{z}\right) = \hat{p}_{out} + \left(\frac{\hat{p}_i-\hat{p}_{out}}{2}-\frac{1}{\sqrt{\beta\hat{L}_p}}\right)\exp\left(4\sqrt{\frac{\hat{L}_p}{\beta}}\hat{z}\right)+\left(\frac{\hat{p}_i-\hat{p}_{out}}{2}+\frac{1}{\sqrt{\beta\hat{L}_p}}\right)\exp\left(-4\sqrt{\frac{\hat{L}_p}{\beta}}\hat{z}\right) \tag{3.141}$$

taking into account the boundary conditions (3.52) and (3.64). Equation (3.139) can be written as:

$$\frac{\dfrac{d\hat{C}_0}{d\hat{z}}}{\hat{C}_0\left(\hat{z}\right)-\hat{C}_{out}\left(0\right)}=\frac{-\dfrac{1}{2}\dfrac{d^2\hat{p}_0}{d\hat{z}^2}+\dfrac{16\hat{P}_s}{\beta}}{\dfrac{d\hat{p}_0}{d\hat{z}}}$$

Integrating over $\hat{z}$, and noting that $\dfrac{d\hat{p}_0}{d\hat{z}}$ can be negative, we have that:

$$\ln\left(\frac{\hat{C}_0\left(\hat{z}\right)-\hat{C}_{out}}{1-\hat{C}_{out}}\right)=-\frac{1}{2}\ln\left|\frac{\beta}{8}\frac{d\hat{p}_0}{d\hat{z}}\left(\hat{z}\right)\right|+\int_0^{\hat{z}}\frac{16\hat{P}_s}{\beta\dfrac{d\hat{p}_0}{d\hat{z}}\left(\hat{z}'\right)}d\hat{z}'$$

or

$$\frac{\hat{C}_0\left(\hat{z}\right)-\hat{C}_{out}}{1-\hat{C}_{out}}=\sqrt{\frac{8}{\beta\left|\dfrac{d\hat{p}_0}{d\hat{z}}\left(\hat{z}\right)\right|}}\exp\left(\int_0^{\hat{z}}\frac{16\hat{P}_s}{\beta\dfrac{d\hat{p}_0}{d\hat{z}}\left(\hat{z}'\right)}d\hat{z}'\right)$$

From equation (3.141) we have that:

$$\int_0^{\hat{z}}\frac{16\hat{P}_s}{\beta\dfrac{d\hat{p}_0}{d\hat{z}}\left(\hat{z}\right)}d\hat{z}'=$$

$$=\int_0^{\hat{z}}\frac{16\hat{P}_s}{4\sqrt{\beta\hat{L}_p}\left[\left(\dfrac{\hat{p}_i-\hat{p}_{out}}{2}-\dfrac{1}{\sqrt{\beta\hat{L}_p}}\right)\exp\left(4\sqrt{\dfrac{\hat{L}_p}{\beta}}\hat{z}'\right)-\left(\dfrac{\hat{p}_i-\hat{p}_{out}}{2}+\dfrac{1}{\sqrt{\beta\hat{L}_p}}\right)\exp\left(-4\sqrt{\dfrac{\hat{L}_p}{\beta}}\hat{z}'\right)\right]}d\hat{z}' \tag{3.142}$$

The solution of this integral is that:

$$\int_0^{\hat{z}} \frac{16\hat{P}_s}{\beta \frac{d\hat{p}_0}{d\hat{z}}\left(\hat{z}\right)} d\hat{z}' = \left[\xi\left(\hat{z}\right)\right]_0^{\hat{z}} \tag{3.143}$$

where

$$\xi\left(\hat{z}\right) = \begin{cases} \dfrac{\hat{P}_s}{\hat{L}_p\sqrt{\Xi}} \arctan\left[\exp\left(4\sqrt{\dfrac{\hat{L}_p}{\beta}}\hat{z}\right)\sqrt{\Theta}\right], & \text{if } \Xi > 0 \\ \dfrac{\hat{P}_s}{2\hat{L}_p\sqrt{-\Xi}} \ln\left|\dfrac{1+\exp\left(4\sqrt{\dfrac{\hat{L}_p}{\beta}}\hat{z}\right)\sqrt{-\Theta}}{1-\exp\left(4\sqrt{\dfrac{\hat{L}_p}{\beta}}\hat{z}\right)\sqrt{-\Theta}}\right|, & \text{if } \Xi < 0 \end{cases} \tag{3.144}$$

and

$$\Xi = \frac{1}{\beta\hat{L}_p} - \frac{\left(\hat{p}_i - \hat{p}_{out}\right)^2}{4} \tag{3.145}$$

and

$$\Theta = \frac{\dfrac{1}{\sqrt{\beta\hat{L}_p}} - \dfrac{\hat{p}_i - \hat{p}_{out}}{2}}{\dfrac{1}{\sqrt{\beta\hat{L}_p}} + \dfrac{\hat{p}_i - \hat{p}_{out}}{2}} \tag{3.146}$$

For $\Xi = 0$, i.e. $\hat{L}_p = \dfrac{4}{\beta\left(\hat{p}_i - \hat{p}_{out}\right)^2}$ the solution of equation (3.142) becomes:

$$\xi\left(\hat{z}\right)=-\int_{0}^{\hat{z}}\frac{2\hat{\mathrm{P}}_{\mathrm{s}}}{\beta\exp\left(-4\sqrt{\frac{\hat{\mathrm{L}}_{\mathrm{p}}}{\beta}}\hat{z}'\right)}d\hat{z}'=-\frac{\hat{\mathrm{P}}_{\mathrm{s}}}{2\sqrt{\beta\hat{\mathrm{L}}_{\mathrm{p}}}}\left[\exp\left(4\sqrt{\frac{\hat{\mathrm{L}}_{\mathrm{p}}}{\beta}}\hat{z}\right)-1\right] \qquad (3.147)$$

Hence the concentration in the sieve tube surrounded by a non-selective membrane (σ = 0) is given by:

$$\hat{\mathrm{C}}_{0}\left(\hat{z}\right)=\hat{\mathrm{C}}_{\mathrm{out}}+\left(1-\hat{\mathrm{C}}_{\mathrm{out}}\right)\exp\left(\xi\left(\hat{z}\right)-\xi\left(0\right)\right)\sqrt{\frac{2}{\sqrt{\beta\hat{\mathrm{L}}_{\mathrm{p}}}}}\times$$

$$\times\frac{1}{\sqrt{\left|\left(\frac{\hat{\mathrm{p}}_{\mathrm{i}}-\hat{\mathrm{p}}_{\mathrm{out}}}{2}-\frac{1}{\sqrt{\beta\hat{\mathrm{L}}_{\mathrm{p}}}}\right)\exp\left(4\sqrt{\frac{\hat{\mathrm{L}}_{\mathrm{p}}}{\beta}}\hat{z}\right)-\left(\frac{\hat{\mathrm{p}}_{\mathrm{i}}-\hat{\mathrm{p}}_{\mathrm{out}}}{2}+\frac{1}{\sqrt{\beta\hat{\mathrm{L}}_{\mathrm{p}}}}\right)\exp\left(-4\sqrt{\frac{\hat{\mathrm{L}}_{\mathrm{p}}}{\beta}}\hat{z}\right)\right|}} \qquad (3.148)$$

$\xi\left(\hat{z}\right)$ is given by (3.144) for $\hat{\mathrm{L}}_{\mathrm{p}}\neq\frac{4}{\beta\left(\hat{\mathrm{p}}_{\mathrm{i}}-\hat{\mathrm{p}}_{\mathrm{out}}\right)^{2}}$ and by (3.147) for $\hat{\mathrm{L}}_{\mathrm{p}}=\frac{4}{\beta\left(\hat{\mathrm{p}}_{\mathrm{i}}-\hat{\mathrm{p}}_{\mathrm{out}}\right)^{2}}$.

Considering the order of magnitude of pressure (§ 3.6.3) and membrane hydraulic conductivity (§ 3.6.4) in sieve tubes we always have that $\hat{\mathrm{L}}_{\mathrm{p}}>\frac{4}{\beta\left(\hat{\mathrm{p}}_{\mathrm{i}}-\hat{\mathrm{p}}_{\mathrm{out}}\right)^{2}}$, thus $\Xi < 0$.

3.6 Physiological Parameters

3.6.1 Sieve Tube Structure

Sieve elements are elongated with the longitudinal axis parallel to the bundle of vascular tissues. Their length is several to many times greater than their width, but both dimensions can vary considerably within the same plant and between species and genera. Typically, the sieve element length varies from 100 to 5000 μm while its width varies between 10 and 400 μm, for an approximately cylindrical shape (Esau, 1969; Parthasarathy, 1975). Therefore, for a sieve tube length, *L*, of 0.5 m we specified the following di-

mensions of the sieve tube elements: radius R = l0 μm; length l = 250 μm; with 0.5 as the fraction of sieve plate area composed of sieve plate pore area; sieve plate pore radius r_p = 0.23 μm; sieve plate pore length, which equals sieve plate thickness, l_p = 0.5 μm. With these dimensions the sieve plate impedance factor β (3.1) is 0.079, which accounts for the sieve plate contribution to the total sieve tube axial conductivity, (3.119).

3.6.2 Sap Viscosity

The phloem sap viscosity depends on both temperature and phloem sap chemical composition (proteins, sugars and other solutes). According to Chirife & Buera (1997) the viscosity of sugar solutions at a given temperature T is given by:

$$\mu(\varphi,\mathrm{T}) = \mu_0(\mathrm{T})\, a(\mathrm{T}) \exp\left(E(\mathrm{T})\, x_s\right) \tag{3.149}$$

where μ_0(T) is the viscosity of the solvent, in this case water, at absolute temperature T; x_s is the mole fraction of sugars and a(T) and E(T) are parameters depending on both temperature and sugar species. Fig. 3.2 shows viscosity of a sucrose solution as a function of sucrose concentration, C, for a temperature of 22 ^{o}C (295.15 K), μ_0 = 9.548×10^{-4} Pa.s (Streeter *et al*., 1998), where a = 0.905 and E = 57.19 (Chirife & Buera, 1997). However,

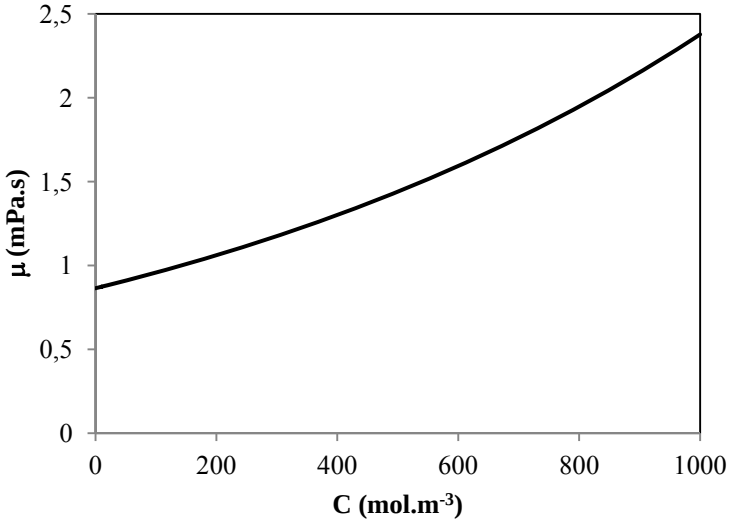

Figure 3.2 – Viscosity of a sucrose solution, μ, given by (3.148) as a function of concentration C.

for convenience, as mentioned in model assumptions (§ 3.1) we consider phloem sap viscosity as constant (μ = 1.5 mPa.s) for the range of sucrose concentration values expected to occur in sieve tubes, 300 to 900 mol.m^{-3} (Taiz & Zeiger, 1998).

3.6.3 Turgor Pressure

There are not many published results of phloem turgor pressure. Considering both the nature and location of phloem in the plant body, it is clearly difficult not only to get access but also to measure its turgor pressure without damage. The first measurement of turgor pressure in the phloem was by Buttery & Boatman (1964) for the laticiferous tissue of Pará rubber tree (*Hevea brasiliensis*). Although not belonging to the translocation pathway, the latex vessel system and sieve tubes are intimately associated elements so that the latex vessel system is considered part of the phloem tissue in *Hevea* and its turgor pressure was assumed to represent values in sieve tubes (Nicole *et al*., 1991). Buttery & Boatman (1964) obtained values ranging from 0.3 to 1.1 MPa using adapted manometers directly inserted in the bark. However, the first measurements of sieve tube turgor pressure (Hammel,1968) used an manometric device, improved from that of Buttery & Boatman (1964), and obtained values ranging from 0.83 to 3.06 MPa in the secondary phloem of red Oak trunk (*Quercus rubra*). Hammel (1968) also observed gradients in turgor and osmotic pressures, the pressures reducing at 0.07 MPa.m^{-1} and 0.03 MPa.m^{-1} respectively in the direction of flow from source to sink. However, those values were surprisingly low. According to the Münch hypothesis, higher values of turgor and osmotic pressure gradients were expected. Later improvements over the phloem needle technique of Hammels (1968) used pressure transducers in other species: 0.73 to 1.73 MPa in white ash trunk (*Fraxinus americana* L.) (Sovonick-Dunford *et al*., 1981); 0.2 to 1.2 MPa also in white ash (Lee, 1981a, b); 0.69 to 1.17 MPa in white ash and Manna ash (*Fraxinus ornus*) (Milburn, 1980); in smaller species, Sheikholeslam & Currier (1977a,b) measured 0.15 to 1.04 MPa turgor pressure in sieve tubes of squirting cucumber (*Ecballium elaterium*) stems. By using a pressure bomb and Bourdon-type gauge Milburn & Zimmermann (1977) measured pressures 0.12 to 0.76 MPa in coconut palm inflorescences (*Cocos nucifera* L.). Milburn (1980), using a glass-spiral pressure gauge, measured 0.9 to 1.09 MPa pressure in *Ricinus communis* sieve tubes. Wright & Fisher (1980) developed another direct way

of measuring sieve tubes turgor pressure using severed aphid stylets with attached capillary micromanometers to indicate pressure. With this method Wright & Fisher (1980) measured 0.79 MPa in sieve tubes of Babylon willow (*Salix babylonica*) stems and, later, 0.63 MPa in bark strips of sandbar willow (*Salix exigua*) (Wright & Fisher, 1983). Following Wright & Fisher (1980), Fisher & Cash-Clark (2000) measured 2.3 MPa in the peduncle of wheat. Following the same method, but with an on-line sensor, Gould *et al*. (2004) presented the second work on a smaller species sow thistle (*Sonchus oleraceus*) in which they measured sieve tube turgor pressures ranging from 0.4 to 1.2 MPa. In an indirect method, phloem turgor pressure was determined by Kaufman & Kramer (1967) from measurements of tissue water potential along with phloem sap osmotic pressure. Their values ranging from 0.39 to 0.56 MPa and turgor pressure gradients of 0.05 to 0.08 $MPa.m^{-1}$ in red maple (*Acer rubrum* L.) were in reasonable agreement with Hammel (1968). Using the same method, Rogers & Peel (1975) observed turgor pressure gradients of 0.05 to 0.27 $MPa.m^{-1}$ in stems of osier (*Salix viminalis*), and purple willow (*Salix purpurea*). Based on these findings, for our modelling purposes turgor pressure at entry to the system was set to $p_i = 1$ MPa.

3.6.4 Sieve Tube Membrane Hydraulic Conductivity, L_p

One of the main parameters describing membrane transport is the membrane hydraulic conductivity. There are not many data on the sieve tube membrane hydraulic conductivity, here represented by L_p. The first measurements, by Milburn (1974) on castor bean (*Ricinus communis* L.) bark segments, gave values between 5.7 and 8.8 $\times 10^{-14}$ $m.s^{-1}.Pa^{-1}$. Sovonick-Dunford *et al*. (1982) obtained a value of 9.6×10^{-15} $m.s^{-1}.Pa^{-1}$ for the sieve tube elements of secondary phloem of red oak stem (*Quercus rubra*). Wright & Fisher (1983) measured 5×10^{-15} $m.s^{-1}.Pa^{-1}$ on sandbar willow (*Salix exigua*) bark strips. Before these investigations, most phloem transport models used the hydraulic conductivity published for membranes of other types of plant cells. However, most of that work was for algal cells. Tyree's (1970) review found the membrane hydraulic conductivity for plant cells to range from 5×10^{-15} to 1×10^{-12} $m.s^{-1}.Pa^{-1}$. Thus, when compared with other cells, it seems that sieve tubes are at the bottom of that range. In this study, sieve tube membrane hydraulic conductivity, L_p, will be taken as 5×10^{-15} $m.s^{-1}.Pa^{-1}$.

3.6.5 Solute Permeability, P_s, and Reflection Coefficient, σ

Of all the biological parameters used to describe phloem transport, the reflection coefficient of sieve tube membrane to solutes, σ, and the membrane permeability to those same solutes, P_s, are the most difficult to determine. By assuming that membrane permeability is determined by the size and distribution of its pores, Kedem & Katchalsky (1958) showed that the membrane parameters P_s and σ should be related:

$$P_S = R_g T \frac{L_p}{\overline{V}_S}(1-\sigma) \tag{3.150}$$

$\overline{V}_S$ is the specific volume of the solute. To our knowledge there are no measurements of these parameters for the sieve tube element/companion cell complexes (SE/CC). Hence, one can only speculate from studies of other types of plant cells. Diamond & Wright (1969) presented an empirical relation between the parameters for non-electrolytes from experimental data of *Nitella mucromata* cells. Although they do not present any theoretical justification, the data show reasonably well that σ decreases closely in parallel with increasing permeability P_s. The permeability was smaller than 10^{-8} m.s^{-1} for σ greater than 0.8, and of the order of 10^{-5} m.s^{-1} for $\sigma \cong 0$. From a survey of experimental data on plant cells, Kargol *et al*. (1997) found a very good agreement with equation (3.150) in measurements from maize roots, but not with measurements from isolated cells *Nitella translucens*. Kargol *et al*. (1997) observed that the linear relationship of Kedem & Katchalsky agrees more with experimental data from artificial membranes. Kargol & Kargol (2000) showed a better agreement with experimental data when the right hand side of the Kedem & Katchalsky (1958) relation between membranes parameters (3.150) is multiplied by $\mathcal{K}$ = 0.021±0.015. Subsequently, Kargol (2001) showed that $\mathcal{K}$ depends on the solute concentration within the membrane: $\mathcal{K} = C_m \overline{V}_S$. However, as a first approach we will adopt the linear relationship (3.150) multiplying the right hand side by $\mathcal{K}$ = 0.031. From the physiological conditions in sieve tubes (Table 3.1), the solute permeability of the sieve tube membrane is given by:

$$P_S = 1.83\times10^{-9}\left(1-\sigma\right)\ (\mathrm{m.s^{-1}}) \qquad (3.151)$$

Hence P_S varies between 10^{-9} m.s^{-1}, for totally permeable membrane ($\sigma = 0$), and 10^{-11} m.s^{-1}, for an almost impermeable membrane ($\sigma = 0.99$).

3.6.6 Apoplastic Environment

Connor *et al*. (1977) and Legge & Connor (1985) measured vertical water potential gradients in mountain ash (*Eucalytus regnans* F. Muell.), between -0.007 and -0.034 MPa.m^{-1}, with increasing height. This agrees with the estimated range of -0.01 to -0.03 MPa.m^{-1} of the total water potential gradient necessary to drive transpiration stream in trees (Zimmermann & Brown, 1971). There are not many studies on solute concentrations in the stem apoplast. Minchin & Thorpe (1984) measured the sucrose concentration in the developing stem of bean (*Phaseolus vulgaris* L.) reducing from basal to apical ends with a gradient of 175 mol.m^{-4} approximately, giving 0.4 MPa.m^{-1}. Connor *et al*. (1977) also observed a reduction in the osmotic pressure with height in mountain ash, thus a decrease in solute concentration with increasing height, of 0.01 MPa.m^{-1}. Hence, taking the estimates of Connor *et al*. (1977) and Zimmermann & Brown (1971), the apoplastic water potential gradient, $\frac{d\Psi_{out}}{dz}$, will be 0.03 MPa.m^{-1} and the apoplastic concentration gradient, $\frac{dC_{out}}{dz}$, 0.01 MPa.m^{-1}, in our model. From these values we have that the apolastic pressure gradient, $\frac{dp_{out}}{dz}$, surrounding the sieve tube in will be 0.04 MPa.m^{-1}, taking the direction of flow from apical to basal ends.

3.7 Results

Equations (3.128), (3.130) and (3.95) are the coupled equations that we need to solve. As there is no analytical solution, these equations were transformed into a first order system of differential equations before we use the MathCad®15.0 differential equations solver routine to solve it (Appendix). The calculated zeroth order terms of concentration, $\hat{C}_0$, and turgor pressure, $\hat{p}_0$, and the first order term of turgor pressure, $\hat{p}_1$, and

their respective derivatives were then used to determine the average first order concentration term $\overline{\hat{C}_1}$ (3.134). Thus, the concentration profile was determined according to equation (3.59) and the sieve tube turgor pressure was then determined following (3.58). The average axial flow speed $\overline{\hat{v}_z}$ (3.57) was determined from $\overline{\hat{v}_{z0}}$ (3.63) and $\overline{\hat{v}_{z1}}$ (3.90). The radial water flow at the sieve tube membrane $\hat{v}_r\left(1,\hat{z}\right)$ (3.56) was determined from the boundary conditions (3.42) and (3.78). Once the concentration and velocity profiles were known, the average axial solute flux was determined according to (3.39) and the radial solute flux through the sieve tube membrane was determined according to boundary condition (3.44). Unless otherwise specified, the model parameter values of Table 3.1 were used:

Table 3.1 –Values of the physical parameters chosen to represent the phloem.

Parameter	**S.I. Unit**	**Value**
Apoplast pressure, $p_{out}(0)$	MPa	0.1
Apoplast solute concentration, $C_{out}(0)$	$mol.m^{-3}$	60
Apoplast osmotic pressure gradient, $\frac{d\Pi_{out}}{dz}$	$MPa.m^{-1}$	0.01
Apoplast pressure gradient, $\frac{dp_{out}}{dz}$	$MPa.m^{-1}$	0.04
Fraction of sieve plate area occupied by pores, α	—	0.5*
Initial flow speed, U	$m.s^{-1}$	1.7×10^{-4}
Initial turgor pressure, p_i	MPa	1.0
Initial sap concentration, C_i	$mol.m^{-3}$	600
Pathway length, L	m	0.5
Sap viscosity, μ	Pa.s	0.0015
Sieve plate pore radius, r_p	μm	0.23*
Sieve plate length, l_p	μm	0.5*
Sieve plate impedance factor, β	—	0.079*
Sieve tube element length, l	μm	250*
Sieve tube membrane hydraulic conductivity, L_p	$m.s^{-1}.Pa^{-1}$	5×10^{-15}
Sieve tube radius, R	μm	10
Sieve tube solute permeability, P_s	$m.s^{-1}$	10^{-10}

Sucrose diffusion coefficient, D	$m^2.s^{-1}$	4.6×10^{-10}†
Sucrose specific volume, $\overline{V}_S$	$m^3.mol^{-1}$	2.155×10^{-4}§
Temperature, T	^{o} C	22
Universal gas constant, R_g	$J.K^{-1}.mol^{-1}$	8.314
Water density, ρ_W	$kg.m^{-3}$	998

* Thompson & Holbrook (2003a)

† Phillips & Dungan (1993)

§ Eszterle (1993)

From the values reported in Table 3.1 we have that $\varepsilon = 2\times10^{-5}$ which makes the first order terms strongly dominate the expansions (3.56) to (3.59). The radial flow Reynolds number $\mathscr{Re} = 1.11\times10^{-3}$ and the Péclet numbers: $\mathscr{Pe}_r = 3.62$ and $\mathscr{Pe}_z = 1.81\times10^5$, which means that the diffusive component of the solute flux in the axial direction is practically negligible compared to the convective component. However this situation is not observed in the radial direction, as the convective flow is only about 4 times the diffusive flow. This shows the importance that diffusive processes (in this case passive) can have in solute exchange between the sieve tube and its surroundings, specifically when the convection flow is reduced. Note also that by definition, sieve tube pressure, $\hat{p}$, is not scaled to 1 or of the order of unity as with the other variables (3.33).

3.7.1 Semipermeable Membrane – The Effect of Radial Water Exchange

When there is no radial exchange across the sieve tube membrane, $L_p = 0$ and $\sigma = 1$, there is an analytical solution for the Navier-Stokes equation (3.3) for the steady state flow in which there is a constant pressure gradient along the pathway, due to viscous losses, given by:

$$\frac{dp}{dz} = -\frac{8\mu U}{\beta R^2} = \Gamma \tag{3.152}$$

The decrease in pressure is due to the viscous losses in the direction of flow and the velocity has the velocity distribution of Poiseuille flow which is parabolic in the radial di-

rection (Kundu & Cohen, 2008). In this special situation, the flow in the sieve tube is identical to the flow in a pipe and the average velocity in any plane normal to the direction of flow is constant with *z* and given by:

$$\bar{v}_{Poiseuille} = -\frac{\beta R^2 \Gamma}{8\mu} = U \tag{3.153}$$

For the more general case of a sieve tube limited by a semipermeable membrane in which there is only radial water exchange but no solute, $L_p \neq 0$ and $\sigma = 1$, the pressure gradient, $\frac{dp}{dz}$, is not constant, as suggested by equation (3.119), and the average zeroth order term of the axial velocity is given by (3.63):

$$\overline{v_{z0}}(z) = -\frac{\beta R^2}{8\mu}\frac{dp_0}{dz}$$

Comparing with equation (3.153) we obtain:

$$\overline{v_{z0}}(z) = \overline{v}_{z\,Poiseuille}\frac{\frac{dp_0}{dz}}{\Gamma} \tag{3.154}$$

Therefore, the deviation from Poiseuille flow, in a sieve tube limited by a semipermeable membrane, is a nonlinear dependence of the pressure profile on the axial coordinate, *z*. There is a pronounced non-linearity of pressure in the direction of flow (Fig 3.3A), with an increasing pressure gradient (curves b, d), compared with the constant linear decrease of pressure with distance, i.e. Poiseuille flow (curves a, c) (Fig. 3.3B). The presence of sieve plates, equivalent to a more viscous fluid (Henton *et al*, 2002; Weir, 1981), gives a greater pressure gradient for both cases of Poiseuille flow (3.152) and when there is radial water exchange (Fig 3.3).

Due to the concentration and pressure differences across the sieve tube membrane (C and p are higher than C_{out} and p_{out}) there is a water potential difference across the sieve tube membrane, $\Delta\Psi$, that draws water into the sieve tube ($\hat{v}_r$ is negative: Fig. 3.4B). As water moves into the sieve tube, conservation of mass for water requires that the average

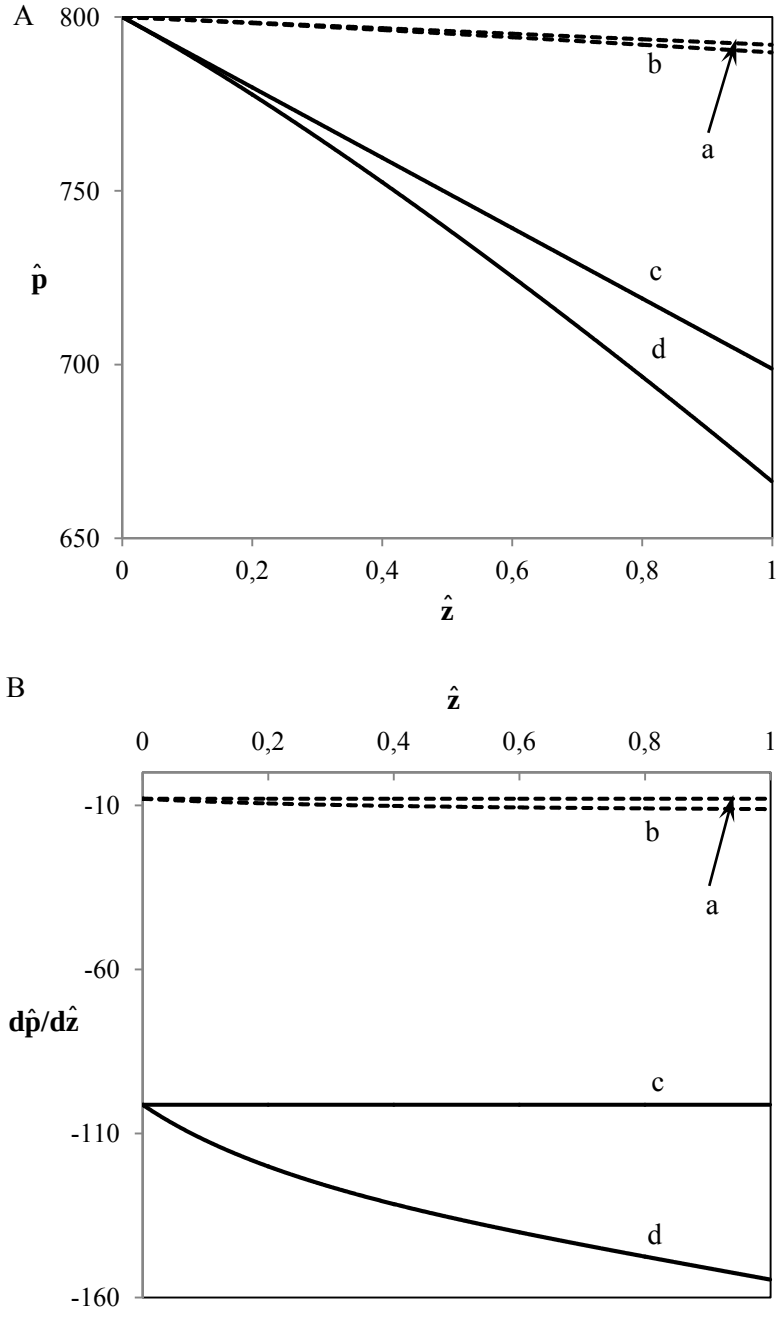

Figure 3.3 – Effect of water permeability on pressure (A) and pressure gradient (B) plotted versus axial position $\hat{z}$ with sieve plates present (——) and ignoring sieve plates (----). Curves: (a) and (c) – impermeable membrane, no water exchange ($L_p = 0$, $\sigma = 1$, Poiseuille flow). Curves (b) and (d) – flow within a sieve tube limited by a semipermeable membrane ($L_p \neq 0$, $\sigma = 1$).

axial velocity, $\overline{v_z}$, increases with distance, as opposed to the constant average axial velocity observed in Poiseuille flow, $\overline{v}_{Poiseuille}$ (3.153), (Fig. 3.4A). Consequently, as there is no solute flux across the membrane, conservation of mass for solute requires that concentration of solute decreases with distance (Fig. 3.5A) as the average axial velocity increases (Fig. 3.4A). Hence, the axial solute flux is kept constant, but with a decreasing concentration gradient (Fig. 3.5B). This is more pronounced for greater radial fluxes (Figs. 3.4B, 3.5B). The pressure gradient also increases and more so if sieve plates are present (Fig. 3.3B, curves b and d), which increase the axial sieve tube resistance (3.1, 3.119). As both concentration and pressure within the sieve tube decrease with distance so does the water potential difference across the sieve tube membrane (Fig. 3.4B). Note that the concentration difference across the membrane becomes smaller as the concentration inside the sieve tube decreases. The same occurs for the pressure difference across the sieve tube membrane, Δp. Hence, less water will flow into the sieve tube with distance. This decreasing radial influx of water with distance is favoured if sieve plates are present (Fig. 3.4B), as the decrease in both pressure (Fig. 3.3A) and concentration (Fig. 3.5A) is bigger with sieve plates present. However, the decrease in pressure observed (Fig. 3.3A) if one ignores sieve plates is sufficient to ensure that the water potential difference across the sieve tube membrane does not increase with flow. This explains why there is less water inflow in the absence of sieve plates (Fig. 3.4B). The effect of sieve plates is more visible, because the combined effects of a "higher viscosity" (§ 3.2) and an increase in velocity cause greater increases in the pressure gradient in the direction of flow. This effect is hardly apparent when neglecting the sieve plates.

3.7.2 Permeable Membrane – The Effect of Radial Solute Exchange

In the more realistic case of a membrane that is permeable to solutes as well as water ($\sigma < 1$), the effects of radial water flow in modifying the Poiseuille solution (as just discussed in § 3.7.1) are attenuated (Figs. 3.6, 3.7).The water influx, dependent on the water potential difference across the sieve tube membrane, which is highly influenced by the concentration difference across the sieve membrane, can be zero (Fig. 3.7B). From the boundary condition (3.18) we have that this water influx ($v_r < 0$) will continue as long as:

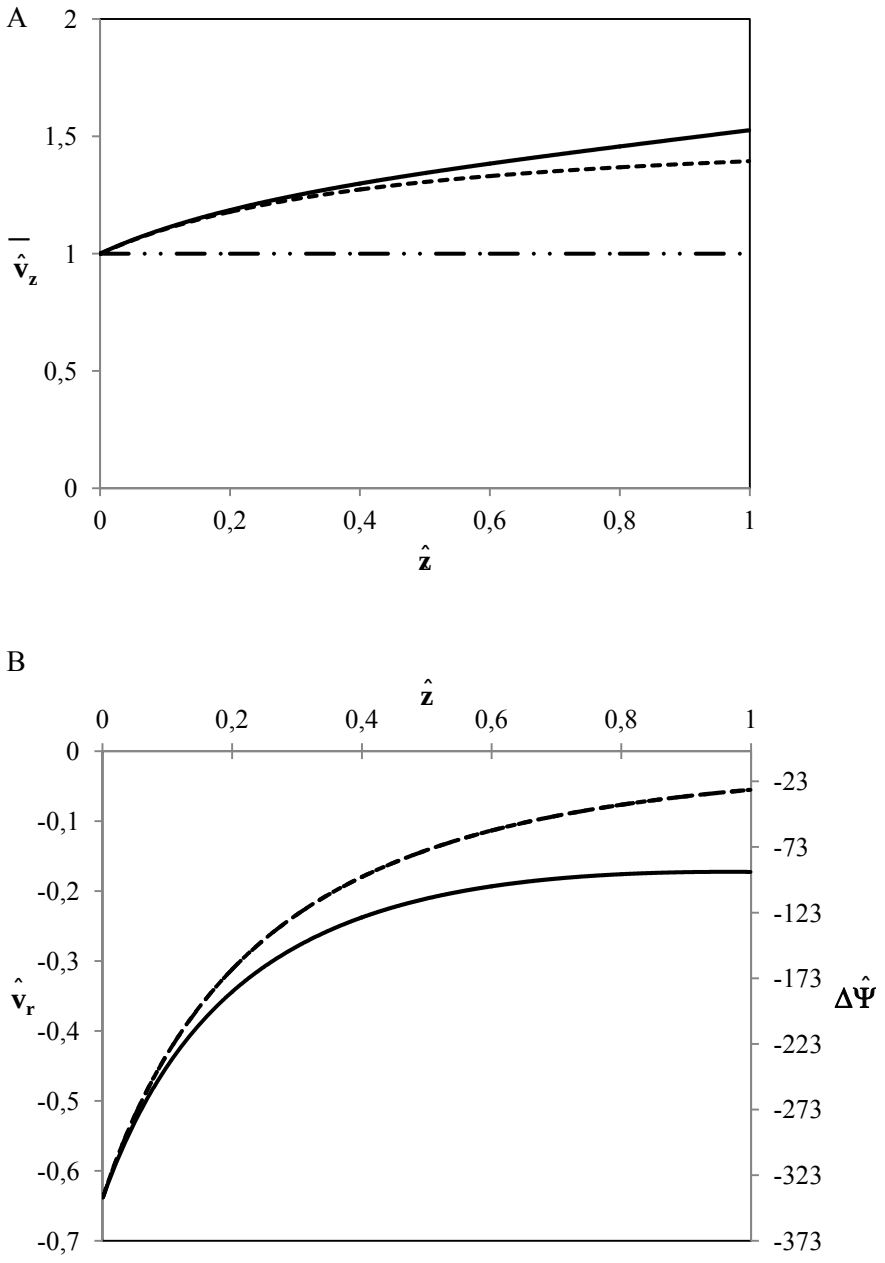

Figure 3.4 – Average axial velocity (A) and radial velocity and water potential difference across the sieve tube membrane (B) versus axial position $\hat{z}$ with sieve plates present (——) and ignoring sieve plates (----) for a flow within a sieve tube limited by a semipermeable membrane ($\sigma = 1$). In A the average axial velocity for the Poseuille flow regime (3.153) is also shown (–···–).

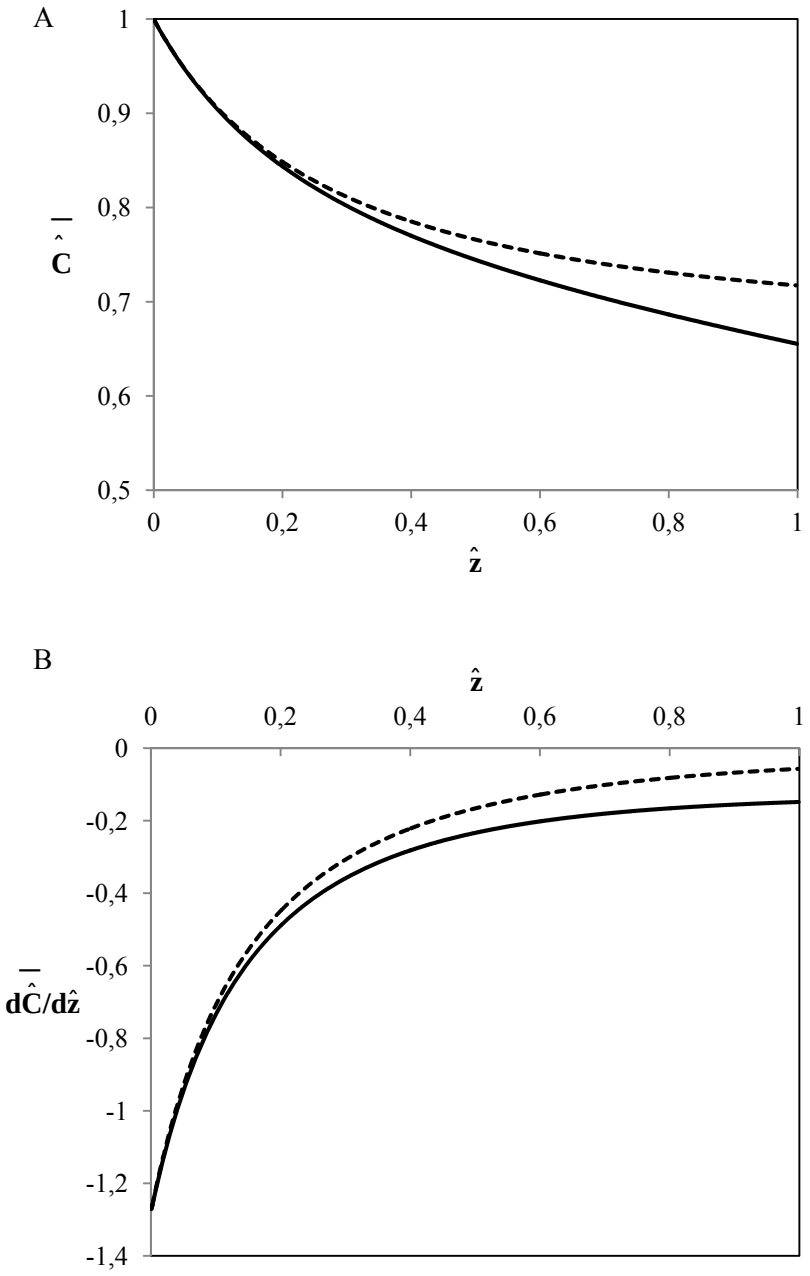

Figure 3.5 – Average concentration (A) and concentration gradient (B) versus axial position $\hat{z}$ with sieve plates present (——) and ignoring sieve plates (----) for a flow within a sieve tube limited by a semipermeable membrane ($\sigma = 1$).

$$\sigma > \frac{\mathrm{p}(R,z) - \mathrm{p}_{\mathrm{out}}(0) - \dfrac{d\mathrm{p}_{\mathrm{out}}}{dz} z}{\mathrm{R_g T}\left(\mathrm{C}(R,z) - \mathrm{C}_{\mathrm{out}}(0) - \dfrac{d\mathrm{C}_{\mathrm{out}}}{dz} z \right)} \tag{3.155}$$

For the normal physiological conditions (Table 3.1), i.e. for the order of magnitude of pressure and concentration expected for sieve tubes, we find that water influx into the sieve tube occurs only if $\sigma > 0.7$ (Fig. 2.7B). As the permeability of the membrane, P_s, increases with decreasing σ (3.150), the pressure gradient in the direction of flow becomes smaller (Fig. 3.6B). This trend arises from two factors that decrease the sieve tube solute concentration (Fig. 3.8). First, the dilution created by water influx, dependent on the water potential difference across the sieve tube membrane, as described before (§ 3.7.1). Second, the passive efflux of solutes across the sieve tube membrane that is dependent on the concentration difference between the sieve tube and the apoplast. The passive loss of solutes is favoured by the higher sieve tube solute concentration compared with the surrounding apoplast. The decrease in concentration as one moves further down the tube, means less water will come in, as the water potential difference across the sieve tube membrane decreases, and more so for the more permeable the membrane (Fig. 3.7B). Simultaneously, and for the same reasons, namely due to a decreasing pressure gradient, the increase in the axial velocity will also be less for more permeable membranes (3.7A) and the same for the axial solute flux (Fig. 3.9A). Due to the concentration difference across the sieve tube membrane there is solute efflux which increases for smaller values of the reflection coefficient, σ (leakier membrane) (Fig. 3.9B). However, the sieve tube membrane solute permeability, P_s, is in the order of 10^{-10} m.s^{-1} (3.150), thus too small to cause dramatic changes in the sieve tube concentration. As the permeability of the sieve tube membrane, P_s, increases with the corresponding decrease in the reflection coefficient, σ, the osmotic effect on water exchange due to the concentration difference across the membrane becomes less important. Eventually, for a very permeable membrane there is a reversal of water exchange and water will move out radially for $\sigma < 0.7$ (Fig. 3.7B). Consequently, the axial velocity will decrease as more water moves out radially (Fig. 3.7A). In its turn and due to mass conservation this will cause the solute concentration to increase as water is drawn out radially (Fig. 3.8). Simultaneously, the pressure inside the sieve tube decreases less and less, and eventually it will increase for

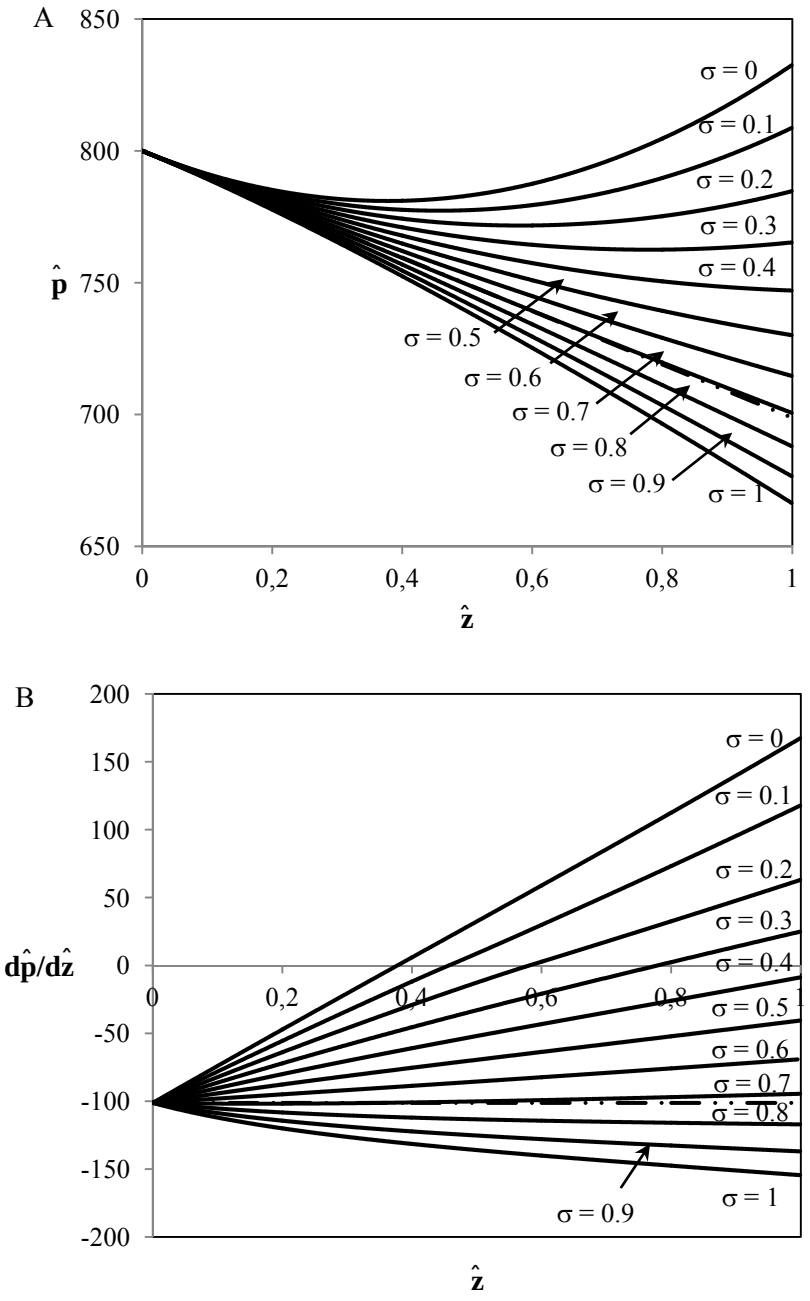

Figure 3.6 – Effect of solute permeability on pressure. Pressure (A) and pressure gradient (B) profiles with position $\hat{z}$ for phloem flow limited by a permeable membrane with different reflection coefficients and solute permeability (3.151) considering the presence of sieve plates. The pressure and pressure gradient profiles for the Poseuille flow regime (3.152) are also shown (–··–).

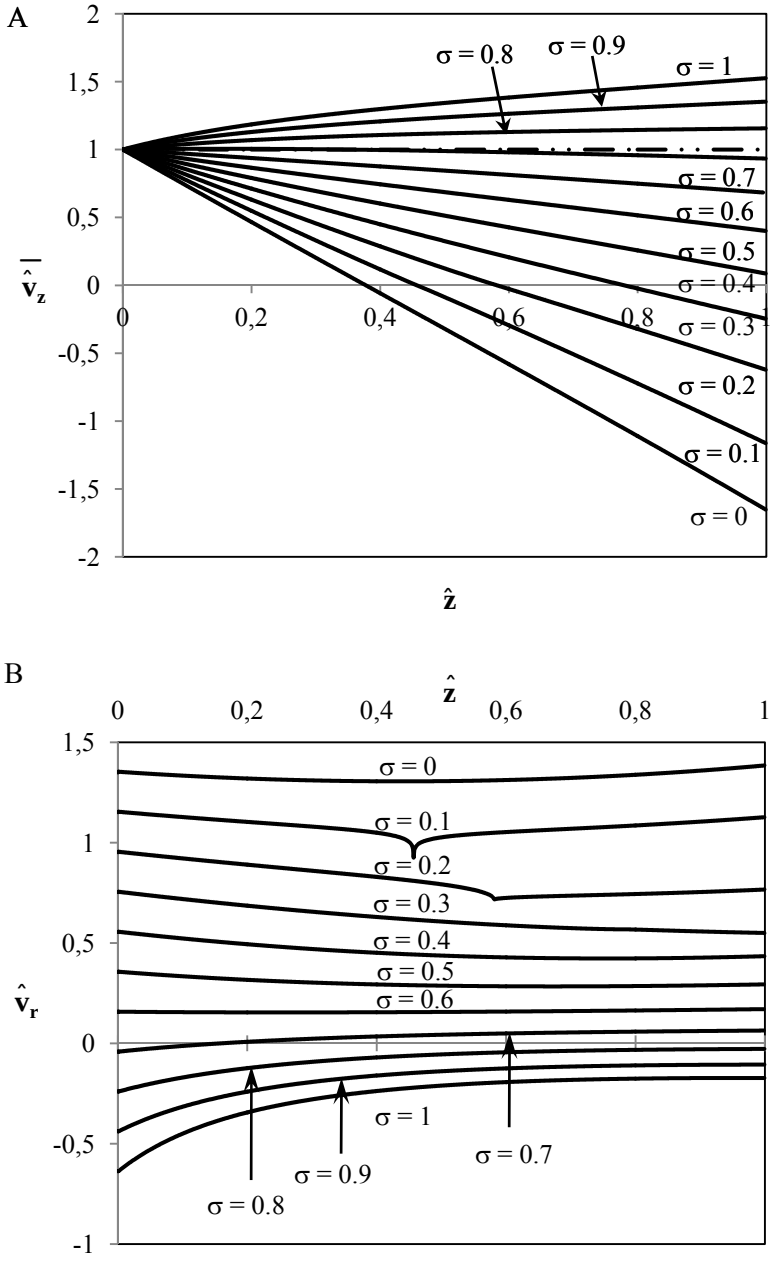

Figure 3.7 – Effect of solute permeability on velocity. Average axial velocity (A) and radial velocity (B) profiles with position $\hat{z}$ for phloem flow limited by a permeable membrane with different reflection coefficients and solute permeability (3.151), considering the presence of sieve plates. In A the average axial velocity for the Poseuille flow regime (3.153) is also shown (–···–).

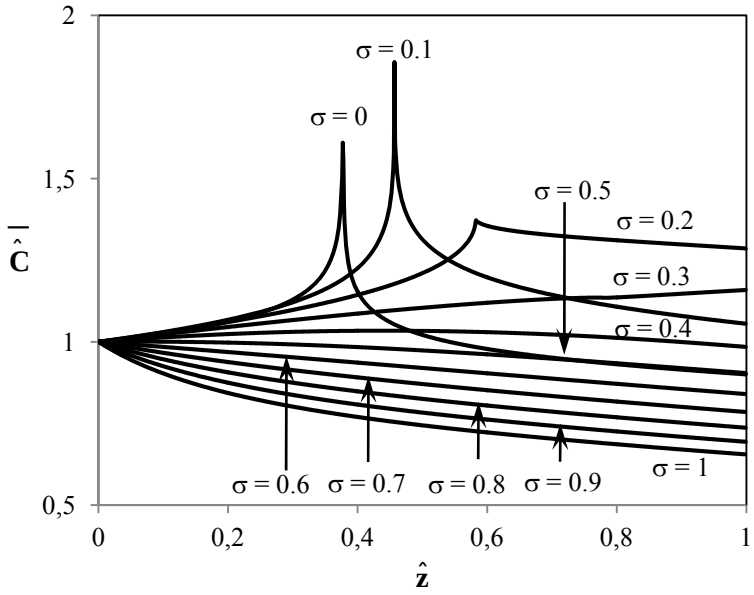

Figure 3.8 – Effect of solute permeability on sieve tube concentration: Average solute concentration profile with position $\hat{z}$ for phloem flow limited by a permeable membrane with different reflection coefficients, σ, and solute permeability, P_s, (3.151), considering the presence of sieve plates.

smaller values of σ so that flow converges from opposite directions. The axial velocity at one point becomes null (Fig. 3.7A) and the solute concentration be comes maximum (Fig. 3.8). Though there is a spike in concentration for smaller values of the reflection coefficient σ, the overall change is more pronounced for $\sigma < 0.2$ only. The occurrence of inflow from the opposite site is a logical conclusion based on the negative sign of the axial velocity beyond the point where it becomes null (Fig. 3.7A) (strictly speaking), and the magnitude is calculable without more information for the model boundaries at higher values of *z*. The extreme of this scenario is seen for $\sigma = 0$ in which the radial water exchange is solely driven by the pressure difference across the sieve tube membrane, and the solute flux is entirely through convection by the water movement across the sieve tube membrane, that dominates for smaller values of σ (3.18; Fig. 3.9B).

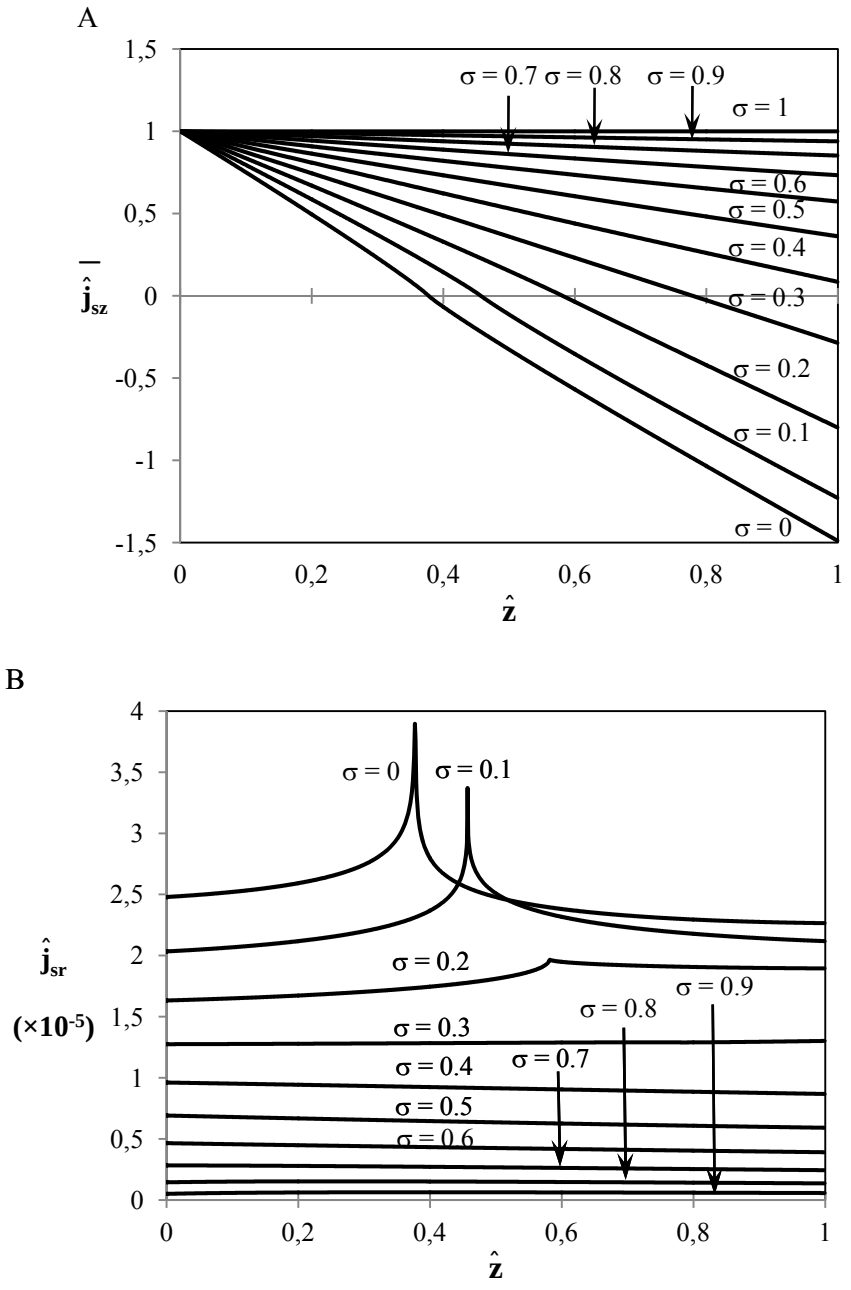

Figure 3.9 – Effect of solute permeability on solute flux. Average axial solute flux (A) and radial solute flux (B) profiles with position $\hat{z}$ for phloem flow limited by a permeable membrane with different reflection coefficients, σ, and solute permeability, P_s, (3.151), considering the presence of sieve plates.

3.7.3 Apoplastic Water Potential

The apoplast surrounding the phloem is considered to have a constant water potential in most phloem transport models; very few authors considered the more realistic situation of a water potential varying with height (e.g. Tyree *et al*. 1974). In Figs. 3.10 to 3.12 we compare transport within a modelled sieve tube being surrounded by water potential being constant, or with the linear gradient chosen for the calculations and simulations in previous sections, as in Table 3.1. In this last case, the apoplastic water potential increases in the direction of flow, giving simultaneous increase in pressure and in solute concentration in the apoplast. This scenario is common in plant stems, where the transpiration stream and phloem transport often, but not always, occur in opposite directions. The solute losses across the sieve tube membrane (§ 3.7.2) are small enough to allow more water to be drawn into the sieve tube surrounded by these water potential gradients (Fig. 3.11B). Nevertheless, for the pressure and concentration gradients in the apoplast of our model (Table 3.1) the differences in sieve tube turgor pressure between the two scenarios are negligible even when the apoplastic water potential gradient is doubled (Fig. 3.10). However, the effects of spatially varying the apoplast water potential are more evident in the axial and radial velocity changes (Fig. 3.11A, B) as well as in the sieve tube solute concentration (Fig. 3.12) when opposed to a constant water potential surrounding the sieve tube. These effects are more pronounced for greater gradients as the water potential difference across the membrane increases, thus driving more water radially through the sieve tube membrane. Consequently the same trend is observed in the sieve tube concentration following the changes in flow velocity (Fig. 3.12).

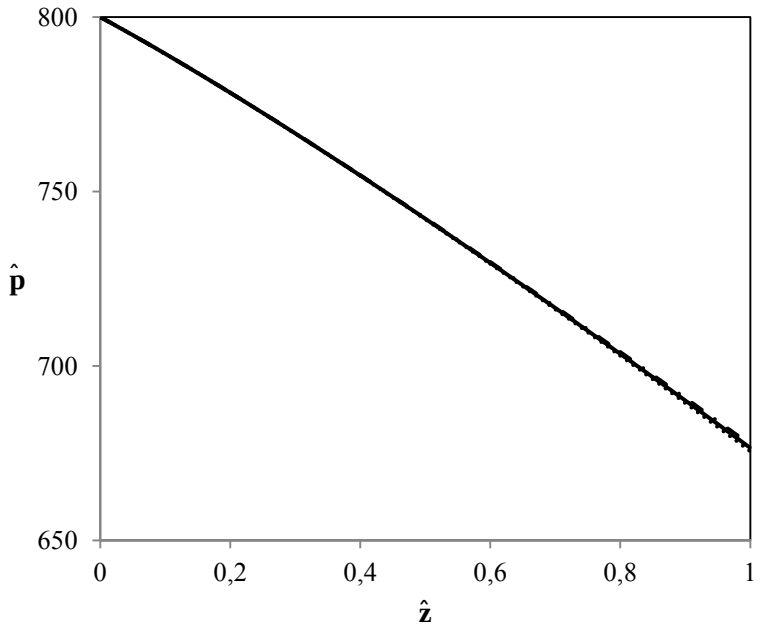

Figure 3.10 – Effect of an apoplast water potential gradient on the sieve tube pressure: pressure profile with position $\hat{z}$ for phloem flow limited by a permeable membrane ($\sigma = 0.9$), considering sieve plates with: a constant water potential (· ─ ·), a water potential gradient (——) (Table 3.1) and (----) a water potential gradient two times the values indicated in Table 3.1.

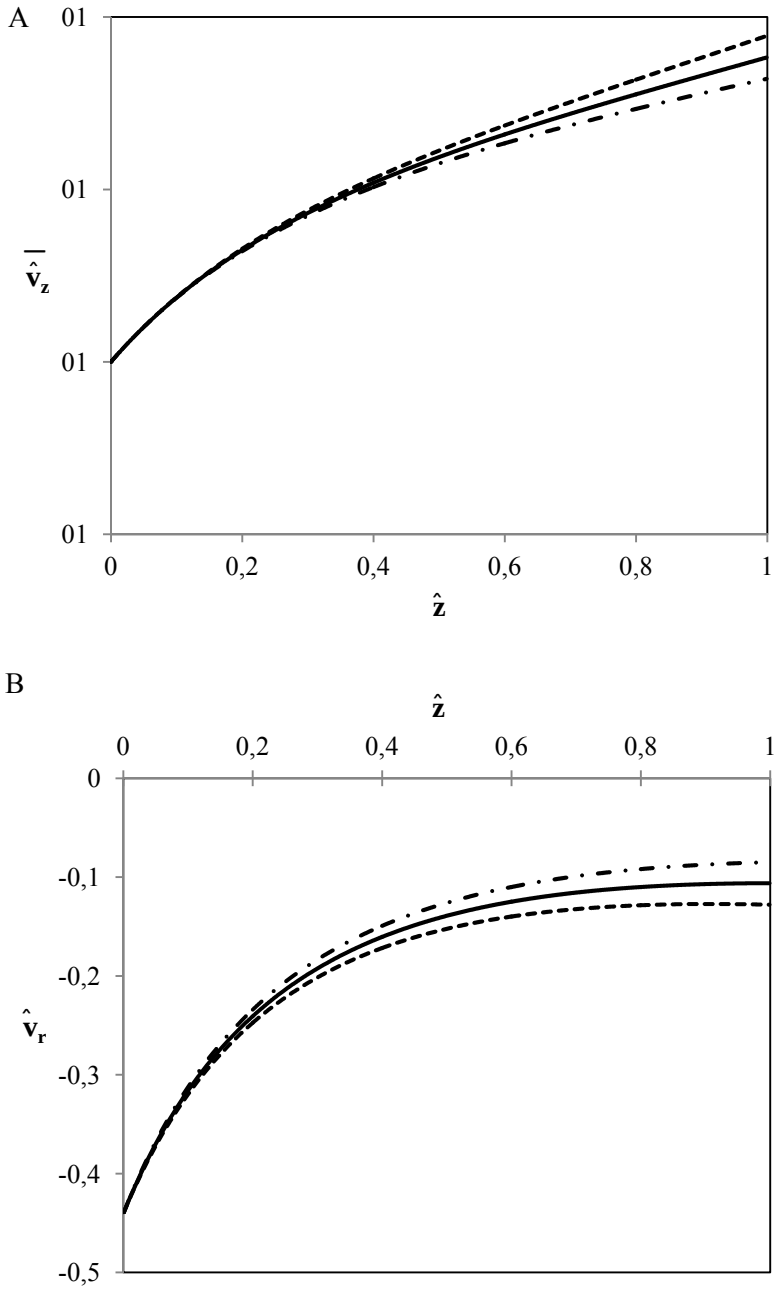

Figure 3.11 – Effect of an apoplast water potential gradient on velocity: average axial velocity (A) and radial velocity (B) profiles with position $\hat{z}$ for phloem flow limited by a permeable membrane (σ = 0.9), considering sieve plates, with: a constant water potential (· ─ ·), a water potential gradient (——) (Table 3.1) and (----) a water potential gradient two times the values indicated in Table 3.1.

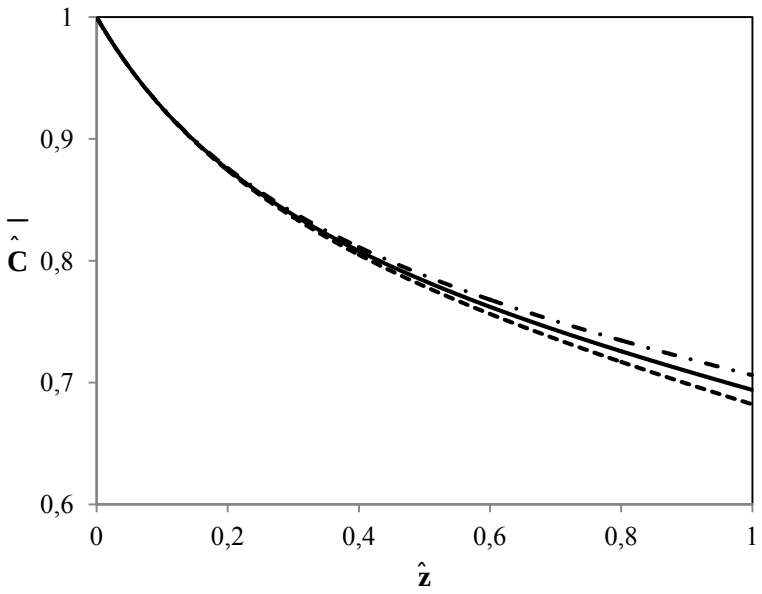

Figure 3.12 – Effect of a gradient in apoplast water potential on average solute concentration profile with position $\hat{z}$. The sieve tube membrane is permeable (σ = 0.9), and sieve plates are accounted for. Apoplast water potential is constant (· ─ ·); gradient of 0.03 MPa.m^{-1} (——) and (- - -) gradient of 0.06 MPa.m^{-1}.

4. Materials & Methods

4.1 Chemicals

All chemicals were purchased from Sigma (Sigma-Aldrich, Taufkirchen, Germany) with the exception of 4-(Chloromercuri)benzenesulfonic acid, sodium salt, PCMBS, that was purchased from TRC (Toronto Research Chemicals Inc., Canada) and silicon based dental impression materials Xantropren VL Plus, Optosil P Plus and Activator Universal for Optosil/Xantopren that were purchased from Heraeus Kulzer GmbH, Germany.

4.2 Plants and Growth Conditions

Wheat plants, *Triticum aestivum* L., were germinated in vermiculate and transferred into a nutrient solution 7 days after sowing. Plants were grown under 12/12 h day/night regime with a temperature period of 22/17 ^{o}C and relative humidity 60/80 %. Nutrient solution was a half-strength Hoagland solution, modified after Hoagland & Arnon (1950) consisting of 1 M KNO_3, 1 M $Ca(NO_3)_2$, 1 M $MgSO_4$, 1 M KH_2PO_4 and 10 µM KCl, 6.3 µM H_3BO_3, 0.4 µM $ZnSO_4$, 0.4 µM $MnSO_4$, 0.1 µM $NaMoO_4$, 0.1 µM $CuSO_4$ and 4 µM Fe-EDTA as trace elements buffered with 0.2 M 2-(N-morpholino)ethanesulfonic acid, MES, at pH 5.3. Nutrient solution was added twice a week and fully changed every two to three weeks. Plants were monitored every week for the formation of tillers that were subsequently removed.

Squash plants, *Cucurbita maxima*, Golden delicious orange variety, seeds purchased from Zaadhandel Jansen, Netherlands, were grown on standard professional pot soil mix, type Typ T Topferde, Einheitserde®, in a growth chamber at 500 to 600 $\mu mol.m^{-2}.s^{-1}$ photon fluency rate, in a 16/8 hour light dark period and 22/18 ^{o}C temperature period with a relative humidity of 60 %.

4.3 ^{11}C Labelling

The carbon isotope ^{11}C decays in a β^+ mode to the boron stable isotope ^{11}B, with a half-live of 20.38 minutes:

$$^{11}_{6}C_5 \rightarrow {}^{11}_{5}B_6 + \beta^+ + v_e + 0.96Mev$$

emitting in opposite directions two identical γ photons of specific energy 0.48 MeV after positron annihilation that will easily penetrate many cm of plant tissue. Detection of a ^{11}C-decay event is therefore possible either by measuring the beta particle directly, e.g. with a Geiger Muller tube, or by measuring one or both annihilation gammas (Thorpe, 1986; Thompson *et al*., 1979). The $^{11}CO_2$ was produced with a compact cyclotron (CV28) with the cooperation of the Institute of Nuclear Chemistry, in the Research Centre Jülich, according to a schedule determined by the medical applications for which the isotope was primarily used. $^{11}CO_2$ was then collected in a trap near the cyclotron and transported to the laboratory where the experiments were running.

Plants 6 to 8 week old were transferred to the climate chamber for acclimation where they were connected to the ^{11}C-labelling and closed circulating air system (Roeb *et al*., 1986b). This was done one day before the start of the ^{11}C labelling experiments to ensure that they had fully recovered from any mechanical disturbances occurred while preparing them for the experiments. For wheat, part of the flag leaf was sealed with a silicon based impression material Xantropren VL Plus in a cylindrical Plexiglas™ chamber (70 mm length and 18 mm diameter) (Fig. 2.1) while the squash load leaf was sealed in a Plexiglas™ chamber (20.8×21.2×3.2 cm) with silicon based impression material Optosil P Plus (Fig. 4.2). Plants were labelled three times with about 100 MBq $^{11}CO_2$ in air at 5, 7.5 and 10.5 h into the light phase.

NaI(Tl) scintillation detectors, for measuring annihilation γ-rays, were positioned within well radiation shielding to avoid incorrect detection of radioactivity, and to be uniformly sensitive to monitor well-defined parts of the plant (Figs. 4.1, 4.2). The counts were corrected for background, dead-time and their different sensitivities to equal amounts of tracer. Plants were treated for approximately 40 to 45 min during the second pulse of ^{11}C when tracer activity in the upper peduncle and the downstream internode

detectors in wheat and squash respectively were at maximum (i.e. equal rates of decay and arrival), being approximately 60 to 80 min after the start of labelling.

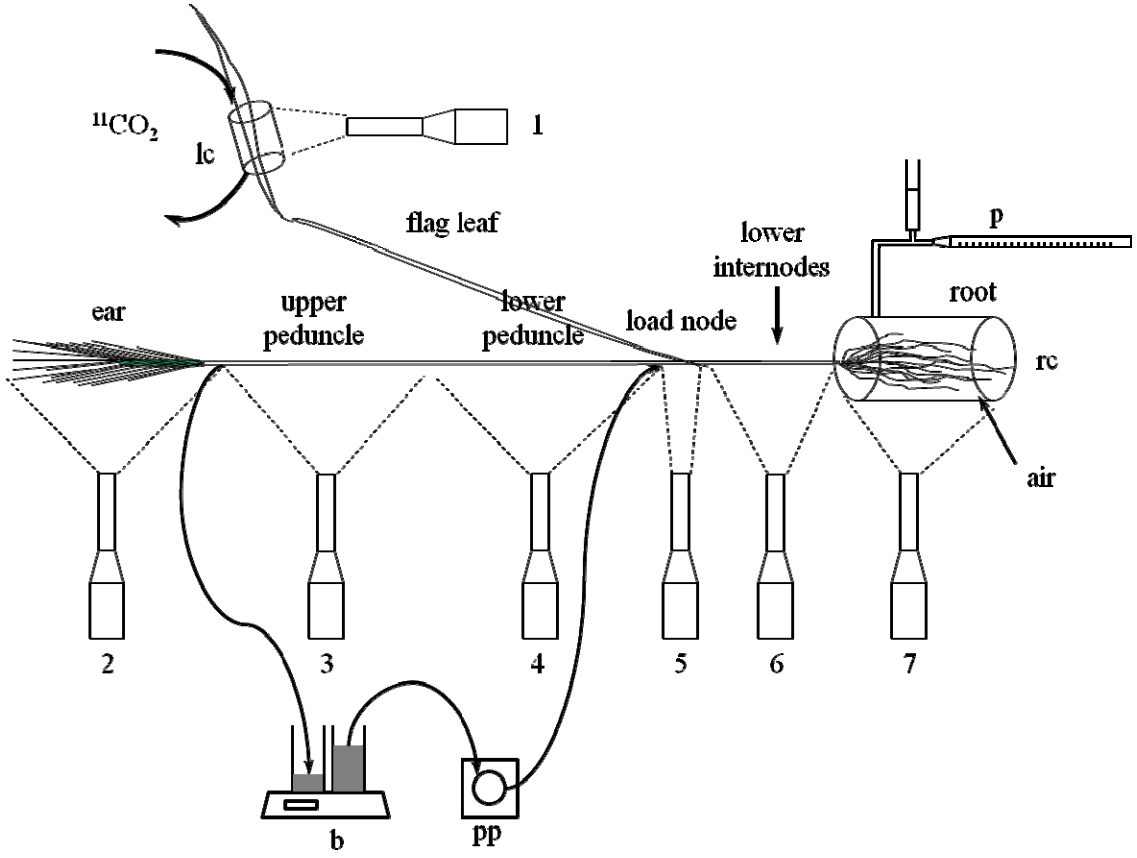

Figure 4.1 – Experimental setup for ^{11}C labelling, perfusion and water uptake measurement of wheat: b – balance; fl – flag leaf; lc – leaf chamber; p – potometer; pp – peristaltic pump; rc – root chamber; 1 to 7 scintillation detectors monitoring the different plant parts.

4.4 Stem Perfusion

Both the peduncle of wheat and the 6th internode of squash (counting from the apex) were perfused during experiments with apoplastic bathing solution (ABS): 1 mM Ca_2SO_4, buffered with 5 mM MES at 6.5 pH, as shown in Figs. 4.1 and 4.2 respectively, with a Gilson miniplus 2 peristaltic pump delivering 0.4 $cm^3.min^{-1}$. In the case of plants used for more than one time the plants were also perfused after the experiments and during the night until the next experiment. The perfusion system was set up as soon as the plants were placed in the climate chamber for acclimation. In the case of squash all leaves between the apex and the load leaf were removed, the internode below the load node was

steam girdled with a steam generator Ariete Vaporì jet 4102 so that all the ^{11}C-labelled photoassimilates would go towards the apex and the load leaf would be the only source supplying all regions between the load node and the apex. It was expected that the transpiration stream would not be affected by the stream girdle. Both the waste bottle and the solution bottle were placed on a Mettler Toledo XS205 analytical balance connected to a computer where the mass change was monitored in 1 minute time intervals with a LabVIEW 8.5 program. To prevent any leakage, the hypodermic needles (0.9x40mm), connecting the perfusion tubing, were sealed to plants with silicon based impression material Xantropren VL Plus. Water uptake into the plant ($mg.cm^{-1}.min^{-1}$) was determined from the slope of the solution mass change monitored from the analytical balance and expressed per unit length of the perfused region.

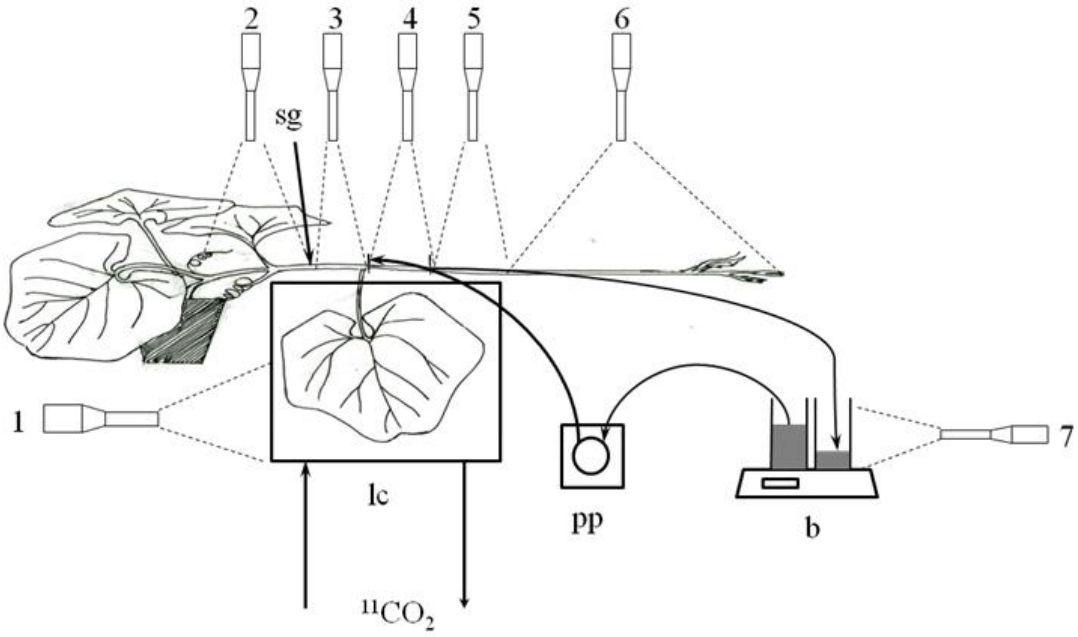

Figure 4.2 – Experimental setup for ^{11}C labelling and perfusion of squash stem: b – balance; lc – leaf chamber; pp – peristaltic pump; sg – steam girdle; 1 to 7 scintillation detectors monitoring the leaf chamber (load zone), lower internodes, load node region, perfused internode, downstream internodes, apex and waste solution bottle.

4.5 Chilling Experiments

The perfusion set up system (Fig. 4.2) was adapted to perform cold block treatments on squash perfused internode. Water at room temperature was pumped by the peristaltic pump to bathe 2 cm of the squash at the middle of 6th internode sealed in half a cylindrical Plexiglas™ chamber (20 mm length and 18 mm diameter). Switching from room temperature water to cold water and vice versa gave a temperature change of the water around the stem in less than one minute.

4.6 Wheat Root Water Uptake

Root water uptake was measured for wheat with a potometer built from a 1.00 ml volumetric pipette. The wheat root was constantly aerated in the root chamber (Fig. 4.1) but for approximately 30 minutes the air supply system was disconnected so that it would not interfere with the potometer measurements. The position of the meniscus was monitored at regular time intervals. A 5 ml syringe connected to the pipette via a T-valve was used to re-position the meniscus intermittently, and to remove any air bubbles.

4.7 Humidity Control in the Squash Leaf Chamber

Due to the high transpiration from the large area of mature squash leaves, a second dehumidifying system was necessary to prevent condensation in the tubing or leaf cuvette. As Fig. 4.3 shows, air was circulated using a Wiese pump in a secondary gas loop first to the leaf chamber, flowing then into a dehumidifier, immersed in a Julabo F32-EH laboratory water bath set at 2 ^{o}C. From there a second copper tube allowed the dry air to warm up again to the climate chamber temperature. With this system the air inside squash leaf chamber had no condensation.

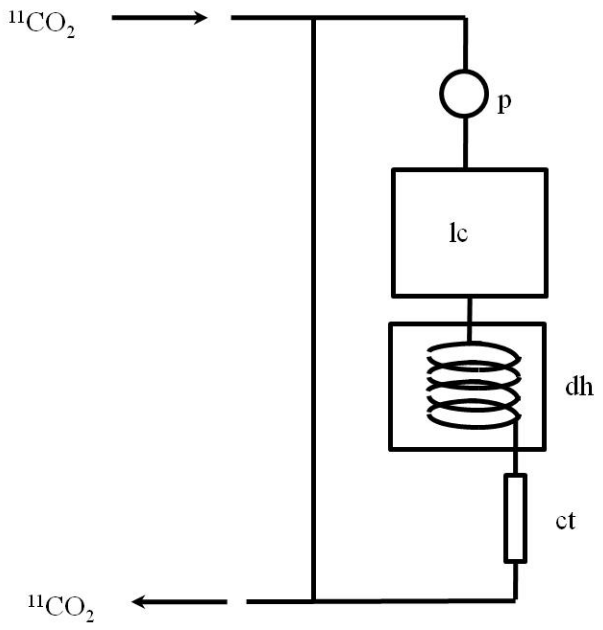

Figure 4.3 – Dehumidifying system for the squash leaf chamber: ct – copper tube; dh – dehumidifier; lc – leaf chamber and p – flat valve gas pump.

4.8 Solution Osmolality

Perfusion solution osmolalities were measured at room temperature (≈ 22 ^{o}C) from their freezing point, using a Fiske® Model 210 Micro Osmometer.

4.9 Light Microscopy

All tissue samples were freehand fresh tissue sections prepared without fixation and observed with a Zeiss Axiophot-2 light microscope. Sections of the 6th internode (counting from the apex) of squash stem were stained with toluidine blue O (a metachromatic dye) and alternatively doubled stained with safranin (which stains red for lignified cell walls) and astra blue (which stains blue for cellulosic cell wall material). Sections from wheat peduncle were stained with Astra Blue. Tissue cross section areas were determined using ImageJ version 1.37a software, from the National Institute of Health, USA.

Both the 6th squash internode and wheat peduncle were injected with approximately 2 ml of a 10% (v/v) fluorescein water solution and let to rest for approximately 10 minutes. Afterwards they were cut and flushed with deionised water and fresh tissue samples were manually sectioned for light microscopy.

4.10 ^{11}C Data Analysis

4.10.1 Input-Output Analysis

For this study, the plants were exposed for a short time to a varying amount of $^{11}CO_2$ by pulse labelling one leaf repeatedly three times during the day. The exported tracer carbon, resulting from photosynthesis from the load leaf (photoassimilates) can be followed as it is transported throughout the plant body by monitoring the tracer that has moved into a well defined part of the plant. The field of view of each detector monitoring tracer movement was defined by the detector collimation which in this study was done by using lead and tungsten blocks defining the geometry presented in Figs. 4.1 and 4.2. Sink detectors are designed to only have tracer moving into their field of view, with the only losses being from isotope decay and respiration of the labelled compound. Sink detectors give a measure of the total tracer that has flowed into their field of view, which is the integral of the flow into this region. It is not necessary to use a single detector to obtain the sink counts, as several detectors activities can be summed, once the observed counts have been corrected for any differences in detector sensitivities.

In order to study tracer movement in a wheat peduncle, the detector geometry was therefore arranged has shown in Fig. 4.1 where the total exported tracer from the load leaf into the rest of the plant is given by the sum of the activities of detectors 2 to 7. The apically transported tracer, the input to the peduncle, can be obtained by summing the 2, 3 and 4 detectors activities. The peduncle output is simply detector 2, the ear activity. The basally transported tracer, to the wheat vegetative part, is given by the sum of 6 and 7 detectors activities.

The detector geometry used with squash is represented in Fig. 4.2. As with wheat, the perfused internode, has input given by summing detectors 4, 5 and 6 activities, while output is given by summing detectors 5 and 6. The downstream internode (detector 5)

output is simply detector 6 which monitors the plant apex as a terminal sink. The load node has input given by summing up detectors 3 to 6 activities, while its output is given by summing detectors 4 to 6 activities.

This data set is used to identify the best quantitative description of the change in shape of the input profile caused by the transport system to produce the output profile. This method is called input-output analysis. Using the mathematical theory of discrete time systems developed for sampled data (Cadzow, 1973), the ^{11}C radioactivity measurements for each transport pathway can be described by a linear difference equation for discrete time observations (Minchin, 1978; Minchin & Troughton, 1980; Minchin & Thorpe, 2003):

$$y_k = -a_1 y_{k-1} + b_j u_{k-j} \tag{4.1}$$

in which the output activity at a given time k of a well defined plant part, y_k, is a function of the previous output activity at time k–1, y_{k-1}, and of the input activity, u_{k-j}, at a time k–j, being j the time delay between the arrive of a given input and its output from the system. Therefore the time delay depends not only on the length of the phloem pathway involved, but also on its intrinsic processes affecting phloem transport. The sampling interval for radiation counting was of 1 minute and of 0.5 minutes in chilling experiments. For modelling purposes the sampling interval was of 5 minutes so that the system can be well described by (2.1) (Minchin & Troughton, 1980). Phloem translocation was described by three parameters, a_1, b_j and j the time delay observed in the transport system (Minchin & Troughton, 1980). Following the algorithm of Minchin & Troughton (1980), model parameters a_1, b_j and j were estimated for every ^{11}C labelling pulse.

From these parameters, the system gain, G, defined as the output for a constant unit input (Minchin & Troughton, 1980) was calculated:

$$G = \frac{b_j}{1 + a_1} \tag{4.2}$$

Therefore, the loss of tracer within the transport system is 1–G. Computing the loss of tracer for each plant part studied we obtain the partitioning of tracer, i.e. the distribution of photoassimilate between the different regions of the plant. Assuming that the net

leakage of photoassimilate per unit length of phloem at position *x* is proportional to the photoassimilate, *P*(*x*), within the sieve tubes from mass conservation we have that:

$$\frac{dP}{dx}(x) = \alpha_{\mathrm{T}} P(x) \tag{4.3}$$

From which we obtain:

$$P(x) = P(0)e^{-\alpha_T x} \tag{4.4}$$

The net leakage of a given length L is:

$$\int_0^L \alpha P(x)dx = \int_0^L \alpha P(0)e^{-\alpha_T x}dx = P(0)\left(1-e^{-\alpha_T L}\right) \tag{4.5}$$

The fractional gain that we obtain from the input-output analysis of tracer profiles is:

$$\mathrm{G} = \frac{P(0)-P(L)}{P(0)} = e^{-\alpha_T L} \tag{4.6}$$

Hence, the fractional net loss of tracer per unit length, α_T (%.cm^{-1}), is given by:

$$\alpha_T = -\frac{\ln(\mathrm{G})}{L} \tag{4.7}$$

in which *L* is the transport system length.

The average transit time, t, for tracer to move through the system length L is given by:

$$\mathrm{t} = \mathrm{T}\left(\frac{\mathrm{j}-\mathrm{a}_1}{1+\mathrm{a}_1}\right) \tag{4.8}$$

where T is the sampling interval defined for modelling. Hence the average translocation speed given by input-output analysis is simply given, by definition, as *L*/t.

4.10.2 Translocation Speed

Translocation speed, the speed at which tracer moves throughout the plant body, was also determined from the half-maximum activity transit time according to Ferrieri *et al*. (2005). To infer the transit time, the time of half-maximum activity was estimated from the time of the maximum of the transform of the input activity decay-corrected data given by:

$$A^{*}(t) = \frac{A_{maximum}}{2} - \left| \frac{A_{maximum}}{2} - A(t) \right| \qquad (4.9)$$

being the maximum activity $A_{maximum}$ the average of several activity values A(t) at the end of the pulse. Equation (2.4) simply gives the inflection point of the activity decay corrected curve at which time one assumes the passing of the front of the pulse. From the times that one observes the maximum $A^{*}(t)$ and having the length of the detection region monitored, L, one gets the average translocation speed of tracer.

4.10.3 Tracer Influx Rate

The tracer influx rate, which gives the accumulation of tracer into a given plant part at each time, was derived from linear regression for the 9 observations centred at that time (4 before and 4 after) which gives the slope of the decay- and background-corrected curves. The influx rate at each time during treatment and during the 20 minutes after treatment removal was then compared with the average tracer influx rate for the 10 minutes before treatment application, giving the relative tracer influx rate.

5. Results

5.1 Solute Penetration into Vascular Bundles through Perfusion

For a better understanding of solute and water exchange processes between the phloem and the surrounding tissue, fluorescein was used as tracer to investigate the penetration of the perfusion solution into the tissue surrounding the air-filled pith cavity of the species studied.

5.1.1 Wheat

There was an extensive radial and uniform penetration of fluorescein (Fig. 5.1A, Fig. 5.1B), that goes beyond the immediate parenchyma cell layers surrounding the pith cavity and diffuses everywhere within the tissue, except for the chlorenchyma regions close to the epidermis (Fig. 5.1B).

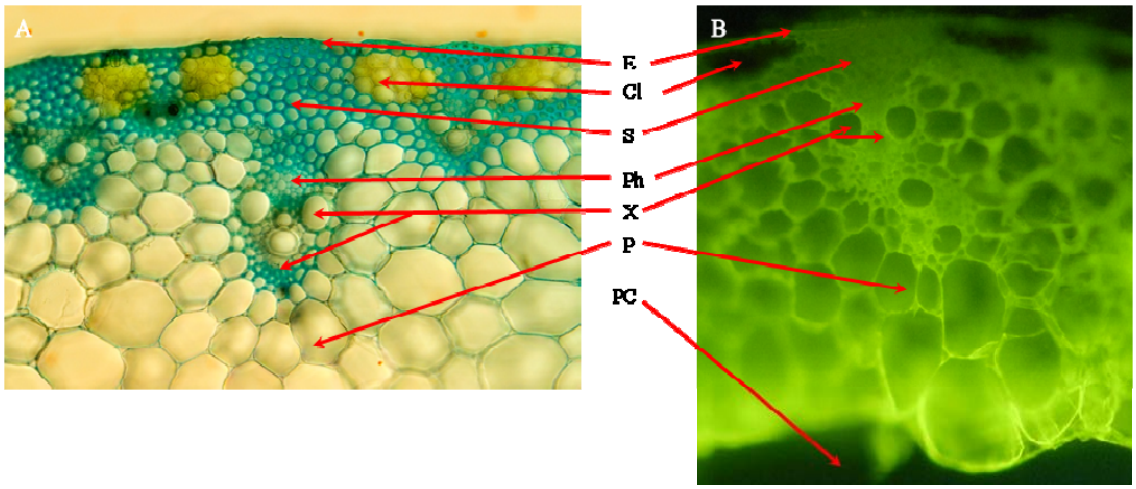

Figure 5.1 – A – Vascular bundles of exposed peduncle of wheat (*Triticum aestivum* L.) peduncle stained with astra blue. B – Fluorescein penetration from the pith cavity through the exposed internode of the wheat peduncle. Both samples are from fresh tissue manually sectioned without

fixation. Cl – chlorenchyma; E – epidermis; P – ground parenchyma; PC – pith cavity; Ph – phloem; S – schlerenchyma; X – xylem (composed of large vessels and narrower tracheids with thick cell walls).

5.1.2 Squash

The relative cross section areas of vascular bundles, phloem and sieve tubes of squash (*Cucurbita maxima*) stems were estimated using the methodology of Braune *et al*. (1999) and Peterson *et al*. (2008). Toluidin staining and alternatively safranin and astra blue double staining were used in fresh tissue samples, manually sectioned and non-fixed, from the 6th internode (the perfused internode) of 3 different 7 week old plants. Toluidin is a very useful general stain for studying plant tissues that produces a range of colours depending on the binding sites in the tissue. Cell walls containing pectic substances stain pink to reddish purple while those containing lignin stain various shades of blue or green. Safranin stains red for lignified cell walls and astra Blue stains blue for polysaccharides of the cell wall such as cellulose and pectins. As Figs. 5.2B and 5.3B show the lignified cells walls occur mostly in the central area of the bundle including the xylem vessels. The pith cavity occupies 19.8 ± 1.8 % of the total stem cross section area, while the 10 vascular bundles compose 8.3 ± 1.8 % of that same area. *Cucurbita maxima* is a classical example of a bicollateral type of vascular bundles (Fig. 5.2). The phloem distributes in external and internal phloem surrounding the central xylem vessels and between the two types of tissues there is interfascicular (or vascular) cambium (Fig. 5.2B). There is another sieve tube network, not associated with xylem, extrafascicular phloem, distributed both axially and longitudinally, mainly imbedded in the ground parenchyma and surrounding the vascular bundles. As indicated in Table 5.1 the external phloem region is not much bigger than the internal phloem, both making up little more than 53 % of the bundle cross sectional area. Note that these values for phloem include sieve tubes and their associated parenchyma cells with both their respective lumen and cell walls. The percentage of sieve tube lumen cross section of the total phloem area in both phloem fascicles differs only a little. It is bigger in the external phloem which is compatible with their larger lumina, comparing with the sieve tubes lumina of the internal phloem. From these results we find that sieve tube lumina comprise about 14 % of the bundle cross sectional area, consequently making approximately 1 % of the stem cross section area.

Fig. 5.3A shows the different areas of the vascular bundles of squash stem internode. There was an extensive radial and uniform penetration of fluorescein that diffused past the parenchyma cell layers surrounding the air-filled pith cavity and penetrated mainly into the internal phloem region and into the xylem vessels in the central part of the vascular bundle (Fig. 5.3A). A lesser amount penetrated the external phloem and cells beyond. This result shows that in squash, as in wheat, dye entered all vascular bundles in the stem (Fig. 5.1B). Therefore, for smaller solutes than fluorescein molecule, such as sugars, the internode anatomy and tissue structure are not expected to be a barrier to penetration and radial diffusion. This perfusion method offers a way of directly affecting phloem transport by simultaneously modifying the apoplastic environment surrounding the generally so well-protected phloem system in plants.

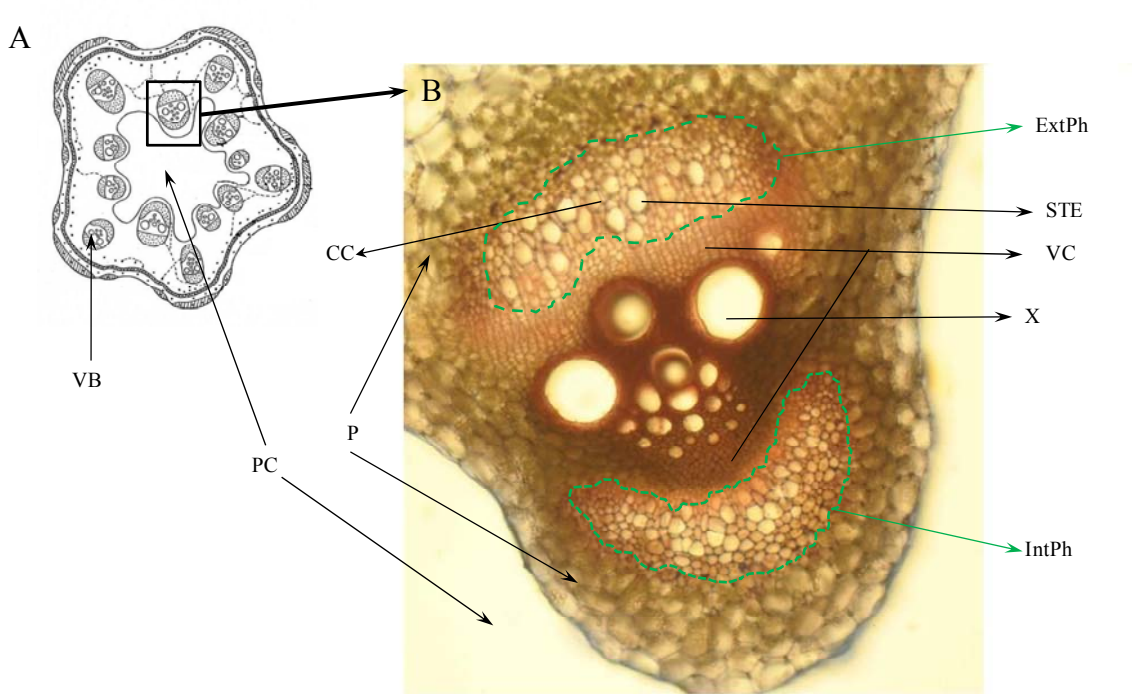

Figure 5.2 – A – *Cucurbita maxima* stem cross section (in Evert & Eichhorn, 2006): VB – vascular bundle. B – External and internal phloem regions of squash (*Cucurbita maxima*) stem vascular bundle doubly stained with safranin and astra blue. Samples are from fresh tissue manually sectioned without fixation: CC – companion cell; ExtPh – external phloem; IntPh – internal phloem; P – ground parenchyma; PC – pith cavity; STE – sieve tube element; VC – vascular cambium; X – xylem.

Table 5.1 – Cross sectional areas of phloem given as percentage of the total vascular bundle cross sectional area, and of sieve tubes given as percentage of the total phloem area. Values refer to means ± SE over 15 samples (5 samples from each of 3 different plants) from the perfused internode. Samples were prepared as indicated in Figs. 5.2 and 5.5.

		$\frac{\text{Phloem}}{\text{Vascular Bundle}}$	$\frac{\text{Sieve Tubes}}{\text{Phloem}}$
% Cross Sectional Area	External Phloem	29.1 ± 4.2	25.6 ± 5.8
	Internal Phloem	25.9 ± 0.8	21.6 ± 4.3

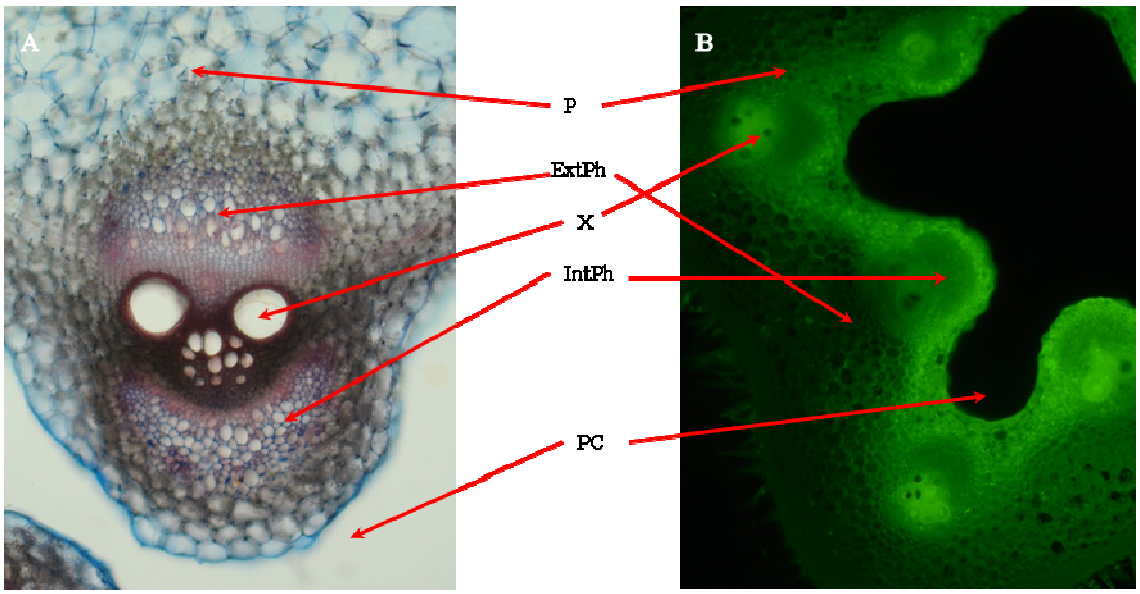

Figure 5.3 – A – Squash stem vascular bundle stained with toluidine blue. B – Fluorescein penetration and radial diffusion through squash stem internode. Both samples are from fresh tissue manually sectioned without fixation: ExtPh – external phloem; IntPh – internal phloem; P – ground parenchyma; PC – pith cavity; X – xylem.

5.2 Typical ^{11}C data for control experiments

Fig 5.4 shows a typical activity profile for the ^{11}C labelling experiments (§ 4.3). The ^{11}C activity is presented for each monitored region in a control experiment for a squash plant perfused with the apoplastic bathing solution (ABS). Following the three daily pulse applications, indicated by the gas detector, tracer accumulates in the load leaf. Subsequently, photoassimilates are transported to all remaining plant parts sequentially from the load node region to the apex, with a very small amount travelling towards the root through the lower region (Figs. 5.4 B, C). The amount of tracer heading towards the root was indeed very small, as the noisier data in Fig. 5.5 suggest. This proves the efficiency of the previous steam girdle treatment. It was observed (not shown here) that if the lower leaves were cut off then there was no activity in the lower internodes, indicating that the tracer moving into that part of the plant was through the xylem stream. Note that the perfused internode becomes a second source of water for the plant. Therefore, after removal of all the leaves downstream of the load node, we assume that the xylem stream in the perfused internode and load node moved mostly towards the lower internodes where the remaining leaves were located (Fig. 5.4A). Therefore, it is most likely that any tracer unloaded into the apoplast in the load node, and eventually in the perfused internode, will end up being transported through the xylem towards the root. This confirms that the steam girdle stopped phloem flow, and also shows that xylem transport continued across the steam girdle.

5.3 Influx of Tracer and Tracer Transport Speed

From the decay- and background-corrected data it is possible to determine tracer accumulation rate (influx rate) in a given plant region and from that to get an idea of the tracer transport speed and the direction in which tracer moves (§ 4.10.2, 4.10.3). Adding up the decay-corrected activity from the detectors monitoring different plant parts gives the total activity of tracer that has flowed into that region of the plant. Adding together the data collected from the apex, the downstream internode and the perfused internode we obtain the activity in the whole plant region downstream of the load node. Basically it

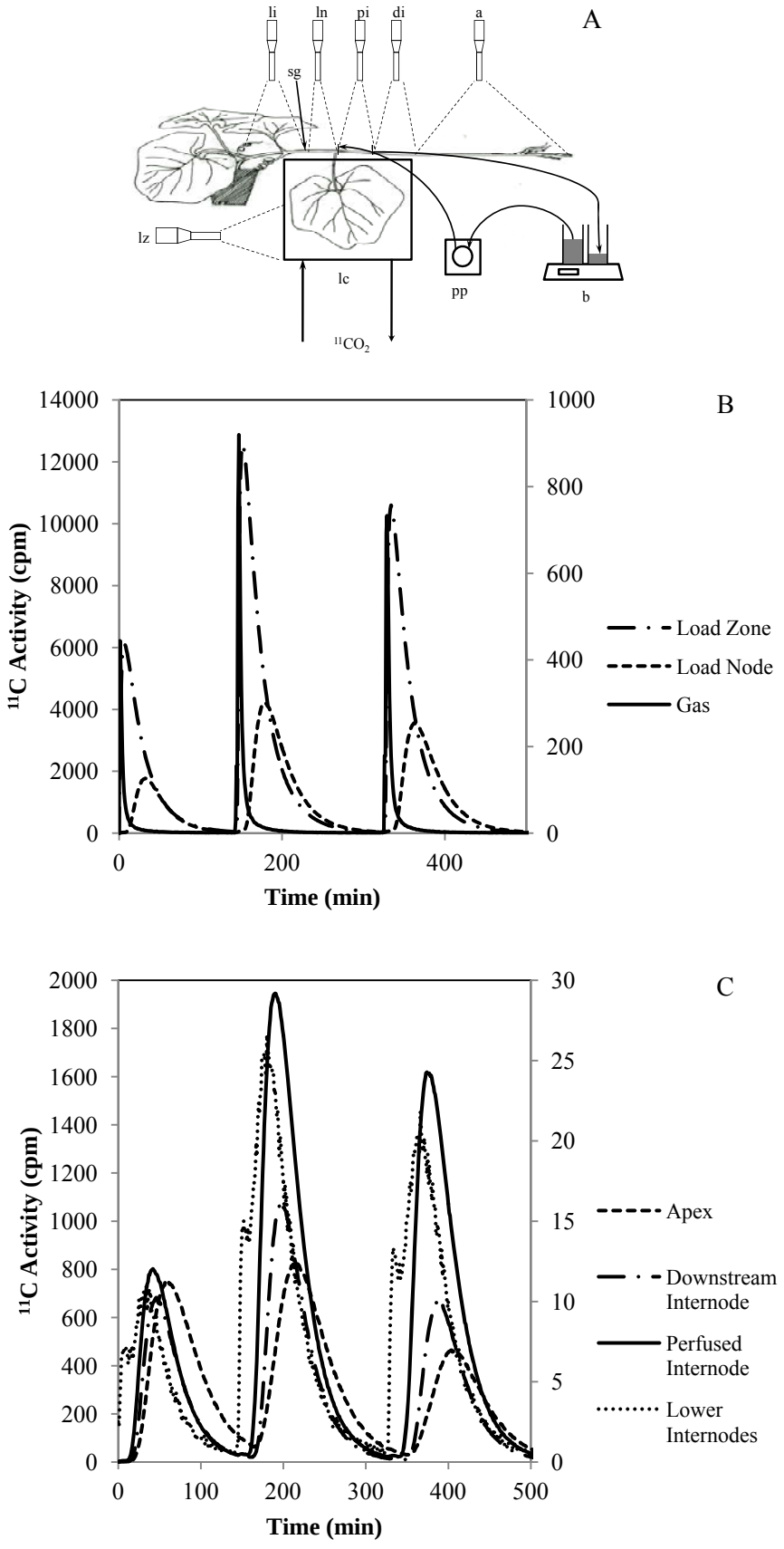
A
li
ln
pi
di
a
sg
lz
lc
pp
b
$^{11}CO_2$
B
^{11}C Activity (cpm)
Time (min)
Load Zone
Load Node
Gas
C
^{11}C Activity (cpm)
Time (min)
Apex
Downstream Internode
Perfused Internode
Lower Internodes

Figure 5.4 – A – Experimental set up for ^{11}C labelling and perfusion of a squash plant: b – balance; lc – leaf chamber; pp – peristaltic pump; sg – steam girdle; scintillation detectors monitoring: a – apex; di – downstream internode; li –lower internodes; ln – load node; lz – load zone; pi – perfused internode. ^{11}C activity profiles of the different parts in a control run experiment of a squash plant labelled with three pulses and perfused with ABS. Data are corrected for detector sensitivities. B – Gas detector, referred to right hand side axis, and higher activity in upstream regions. C – Lower activity in downstream regions; lower internodes activity is referred to the right hand side axis.

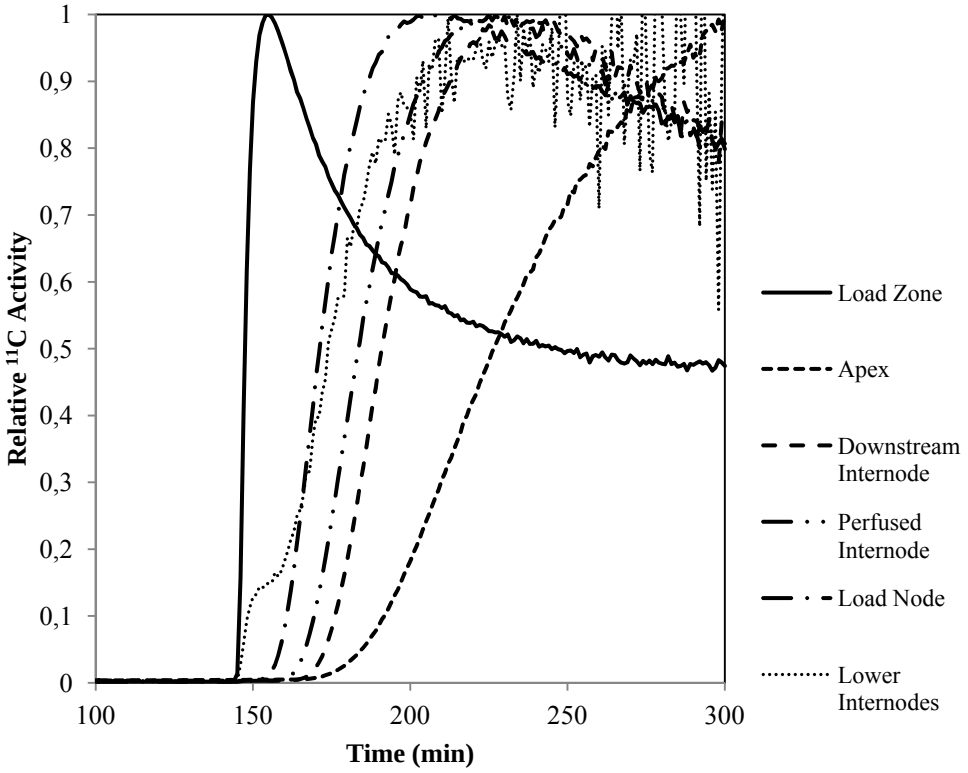

Figure 5.5 – Relative ^{11}C activity profiles of the different plant parts for the second pulse of Fig. 5.4. Data are relative to the maximum count rate for each detector and are corrected for background and decay.

would be equivalent to having just one detector, a "sink detector", monitoring that same whole region. In this manner, we obtain the total influx of tracer to that specific region of the plant. Hence, after decay and background correction, its profile would be very similar to the ones shown in Fig. 5.5. Determining the slope of the decay-corrected data, of the accumulation of tracer in a given plant part, we get the influx rate of tracer into that re-

gion (§ 4.10.3). The time of maximum influx rate (Fig. 5.6), i.e. the time of inflexion of the decay corrected curves (Fig. 5.5), is roughly the time at half-height in Fig. 5.5. In its turn, this time corresponds to the time of maximum raw activity in curves from Fig. 5.4. For our purposes, we define this time of highest influx rate, as the time at which the front of the pulse enters that monitored region. From the times at which the front arrives at each detector, a speed can be inferred, which we call the tracer transport speed, or tracer translocation speed, although we do not have a sharp well defined pulse in one sieve tube, rather one which is in many sieve tubes and vascular bundles.

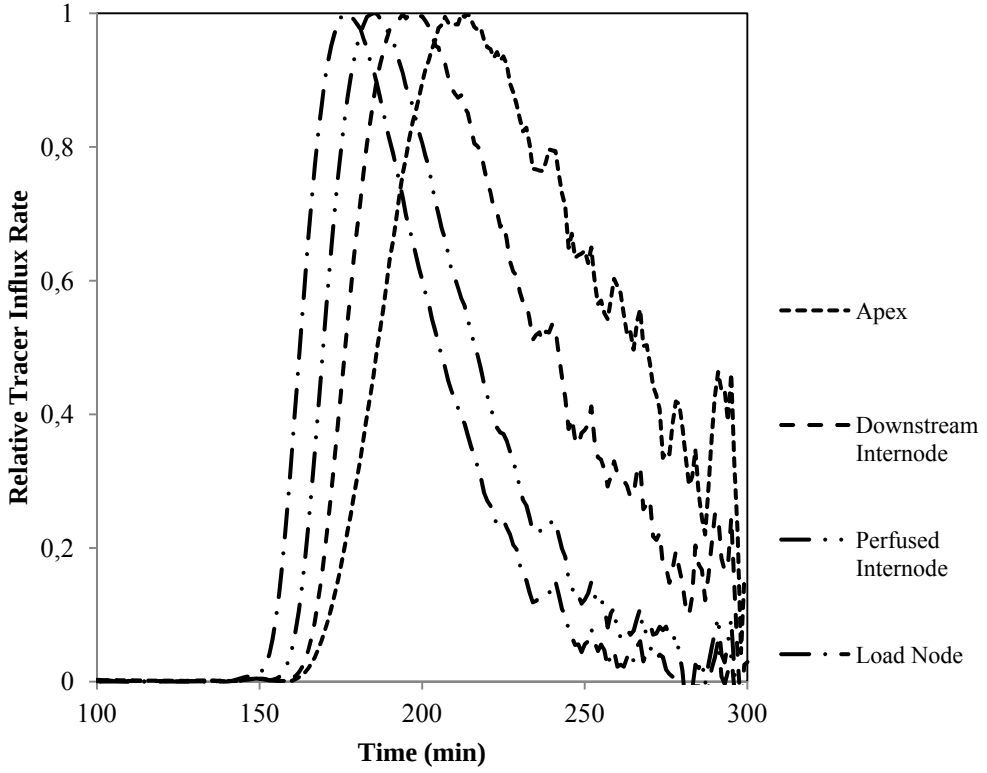

Figure 5.6 – Relative ^{11}C influx rate into several parts of the squash plant for the decay- and background-corrected data of second pulse of Fig. 5.4. Each plot is scaled relative to the maximum influx rate.

Following Ferrieri *et al*. (2005), from the half-maximum activity transit time (midpoint of the front of pulse) it is possible to determine a tracer translocation speed (§4.10.2). Due to the geometry of its vascular system (Patrick, 1971), in wheat it was not possible to identify a front of tracer and determine tracer translocation speed in the load

node, or immediate downstream regions towards the root. Tracer coming from the wheat flag leaf will firstly move down the internode below the flag leaf node, possibly reaching further internodes below, before some movement towards the ear as well as root. This means that both in the load node and in the lower internodes detected regions (Fig 5.4A) there is simultaneous movement of tracer in opposite directions in different bundles. Thus, it is not possible to distinguish which fraction of tracer will move in a given direction nor consequently to determine tracer translocation speed. For the region in which flow was uni-directional, so that speed could be measured, perfusion by the apoplastic bathing solution (ABS) did not significantly affect tracer translocation speed (Fig. 5.7). For both perfused and non-perfused plants tracer translocation speed ranges from 1.3 to 1.6 cm.min^{-1}.

The translocation speed measured for the perfused and downstream internodes of squash were similar, and were not affected by ABS perfusion, but speed in the load node region was reduced by perfusion (Fig 5.8). Comparing the speed in both species we see that tracer moves faster in wheat peduncle than in squash internodes, in both perfused and non-perfused plants. In the absence of treatment solutes, perfusion did not affect speed in either the downstream regions of both species. In both wheat and squash speed did not change significantly during the day for any of the regions (Fig. 5.7, 5.8). Tracer translocation speed estimates obtained from the transit time determined from transfer function analysis (§ 4.10.1) agree well with the estimates from the half-maximum activity transit time (Figs. 5.7B, 5.8B).

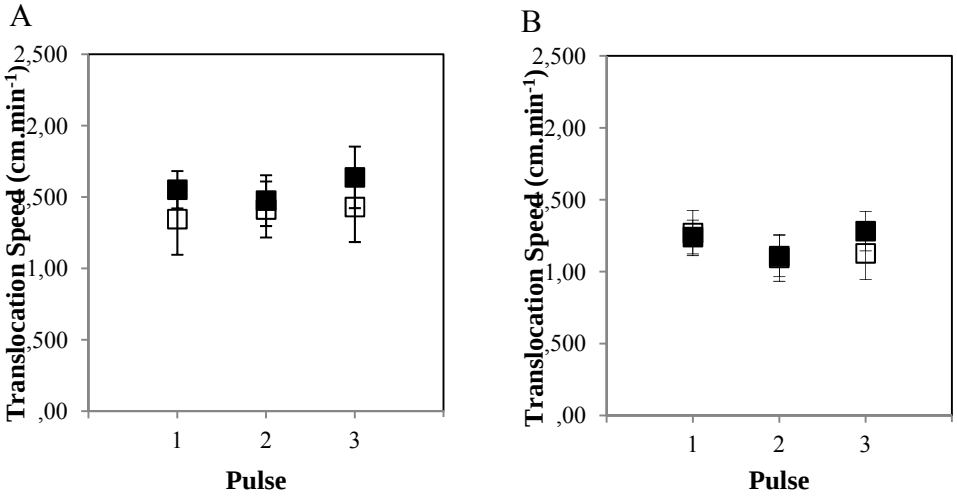

Figure 5.7 – Translocation speed estimates (mean ± SE) in the wheat perfused peduncle: A – from the half-maximum activity transit time; B – from transfer function analysis. (■) plants perfused with the apoplastic bathing solution (ABS) (n = 5) and (□) non-perfused plants (n = 4), both submitted to the three ^{11}C labelling pulses.

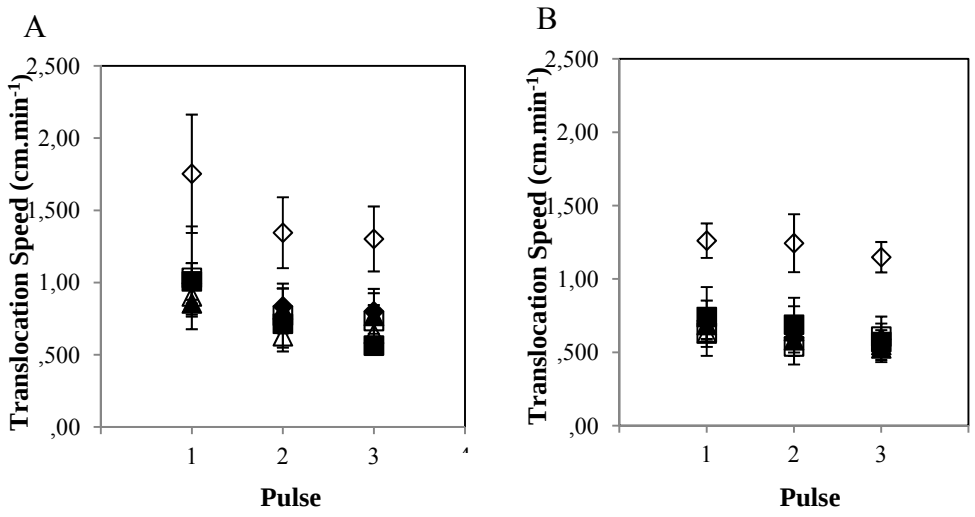

Figure 5.8 – Translocation speed estimates (mean ± SE) in the squash stem: A – from the half-maximum activity transit time; B – from transfer function analysis. Load node (♦, ◊), perfused internode (■, □) and downstream internode (▲,△). Filled markers refer to plants perfused with the apoplastic bathing solution (ABS) (n = 9) and non-filled markers refer to non-perfused plants (n = 6) both submitted to the three ^{11}C labelling pulses.

5.4 Tracer Loss

Measurements of the loss of tracer, which can be expressed as the percentage per unit length of the photoassimilate flow within the transport pathway, and how it can be affected can give us clues about the solute exchange processes happening in the phloem pathway. First we checked the effect of perfusion on loss. Tracer loss was hardly affected by ABS perfusion, in either species (Figs. 5.9, 5.10, 5.11). Tracer loss in the wheat peduncle was less than 1 $\%.cm^{-1}$. This is clearly less than we saw in squash (compare values of Figs. 5.10 and 5.11). For wheat it shows that almost all of the tracer entering through the peduncle ended up in the ear and very little was unloaded in the peduncle. As Fig. 5.9 shows, the partitioning of tracer (§ 4.10.1), and similarly of photoassimilates, favours

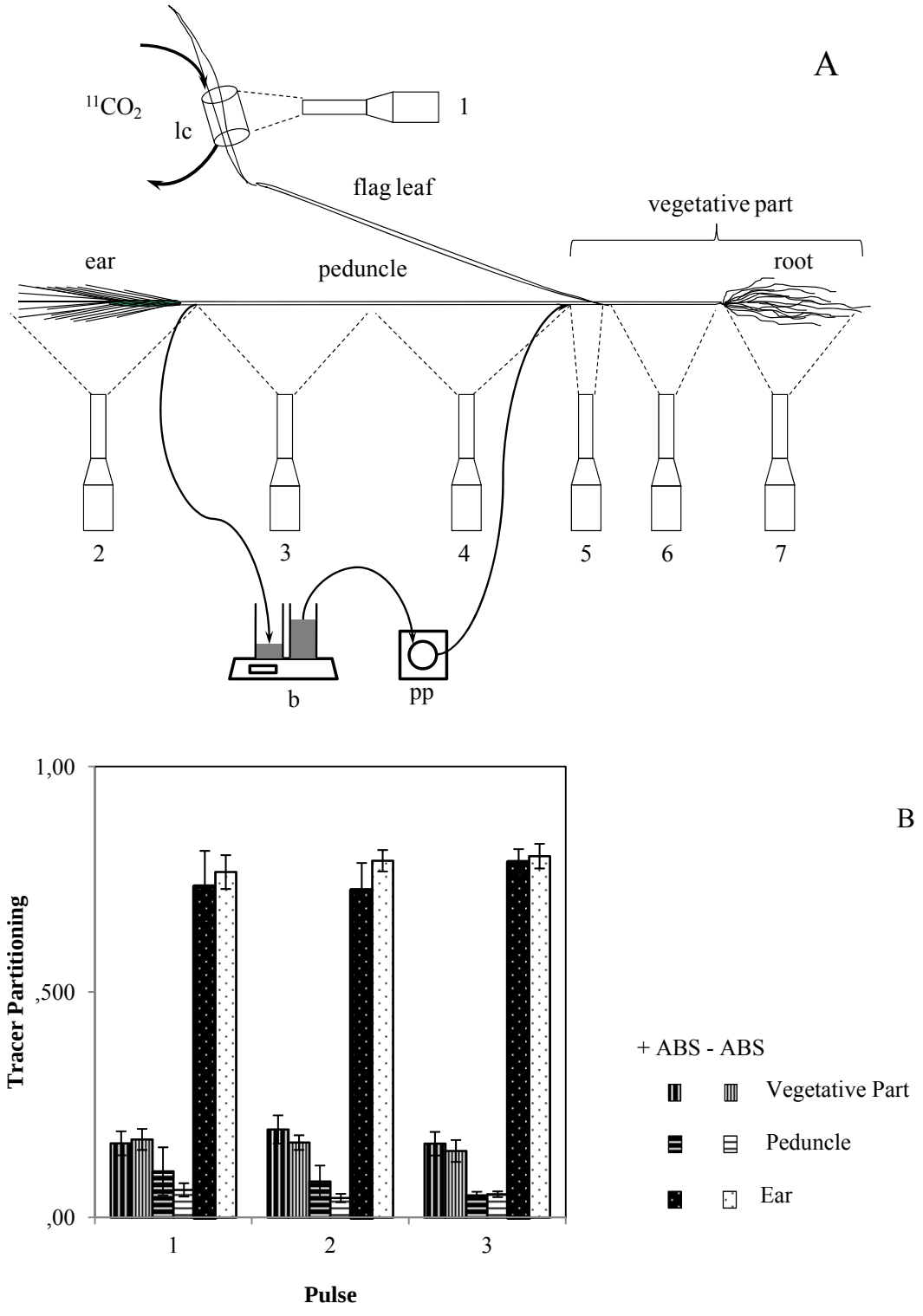

Figure 5.9 – A – Experimental setup for ^{11}C labelling on wheat: b – balance; lc – leaf chamber; pp – peristaltic pump; from 1 to 7 scintillation detectors monitoring the different plant parts. B – ^{11}C partitioning (mean ± SE) between the wheat vegetative part, peduncle and ear in plants per-

fused with the apoplastic bathing solution (ABS) (n = 5) and non-perfused plants (n = 4), both submitted to the three ^{11}C labelling pulses.

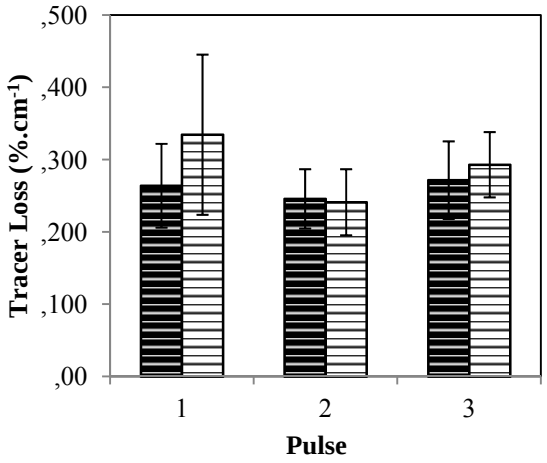

Figure 5.10 – ^{11}C loss (mean ± SE) in wheat peduncle in plants perfused with the apoplastic bathing solution (ABS) (▤) (n = 5) and non-perfused (▤) (n = 4), both submitted to the three ^{11}C labelling pulses.

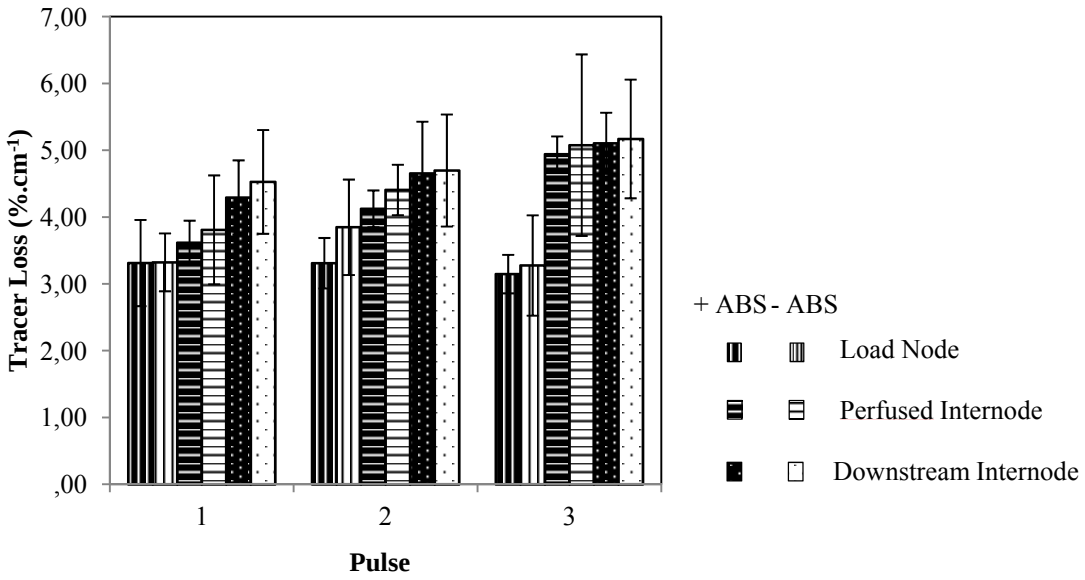

Figure 5.11 – ^{11}C loss (mean ± SE) in the load node, perfused internode and downstream internode of squash plants perfused with the apoplastic bathing solution (ABS) (n = 9) and non-perfused (n = 6), both submitted to the three ^{11}C labelling pulses.

greatly the ear as a very strong sink. More than 2/3 of all the recently assimilated carbon supplied to the plant from the flag leaf ended up in the ear, a small fraction in the peduncle while the rest was delivered into the vegetative part, which includes the load node and all the lower internodes plus the root. The short-term partitioning of tracer between the three wheat plant parts did not change during the day nor was affected by ABS perfusion (Fig. 5.9). The same behaviour was observed with tracer loss in the wheat peduncle. Whereas in squash there was a trend towards the end of the day showing bigger values for the third pulse in both perfused and downstream internodes, for both perfused and non-perfused plants (Fig. 5.11). In squash, in both cases, the load node region has smaller values of tracer loss, ranging from 3.2 to 3.8 $\%.cm^{-1}$, than the perfused internode and the downstream internode adjacent to it, of 3.8 to 5.2 $\%.cm^{-1}$.

In some experiments with squash a detector was used for any tracer that might be washed out in the perfusion solution, thus leaving the plant (Fig. 4.2). The count rate was very low, and not suitable for transfer-function analysis of the time series. For this reason, we measured the amount of tracer in the waste solution bottle (output) and the amount of tracer downstream of the load node (input), at one specific time as a measure of the total fractional loss of tracer into the perfusion solution. For the pump speed and tubing used, the peak of the output raw activity curve in the waste solution bottle occurred 10 to 20 minutes after the peak of the perfused internode raw activity curve. Hence, 50 minutes after the peak of the input activity curve into the perfused internode ensures a sufficient amount of tracer to be detected and it was distinguishable from the background. This is adequate for seeing any effects caused by perfusion by different solutes as the treatments were also applied in that time range. Determined this way, the loss of mobilized tracer per unit length to ABS was $4.5 \pm 0.1 \times 10^{-4}$ $\%.cm^{-1}$ (n = 4).

5.5 Effect of Sucrose and Mannitol Perfusion on Tracer Loss in Wheat

Sucrose is the only sugar species transported in wheat, thus quite likely to be taken up from the apoplast (Hayashi & Chino, 1986); hence it cannot be used as an osmoticum. However, it can be used to investigate sucrose retrieval in the phloem by observing if the presence of sucrose in the apoplast, due to perfusion, affects tracer loss in the

phloem. Mannitol is not transported in wheat and so it was used as osmoticum with which the effects of water exchange on tracer loss in the phloem were investigated. In the peduncle, tracer loss was affected by perfusion by sucrose or mannitol for concentrations of 500 mM or more only: concentrations of 100 or 300 mM of either sugar showed no effect (data not shown). There were responses at 500 and 700mM although some plants did not respond for the latter. Where there was a response, there was a clear difference between effects of mannitol and sucrose: mannitol gave a *prolonged* depression of tracer loss in the peduncle (Fig. 5.12), showing no effect when the treatment was removed; sucrose gave a *transient* increase, starting to recover during the treatment, and showing some signs of an accelerated recovery when the treatment ended (Fig. 5.13). The response of tracer loss to the lower region of wheat on perfusing with sucrose or mannitol was not reproducible. Although perfusion by 500 mM mannitol or sucrose always decreased parti-

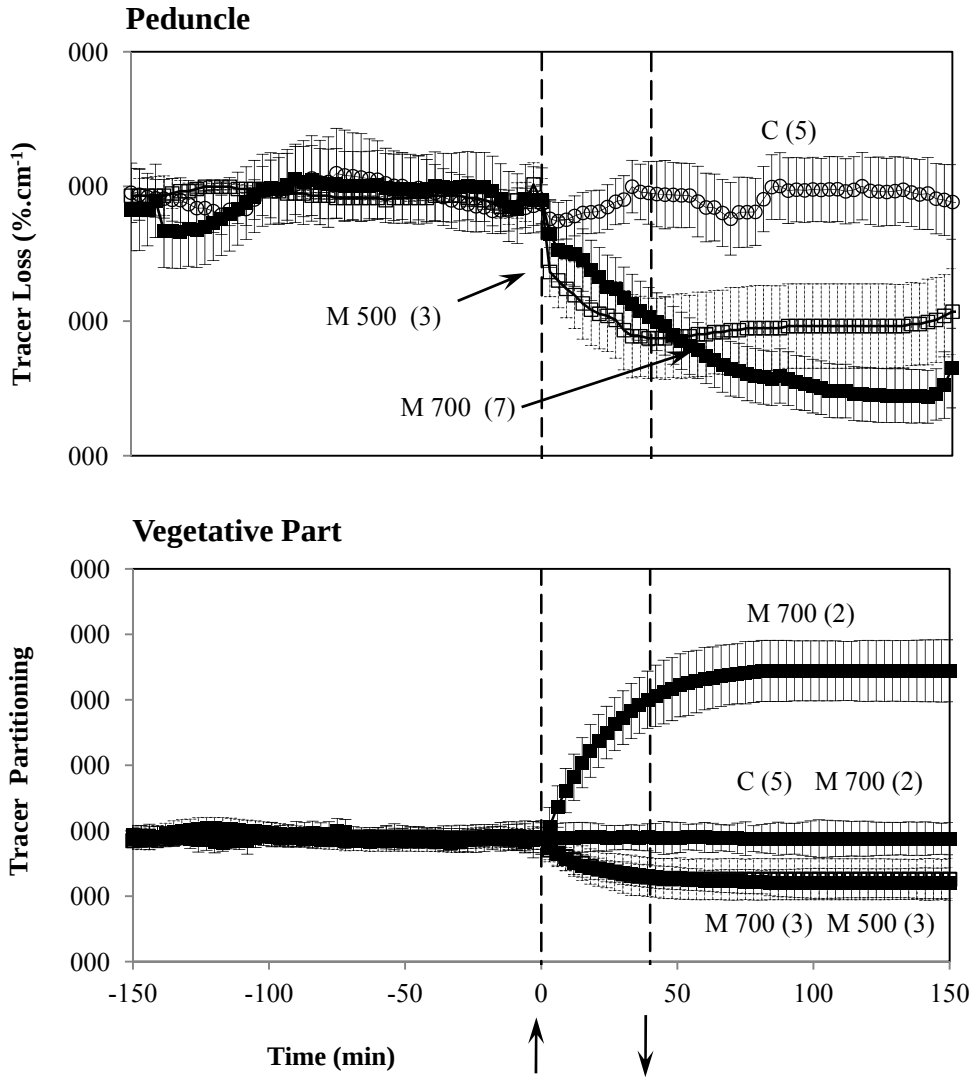

Figure 5.12 – Effect of mannitol perfusion on ^{11}C loss in the wheat (mean ± SE): C – control run; M – mannitol at 500 and 700 mM. Number of samples in brackets. Treatments were applied at 0 time and removed 40 minutes later as indicated by the arrows.

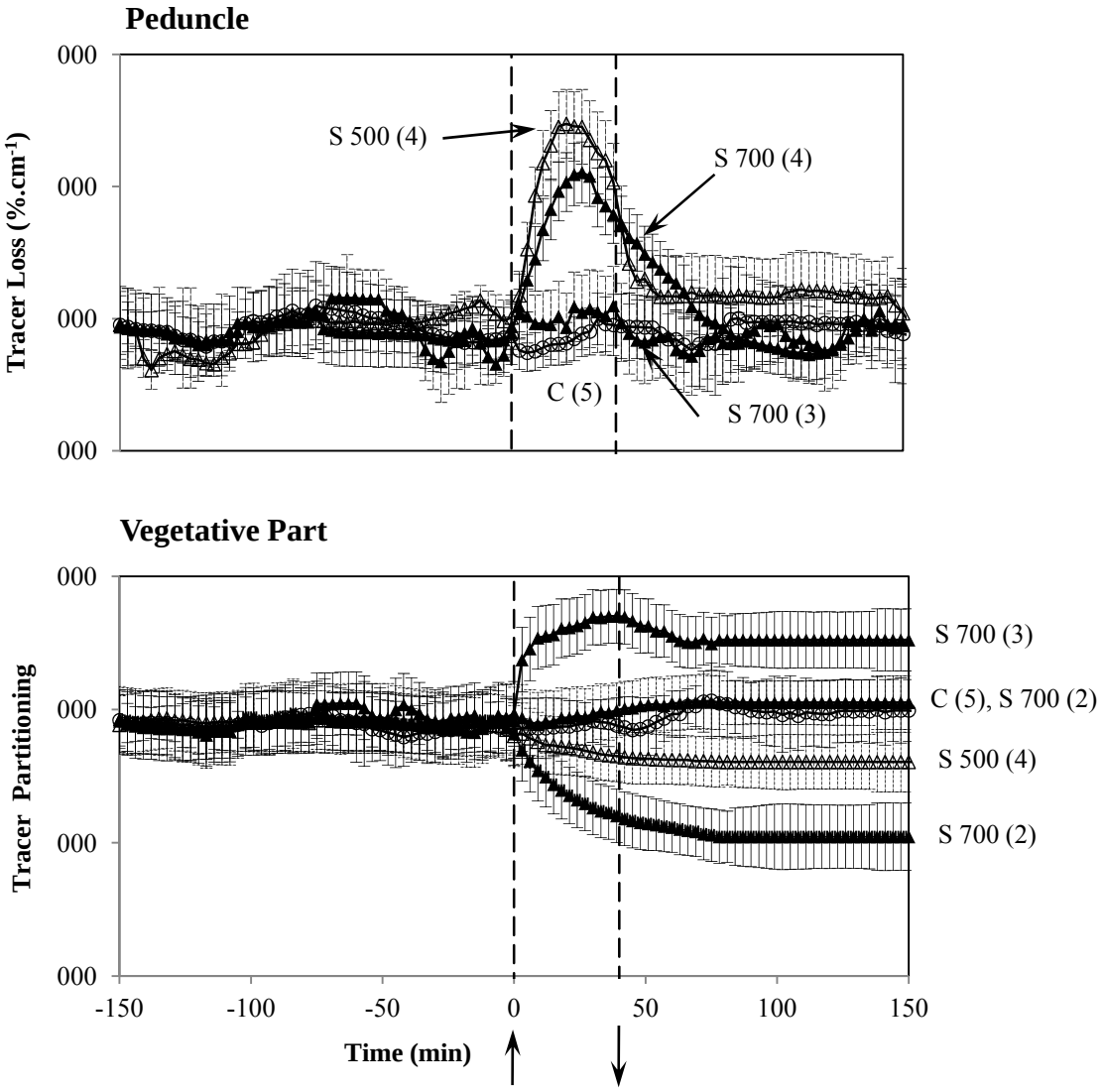

Figure 5.13 – Effect of sucrose perfusion on ^{11}C loss in wheat (mean ± SE): C – control run; S – sucrose at 500 and 700 mM. Number of samples in brackets. Treatments were applied at 0 time and removed 40 minutes later as indicated by the arrows.

tioning downward, at 700 mM tracer loss in that region increased, decreased or did not change at all (Fig. 5.12). Unlike responses within the perfused peduncle, the effects of sucrose and mannitol were not different: both solutes gave variable responses, the responses were prolonged, and showed no influence of a treatment ending.

5.6 Effect of Sucrose, Mannitol, Raffinose and PEG Perfusion on Tracer Loss in Squash

Sucrose and oligosaccharides (RFO, such as stachyose, raffinose and verbascose) are transported through the phloem in the *cucurbitaceae* family (Webb & Gorham, 1964; Hendrix, 1968, 1982; Hsiang Bush, 1992). Stachyose generally comprises more than half of the total carbohydrate in their phloem sap, with sucrose being about 20% (Webb & Gorham, 1964). However, the transported sugar is dependent on species (Kenneth *et al*., 1964; Hendrix, 1982). As with wheat, we asked whether perfusing the apoplast with the transported sugars, sucrose and raffinose, affects tracer transport. For the question, does apoplast water potential affect tracer transport, we initially perfused with mannitol, since mannitol is not transported in the phloem of *cucurbitaceae* (Richardson & Baker, 1982; Fiehn, 2003). However, as we will see, the possibility of mannitol uptake from the apoplast was raised, as it seemed to have effects beyond mere water relations. For this reason polyethylene glycol (PEG) was used as an osmotic agent, since it does not penetrate into the plant, and we will have water but not PEG exchange between the perfusion solution and the plant tissue (Carpita *et al*., 1979; Oertli, 1986).

Perfusion by 100 mM sucrose caused an increase in the tracer loss both in the perfused internode and in its following downstream internode, while in the load node region, upstream located, there was an opposite effect: a slight decrease in the tracer loss (Fig. 5.14). In all regions the increased values were maintained after treatment removal. Perfusion by mannitol at the same concentration caused similar responses to sucrose perfusion in all three regions but its effects were more pronounced in both the perfused and downstream internodes (Fig. 5.14). In the load node region sucrose, mannitol and raffinose all had a similar effect in decreasing tracer loss, although there was recover from the plant once mannitol was replaced by ABS. This apparent recovery to a similar tracer loss value before teatment was seen with neither raffinose nor sucrose (Fig. 5.14). When compared with the sucrose and mannitol raffinose perfusion caused a smaller increase, particularly in the perfused internode. However in the downstream internode this difference becomes smaller when compared with sucrose effect while still being much less than the increased caused by mannitol perfusion. As with sucrose, the tracer loss changes caused by mannitol and raffinose are also maintained after removal of treatment in both the perfused and

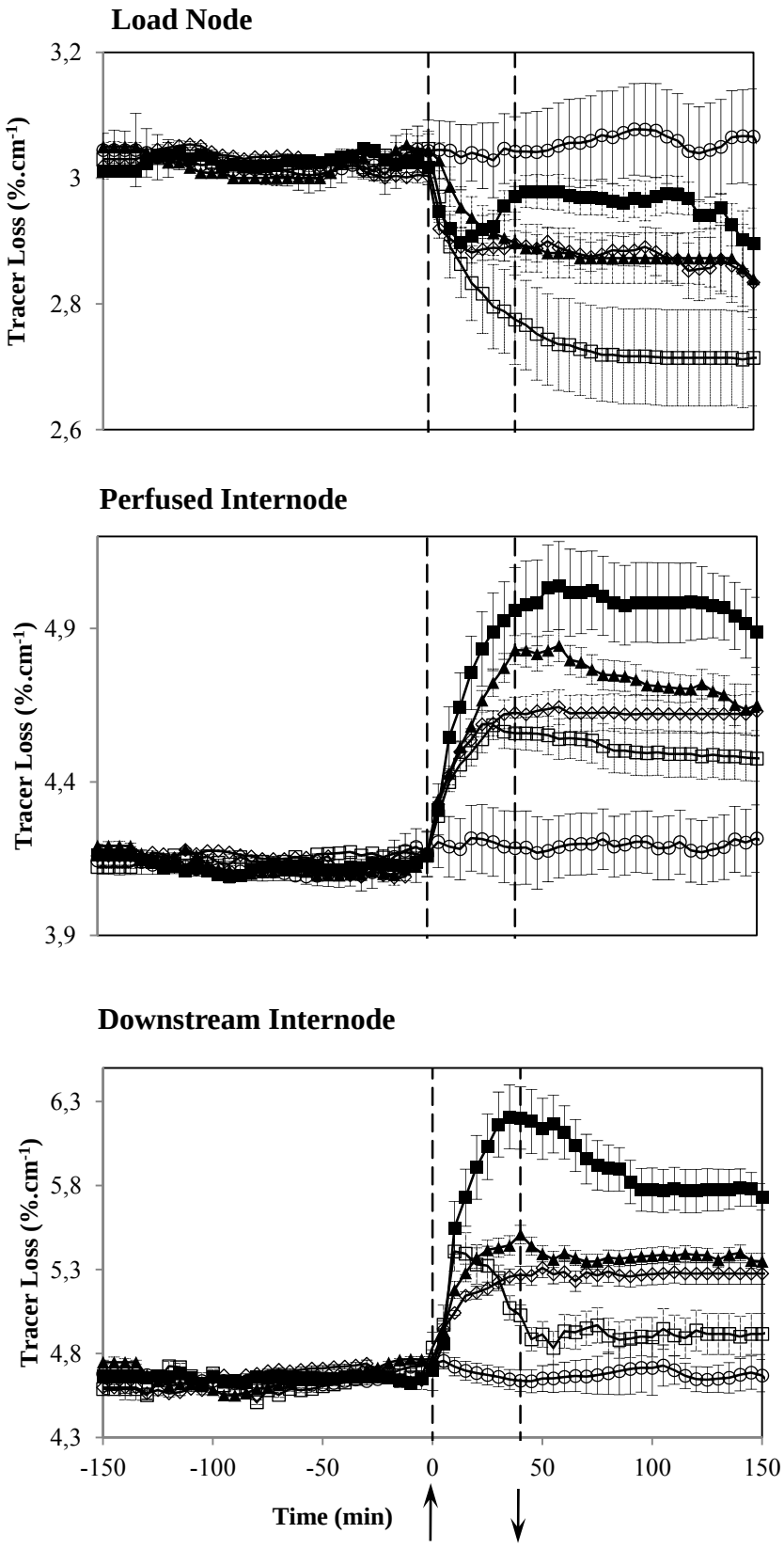
Load Node
Tracer Loss (%.cm-1)
3,2
3
2,8
2,6
Perfused Internode
Tracer Loss (%.cm-1)
4,9
4,4
3,9
Downstream Internode
Tracer Loss (%.cm-1)
6,3
5,8
5,3
4,8
4,3
-150
-100
-50
0
50
100
150
Time (min)

Figure 5.14 – Effect of 100 mOsmolal perfusion on ^{11}C loss in squash internodes (mean ± SE): ○ – control run (n = 7); ■ – mannitol (n = 5); □ – PEG (n = 5); ◊ – raffinose (n = 4); ▲ – sucrose (n = 7). Treatments were applied at 0 time and removed 40 minutes later as indicated by the arrows.

the downstream internodes.

Using a PEG solution that was osmotically equivalent to the other 100 mM sugar solutions the effect was similar to sucrose, mannitol and raffinose perfusions, on increasing the tracer loss in the perfused and downstream internodes and causing the opposite in the load node. However, in the perfused internode the effect PEG perfusion was significantly less than the effects observed with sucrose and mannitol and was slightly less than the effect observed with perfusion by raffinose (Fig. 5.14). In addition, in the downstream internode there was recovery from the plant that started before PEG was replaced by ABS that did not happen with sugars. In the load node is where PEG effects were more visible when compared with sugars as it decreased much more the tracer loss in that region and this status was maintained after PEG removal. As with the other solutes, its effect was maintained after treatment removal.

As a way of investigating changes in translocation speed and in tracer amount in each part of the plant, we compare the rate of influx of tracer, from the half-life corrected data, just before and after treatment (§ 4.10.3). Hence by comparing the influx rate of tracer into a given plant part after treatments with the average influx rate of the last 10 minutes before treatment, we obtain what we called the relative influx rate of tracer. At the same osmolal concentration, a nominal 100 mOsmolal, sucrose and raffinose behaved more or less similarly to control experiments (ABS) regarding the tracer influx rate in the perfused internode (Fig. 5.15). Raffinose and sucrose perfusions reduce the influx rate when compared with control runs. This difference is also observed more pronounced after mannitol and sucrose treatments removal. During treatment the tracer influx rate was already declining in the perfused internode, meaning that the pulse front has already passed that region by that time, going into the adjacent downstream internode (Figs. 5.5, 5.6), as indicated by the increase in the tracer influx rate (Fig 5.16). In the downstream internode the effect of sucrose perfusion seems more evident than in the perfused internode as it reduced the tracer influx rate compared with the control runs and mannitol. Raffinose effect is not evident (Fig. 5.16). However, the removal of treatments and their replacement by ABS perfusion seems not to disturb that much tracer flux in the downstream internode (Fig. 5.16). From this, we can infer that at this concentration the treatments had minute effects

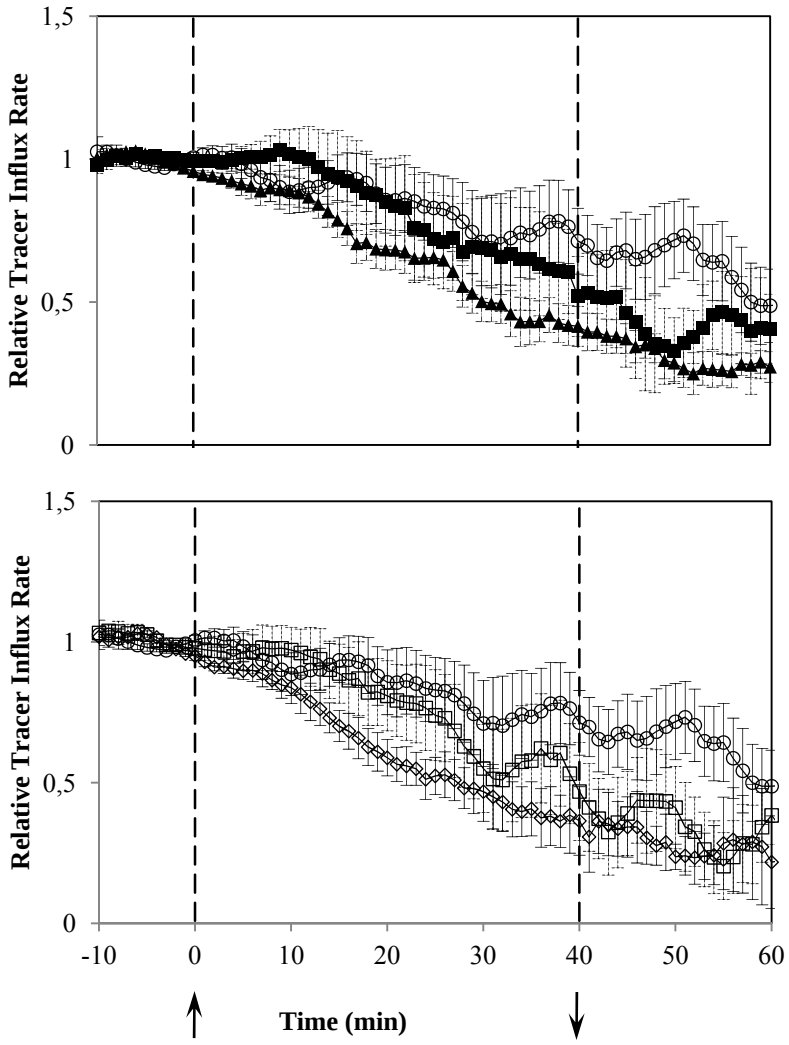

Figure 5.15 – Perfusion effect on the relative influx rate of mobilized tracer into the perfused internode during treatments of 100 mOsmolal solutions (mean ± SE): ○ – control run (n = 7); ■ – mannitol (n = 5); □ – PEG (n = 5); ◊ – raffinose (n = 4); ▲ – sucrose (n = 7). Treatments were applied at 0 time and removed 40 minutes later as indicated by the arrows.

on tracer influx rate.

With perfusion by 300 mM solutions there were striking differences between responses to sucrose and mannitol on the one hand and PEG on the other (Fig. 5.17), when compared with 100 mM solutions (Fig. 5.14). With 300 mM both sucrose and mannitol caused a similar and significant increase in the tracer loss in both the perfused and downstream internodes, almost doubling it in the perfused region (Fig. 5.17). Neither change was reversed when treatments were removed. In the load node region, sucrose and manni-

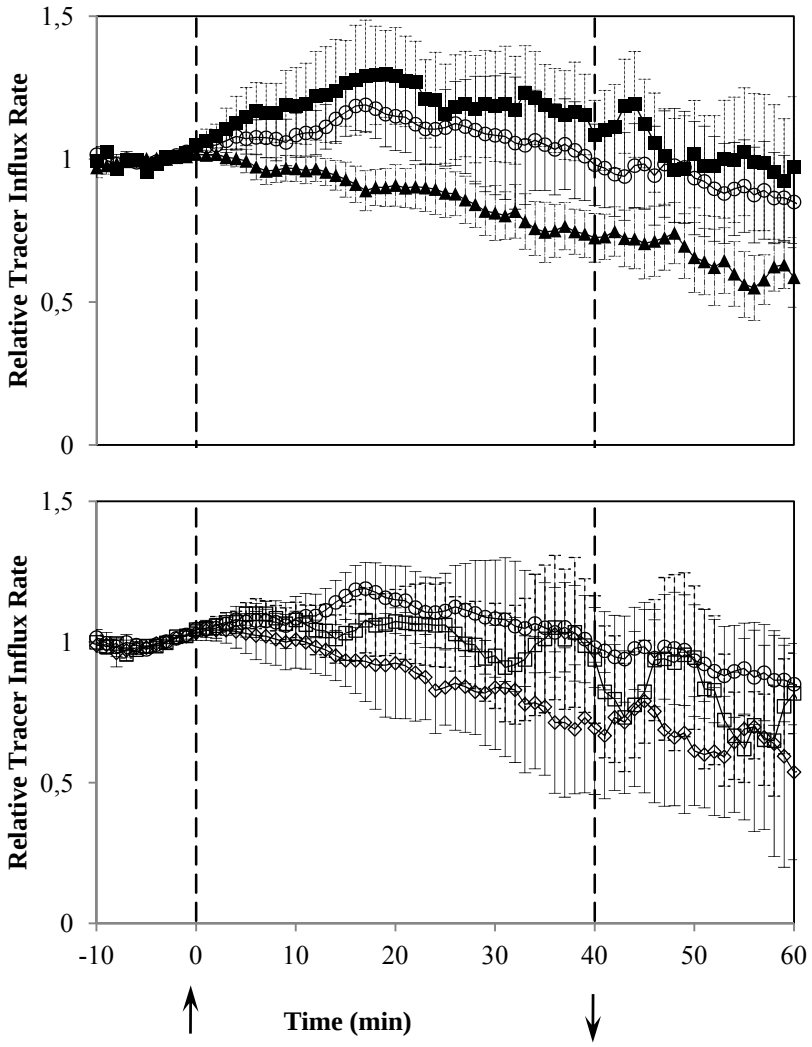

Figure 5.16 – Perfusion effect on the relative influx rate of mobilized tracer into the downstream internode during treatments of 100 mOsmolal solutions (mean ± SE): ○ – control run (n = 7); ■ – mannitol (n = 5); □ – PEG (n = 5); ◊ – raffinose (n = 4); ▲ – sucrose (n = 7). Treatments were applied at 0 time and removed 40 minutes later as indicated by the arrows.

tol effects differ; there was a recovery from the initial effect of sucrose, a decrease in tracer loss, while it was still being perfused. This did not happen for a 300 mM mannitol perfusion nor did it happen when using 100 mM sucrose (Fig. 5.13). In both the perfused internode and its following downstream internode, the PEG effect, increasing tracer loss, was significantly smaller than the effects of 300 mM sucrose or mannitol (Fig. 5.17). Contrary to 100 mOsmolal PEG (Fig. 5.13), the effect of 300 mOsmolal in the downstream internode was not reversible (Fig. 5.17). In the load node region, on the other hand

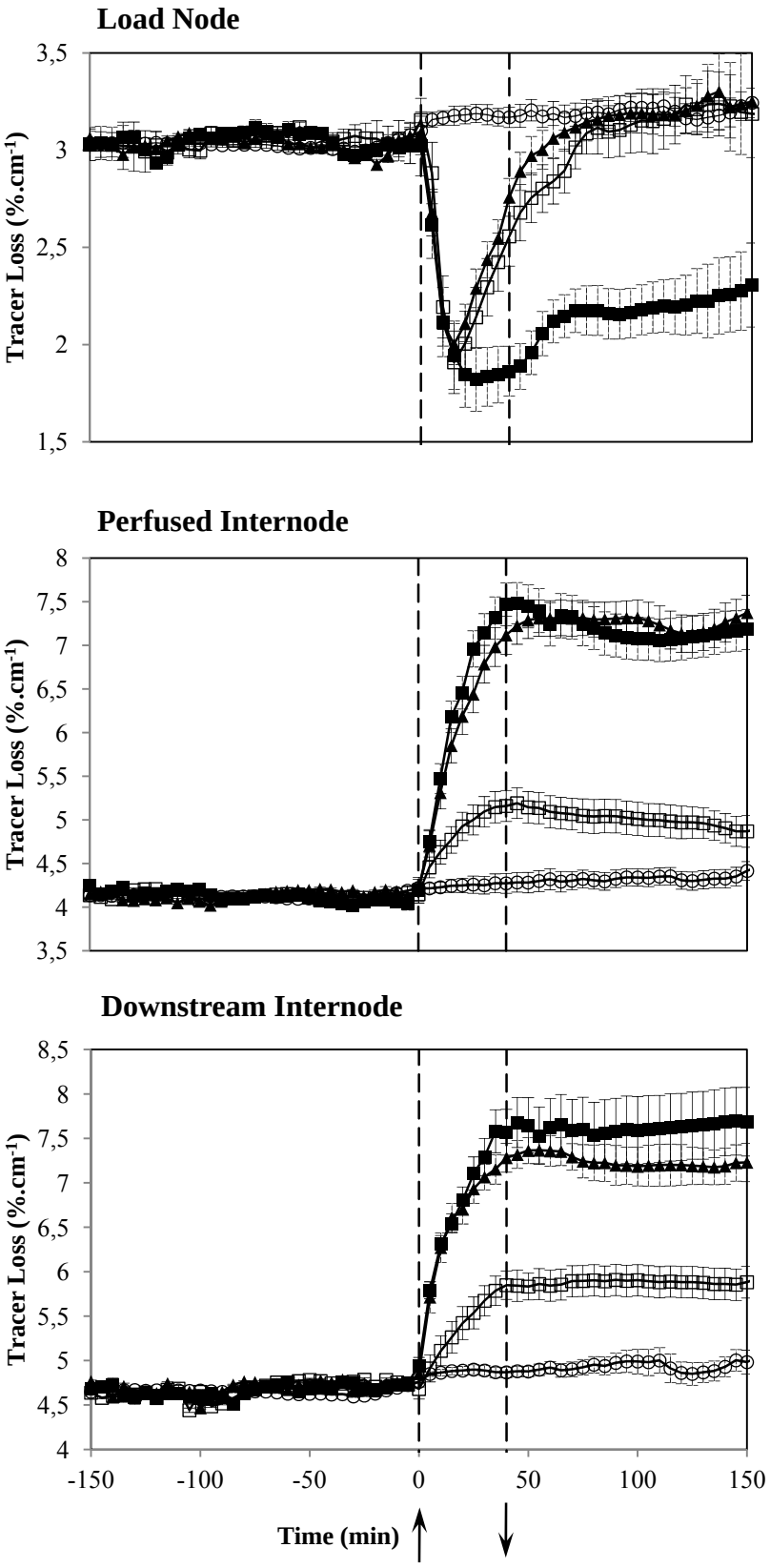
Load Node
Tracer Loss (%.cm-1)
3,5
3
2,5
2
1,5
Perfused Internode
Tracer Loss (%.cm-1)
8
7,5
7
6,5
6
5,5
5
4,5
4
3,5
Downstream Internode
Tracer Loss (%.cm-1)
8,5
8
7,5
7
6,5
6
5,5
5
4,5
4
-150
-100
-50
0
50
100
150
Time (min)

Figure 5.17 – Effect of 300 mOsmolal perfusion on ^{11}C loss in squash internodes (mean ± SE): ○ – control run (n = 7); ■ – mannitol (n = 5); □ – PEG (n = 5); ◊ – raffinose (n = 4); ▲ – sucrose (n = 7). Treatments were applied at 0 time and removed 40 minutes later as indicated by the arrows.

there was recovery towards the initial state, while still being perfused with PEG (Fig. 5.17), like the response to sucrose. This recovery did not occur with 100 mOsmolal PEG solution (Fig. 5.14).

Unlike 100 mOsmolal (Figs. 5.15, 5.16), perfusion by 300 mOsmolal sucrose, mannitol or PEG caused an increase in the tracer influx rate into the perfused internode (Fig 5.18). In the downstream internode, following the perfused internode, all solutions had a similar effect on the tracer influx rate, reaching a maximum later in time during treatment (Fig. 5.18). In this region, sucrose perfusion caused a smaller increase when compared with both mannitol and PEG and the increase was not affected by treatment removal. These changes in tracer influx rate suggest an increase in the translocation speed.

With 500 mM perfusion showed again the different effects of sugars and PEG on tracer loss at 300 mM (Fig. 5.16), and also demonstrated a clear difference between sucrose and mannitol. Fig. 5.19 shows that sucrose 500 mM perfusion increased the tracer loss irreversibly in both perfused internode and its following internode, while again it had an opposite effect in the load node region, upstream from the perfused internode. With perfusion by 500 mM sucrose, the decrease in tracer loss in the load node region was almost double that at 300 mM (Fig. 5.19). The was no recovery to the pre-treatment state, as at 300 mM, although there was subsequent tracer loss increase after a minimum was reached during treatment that continued after treatment removal (Fig. 5.19). In the perfused internode, the increase in tracer loss was double that at 300 mM sucrose. 600 mOsmol PEG caused a smaller effect than sucrose 500 mM in both perfused and downstream internodes (Fig. 5.19) but greater than at 300 mOsmol PEG. Between the two concentration values, the main difference goes to the load node region where the decrease caused in the tracer loss is much bigger, although similar to the one observed with the perfusion by 500 mM sucrose. It doubles the decrease observed by perfusing with 300 mOsmol PEG solution. And unlike what happened at that concentration, at 500 mOsmol PEG perfusion the plant does not return to its previous state, either during or after treatment.

At 500 mM, the response to mannitol and sucrose was quite different in terms of

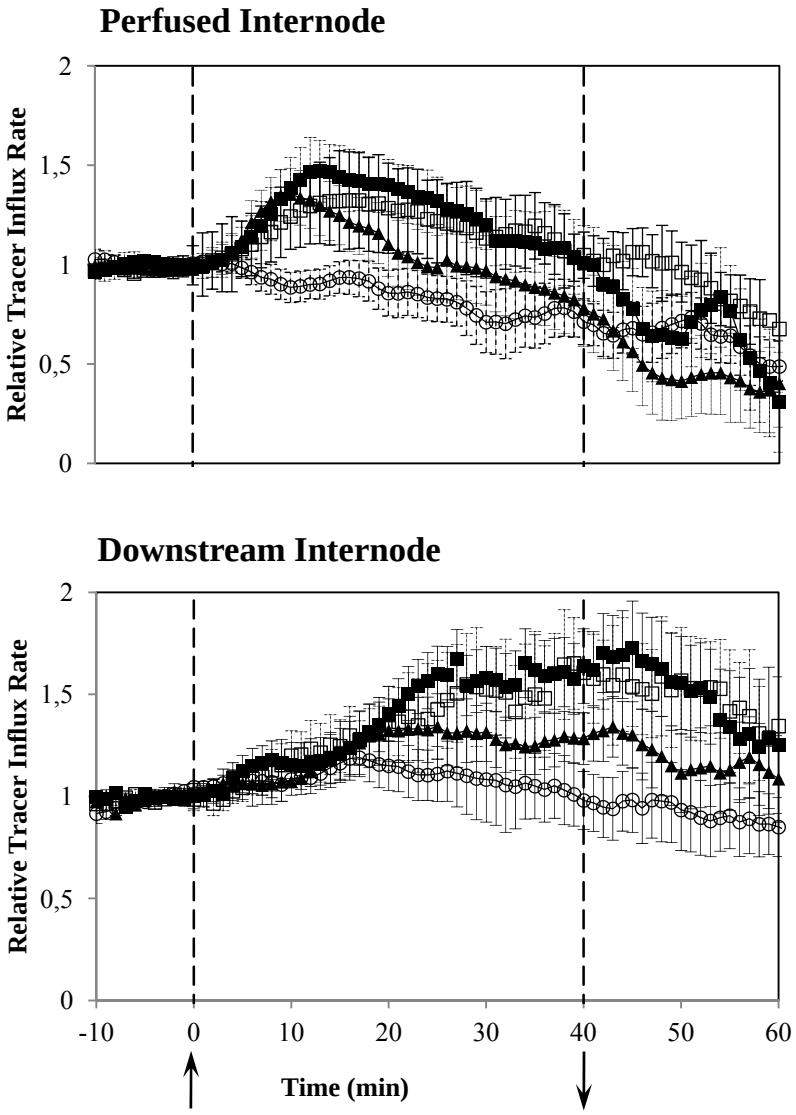

Figure 5.18 – Perfusion effect on the relative influx rate of mobilized tracer into the perfused internode and downstream internode during treatments of 300 mOsmolal solutions (mean ± SE): ○ – control run (n = 7); ■ – mannitol (n = 5); □ – PEG (n = 5); ▲ – sucrose (n = 7). Treatments were applied at 0 time and removed 40 minutes later as indicated by the arrows.

tracer transport (Figs. 5.20, 5.21). This difference was not observed at smaller concentration values of either sugars. With 500 mM mannitol perfusion, there was a stoppage of phloem transport immediately after treatment application in both the perfused internode and the downstream internode while both the load node and the apex slowed down. This situation lasted for 12 ± 2 min (n = 5). Therefore, there is no data for input-output analysis, as no tracer input function exists. Therefore we turn to the raw data. This stoppage of

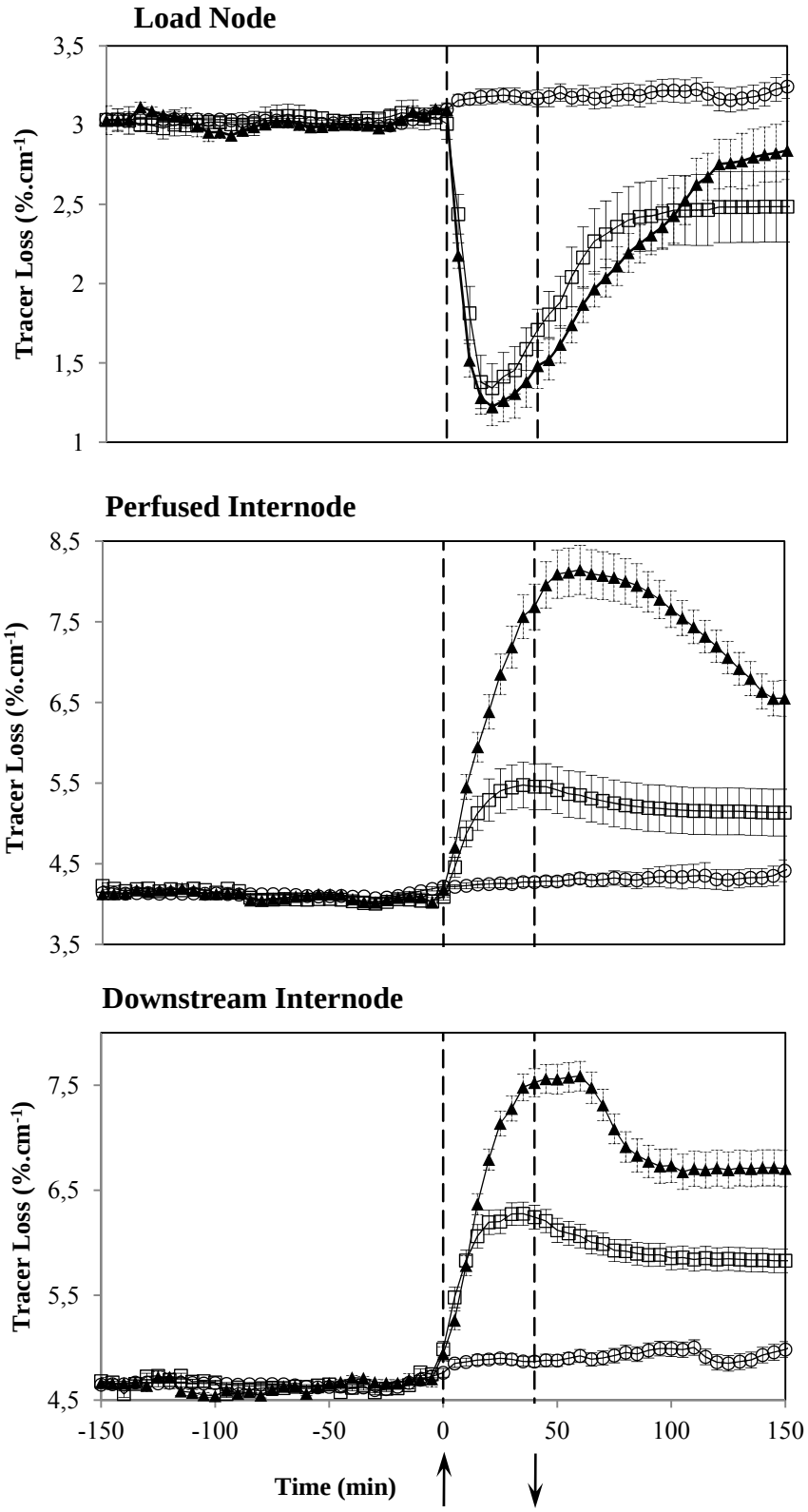
Load Node
Tracer Loss (%.cm-1)
3,5
3
2,5
2
1,5
1
Perfused Internode
Tracer Loss (%.cm-1)
8,5
7,5
6,5
5,5
4,5
3,5
Downstream Internode
Tracer Loss (%.cm-1)
7,5
6,5
5,5
4,5
-150
-100
-50
0
50
100
150
Time (min)

Figure 5.19 – Effect of 600 mOsmolal perfusion on ^{11}C loss in squash internodes (mean ± SE): ○ – control run (n = 7); □ – PEG (n = 4); ▲ – sucrose (n = 4). Treatments were applied at 0 time and removed 40 minutes later as indicated by the arrows.

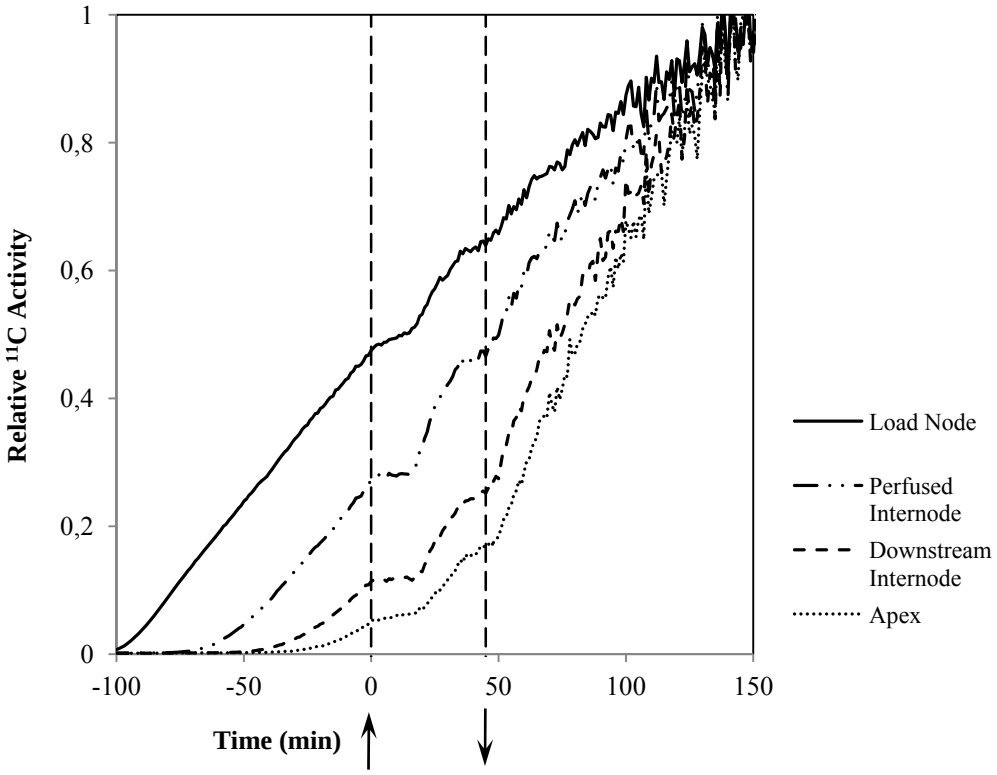

Figure 5.20 – Effect on the rate of accumulation of mobilized ^{11}C in the stem of 500 mM mannitol perfusion. Half-life and background corrected data for the detectors monitoring the different plant parts considered.

phloem transport is also shown by the fast decrease of tracer influx rate in both internodes and it is even more evident in the downstream internode as the influx rate reaches 0 (Fig. 5.22). While treatment continued, tracer accumulation recovered to higher rates than before treatment, reaching a maximum and than decreasing again (Figs. 5.20, 5.22). The rate decreased afterwards even further after the removal of treat ment (Fig. 5.22). Although only one example is shown in Fig 5.20, this behaviour was always observed in the 5 different specimens studied. The slowing down of tracer influx especially after treatment removal was not always evident (Fig. 5.20). These results clearly indicate changes

in phloem translocation speed. However, it is not possible to specify spatially where and how far in the plant the stoppage of phloem transport really occurs.

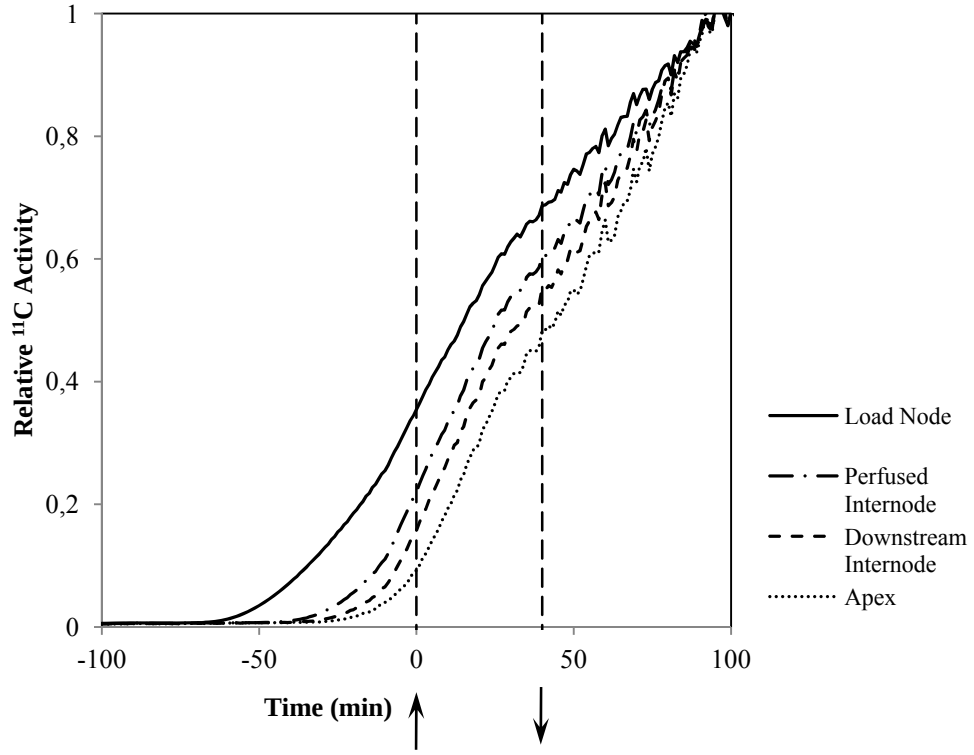

Figure 5.21 – Effect on the rate of accumulation of mobilized ^{11}C in the stem of sucrose 500 mM perfusion. Half-life and background-corrected data for the detectors monitoring the different plant parts considered.

With 500 mM sucrose, perfusion did not stop phloem transport (Fig 5.21), and in contrast to 500 mM mannitol, there was an increase of the tracer influx rate into both the perfused internode and downstream internode (Fig. 5.22). This suggests an increase in phloem translocation speed. Perfusion by 500 mM sucrose had a much more severe effect in raising the ^{11}C influx rate in both the perfused internode and its downstream internode than did perfusion by 300 mM. Adding to that, at 500 mM there was a clear response from the plant after treatment removal, with a fast decrease of the rate of tracer influx in both internodes (Fig. 5.22). This was not observed with perfusion by lesser amounts of sucrose. The effects on the rate of influx of ^{11}C by perfusion by 600 mOsmol PEG solution do not differ much from the effects observed with 300 mOsmol (Fig. 5.17). Neither does treatment removal seem to have any effect in both internodes for both situations.

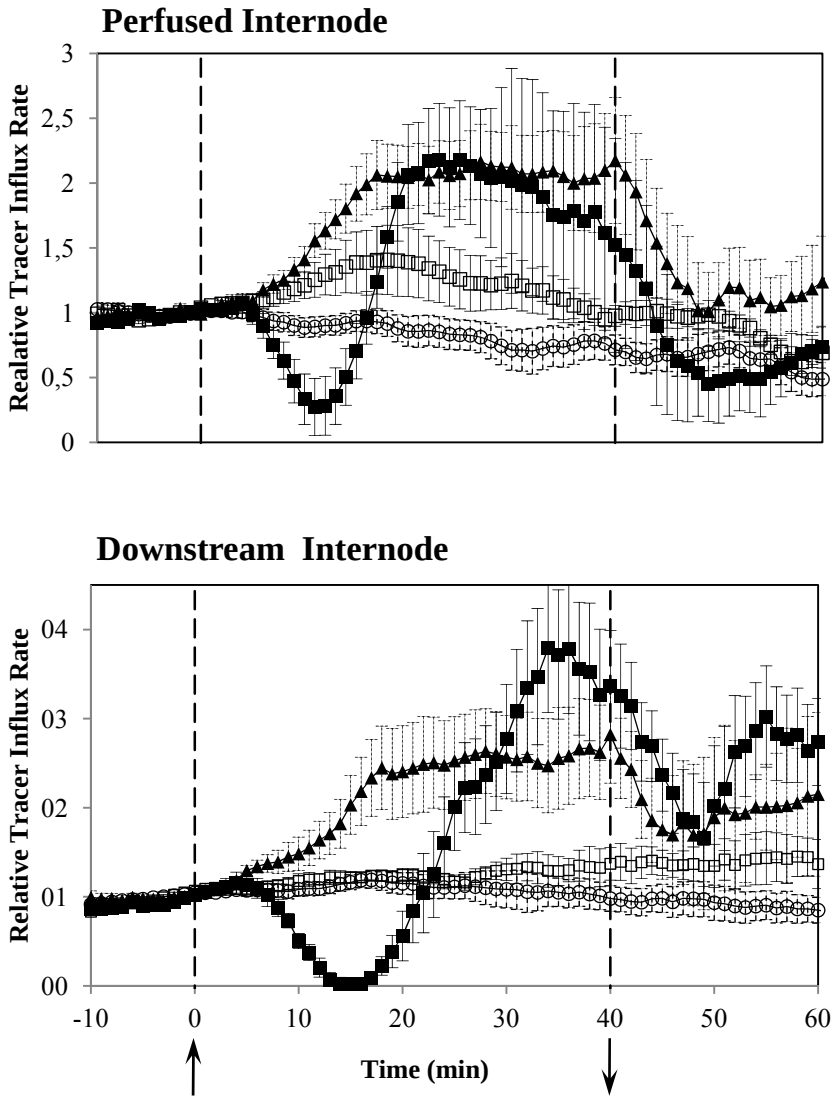

Figure 5.22 – Effect of perfusion by 500 mOsmolal solutions on the relative influx rate of mobilized tracer into the perfused internode and downstream internode (mean ± SE): ○ – control run (n = 7); ■ – mannitol (n = 5); □ – PEG (n = 5); ▲ – sucrose (n = 7). Treatments were applied at 0 time and removed 40 minutes later as indicated by the arrows.

Monitoring the tracer accumulation in the perfusion solution was not always possible. However, the results presented in Table 5.2 show that the different solutes used as treatments did not affect tracer accumulation in the perfusion solution, as there is no difference with the tracer loss observed when only ABS is being perfused and are far less than the tracer loss observed in squash internodes during treatments (Figs. 5.14, 5.17 and 5.19).

Table 5.2 – Tracer loss into the perfusion solution (mean ± SE).

Treatment	Loss ($\times 10^{-4}$ %.cm^{-1})
Control (n = 4)	4.5 ± 0.1
Mannitol (300 mM) (n = 3)	4.4 ± 0.3
PEG (300 mOsmolal) (n = 3)	4.6 ± 0.2
PEG (500 mOsmolal) (n = 1)	4.3
Sucrose (300 mM) (n = 1)	4.3
Raffinose (100 mM) (n = 1)	4.7

5.7 Solutions Osmolality

In order to better compare the effects of perfusion by the different solutes on ^{11}C transport and on water exchange between the plant and solutions, we measured the osmotic strength of the solutions. The solvent solution was not simply water but rather an aqueous strongly pH buffered solution – ABS – with an osmolality of 7.5 ± 0.6 mOsmol (n = 7). PEG osmolality varied non-linearly with the amount dissolved (Fig. 5.23), confirming previous results of osmotic pressure of culture solutions with PEG (Lagerwerff *et al*., 1961; McClendon, 1981; Michel, 1983; Michel *et al*., 1983; Michel & Kaufman, 1973). For the concentration range used in this study the best fit was a quadratic function from which we determined PEG osmolalities for the treatments to use (Fig. 5.23). The formula was different from what other authors have used (e.g. Michel, 1983) since it refers to a different solvent solution, but it confirms the quadratic variation of PEG solutions osmolality with the mass of PEG used in previous studies. Raffinose and mannitol osmolalities vary linearly with their concentration (Fig. 5.24). Sucrose osmolality varies non-linearly with concentration, but for concentrations up to 300 mM its variation is pretty much similar to mannitol osmalilty, giving similar values (cf. Fig. 5.24). This confirms the results of Michel (1972) and Michel *et al*. (1973).

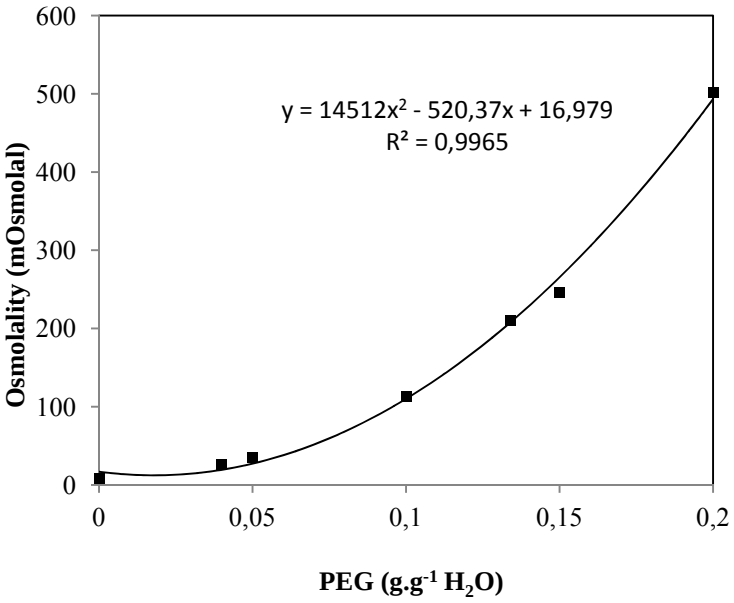

Figure 5.23 – PEG osmolality as a function of PEG mass using ABS as the solvent solution, n = 5. SE is on the order of 1 for all points, for this reason it is not displayed as it is smaller than symbols used.

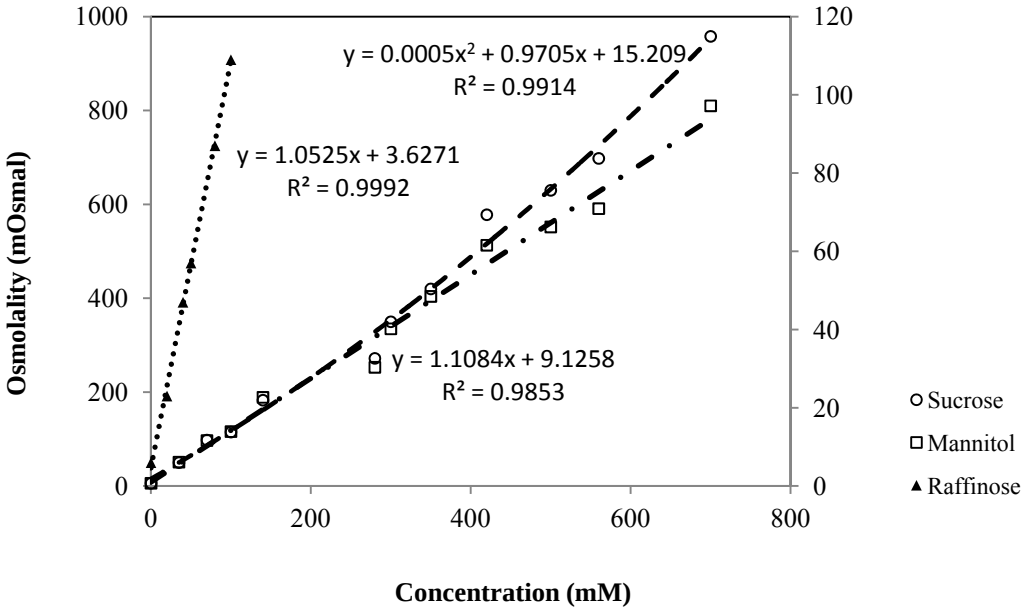

Figure 5.24 – Sucrose, mannitol and raffinose osmolalities as a function of concentration using ABS as the solvent solution, for all solutes n = 5. SE is on the order of 1 for all points, for this reason it is not displayed as it is smaller than symbols used. Raffinose osmolality is referenced to the right hand side axis.

5.8 Effect of Sucrose and Mannitol Perfusion on Water Exchange in Wheat Peduncle and Root

During ^{11}C experiments water exchange in the perfused region between the solution and the tissue was measured. When wheat peduncle was perfused by ABS, the plant took up water (0.19 ± 0.03 $mg.min^{-1}.cm^{-1}$, n = 15) and the uptake rate did not change during a control run experiment. Perfusion by both sucrose and mannitol at 100 mM showed no effect on water uptake, nor did it change the tracer loss in the peduncle (data not shown). Changes in the water uptake were only observed for 500 and 700 mM concentrations (Figs. 5.25 and 5.26). There was no difference between the effects of perfusion by the sugars at 500 mM, both causing a decrease in water uptake, making the plant take up less water while being perfused with mannitol or sucrose at 0.08 ± 0.03 and 0.07 ± 0.02 $mg.min^{-1}.cm^{-1}$ respectively (Fig. 5.25). A different scenario occurs when solute concentration rises to 700 mM (Fig. 5.26). At this concentration not only we had a reverse in the direction of water uptake but this effect was more pronounced for mannitol than for sucrose (Fig. 5.26). The peduncle water uptake reversed to –0.11 ± 0.02 and to –0.07 ± 0.02 $mg.min^{-1}.cm^{-1}$ for sucrose and mannitol. At this concentration a potometer was used for measuring the plant water uptake, taking advantage of the fact the plants were grown hydroponically (§ 4.6). However, with this setup (Fig. 4.1), it was not possible to measure the root water uptake continuously, as the roots needed aeration and the air supply to the root had to be stopped during measurements (Fig. 4.1). So, in order to minimize this effect, while still getting a good compromise between that and the necessary measurements, a time interval of 40 minutes was chosen. The treatment (the change of perfusion solution) was done at 20 minutes after the start of measurements. Perfusion by both sucrose and mannitol at 700 mM caused a similar effect on increasing the root water uptake to about 22 $mg.min^{-1}$ from the 18 $mg.min^{-1}$ observed before treatment application (Fig. 5.27). Returning to ABS perfusion, root water uptake, and peduncle uptake, both recovered to control run condition. These potometer results are quite useful as they show the good hydraulic coupling between the peduncle and the roots, consequently indicating its healthy state. They show that for the maintenance of such condition, when submitted to a forced loss of water in some part of the plant, there is compensation by increasing the root water uptake and it is sustained as long as the treatment lasts.

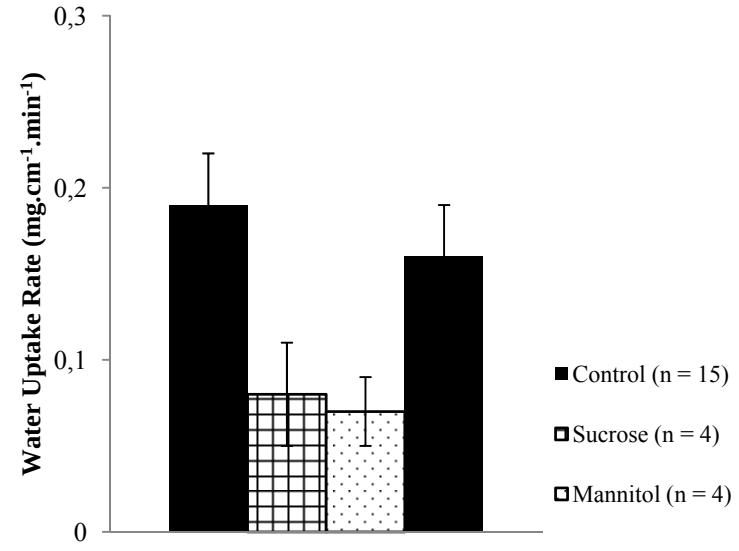

Figure 5.25 – Water uptake rates into wheat peduncle for 500 mM perfusion (mean ± SE). Control measurements refer to before treatment (left) and after treatment (right).

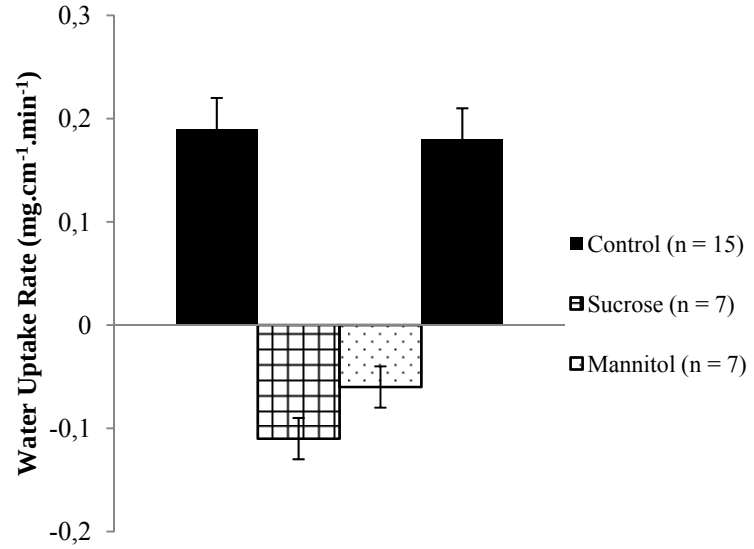

Figure 5.26 – Water uptake rates into wheat peduncle for 700 mM perfusion (mean ± SE). Control measurements refer to before treatment (left) and after treatment (right).

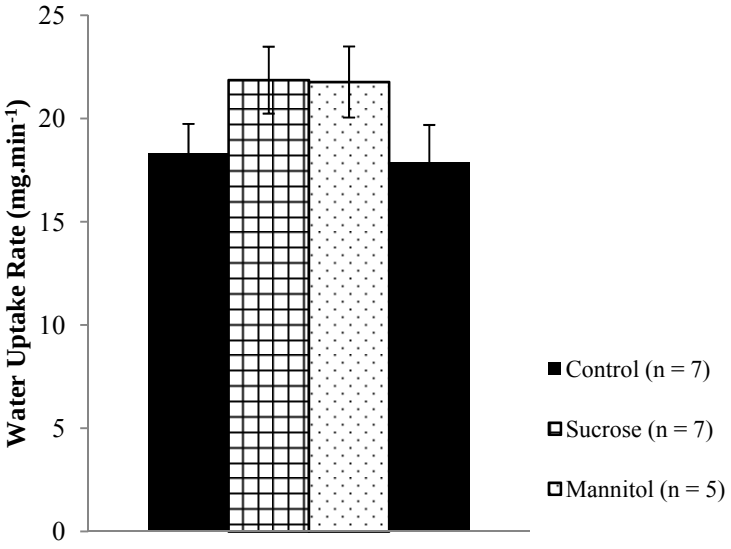

Figure 5.27 – Water uptake rates in the wheat root during 700 mM perfusion (mean ± SE). Control measurements refer to before treatment (left) and after treatment (right).

5.9 Effect of Sucrose, Mannitol, Raffinose and PEG Perfusion on Water Exchange in Squash Internodes

The 6th internode of a 6 to 8 week old squash plant (*Cucurbita maxima*) took up water at 0.82 ± 0.04 mg.min^{-1}.cm^{-1} when perfused with ABS (n = 13, including labelled and non-labelled plants) throughout the day. Perfusion by 100 mM sucrose and mannitol decreased the plant water uptake to 0.52 ±0.05 and 0.5 ± 0.03 mg.min^{-1}.cm^{-1} respectively (Fig. 5.28). Their effect was more pronounced than the decrease caused by the perfusion by 100 mOsmol PEG solution, which slightly decreased the plant water uptake to 0.76 ± 0.02 mg.min^{-1}.cm^{-1}. The perfusion by 100 mM raffinose caused an intermediate response between those of sucrose, mannitol and PEG effects, on decreasing the plant water uptake to 0.65 ± 0.08 mg.min^{-1}.cm^{-1}. Perfusion by 300 mM sucrose and mannitol caused similar effects; both reversed the water uptake making the plant to lose water to the perfusion so lution at 0.28 ± 0.04 and 0.25 ± 0.05 mg.min^{-1}.cm^{-1} respectively (cf. Fig. 5.29). This was not observed when 300 mOsmol PEG solution was perfused as the plant water uptake was not reversed but decreased more than at a 100 mOsmol of PEG to 0.66 ± 0.07 mg.min^{-1}.cm^{-1}.

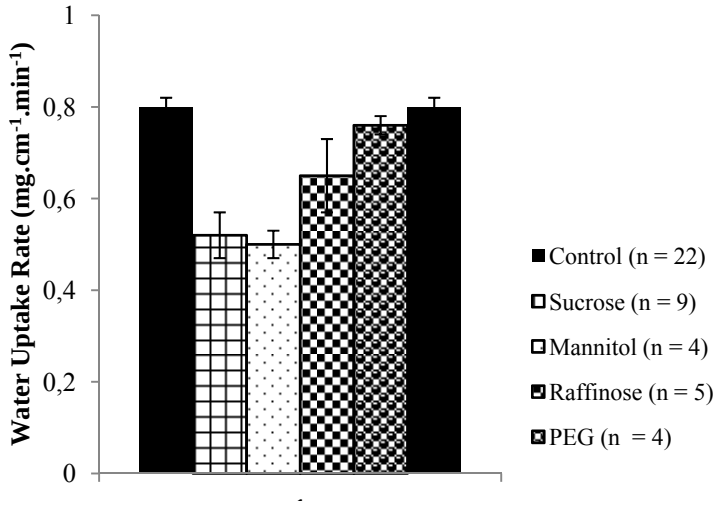

Figure 5.28 – Water uptake rates in the perfused internode of squash for 100 mOsmolal perfusion (mean ± SE). Control measurements refer to before treatment (left) and after treatment (right).

At 500 mM both sucrose and mannitol maintained their similar effects, reversing the water uptake by the plant to a more severe state, causing the plant to lose water to the perfusion solution at a rate of 0.67 ± 0.10 and 0.63 ± 0.11 $mg.min^{-1}.cm^{-1}$ respectively (cf. Fig. 5.30). PEG effect was still different from sucrose and mannitol at an equivalent osmotic strength as it did not reverse the plant water uptake but just reduced it to 0.26 ± 0.02 $mg.min^{-1}.cm^{-1}$. As with previous treatments at smaller concentrations, the plant water uptake resumed to its previous pre-treatment state with a similar uptake rate (Figs. 5.28, 5.29, 5.30).

5.10 PCMBS Effect on Tracer Loss

PCMBS was used to investigate the possible apoplastic step – membrane transport – for phloem reloading along the transport pathway in both wheat and squash.

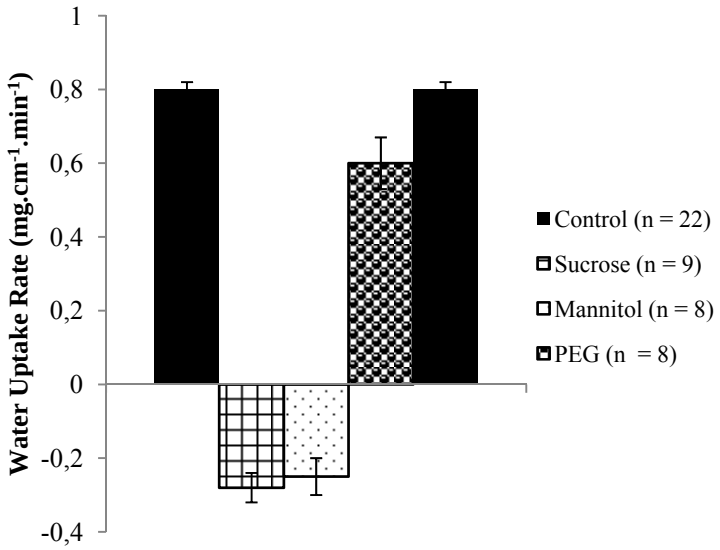

Figure 5.29 – Water uptake rates in the perfused internode of squash for 300 mOsmolal perfusion (mean ± SE). Control measurements refer to before treatment (left) and after treatment (right).

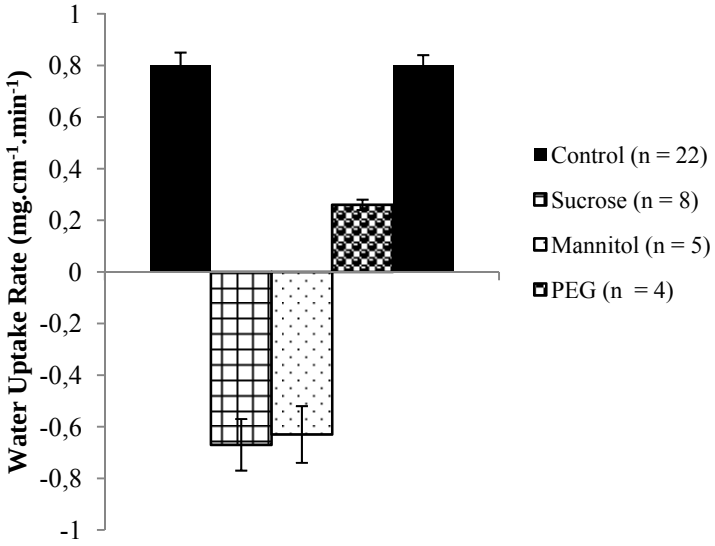

Figure 5.30 – Water uptake rates in the perfused internode of squash for 500 mM perfusion (mean ± SE). Control measurements refer to before treatment (left) and after treatment (right).

5.10.1 Wheat

The effect of perfusion by 2 mM PCMBS on tracer loss in wheat caused very different responses both in the perfused peduncle and in the vegetative part. In the peduncle, a clear increase in the tracer loss was evident on two cases that were also observed in the vegetative part (Fig. 5.31). However, the second case not only was less than observed in the first specimen, but it was also slower and more noticeable in the peduncle. The increase in tracer loss occurred mostly at the end of treatment and continued after treatment removal, similarly in the vegetative part. On the other two specimens the effect of PCMBS perfusion went from no response to a very slow decrease in tracer loss in the vegetative part of the plant which than became faster after treatment replacement by ABS (Fig. 5.31). As Fig. 5.31 shows the scenario in the vegetative part is more diverse and thus less suitable for interpretation, as the effects can go from no response to increase or decrease. This together with the various responses observed in the peduncle of the 4 different specimens used makes the PCMBS effect on the tracer loss in wheat very difficult to interpret.

5.10.2 Squash

PCMBS effects on squash, as opposed to wheat, were reproducible. PCMBS by itself at 2 mM caused an increase in tracer loss in both the perfused internode and the downstream internode (Fig 5.32), but did not affect transport in the load node region. In the perfused internode, if 2 mM PCMBS was included with 100 mM sucrose, the tracer loss increased much more than with sucrose or PCMBS alone (Fig. 5.32). In the downstream internode, 2 mM PCMBS alone gave a similar effect to 100 mM sucrose alone, but unlike the perfused internode, the sucrose response was the same with or without PCMBS (Fig. 5.32). In the load node region, the effect of perfusion by 100 mM sucrose (Fig 5.14) was completlely abolished when 2 mM PCMBS was also added (Fig. 5.32). The perfusion by 2mM PCMBS alone had no effect on tracer loss in the load node. For tracer accumulation, PCMBS increased the rate in both the perfused internode and the downstream internode (Fig. 5.33). And although sucrose caused a decrease in tracer in-

flux rate into both regions (Fig 5.16), with PCMBS there was an increase in tracer influx rate. The effect of PCMBS continued even after treatment removal (Fig. 5.33). Concerning tracer transfer into the perfusion solution, PCMBS had no effect (Fig. 5.34). The loss of tracer into the perfusion solution was not affected if the stem was perfused by PCMBS, and the situation did not change when PCMBS was removed.

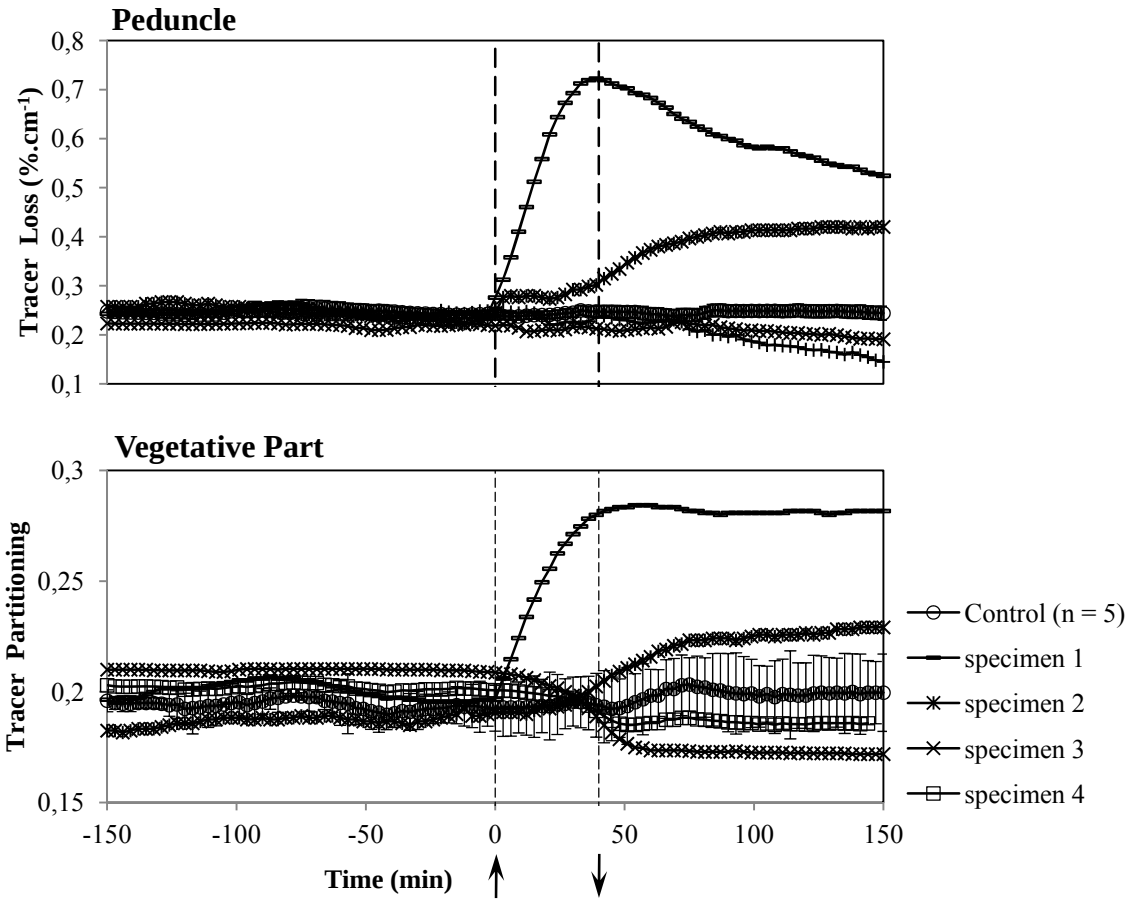

Figure 5.31 – Effect of perfusion by 2mM PCMBS on ^{11}C loss in wheat (mean ± SE for the control only). Treatments were applied at 0 time and removed 40 minutes later as indicated by the arrows.

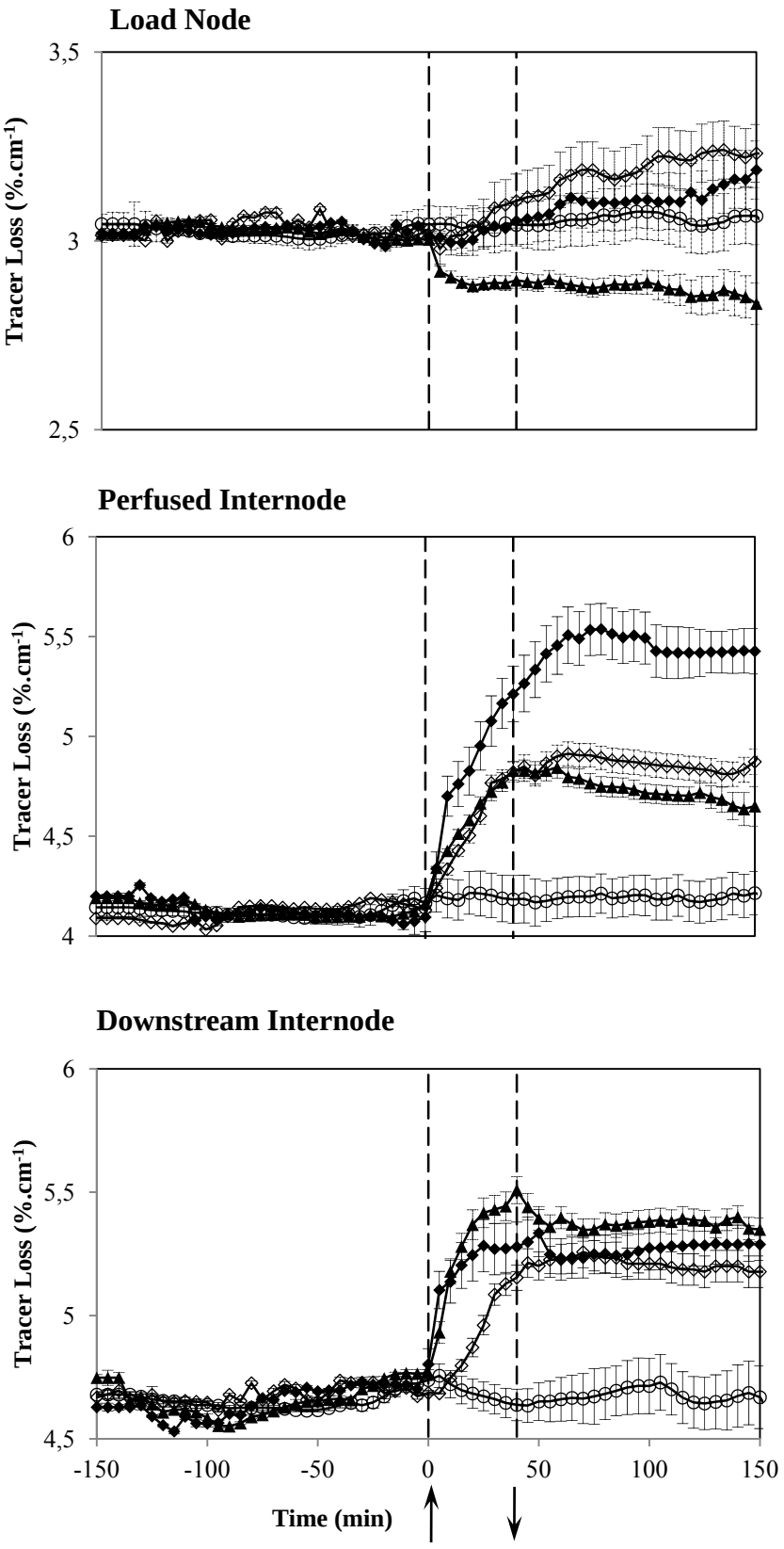
Load Node
Tracer Loss (%.cm-1)
3,5
3
2,5
Perfused Internode
Tracer Loss (%.cm-1)
6
5,5
5
4,5
4
Downstream Internode
Tracer Loss (%.cm-1)
6
5,5
5
4,5
-150
-100
-50
0
50
100
150
Time (min)

Figure 5.32 – Effect of perfusion by PCMBS on ^{11}C loss in squash internodes (mean ± SE): ○ – control run (n = 7); ◊ – 2 mM PCMBS (n = 4); ♦ – 100 mM sucrose + 2 mM PCMBS (n = 5); ▲ – sucrose (n = 7). Treatments were applied at 0 time and removed 40 minutes later as indicated by the arrows.

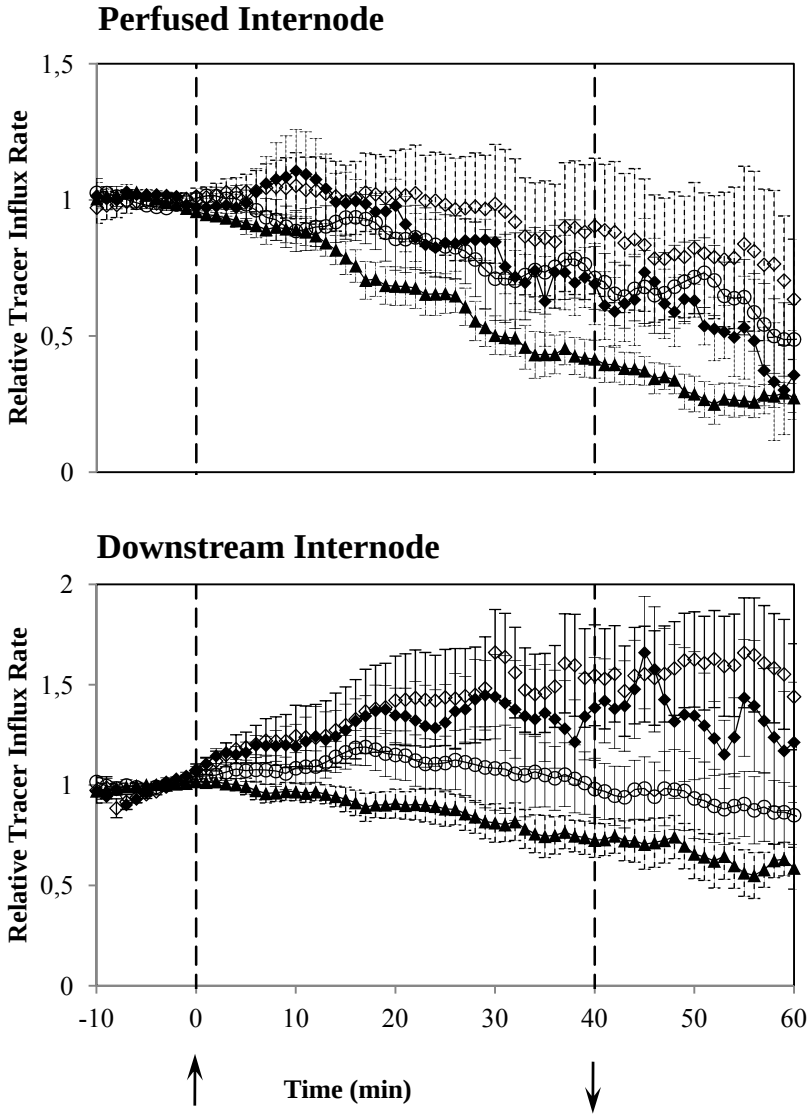

Figure 5.33 – Effect of of PCMBS on the relative influx rate of mobilized tracer into the perfused internode and downstream internode (mean ± SE): ○ – control run (n = 7); ◊ – 2 mM PCMBS (n = 4); ♦ – 100 mM sucrose + 2 mM PCMBS (n = 5); ▲ – sucrose (n = 7). Treatments were applied at 0 time and removed 40 minutes later as indicated by the arrows.

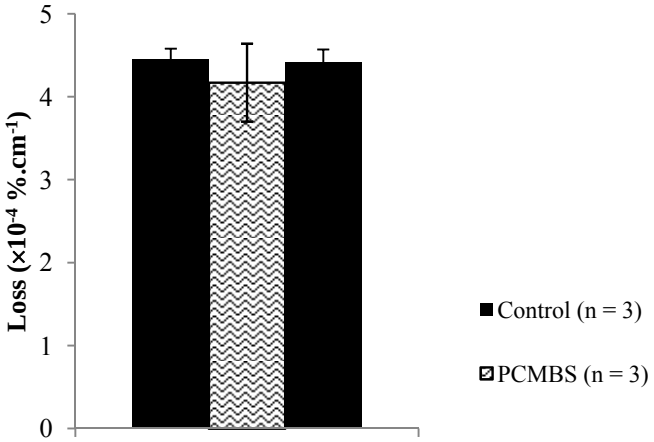

Figure 5.34 – Tracer loss into the perfusion solution during PCMBS (2 mM) perfusion (mean ± SE). Control measurements refer to before treatment (left) and after treatment (right).

5.11 PCMBS Effect on Water Uptake in Squash

Perfusion by 2 mM PCMBS caused a reduction of water uptake from the perfusion solution to the stem, and to the same extent as 100mM sucrose (Fig. 5.35). However, the effect was no different if 100mM sucrose was added with PCMBS. Water uptake recovered when treatments were removed and replaced by ABS (Fig. 5.35).

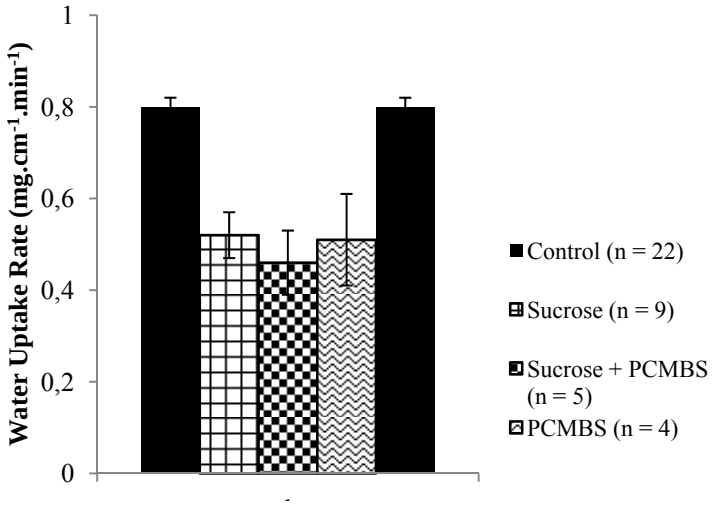

Figure 5.35 – Water uptake rates in the perfused internode of squash for perfusion by PCMBS (mean ± SE). Control measurements refer to before treatment (left) and after treatment (right).

5.12 Chilling Effect on ^{11}C Transport in Squash

The peristaltic pump (as normally used to perfuse squash internodes) was used to perfuse by water, that could be chilled quickly, 2 cm of the 6th internode (perfused internode) central region (§ 4.5). Fig. 5.36 shows the results obtained with one specimen in which two successive chilling treatments were applied followed by warming up back to ambient temperature. The initial ambient temperature of the bathing water was around around 27 ^{o}C and it was suddenly dropped in less than 30 s to around 15 ^{o}C in both treatments, by replacing the supply to be cold water instead of ambient water. The second treatment was longer than the first one. As it is already known for this family, *cucurbitaceae*, chilling inhibits phloem transport temporarily (Lang & Minchin, 1986). Tracer transport stopped downstream of the treated region in both the apex and the immediate downstream internode (Fig. 5.36), and recovered simultaneously in both regions while still at the lower temperature, but at a slower rate. The perfused internode did not show entirely the same behaviour as the downtstream internode; the chilled region was just 2 cm of the perfused internode and the detected region includes both upstream and downstream parts relative to the chilled region. Thus, while downstream of the treated segment phloem transport stops, on the opposite side (upstream of the treated segment) there is some transport and tracer accumulation. This is indicated by the decrease in the slope of the decay-corrected curve of the perfused internode (Fig. 5.36) for both treatments which is not zero.

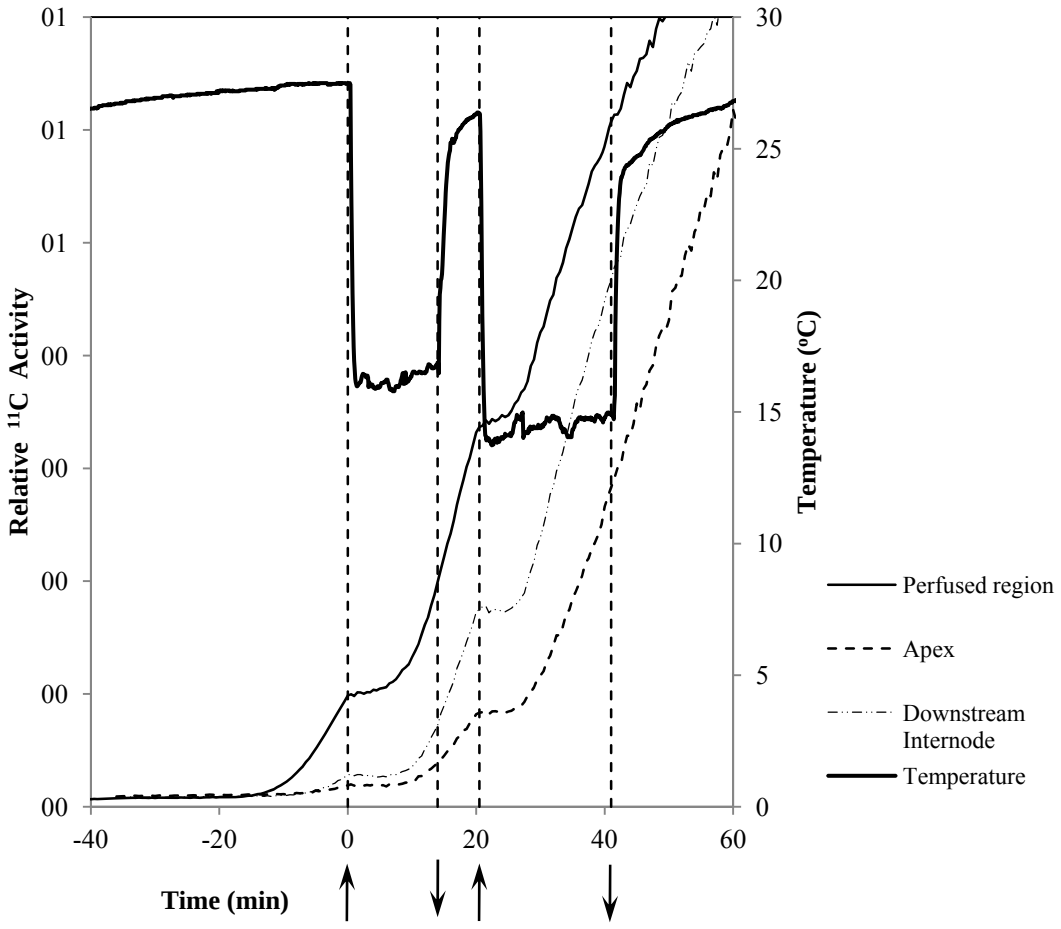

Figure 5.36 – Effect of abruptly dropping the temperature in 2 cm of the squash perfused internode on local transport of ^{11}C-photoassimilate. Half-life and background-corrected data for the detectors monitoring the different plant parts considered.

6. Compartmental Model of Phloem Transport

6.1 Compartmental System

A simple compartmental model was developed in order to interpret the ^{11}C experimental results for squash. The model represents the perfused internode of squash as three different compartments: the perfused pith cavity, the sieve tubes, and a third compartment, representing the xylem and ground parenchyma surrounding the vascular bundles (Fig. 6.1).

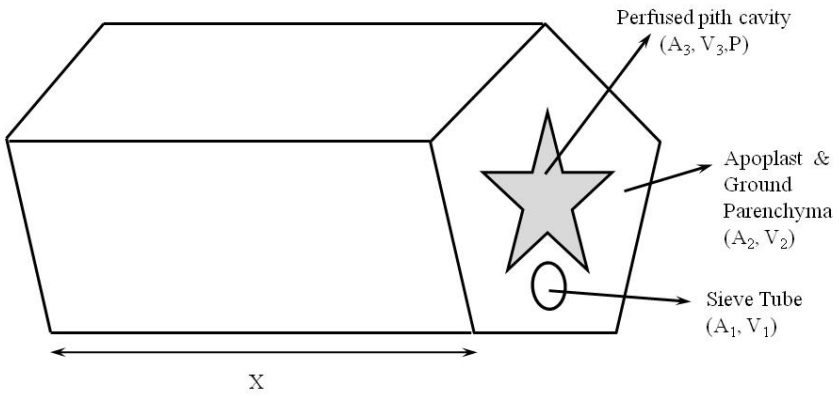

Figure 6.1 – Compartmental model of the perfused squash internode of length X and divided in three compartments of cross sectional area A_i and volume V_i, i = 1, 2, 3. The internode pith cavity of perimeter P is shown here as a pentagrammic prism.

A stem internode (Fig. 6.2) is represented as a phloem translocation pathway imbedded within an apoplastic volume which is bounded by the perfusion solution. There is no immediate output of tracer when input arrives at a given time at the perfused internode. For this reason, and to account for all the different processes happening in the internode contributing to tracer translocation, a time delay θ is specified before any tracer will appear as output. The translocation pathway is regarded as a time delay, θ, followed by a well-

stirred compartment of fixed volume at pressure p_1 and concentration C_1. Photoassimilates are delivered into compartment 1 at pressure p_{in} with concentration C_{in} through the input solution flux j_{in}. In the same way, it leaves this phloem compartment with a solution flux j_{out} at pressure p_{out} and concentration C_1. Between adjacent compartments there are lateral water and solute exchanges. Considering the symplastic constriction at the interface between the sieve element/companion cell complex, SE/CC, and the phloem parenchyma cells in the stem of squash characterized by very low plasmodesmal frequencies and densities (Kempers *et al*., 1998), the main interaction between the phloem and the rest of the internode tissue was taken to be through the apoplast. j_{lm} represents the solution exchange between compartments *l* and *m*, whereas the lateral flux of solute j_{Slm} between compartments *l* and *m* is the product of a transfer coefficient k_{lm} by the concentration of solute in compartment *l*:

$$j_{Slm} = k_{lm} C_l \tag{6.1}$$

In this model, loss of solutes is from the sieve tube considered as a linear concentration-dependent process. Given p_{in}, p_{out}, p_3, C_{in}, $C_1(t=0)$, $C_2(t=0)$, C_3, tracer input activity and the physiological and structural parameters as model inputs, the goal is to determine $p_1(t)$, $p_2(t)$, $C_1(t)$, $C_2(t)$ and the tracer distribution in the several compartments. From the

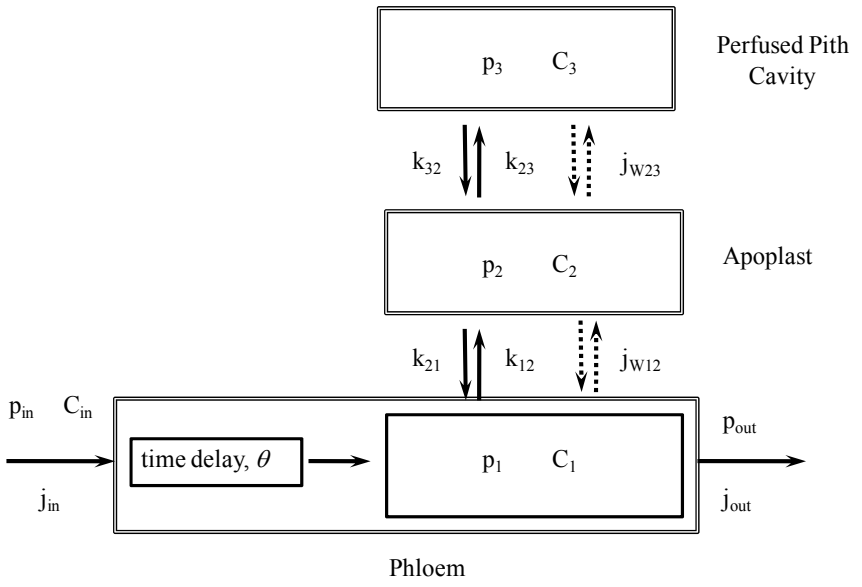

Figure 6.2 – Solute (⟶) and water (⇢) exchanges in the compartmental model of the perfused squash internode.

tracer distribution in compartment 1 together with j_{out} the model prediction of the tracer output activity can be calculated which is then compared with experimental data.

6.2 Model Equations

6.2.1 Volume Conservation

Volume conservation in the phloem compartment requires that any solution moving into compartment 1 leaves both radially and axially such that:

$$J_{in} = J_{out} + J_{12} \tag{6.2}$$

in which J is the volume flow rate which relates to flux j as:

$$J = jA \tag{6.3}$$

where A is the area through which flow occurs. The axial volume flux is given by Darcy's equation (2.15):

$$j = -\frac{k}{\mu}\frac{dp}{dx}$$

According to compartment dimensions, specifically its length, the axial volume influx and efflux of compartment 1 can be written as:

$$j_{in} = \frac{k}{\mu(C_{in})X}(p_{in} - p_1) \tag{6.4}$$

and

$$j_{out} = \frac{k}{\mu(C_1)X}(p_1 - p_{out}) \tag{6.5}$$

where X is the compartment length (the internode length), which is the same for all compartments (Fig. 6.1); μ is the phloem sap viscosity, a function of both solute concentration and temperature (see § 3.6.2); and k is the sieve tube axial conductivity, depending only on anatomical and structural features of the sieve tubes. Such features as lumen dimensions, the sieve plate pore density and dimensions, and the presence of other intracellular structures affect phloem flow via the parameter k. However the contribution of these different factors to sieve tube axial conductivity is not explicitly specified. The radial water exchange between compartment 1 and 2 is given by Starling's equation (2.6):

$$j_{W12} = L_1\left[p_1 - p_2 - \sum_{i=1}^{N}\sigma_{i12}(\Pi_{i1} - \Pi_{i2})\right] \tag{6.6}$$

where j_{W12} is the water flux. As there is also solute exchange between the two compartments, the solution volume flux j_{12} between compartment 1 and 2 is given by:

$$j_{12} = \frac{j_{W12}}{1 - \sum_{i=1}^{N}\bar{V}_i C_{i1}} = L_1^*\left[p_1 - p_2 - \sum_{i=1}^{N}\sigma_{i12}(\Pi_{i1} - \Pi_{i2})\right] \tag{6.7}$$

in which

$$L_l^* = \frac{L_l}{1 - \sum_{i=1}^{N}\bar{V}_i C_{il}} \tag{6.8}$$

for compartment l = 1,2,3; N is the number of different solutes considered; L_1 is the sieve tube membrane hydraulic conductivity; $\bar{V}_i$ is the molar volume of solute i at concentration C_{il} and is independent of concentration as long as the solution is not saturated; σ_{i12} is the reflection coefficient of the sieve tube membrane for the solute i moving across it, and

the osmotic pressure of solute *i* in compartment *l*, Π_{il}, according to Michel (1972), is given by:

$$\Pi_{il} = \rho_W R_g T\left(0.998 m_{il} + 0.089 m_{il}^{\,2}\right) \tag{6.9}$$

m_{il} being the molality of solute *i* in the compartment *l*, that is:

$$m_{il} = \frac{C_{il}}{\rho_W\left(1 - \bar{V}_i C_{il}\right)} \tag{6.10}$$

ρ_W is density of water at absolute temperature T and R_g is the universal gas constant. In our case, we distinguish treatment solutes from the endogenous solutes (sucrose), thus N = 2. In the model there is no axial movement of solution in compartment 2, so the volume conservation between compartments 2 and 3 requires that:

$$J_{12} = J_{23} \tag{6.11}$$

in which the solution flux, j_{23}, between the two compartments is:

$$j_{23} = L_2^*\left[p_2 - p_3 - \sum_{i=1}^{N}\sigma_{i23}\left(\Pi_{i2} - \Pi_{i3}\right)\right] \tag{6.12}$$

where L^*_2 is given by (6.8), L_2 is the hydraulic conductivity and σ_{23} is the reflection coefficient of solute *i* for the boundary between compartments 2 and 3. Substitution of equations (6.4), (6.5) and (6.7) into equation (6.2) and considering (6.3) yields:

$$p_1 = \frac{\left(L_1^* A_{lat1} + L_2^* A_{lat2}\right)\frac{kA_1}{X}\left(\frac{p_{in}}{\mu(C_{in})} + \frac{p_{out}}{\mu(C_1)}\right)}{L_1^* A_{lat1} L_2^* A_{lat2} + \frac{kA_1}{X}\left(L_1^* A_{lat1} + L_2^* A_{lat2}\right)\left(\frac{1}{\mu(C_{in})} + \frac{1}{\mu(C_1)}\right)} +$$

$$+ \frac{L_1^* A_{lat1} L_2^* A_{lat2}\left[p_3 + \sum_{i=1}^{N}\sigma_{i23}\left(\Pi_{i2} - \Pi_{i3}\right) + \sum_{i=1}^{N}\sigma_{i12}\left(\Pi_{i1} - \Pi_{i2}\right)\right]}{L_1^* A_{lat1} L_2^* A_{lat2} + \frac{kA_1}{X}\left(L_1^* A_{lat1} + L_2^* A_{lat2}\right)\left(\frac{1}{\mu(C_{in})} + \frac{1}{\mu(C_1)}\right)} \quad (6.13)$$

and combining equations (6.11) and (6.12) leads to:

$$p_2 = \frac{L_1^* A_{lat1}\left[p_1 - \sum_{i=1}^{N}\sigma_{i12}\left(\Pi_{i1} - \Pi_{i2}\right)\right] + L_2^* A_{lat2}\left[p_3 + \sum_{i=1}^{N}\sigma_{i23}\left(\Pi_{i2} - \Pi_{i3}\right)\right]}{\left(L_1^* A_{lat1} + L_2^* A_{lat2}\right)} \quad (6.14)$$

in which A_1 is the cross sectional area of compartment 1; A_{lat1} is the lateral area between compartments 1 and 2, i.e. the area of sieve tube membrane, and A_{lat2} is the area of the boundary between compartments 2 and 3.

6.2.2 Solute Conservation

The rate of change in the amount of endogenous solutes, N_l, in compartments 1 and 2 is given by:

$$\frac{dN_1}{dt} = J_{Sin} - J_{Sout} + J_{Slat.in} - J_{Slat.out} \quad (6.15)$$

and

$$\frac{dN_2}{dt} = J_{Slat.in} - J_{Slat.out} \quad (6.16)$$

where J_{Sin} and J_{Sout} are the solute axial input and output flows respectively and $J_{Slat.in}$ and $J_{Slat.out}$ are the solute lateral input and output flows respectively for each compartment. According to model assumptions, equations (6.15) and (6.16) can be written as:

$$\frac{dC_1}{dt} = -\left(k_{12} + \frac{j_{out}A_1}{V_1}\right)C_1 + k_{21}\frac{V_2}{V_1}C_2 + \frac{j_{in}A_1C_{in}}{V_1} \tag{6.17}$$

and

$$\frac{dC_2}{dt} = -\left(k_{21}+k_{23}\right)C_2 + k_{12}\frac{V_1}{V_2}C_1 \tag{6.18}$$

V_1, V_2 and V_3 are the volumes of compartments 1, 2 and 3 respectively. Any endogenous solute eventually moving into compartment 3 is washed out by the perfusion solution and will not be taken up. Thus, the rate of change in the amount of endogenous solutes in compartments 3, N_3, is given by:

$$\frac{dN_3}{dt} = J_{Slat.in} - J_{Sperfusion} \tag{6.19}$$

where $J_{Sperfusion}$ is the solute flow washed out by perfusing the pith cavity (V_3, Fig. 6.1). Hence, we have that:

$$\frac{dC_3}{dt} = k_{23}C_2 - q\frac{C_3}{V_3} \tag{6.20}$$

where q is the perfusion flow delivered by the peristaltic pump, which is constant. Thus $q\frac{Q_3}{V_3}$ is the solute bulk outflow that will end up in the waste bottle solution.

From Fig. 6.1 one can write $\frac{A_1}{V_1} = \frac{1}{X}$. Substituting the influx and efflux, equations (6.4) and (6.5), into equation (6.17) we obtain:

$$\frac{dC_1}{dt} = -\left[k_{12} + \frac{k}{\mu(C_1)X^2}(p_1 - p_{out}) \right] C_1 + k_{21}\frac{V_2}{V_1}C_2 + \frac{k}{\mu(C_{in})X^2}(p_{in} - p_1)C_{in} \tag{6.21}$$

where the pressure inside compartment 1, p_1, is given by equation (6.13). It is also necessary to consider the solutes that are supplied in treatments, which may not be the same as the endogenous solutes. The conservation of mass requires that the changes in the amount of treatment solute for compartments 1 and 2 are similar to what was considered to endogenous solutes (6.15) and (6.16). That is:

$$\frac{dC_{1t}}{dt} = -\left(k_{12t} + \frac{j_{out}A_1}{V_1} \right) C_{1t} + k_{21t}\frac{V_2}{V_1}C_{2t}$$

or

$$\frac{dC_{1t}}{dt} = -\left[k_{12t} + \frac{k}{\mu(C_1)X^2}(p_1 - p_{out}) \right] C_{1t} + k_{21t}\frac{V_2}{V_1}C_{2t} \tag{6.22}$$

and

$$\frac{dC_{2t}}{dt} = -(k_{21t} + k_{23t})C_{2t} + k_{12t}\frac{V_1}{V_2}C_{1t} + k_{32t}\frac{V_3}{V_2}C_{3t} \tag{6.23}$$

in which the subscript t refers to treatments solute. In compartment 2 the treatment solute follows the same path as the endogenous solutes present, whilst in compartment 1 the treatment solute will leave through bulk flow within the sieve tube or it will be exchanged with compartment 2 in a similar way as the other solutes. The main differences may be the various transport coefficients that different solutes can have, as indicated by the subscript t when compared with the endogenous solutes. Equations (6.21) and (6.22) are non-linear in the solute concentrations due to the explicit non-linear concentration dependence of p_1 as shown by equations (6.9) and (6.13), and the concentration dependence of phloem sap viscosity μ (3.137). For this reason equations (6.18), (6.20) to (6.23) were

solved numerically, using Euler's method where the solute concentration in compartment $l = 1, 2, 3$ is given by:

$$C_l(t_{n+1}) = C_l(t_n) + (t_{n+1} - t_n)\frac{dC_l}{dt}(t_n) \tag{6.24}$$

Hence, from equations (6.18), (6.20) and (6.21), one obtains, for the endogenous solutes:

$$C_1(t_{n+1}) = C_1(t_n) + (t_{n+1} - t_n)\left\{-\left[k_{12} + \frac{k}{\mu(C_1(t_n))X^2}(p_1(t_n) - p_{out})\right]C_1(t_n) + \right.$$
$$\left. + k_{21}\frac{V_2}{V_1}C_2(t_n) + \frac{k}{\mu(C_{in})X^2}(p_{in} - p_1(t_n))C_{in}\right\} \tag{6.25}$$

and

$$C_2(t_{n+1}) = C_2(t_n) + (t_{n+1} - t_n)\left[-(k_{21}+k_{23})C_2(t_n) + k_{12}\frac{V_1}{V_2}C_1(t_n)\right] \tag{6.26}$$

and

$$C_3(t_{n+1}) = C_3(t_n) + (t_{n+1} - t_n)\left[k_{23}C_2(t_n) - q\frac{C_3}{V_3}(t_n)\right] \tag{6.27}$$

For the treatment solutes, considering equations (6.22) and (6.23) one obtains respectively:

$$C_{1t}(t_{n+1}) = C_{1t}(t_n) + (t_{n+1} - t_n)\left\{-\left[k_{12t} + \frac{k}{\mu(C_1(t_n))X^2}(p_1 - p_{out})\right]C_{1t}(t_n) + \right.$$
$$\left. + k_{21t}\frac{V_2}{V_1}C_{2t}(t_n)\right\} \tag{6.28}$$

and

$$C_{2t}(t_{n+1}) = C_{2t}(t_n) + (t_{n+1} - t_n)\left[-(k_{21t}+k_{23t})C_{2t}(t_n) + k_{12t}\frac{V_1}{V_2}C_{1t}(t_n) + \right. \\ \left. + k_{32t}\frac{V_3}{V_2}C_{3t}(t_n) \right] \tag{6.29}$$

For the numerical evaluation of equations (6.25) to (6.27), initial conditions of concentrations have to be provided. The total solute concentration in each compartment at time t_n is given by:

$$C_{l\text{total}}(t_n) = C_l(t_n) + C_{lt}(t_n) \tag{6.30}$$

for $l = 1,2$.

6.2.3 Tracer Conservation

By definition, no tracer has any osmotic role and as such the rate of change in the amount of tracer in a compartment is linear with the amount of tracer in that compartment. Note also that tracer decays. Using the same reasoning as for solute movement, the rate of change of Q_1, the tracer amount in compartment 1, is given by:

$$\frac{dQ_1}{dt} = J_{\text{Tracer in}} - J_{\text{Tracer out}} + J_{\text{Tracer lat.in}} - J_{\text{Tracer lat.out}} - \left(\frac{dQ_1}{dt}\right)_{\text{decay}}$$

which gives,

$$\frac{dQ_1}{dt} = \left(\frac{j_{in}Q_{in}}{V_0} - \frac{j_{out}Q_1}{V_1}\right)A_1 + k_{21}Q_2 - k_{12}Q_1 - \lambda Q_1 \tag{6.31}$$

in which λ is the decay constant for ^{11}C, equal to $\lambda = \frac{\ln 2}{t_{1/2}}$, $t_{1/2}$ = 20.3 min and V_0 is the volume of the compartment preceding compartment 1 (the perfused internode). The incremental input and output activities entering and leaving the perfused internode are respectively:

$$\frac{dQ_{in}}{dt} = J_{Tracer\,in} - \left(\frac{dQ_{in}}{dt}\right)_{decay} = \frac{j_{in}Q_{in}}{V_0}A_1 - \lambda Q_{in} \tag{6.32}$$

$$\frac{dQ_{out}}{dt} = J_{Tracer\,out} - \left(\frac{dQ_{out}}{dt}\right)_{decay} = \frac{j_{out}Q_1}{V_1}A_1 - \lambda Q_{out} \tag{6.33}$$

where λQ_{in} is the measured activity of tracer that has entered the perfused internode and λQ_{out} is the measured activity of tracer that has left the perfused internode. The total amount of tracer detected in the perfused internode region only is given by:

$$Q_{in} - Q_{out} - Q_{perfusion} = Q_1 + Q_2 + Q_3 \tag{6.34}$$

in which Q_3 is the amount of tracer in the perfused pith cavity, and $Q_{perfusion}$ is tracer that has been collected after coming out of the plant in the perfused solution (§ 5.4, 5.6). According to Fig. 6.1, $\frac{1}{X} = \frac{A_1}{V_1} \cong \frac{A_1}{V_0}$, considering that the input tracer Q_{in} is somehow contained in a similar compartment as compartment 1 with the same cross sectional area A_1 and approximately the same length X. This is justified if one defines compartment 1 as the sieve tube element/companion cell complexes in the perfused internode so that its immediate upstream compartment will be also the sieve tube element/companion cell complexes of the upstream internode. In the experimental setup this corresponds to the internode immediately after the load node in the direction of flow and with very similar dimensions to the perfused internode. The activity of tracer coming into the perfused internode is the sum of the activities of the detectors monitoring the perfused internode, the downstream internode and the apex. For compartment 2, where no axial flow occurs, the rate of change in the amount of labelled photoassimilates is given by:

$$\frac{dQ_2}{dt} = J_{\text{Tracer lat.in}} - J_{\text{Tracer lat.out}} - \left(\frac{dQ_2}{dt}\right)_{\text{decay}}$$

or

$$\frac{dQ_2}{dt} = -(k_{21}+k_{23}+\lambda)Q_2 + k_{12}Q_1 \tag{6.35}$$

Any tracer leaking into compartment 3 (the perfused pith cavity) will be eventually washed out of the system by the perfusion stream and will not be taken up. Thus:

$$\frac{dQ_3}{dt} = J_{\text{Tracer lat.in}} - \left(\frac{dQ_3}{dt}\right)_{\text{decay}} - \frac{dQ_{\text{perfusion}}}{dt}$$

or

$$\frac{dQ_3}{dt} = k_{23}Q_2 - \lambda Q_3 - q\frac{Q_3}{V_3} \tag{6.36}$$

is the change in the amount of tracer in the internode pith cavity (compartment 3), q the perfusion flow delivered by the peristaltic pump as described before.

As mentioned before, due to the nonlinear dependence of both j_{in} and j_{out} together with μ on sugar concentration and the fact that the transfer coefficients and p_{in} and p_{out} might change with time due to treatments, equations (6.31) and (6.35) have time-dependent coefficients for Q_1 and Q_2 variables. Therefore, these equations will also be solved numerically following the same method used for determining the concentrations of endogenous and treatment solutes (§ 6.2.2). From equation (6.31) together with equations (6.4) and (6.5), one obtains the tracer amount in compartments 1:

$$\begin{aligned} Q_1(t_{n+1}) = Q_1(t_n) + (t_{n+1}-t_n)\Bigg[& \frac{kQ_{in}(t_n-\theta)(p_{in}(t_n)-p_1(t_n))}{X^2\mu(C_{in}(t_n))} - \\ & \frac{kQ_1(t_n)(p_1(t_n)-p_{out}(t_n))}{X^2\mu(C_1(t_n))} + k_{21}Q_2(t_n) - (k_{12}+\lambda)Q_1(t_n)\Bigg] \end{aligned} \tag{6.37}$$

where θ is the translocation time delay (Fig. 6.2). The amount of tracer in compartment 2 is:

$$Q_2(t_{n+1}) = Q_2(t_n) + (t_{n+1} - t_n)\left[-(k_{21} + k_{23} + \lambda)Q_2(t_n) + k_{12}Q_1(t_n)\right] \quad (6.38)$$

and the amount of tracer in the internode pith cavity is:

$$Q_3(t_{n+1}) = Q_3(t_n) + (t_{n+1} - t_n)\left[k_{23}Q_2(t_n) - \lambda Q_3(t_n) - q\frac{Q_3(t_n)}{V_3}\right] \quad (6.39)$$

From equations (6.33), the amount of tracer coming axially out of the perfused internode, Q_{out}, can be calculated numerically by:

$$Q_{out}(t_{n+1}) = Q_{out}(t_n) + (t_{n+1} - t_n)\left[\frac{k}{\mu(C_1(t_n))X^2}(p_1(t_n) - p_{out})Q_1(t_n) - \lambda Q_{out}(t_n)\right] \quad (6.40)$$

and $\lambda Q_{out}(t_n)$ will be the model output activity of the perfused internode that will be compared with the corresponding experimental data: the sum of the activities of the detectors monitoring both the apex and the downstream internode.

6.2.4 Translocation Time Delay, θ

In a steady state situation the time θ that it takes for any volume V of solution to be translocated through the phloem (compartment 1) with an average volume flow rate $\bar{J}$ is such that:

$$\theta = \frac{V_1}{\bar{J}} = \frac{2V_1}{(j_{in} + j_{out})A_1} \quad (6.41)$$

Hence, considering the solution flux densities given by equations (6.4) and (6.5), one can write:

$$\theta = \frac{2X^2}{k\left(\frac{p_{in} - p_{out}}{\mu(C_{in})} + \frac{p_1 - p_{out}}{\mu(C_1)}\right)} \tag{6.42}$$

confirming that, other things being equal, the more viscous the solution, the more slowly translocation occurs. Considering the values observed for the translocation speed in squash (Fig. 5.8) and perfused length X = 10 cm, one obtains θ from 10^2 to 10^3 s, thus well within the time expected for tracer to appear at the end of the perfused internode.

6.3 Model Parameters

As can be seen from the model equations, anatomical and physiological information are needed in order to best apply the model to experimental data.

6.3.1 Sugar Concentration

One of the most intriguing facts about phloem transport in *cucurbitaceae* is the apparent low sugar concentration and very high protein content measured from phloem exudates when compared to other species (Crafts, 1931, 1932; Fiehn, 2003; Richardson & Baker, 1982; Richardson *et al*., 1984). This high protein content has been considered a peculiar feature of this family and is hard to reconcile with the Münch pressure flow mechanism that depends on high osmotic sugar contents in sieve tubes. However, high osmotic pressures have been observed in plasmolysis experiments in mature sieve tube elements of the vascular bundles in callus tissue in *Cucurbita pepo* (Lackney & Sjolund, 1991). Haritatos *et al*. (1996) have also measured high RFO concentrations in SE/CCs in minor veins. But, most if not all the phloem exudates, as typically collected from *cucurbitaceae* species, have been shown to come from extrafascicular sieve tubes not from the external and internal phloem of vascular bundles (Zhang 2005; Zhang *et al*., 2010). The extrafascicular sieve tubes have been known from the very early studies in *cucurbitaceae,*

and compose an anastomozing system scattered throughout the ground parenchyma (Crafts, 1931, 1932). They connect the different vascular bundles and also run parallel surrounding the vascular bundles and the stem sclerenchyma (Cronshaw & Esau, 1968b; Kempers *et al*., 1993). Zhang (2005) suggested that this close proximity to the vascular bundles has led to exudate being mistakenly taken to come from the bundles. The composition of sugar and proteins differ between vascular and extrafascicular phloem, and the sugar content is much less in the extrafascicular system (Zhang, 2005; Zhang *et al*., 2010). Zhang (2005) also observed that the sugar concentration of the vascular phloem was closer to the values in minor veins (i.e. Haritatos *et al*. 1996). In the present model the extrafascicular sieve tubes are not considered as a separate compartment and they are not specifically identified and characterized in microscopy observations (Figs. 5.2, 5.3). The solute values here were therefore constrained to resemble those in vascular phloem, with input and content of compartment 1, C_{in}, and $C_1(0)$, in the range of 500 to 800 mM, and for compartment 2 the initial concentration, $C_2(0)$ in the range 50 to 300 mM. The value for $C_3(t)$ is that of the perfusing solution.

6.3.2 Sap Viscosity

Phloem sap viscosity was specified to depend on both temperature and phloem sap chemical composition, according to equation (3.138). Fiehn, (2003) showed that the main fraction of sugars for squash is of stachyose and raffinose, thus for the temperature during experiemtns, 22 ^{o}C, we specified parameters a = 1.07 and E = 94.46 (Chirife & Buera, 1997).

6.3.3 Anatomy and Structure

From the experimental results presented (§ 5.1.2) the lumina of all sieve tubes makes up about 1% of the total stem cross sectional area, while the pith cavity occupies about 20 %. Therefore, the cross sectional area of compartment 2, A_2, (being everything but the sieve tubes lumina and the pith cavity) is about 79 % of the stem cross section. Hence, for a perfused internode length X of 10 cm: $\frac{V_1}{V_2}$ = 1/79 and $\frac{V_3}{V_2}$ = 20/79. As an approximation and considering the stem anatomy described before (§ 5.1.2), for a typical

squash stem of pentagonal cross section of side length 6 mm, its cross sectional area is approximately 6.2×10^{-5} m^2. Hence, the perfused internode volume is 6.2×10^{-6} m^2. Giving its convoluted nature resembling a star shape, we can approximate the pith cavity cross sectional area, $A_3 \cong 1.2\times10^{-5}$ m^2, as a pentagram for which its perimeter P ≅ 2.1 cm (Fig. 6.1). The lateral area A_{lat2} of the pith cavity, separating compartments 2 and 3, was thus considered a pentagrammic prism, with $A_{lat2} \cong 2.1\times10^{-3}$ m^2. Considering the sieve tube lumina and vascular bundles cross sections relative to the cross section of the stem (§ 5.1.2), the total cross sectional area of compartment 1 is 1% of the total stem cross section, thus $A_1 = 6.2\times10^{-7}$ m^2 while the total lateral area of compartment 1 representing the sieve tubes, A_{lat1}, is approximately 2.8×10^{-4} m^2.

6.3.4 Membrane Hydraulic Conductivities

The sieve tube membrane hydraulic conductivity, L_1, will be taken between 5×10^{-15} and 1×10^{-13} $m.s^{-1}.Pa^{-1}$ (see § 3.6.4). The conductivity, L_2, for the border between compartment 2 (apoplast) and the compartment 3 (internode pith cavity) can be estimated from the water uptake data of the perfused internode during PEG treatments (§ 5.9). As PEG does not penetrate into the plant tissue (Carpita *et al*. 1979; Oertli, 1986), the solution flow between the two compartments will only be water exchange, so that for PEG perfusion, the reflection coefficient between compartments 2 and 3 becomes $\sigma_{23} = 1$ and equation (6.6) can be written as:

$$j_{W23} = L_2\left[\left(p_2 - \Pi_2\right) - \left(p_3 - \Pi_3\right)\right] = L_2\left(\Psi_2 - \Psi_3\right)$$

in which Ψ_1 and Ψ_2 are the water potential of compartments 2 and 3 respectively. So, in a steady state situation of constant water exchange between the two compartments as it was observed, one can write:

$$j_{W23} = L_2\Psi_2 - L_2\Psi_3$$

The water uptake measured ($Kg.s^{-1}.m^{-1}$) is given by:

$$j_{23W} = L_2 \rho_W P \Psi_2 - L_2 \rho_W P \Psi_3 \qquad (6.43)$$

where P is the internode pith cavity perimeter (see § 6.3.3). P can be larger than the internode perimeter itself due to its convoluted nature. The density of water, ρ_W, at 22 ^oC is 997.735 kg.m^{-3} (Streeter *et al*., 1998). As equation (6.43) shows j_{23W} (Ψ_3) is linear in Ψ_3, thus the slope is $-L_2\rho_W P$. From water uptake rates for the different PEG treatments (Figs. 5.27, 5.28 and 5.29) as a function of pith cavity osmotic pressure, Ψ_3 (Fig.6.3) one obtains $L_2 \cong 3\times10^{-14}$ m.s^{-1}.Pa^{-1}. Note that L_2 represents the hydraulic conductivity of the border of a very diverse compartment 2, which includes both apoplastic and symplastic intercellular pathways for water movement together with the xylem stream. The well known, and already mentioned, symplastic constriction at the interface between the sieve element/companion cell complex (SE/CC) and the phloem parenchyma cells in the stem of squash (Kempers *et al*., 1998) may contribute to the fact that it is smaller than sieve tube membrane conductivity L_1.

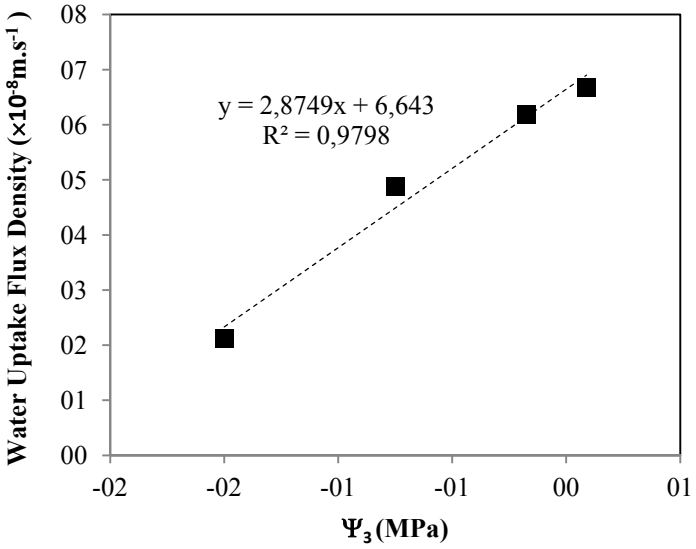

Figure 6.3 – Water uptake of the squash perfused internode pith cavity during PEG perfusion.

From comparison of equation (6.43) with the data presented by Fig. 6.3 one obtains $\Psi_2 \cong -2.3$ MPa for compartment 2 (intercept for zero flow). However, values like this are reported for water-stressed plants which we believe is not the case with the plants we used (Chone *et al*., 2001; Fisher & Cash-Clark, 2000; Sdoodee & Somjun, 2008).

Note also that, unlike the model assumption, represented by equation (6.11), all water uptake data presented in this work do not represent the water uptake by the sieve tubes. In fact the latter is most probably much less than the values presented.

6.3.5 Sieve Tube Axial Conductivity

Measurements of the sieve tube axial conductivity, k, have been more frequent than measurements on the sieve tube membrane hydraulic conductivity, L_1, as they can be obtained from combining translocation velocity and turgor pressure gradients data. The review of Milburn (1975) on pressure flow hypothesis over the experimental work done up to that time found that k/μ ranged from 0.58 to 9.72×10^{-10} $m^2.s^{-1}.Pa^{-1}$. Most of the combined studies were performed on tree species. From the fewer studies of herbaceous, Milburn (1975) pointed out the values were smaller compared with those for trees. However, due to different methodologies and the limited range of species studied, that difference might not be real. The anatomy and structure of sieve tubes data are well suited to being used in Hagen–Poiseuille equation. This made its application on phloem transport almost universal and convincing to a lot of authors. Its simplicity and ease of interpretation also contributed. Perhaps its most powerful feature was the fact that it allows anatomy, physiology and structural data for different plant species, i.e. sieve tube element lumen, sieve plate pore dimensions and density, together with phloem sap viscosity, as equations (2.7) and (2.14) show, to be related to measured turgor pressure gradients and velocity. In this way, Tyree, Christy & Ferrier (1974) estimated k/μ to vary between 0.2 and 22×10^{-9} $m^2.s^{-1}.Pa^{-1}$ in a survey of different species including herbaceous and tree species. This range of values was commonly used in several other works (i.e. Goeschl *et al*., 1976). Rand *et al*. (1980), applying Stokes' equation (2.13) and from a small survey of different plant species, showed that sieve tube axial conductivity could be reduced by 15 to 75 % of the values estimated by Tyree, Christy & Ferrier (1974). This broadens the range of values of k/μ from 4×10^{-11} to 2×10^{-8} $m^2.s^{-1}.Pa^{-1}$, which makes it closer to the values estimated from experimental data (Milburn, 1974). Thompson & Holbrook (2003a) improved the approach used by Tyree, Christy & Ferrier (1974) to estimate the sieve tube axial conductivity (2.14) and obtaining values in order of 10^{-13} $m^2.s^{-1}.Pa^{-1}$, about 13% of the value in the absence of sieve plates. Thus the estimates of Tyree, Christy & Ferrier (1974) were thereby decreased by one order of magnitude, to values which agree more

with the experimental data (Milburn, 1975). Note that sap viscosity μ(T, ^{o}C) is an inherent part of sieve tube axial conductivity in most experimental considerations (Milburn, 1975) and in most theory (Tyree, Christy & Ferrier, 1974; Thompson & Holbrook, 2003a), whereas here the conductivity is a purely geometrical factor and sap viscosity is a separate parameter. It is viscosity that appears in Darcy's equation (2.15). The influence of geometry comes in via boundary conditions. Since phloem sap viscosity is of the order 10^{-3} Pa.s, sieve tube conductivity k is much smaller than the values surveyed above, as well as having different dimensions. With the translocation speed we observed in the squash perfused internode (Fig. 5.8), Darcy's equation (2.15), the expected order of magnitude for phloem sap viscosity (10^{-3} Pa.s), and the turgor pressure gradients mentioned before (§ 3.6.3) (10^{-1} MPa.m^{-1}), the order of magnitude of the sieve tube axial conductivity k is 10^{-12} to 10^{-11} m^2.

6.3.6 Model Evaluation and Transfer Coefficients

Not all parameter values are readily available from experimental and theoretical work. Furthermore in some cases they arise from model assumptions, not particularly or directly attributed to known physiological measurements. Hence, evaluation of a model like this one presented becomes crucial and more difficult. The criteria for finding the best values of model parameters were chosen after Thornley & Johnson (2000) and setting the biological range of all the parameters previously described. First, the model residual, r_i, for time i is calculated as:

$$r_i = \ln\left(\frac{y_i}{Y_i}\right) \tag{6.44}$$

y_i being the measured value and Y_i the corresponding model prediction for that measured variable at time i. The best model is the one that gives the minimum sum of squares up to time N:

$$R=\sum_{i=1}^{N} g_i r_i^2 \tag{6.45}$$

using a weighing factor g_i if required. For our case, all residues were taken as equally important ($g_i = 1$), the model output Y_i was the activity of the simulated output of the perfused internode, with measured values y_i. The best model was estimated by varying the transfer coefficients k_{ij} to minimize R, while ensuring that corresponding values of pressure, translocation speed, and water exchange between the compartments were physiologically reasonable (i.e. within the ranges specified above). To this end, the appropriate fitting involved fixing the ranges for pressure (p_{in}, p_{out}, andp_3), k, L_1, L_2, $C_1(0)$, and $C_2(0)$, then varying k_{ij}, to improve R and evaluating whether the predicted output values of pressure, translocation speed and water exchange, between the compartments, fall within their expected biological range. Their "biological likelihood" was the main criteria for deciding the possible values for the transfer coefficients to be used. The goal here is not to infer parameter values per se but to describe tracer data under the proposed model.

6.4 Model Results

Unless otherwise specified the following model parameter values were used:

Table 6.1 –Values of the physical parameters used in the compartmental model.

Parameter	S.I. Units	Value
^{11}C half life, $t_{1/2}$	min	20.3
Compartment length, X	m	0.1
Compartment 1 cross sectional area, A_1	m^2	6.2×10^{-7}
Hydraulic conductivity, L_2	$m.s^{-1}.Pa.^{-1}$	3×10^{-14}
Initial solute concentration in compartment 1, $C_1(0)$	$mol.m^{-3}$	600
Initial solute concentration in compartment 2, $C_2(0)$	$mol.m^{-3}$	200
Initial solute concentrations: $C_{1t}(0)$, $C_{2t}(0)$	$mol.m^{-3}$	0
Input pressure, p_{in}	MPa	0.995 to 1.0[†]
Input solute concentration, C_{in}	$mol.m^{-3}$	600
Lateral area, A_{lat1}	m^2	2.8×10^{-4}
Lateral area, A_{lat1}	m^2	2.1×10^{-3}
Output pressure, p_{out}	MPa	0.99 to 0.995[†]
Pith cavity volume, V_3	m^3	1.24×10^{-7}

Reflection coefficients: $\sigma_{12} = \sigma_{23}$	—	0.5
Sap viscosity, μ	Pa.s	0.0015
Sieve tube axial conductivity, k	m^2	10^{-12} to 10^{-11}
Sieve tube membrane hydraulic conductivity, L_1	$m.s^{-1}.Pa.^{-1}$	7.5×10^{-14}
Mannitol specific volume, $\overline{V}_{MannS}$	$m^3.mol^{-1}$	1.192×10^{-4}‡
Sucrose specific volume, $\overline{V}_S$	$m^3.mol^{-1}$	2.155×10^{-4}*
Temperature, T	^oC	22
Universal gas constant, R_g	$J.K^{-1}.mol^{-1}$	8.314
Volume ratio, V_1/V_2	—	1/79
Volume ratio, V_2/V_3	—	20/79
Water density, ρ_W	$kg.m^{-3}$	998

† See § 3.6.3

‡ Kiyosawa (1991)

* Eszterle (1993)

6.4.1 Control Runs

In order to estimate the model parameters, the model examination started with the control runs (ABS perfusion only), and this also gives some illustrations of the fitting procedure. The model itself allows different hypothetical scenarios. In a first case there is no solute exchange between the phloem and surrounding tissue. As a consequence, all the transfer coefficients k_{ij} are null, reflection coefficients σ_{ij} are equal to 1, and tracer leaves compartment 1 axially, by bulk flow only. Other parameters were set at the middle of their expected physiological ranges, as listed in Table 6.1: the sieve tube turgor pressure difference, $\Delta p = p_{in} - p_{out} = 0.001$ MPa; sieve tube axial conductivity, $k = 5\times10^{-12}$ m^2; sieve tube membrane conductivity, L_1; C_1 (0); C_2 (0) and L_2. With these values, the model translocation speed is less than the observed values, as indicated by the time lag between the model prediction and the experimental data (Fig.6.4). To increase the speed, a higher turgor pressure gradient or much higher axial conductivity seem to be needed, but either change produces scenarios that are not physiologically reasonable. For example if the sieve tube axial conductivity, k, was increased to 2.4×10^{-11} m^2 (Fig. 6.5) the model output tracer activity was initially similar to the experimental data but reached a much too high tracer activity. Changing either the turgor pressure difference or the sieve tube axial con-

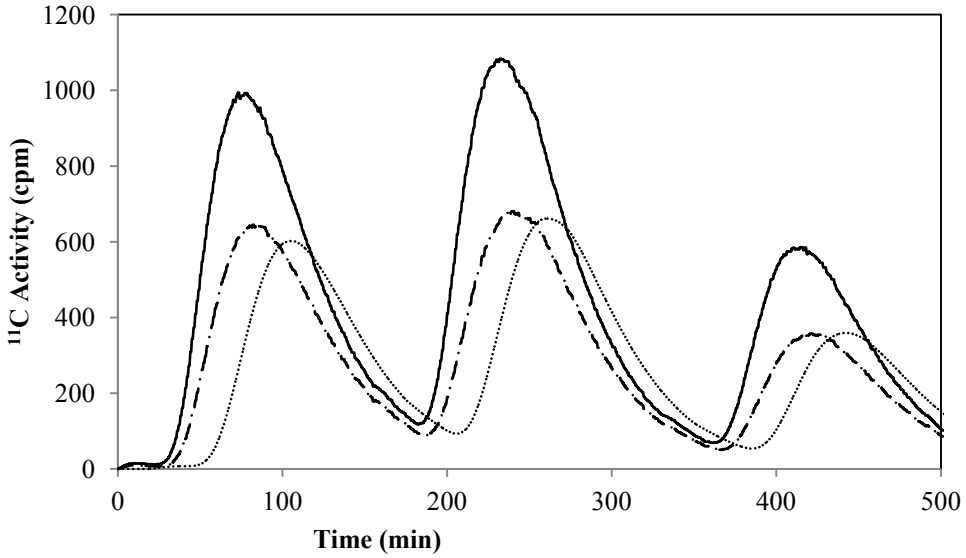

Figure 6.4 – Experimental data of input activity (–) and output activity (· –) for the perfused internode and model prediction for the output activity (···) where there is no solute exchange between the phloem and the surrounding tissue, and transfer coefficients: $k_{12} = k_{21} = k_{23} = k_{32} = 0$. Other parameters were set to: $\sigma_{12} = \sigma_{21} = 1$; $p_{in} = 1$ MPa; $p_{out} = 0.99$ MPa; $\Delta p = p_{in} - p_{out} = 0.01$ MPa; $k = 5\times10^{-12}$ m^2; $L_1 = 7.5\times10^{-14}$ m.Pa^{-1}.s^{-1}; $L_2 = 3\times10^{-14}$ m.Pa^{-1}.s^{-1}; C_1 (0) = 600 mM and C_2 (0) = 200 mM.

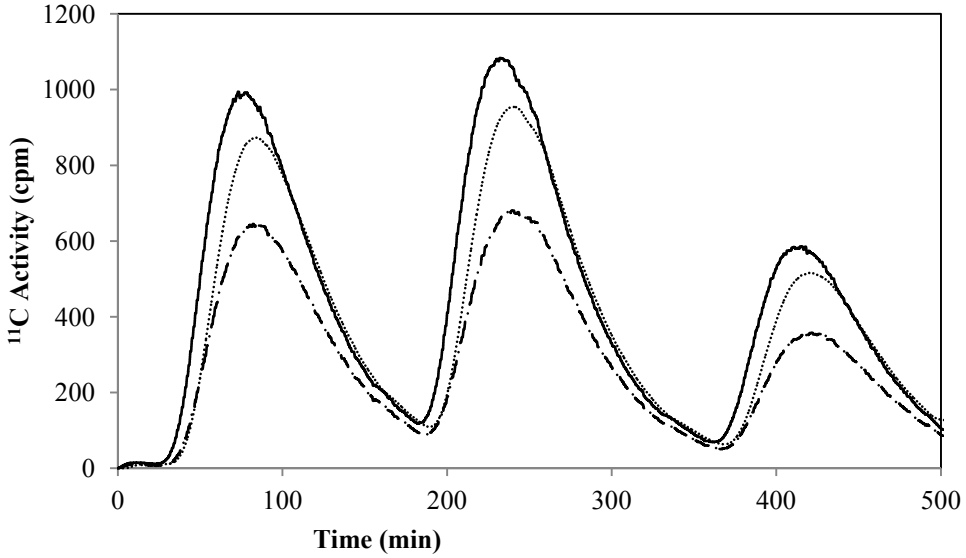

Figure 6.5 – Experimental data of input activity (–) and output activity (· –) for the perfused internode and model prediction for the output activity (···) where there is no solute exchange be-

tween the phloem and the surrounding tissue, all parameters are the same as in Fig. 6.4 except for $k = 2.4\times10^{-11}$ m^2.

ductivity inside their respective physiological ranges, produces scenarios that do not match the experimental output activity profiles. The results are either slower or not delivering the observed amount of tracer.

If there is solute exchange between the three compartments, as experimentally observed with tracer (§ 5.4, 5.6 and 5.9), but maintaining the same physiological conditions of the cases shown in Figs. 6.4 and 6.5, the best fit, according to criterion (6.45), corresponds to $k_{12} = 1.85\times10^{-3}$ s^{-1}, $k_{21} = 7.0\times10^{-5}$ s^{-1} and $k_{23} = 5.3\times10^{-6}$ s^{-1} and a sieve tube axial conductivity $k = 2.4\times10^{-11}$ m^2 (Fig 6.6). In this model, the tracer distribution among the three compartments does not explicitly depend on the reflection coefficients σ_{12} and σ_{23} which affect only pressures p_1, p_2 and the water exchange between compartments. So, the criteria for deciding the best reflection coefficient values were to have both a positive pressure p_2, and a positive radial water flow outward from compartment 1, as expected if there is solute unloading in the phloem. With these two additional conditions, two scenarios give water outflow from compartment 1: (i) all boundaries are permeable to solutes and tracer (thus σ_{12}, $\sigma_{23} < 1$); or (ii) tracer moves only between compartments 1 and 2, not crossing to compartment 3, hence $\sigma_{12} < 1$ and $\sigma_{23} = 1$. However, since $k_{23} = 5.3\times10^{-6}$ s^{-1}, although small is not zero, so it is not logical for tracer to be therefore moving out of compartment 2 to 3, but at the same time the border is impermeable to tracer, and $\sigma_{23} = 1$. Therefore the first scenario is considered as representative of the control run situation. Having both barriers permeable to tracer, but with no way of discriminating between different reflection coefficient values, we put $\sigma_{12} = \sigma_{23} = 0.5$. This recognizes that each compartment boundary is permeable to tracer and endogenous solutes. Our choice of σ_{12} and σ_{23} is somewhat arbitrary but justified by the insensitivity of the model output to changes of σ_{12} and σ_{23} and by the fact that these parameters have not been measured for sieve tubes. Fig. 6.7 shows the fitting of the model prediction to experimental data presented in Fig. 6.6, represented by the model residuals, r_i, (6.44) and by the ratio between the curves at each time. Note the very good fitting represented by the small residues equal to zero and the ratio of model prediction to experimental data very close to 1 throughout most of the time. For the control run presented in Fig. 6.6, pressure inside compartment 1, 0.995 MPa, lies between model inputs p_{in} and p_{out}, while pressure inside compartment 2 is around 0.35 MPa, well below the value for compartment 1 (Fig. 6.8). This may be not to-

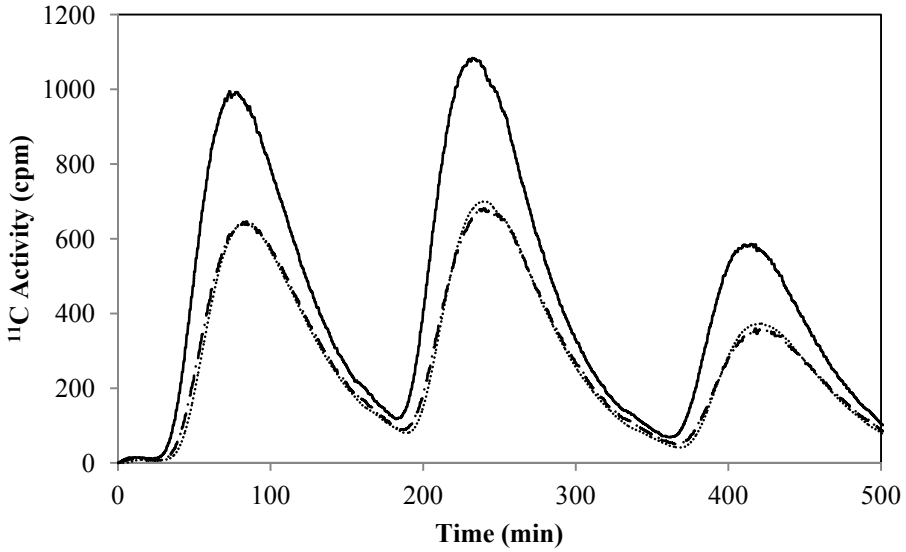

Figure 6.6 – Experimental data of input activity (–) and output activity (· –) for the perfused internode and model prediction for the output activity (···) with solute exchange between the phloem and the surrounding tissue described by the transfer coefficients: $k_{12} = 1.85\times10^{-3}$ s^{-1}; $k_{21} = 7.0\times10^{-5}$ s^{-1}; $k_{23} = 5.3\times10^{-6}$ s^{-1} and $k_{32} = 0$. All other parameters are the same as in Fig. 6.4 except for: $\sigma_{12} = \sigma_{21} = 0.5$ and $k = 2.40\times10^{-11}$ m^2.

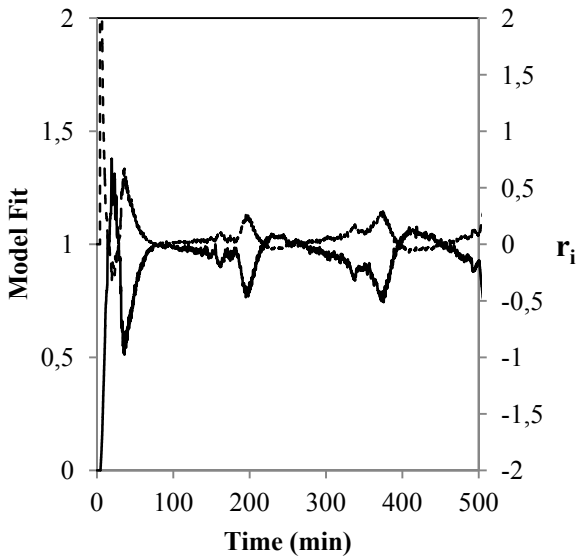

Figure 6.7 – Model fitting evaluated by the ratio between model prediction and experimental data (—) and model residuals r_i (----) for the control run shown in Fig. 6.6.

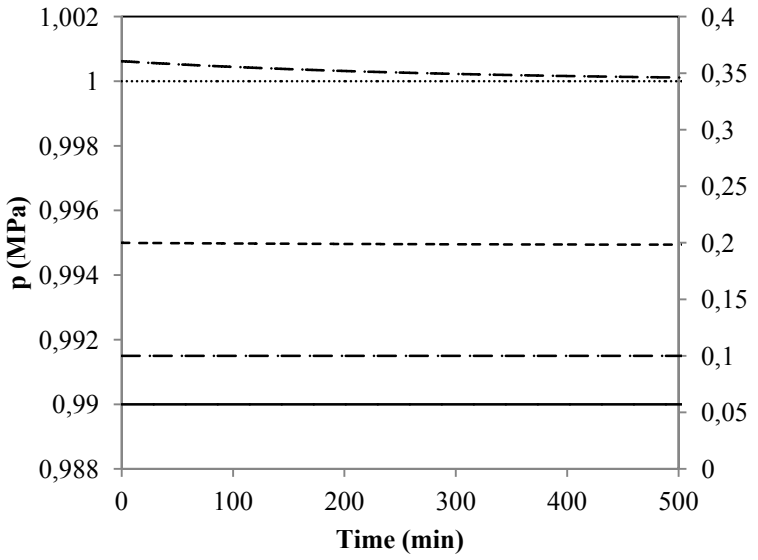

Figure 6.8 – Pressure values for the control run presented in Fig. 6.6: (·····) p_{in}; (—) p_{out}; (----)·p_1; (· · –) p_2 and (· –) p_3. p_2 and p_3 are both referenced to the right hand side axis.

tally unrealistic given the very diverse types of tissue grouped together that compartment 2 represents. However, the concentration difference between compartment 1 and 2 (Fig. 6.9) is not sufficient to counterbalance the pressure difference between the two compartments (Fig. 6.8). Thus, according to (6.6), there is a water efflux from compartment 1 to compartment 2 which reflects the water potential difference between the two compartments. For the same reasons and due to volume conservation (6.11) the same situation occurs between compartments 2 and 3 (Fig. 6.10). Although we did not observe these radial solution fluxes directly, in control runs the plant typically did take up water. Note also the very small amount of solutes in the pith cavity, when compared with the values for compartments 1 and 2 (Fig. 6.9) predicted by (6.20).

Considering a second control run from a different squash plant, the model prediction (Fig. 6.11) gave best agreement with the experimental data using: $k = 1.30\times10^{-11}$ m^2, which lower than in the first plant; $k_{12} = 1.74\times10^{-3}$ s^{-1}; $k_{21} = 6.6\times10^{-5}$ s^{-1} and $k_{23} = 5.0\times10^{-5}$ s^{-1} and all the other parameters as before (Fig. 6.6). Because k is lower in the model for this second plant, the axial flow is less. All the other model predictions for both cases are similar and show the same behaviour, namely pressure and concentration changes as shown in Figs. 6.8 and 6.9 respectively. In this second case, we have a plant

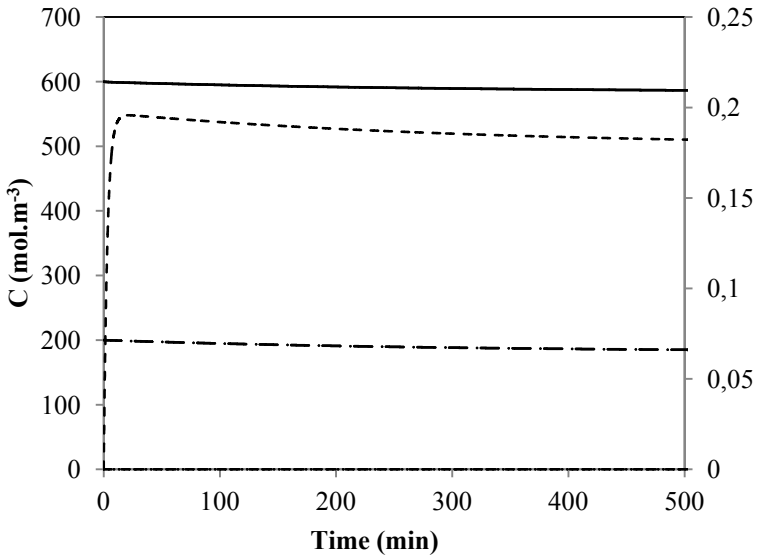

Figure 6.9 – Solute concentration for the control run presented in Fig. 6.6: (—) C_1 (· –) C_2 and (----) C_3. C3 only is referenced to right hand side axis.

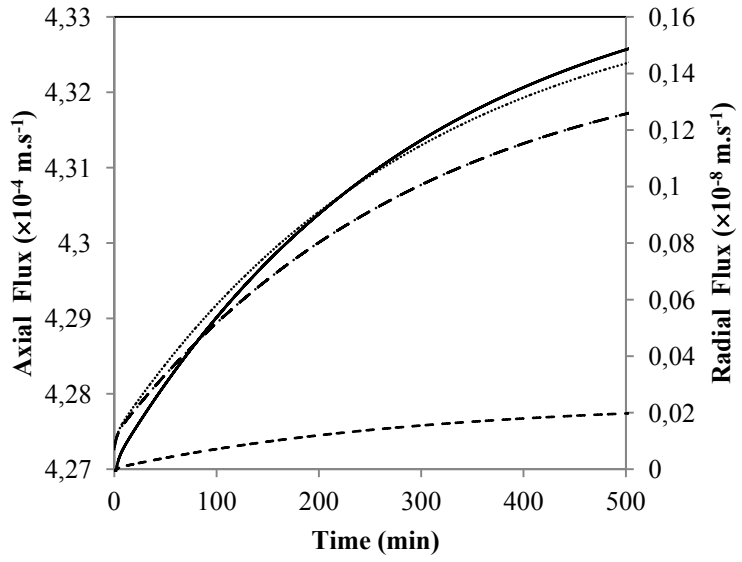

Figure 6.10 – Axial: (·····) j_{in} and (· –) j_{out} and radial: (—) j_{12} and (----)·j_{23} fluxes for the control run presented in Fig. 6.6.

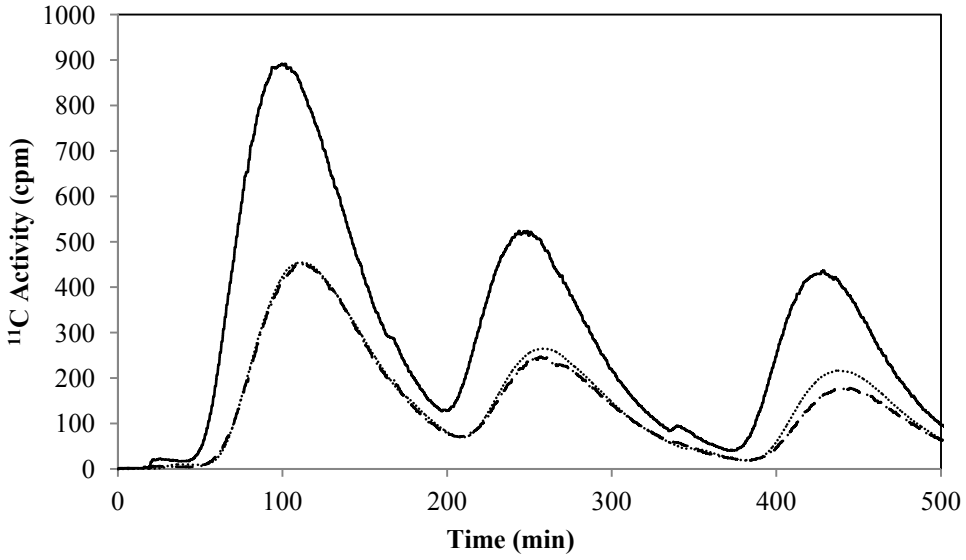

Figure 6.11 – Experimental data of input activity (–) and output activity (· –) for the perfused internode and model prediction for the output activity (···) with solute exchange between the phloem and the surrounding tissue for a control run of a second squash plant. $k = 1.30\times10^{-11}$ m^2, $k_{12} = 1.74\times10^{-3}$ s^{-1}; $k_{21} = 6.6\times10^{-5}$ s^{-1}; $k_{23} = 5.0\times10^{-6}$ s^{-1}; all other parameters are the same as in Fig. 6.6.

that is slower in transport, as indicated by the smaller sieve tube axial conductivity of its model, when submitted to same turgor pressure difference as before. However, it presents a similar physiological state to the first case as suggested by similarity of model transfer coefficients. Note that, even though we are presenting only one solution for each of the two different plants, several other equally likely scenarios could have been also presented, for example if we had chosen to assume different turgor pressure differences. In fact, we might attribute the deviation of the fit, more evident in the third pulse of the second plant (Fig. 6.11), to changes in the turgor pressure difference later in the day. This explains, for example, why the predicted activity was too high, and suggests a slowing down of bulk flow in the plant. Or, as an alternative explanation, an increase in the tracer unloading could also be responsible for the predicted activity being too high.

If we assume input pressures p_{in} decreasing linearly with time (Fig. 6.13), given by:

$$p_{in}(t_{n+1}) = p_{in}(t_n) - \frac{dp_{in}}{dt}(t_{n+1} - t_n) \tag{6.46}$$

in order to have a decreasing pressure difference, $\Delta p = p_{in} - p_{out}$, driving bulk flow through compartment 1, we obtain a much better fit for the whole control run presented in Fig. 6.11, namely for the second and third pulses (Fig. 6.12). In this case we found $\frac{dp_{in}}{dt}$ = –2.8 Pa.min^{-1}. Consequently both the input and output axial flows in compartment 1 decrease (Fig. 6.15). The changes in concentration are similar to the first plant as the transfer coefficients do not differ much from the first plant (Fig. 6.14). The translocation speed obtained for both plants (Fig. 6.10, 6.15), although higher than the values measured from ^{11}C transport for perfused plants (Fig. 5.8), is consistent with the values normally reported for phloem transport. From these results we conclude that solute exchange between compartments is needed to best simulate the experimental profiles of tracer activity.

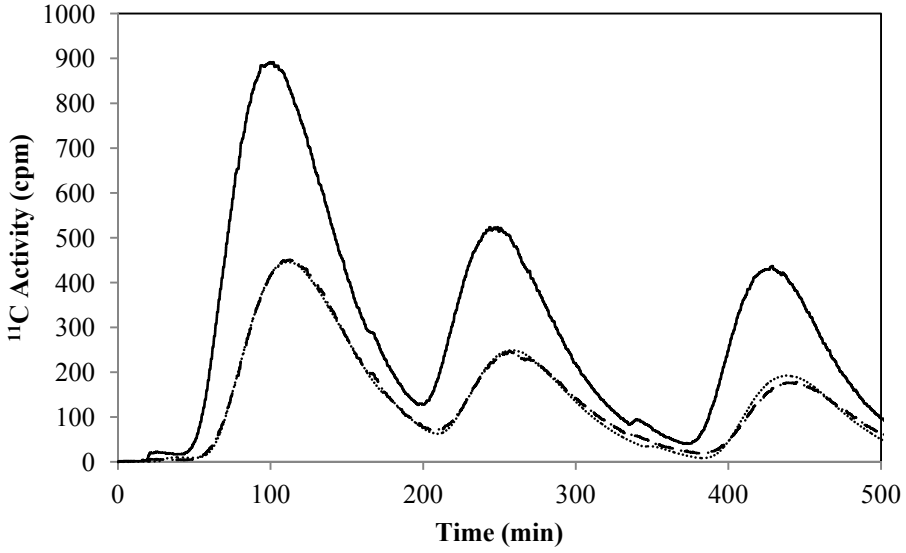

Figure 6.12 – Experimental data of input activity (–) and output activity (· –) for the perfused internode and model prediction for the output activity (···) for the control run presented in Fig. 6.11 but with a decreasing input pressure $\frac{dp_{in}}{dt}$ of –2.8 Pa.min^{-1} linear with time.

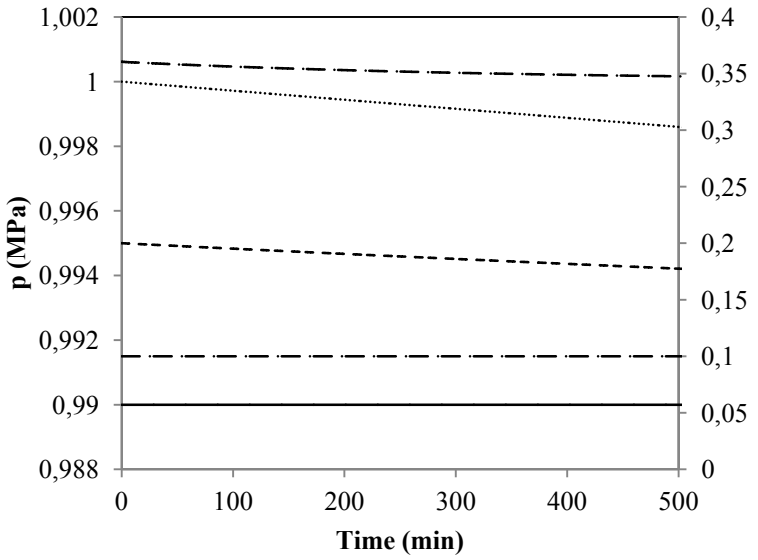

Figure 6.13 – Pressure values for the control run presented in Fig. 6.12: (·····) p_{in}; (—) p_{out}; (----)·p_1; (· · –) p_2 and (· –) p_3 are both referenced to the right hand side axis.

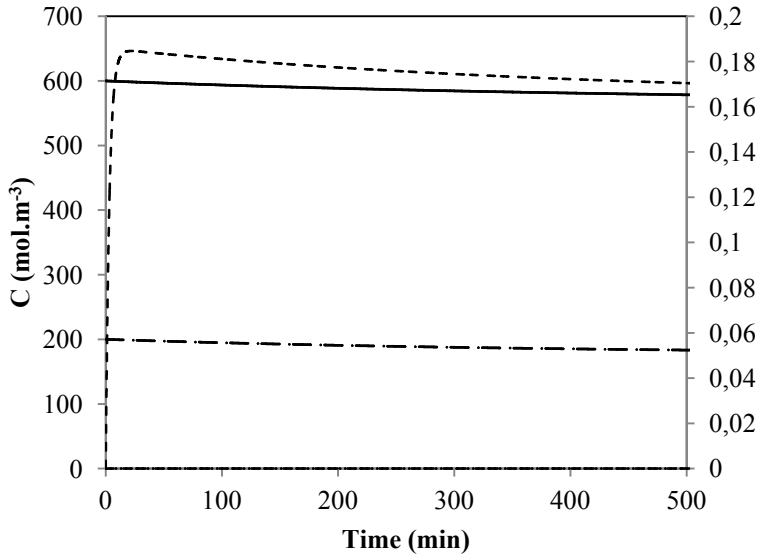

Figure 6.14 – Solute concentration for the control run presented in Fig. 6.12: (—) C_1 (· –) C_2 and (----) C_3. C_3 is referenced to right hand side axis.

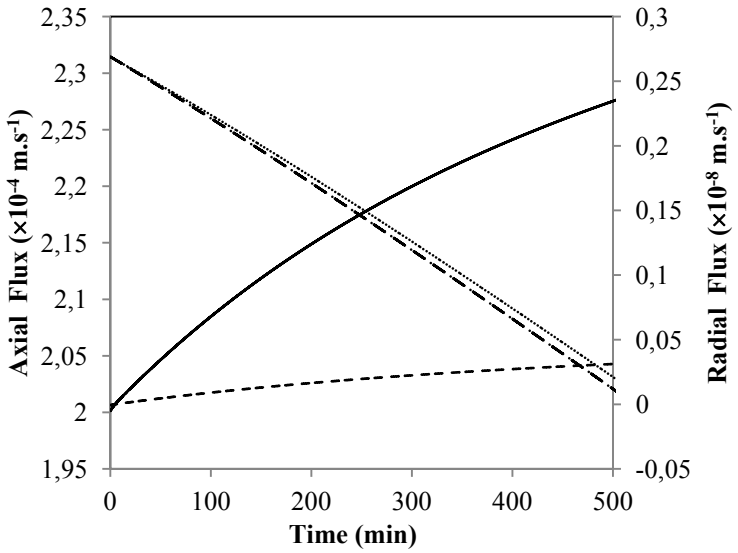

Figure 6.15 – Axial: (·····) j_{in} and (· –) j_{out} and radial: (—) j_{12} and (----)·j_{23} fluxes for the model solution for the control run presented in Fig. 6.12.

6.4.2 Effects of PEG on ^{11}C Translocation in Squash

PEG, a non-penetrating molecule, was used as an osmotic agent in order to affect the apoplastic water potential of the perfused internode without chemical modification. PEG is not taken up by the plant but its presence in the squash internode pith cavity changes the plant water uptake, due to the change in the pith cavity water potential (Figs. 5.28, 5.29 and 5.30). For perfusion of an impermeable solute the transport coefficients referring to treatment solutes, k_{ijt}, are zero. Hence, there is no reason for the transport coefficients of the endogenous solutes, k_{ij}, to change due to PEG perfusion. Lowering the water potential of the pith cavity by perfusing it with PEG changes the radial water exchange, as more water is drawn from the plant into the perfusion solution. This water efflux is greater for the higher PEG concentration in the second treatment. Consequently, pressure decreases in both compartments 1 and 2, but with unrealistic (negative) values in the latter (Fig. 6.17B). The changes in pressure in compartment 1 are not as severe as the changes in compartment 2. If p_3 were to change, negative minimums of p_2 could be avoided but only by increasing p_3 5 times or more, which is totally unrealistic as the perfusion p_3 is done at normal atmospheric pressure. The negative pressure in compartment 2

is a result of the model limitations, to be discussed later in the discussion chapter. Once the treatment is removed, the conditions before treatment resume. These effects are more pronounced in the second treatment (Fig. 6.17B) when a higher PEG concentration was used.

To better fit the model to data, the output pressure pout is decreased during PEG treatments (Table 6.2), in addition to the change in pith cavity osmolality. The changes in pressure difference between compartment 1 ends affect the axial flow (Fig. 6.19). The peaks observed in Fig. 16 at the beginning and at the end of treatments are artefacts caused by the change in $p_1 - p_{out}$ at the time of treatments being greater than the change in $p_1 - p_{out}$ for the time step chosen in the numerical method used. However, two factors contribute to the change in flow during PEG perfusion. First, the decrease in pressures p_1 and p_{out} favours a decrease in j_{out} (6.5) while at the same time increases j_{in} as the difference between p_{in} and p_1 increases. The changes in both axial flows affect solute concentration for compartment 1. As more solute is coming in and less is flowing out, there is an

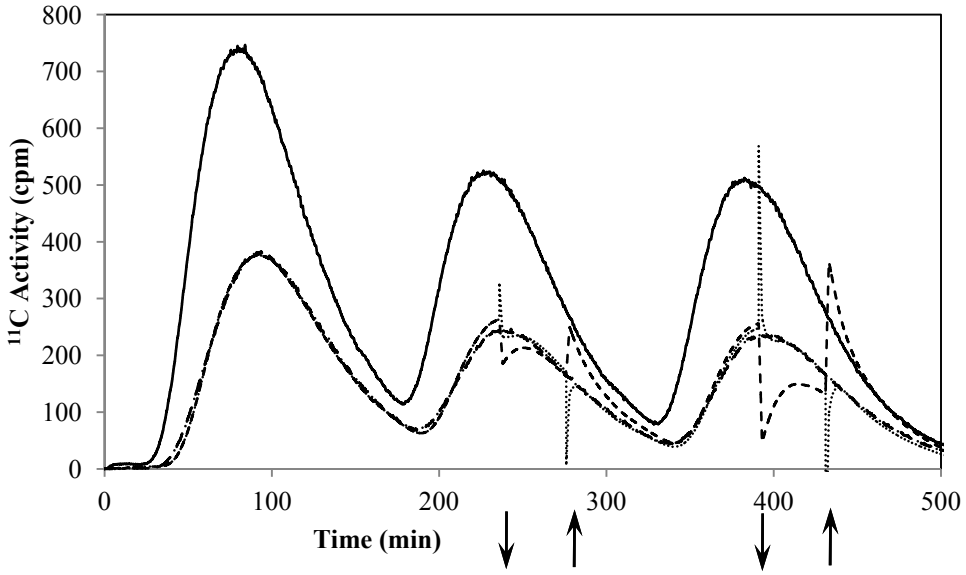

Figure 6.16 – Experimental data of input activity (–) and output activity (· –) for the perfused internode. The model prediction is shown for the output activity for an experiement with two PEG treatments of 300 and 600 mOsmol respectively: (····) for constant pressure difference as indicated in Fig. 6.6; (·····) for the variable output pressure p_{out} (Fig. 6.17A) and pressure difference Δp (Table 6.2). Other parameters: $k_{12} = 1.64\times10^{-3}$ s^{-1}, $k_{21} = 6.2\times10^{-5}$ s^{-1}, $k_{23} = 5.0\times10^{-6}$ s^{-1}; $k_{12t} = k_{21t} = k_{23t} = k_{32t} = 0$; $\sigma_{12} = \sigma_{23} = 0.5$; $\sigma_{t12} = \sigma_{t23} = 1$; $k = 1.25\times10^{-11}$ m^2, all other parameters the same as in Fig.6.6. Treatment times are indicated by arrows.

increase in compartment 1 concentration (Fig. 6.18A). Of course, the solution viscosity also changes (Fig. 6.20). Second, the increase in compartment 1 viscosity causes a decrease in $j_{out,}$ as suggested by (6.5). During PEG treatment the concentration in compartment 2 increases because of the increase in compartment 1 concentration, as more solute is available and thus more is lost radially increasing compartment 2 concentration (Fig. 6.18B). However, this situation is transient as it stops once treatment is removed and concentration C_1 decreases. These results show that tracer loss can be affected by PEG perfusion, due to a change in speed, without any change in the transport coefficients.

Table 6.2 – Values of the pressure difference $\Delta p = p_{in} - p_{out}$ for the experiment of Fig.6.16.

	Before Treatment	**During 1st Treatment**	**After 1st Treatment**	**During 2nd Treatment**	**After 2nd Treatment**
Δp (MPa)	0.0100	0.0104	0.0095	0.0108	0.0093

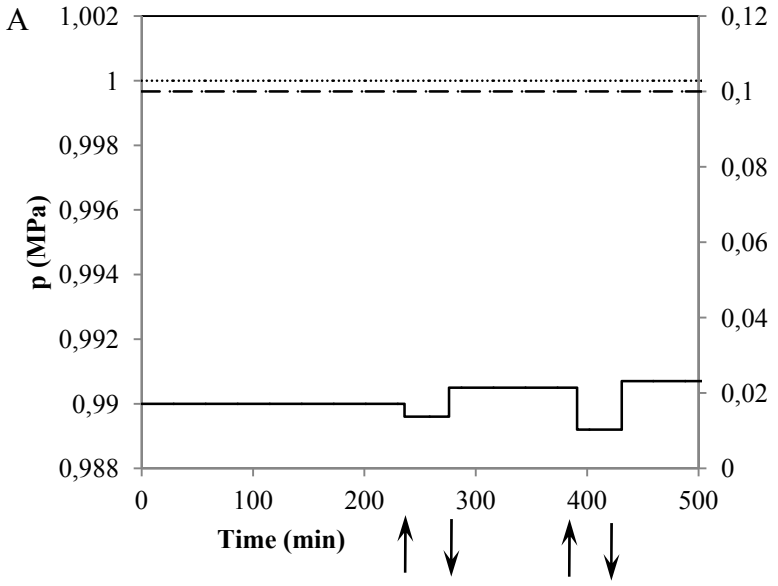

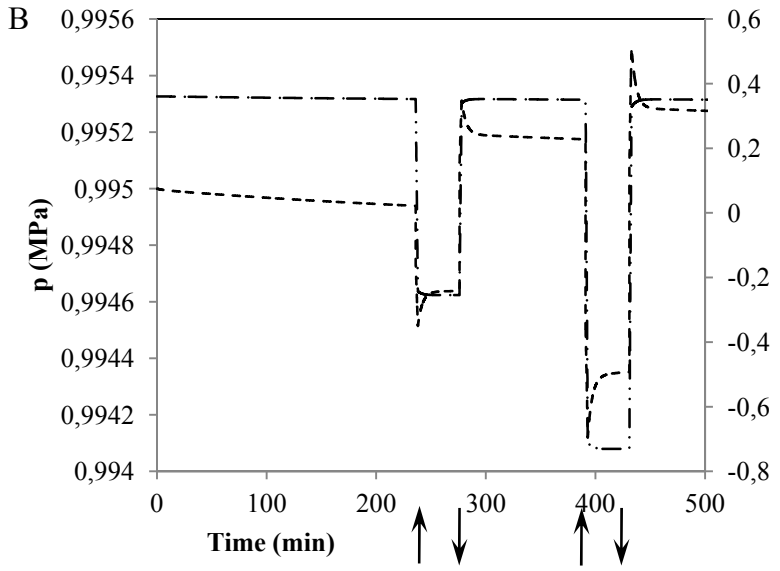

Figure 6.17 – Pressure values for the PEG treatments presented in Fig. 6.16: A – (·····) p_{in}; (—) p_{out}; (· –) p_3 referenced to the right hand side axis; B – (----)·p_1; (· · –) p_2 referenced to the right hand side axis.

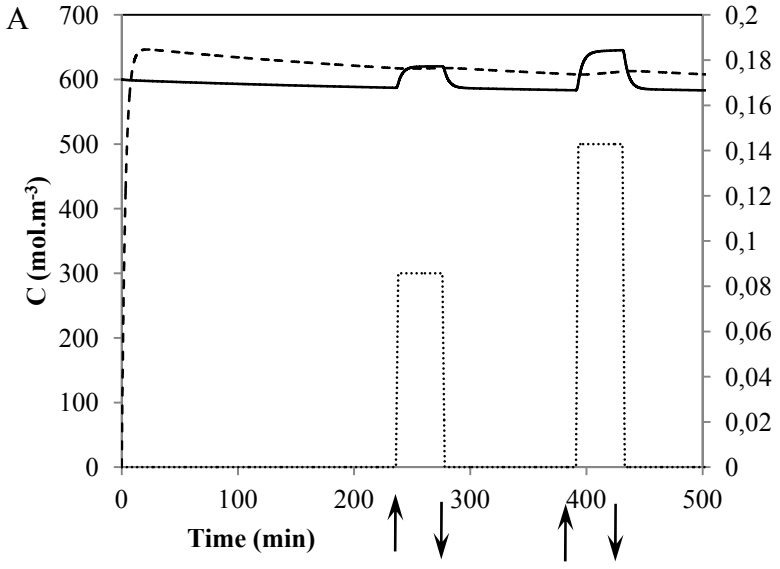

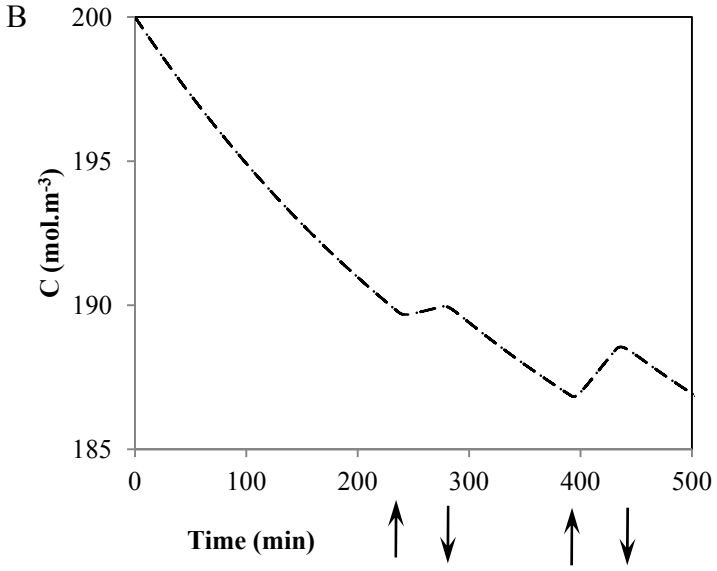

Figure 6.18 – Solute concentration for the PEG treatments presented in Fig. 6.16: A – (—) C_1; (- - -) C_3 referenced to right hand side axis and (·····) PEG concentration,C_{3t}.; B – (· –)C_2. Treatment times are indicated by arrows.

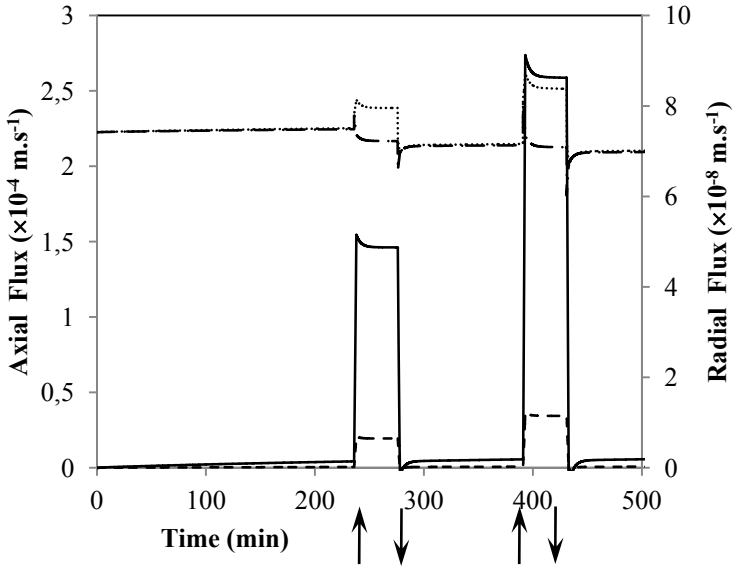

Figure 6.19 – Axial: (·····) j_{in} and (· –) j_{out} and radial: (—) j_{12} and (----)·j_{23} fluxes for the PEG treatments presented in Fig. 6.16. Treatment times are indicated by arrows.

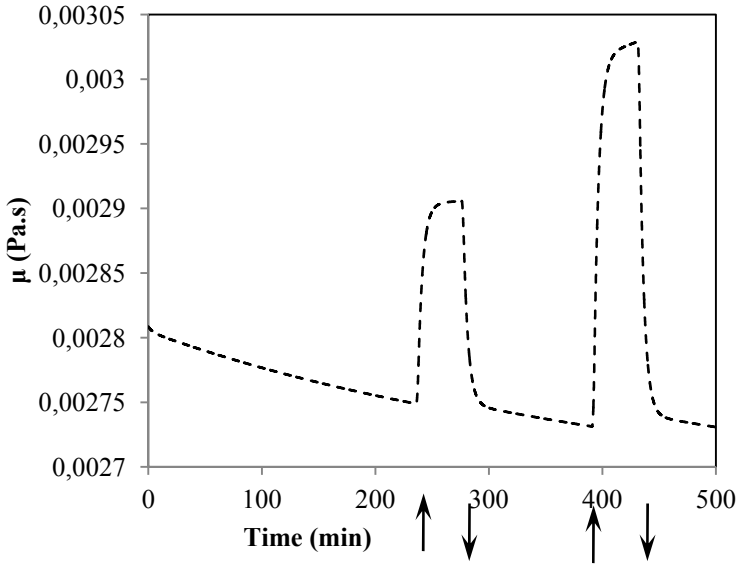

Figure 6.20 – Viscosity in compartment 1 (·····) for the PEG treatments presented in Fig. 6.16. Treatment times are indicated by arrows.

6.4.3 Effects of Sucrose on ^{11}C Translocation in Squash

The effects of sucrose perfusion on ^{11}C transport in squash were similar in nature to the effects of PEG perfusion, specifically when using solutions of similar osmotic strength. To better fit the model to data, the output pressure p_{out} is decreased during sucrose treatments (Table 6.3), in addition to the change in pith cavity osmolarity. However, unlike PEG, sucrose should be taken up by the plant. For this reason there is a very good agreement of model with the experimental data if we consider the transport coefficients k_{ijt} and associated reflection coefficient for exogenous sucrose transport equal to the corresponding coefficients for the endogenous solutes (Fig. 6.21). In the same way as observed with PEG, perfusion of 500 mM sucrose decreases the water potential in the perfused pith cavity drawing more water from compartments 1 and 2 (Fig. 6.25) and decreasing pressure in both compartments 1 and 2 (Fig. 6.22). Consequently, there will be a decrease in the axial outflow (Fig. 6.25) which will lead to an increase in C_1, the solute concentration in compartment 1 (Fig. 6.23). The pressure difference $\Delta p = p_{in} - p_{out}$ during the sucrose second treatment (Table 6.3) was similar to Δp verified for an osmotically equivalent PEG solution (2^{nd} treatment in Table 6.2).

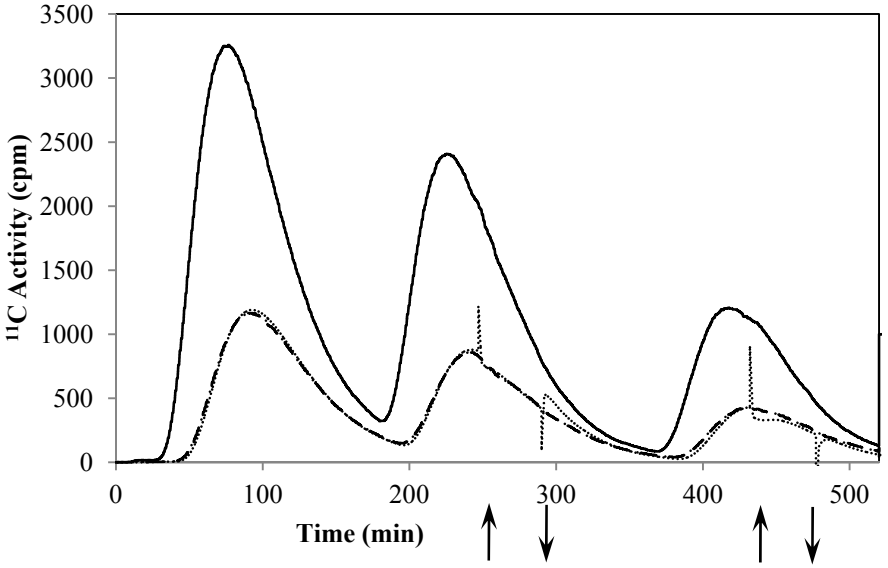

Figure 6.21 – Experimental data of input activity (–) and output activity (· –) for the perfused internode and model prediction for the output activity (····) for an experiement with two 500 mM sucrose treatments: variable p_{out} (Fig. 6.22) giving variable Δp (Table 6.3); $k_{12} = 2.0\times10^{-3}$ s^{-1}, $k_{21} = 7.6\times10^{-5}$ s^{-1}, $k_{23} = 5.0\times10^{-6}$ s^{-1}, k_{32} the same as in Fig. 6.6; $k_{12t} = 2.0\times10^{-3}$ s^{-1}; $k_{21t} = 7.6\times10^{-5}$ s^{-1}; $k_{23t} = k_{32t} = 5.0\times10^{-6}$ s^{-1}; $\sigma_{12} = \sigma_{21} = \sigma_{12t} = \sigma_{21t} = 0.5$; $k = 0.8\times10^{-11}$ m^2, p_{in}; all other parameters the same as in Fig. 6.6. Treatment times are indicated by arrows.

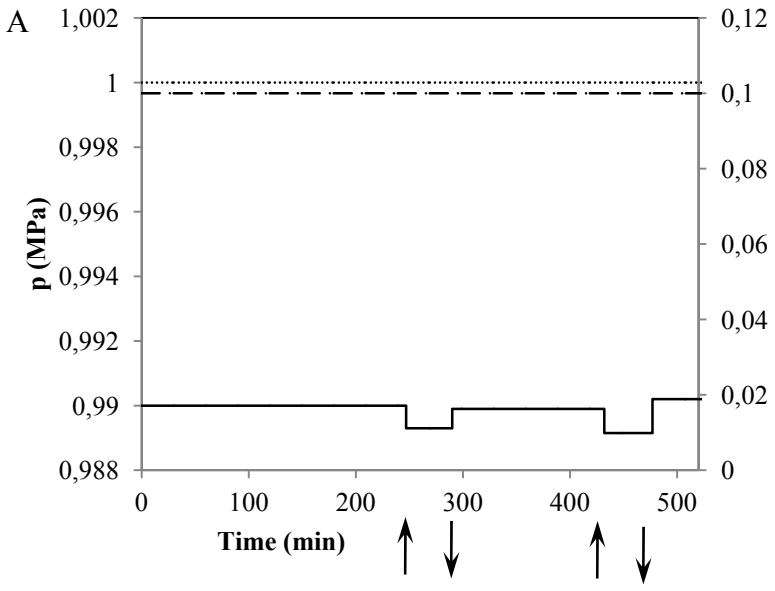

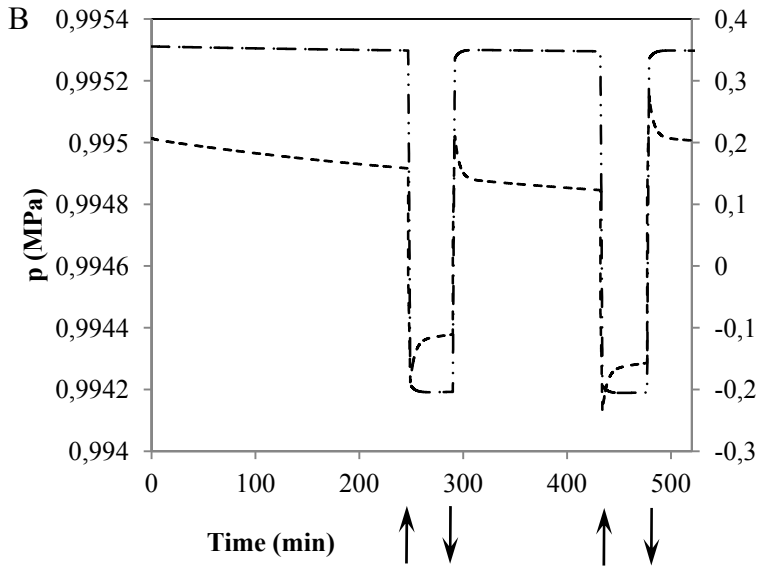

Figure 6.22 – Pressure values for the sucrose treatments presented in Fig. 6.21: A – (·····) p_{in}; (—) p_{out}; (· –) p_3 referenced to the right hand side axis; B – (----)·p_1; (· · –) p_2 referenced to the right hand side axis.

Table 6.3 – Values of the pressure difference $\Delta p = p_{in} - p_{out}$ for the experiment of Fig.6.21.

	Before Treatment	**During 1st Treatment**	**After 1st Treatment**	**During 2nd Treatment**	**After 2nd Treatment**
Δp (MPa)	0.0100	0.0107	0.00985	0.01075	0.00980

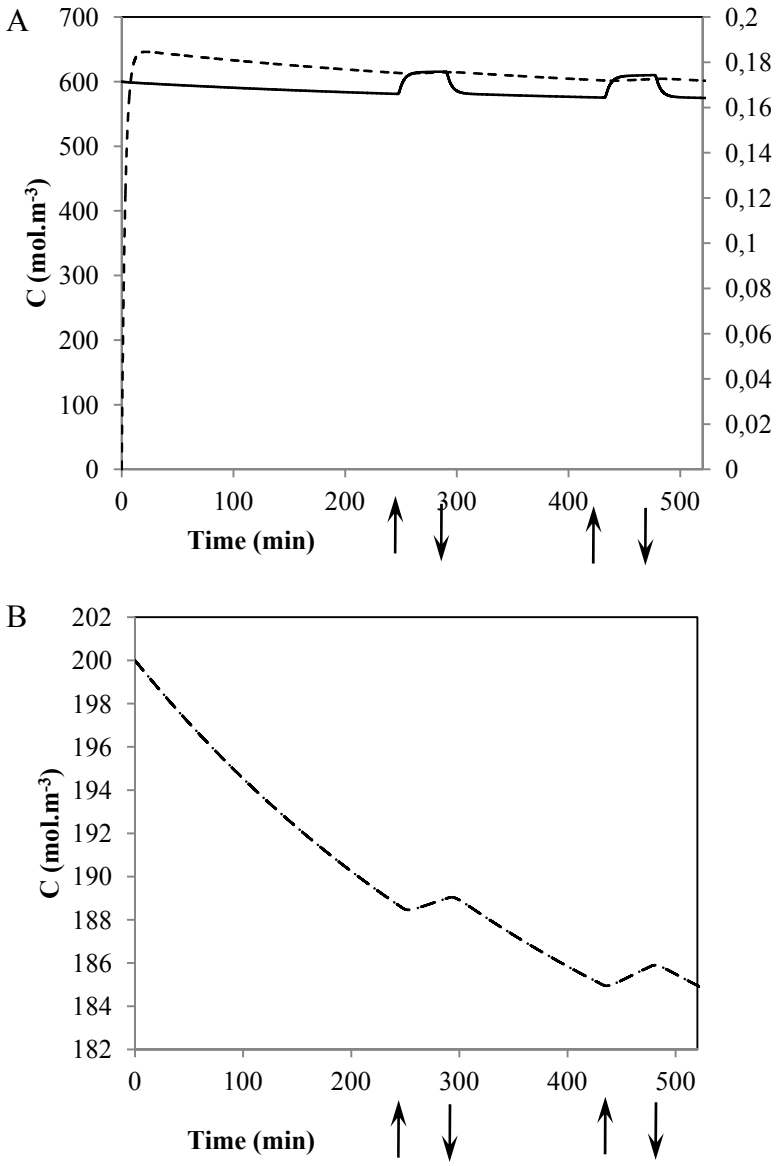

Figure 6.23 – Solute concentration for the sucrose treatments presented in Fig. 6.21: A – (—) C_1; (----) C_3 referenced to right hand side axis; B – (· –)C_2. Treatment times are indicated by arrows.

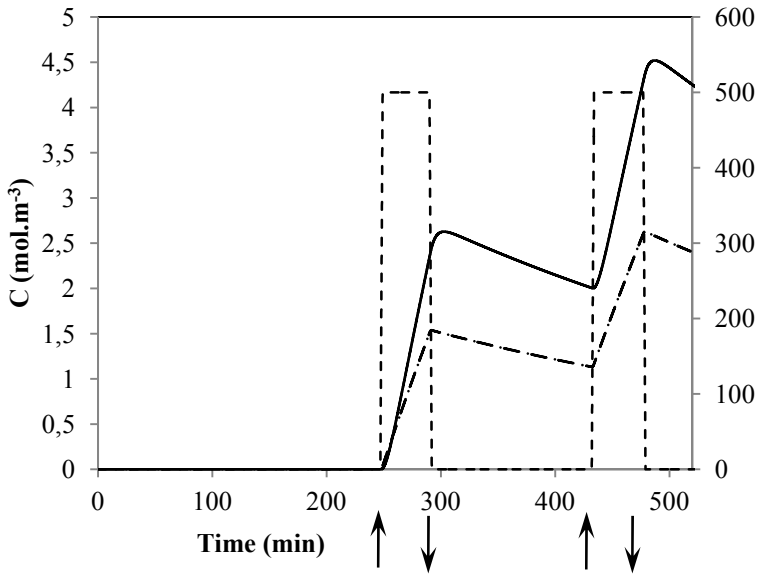

Figure 6.24 – Sucrose concentration for the sucrose treatments presented in Fig. 6.21: (—) compartment 1, C_{1t}, (· –) compartment 2, C_{2t}; (----) concentration in compartment 3, C_{3t}, referenced to the right hand side axis.

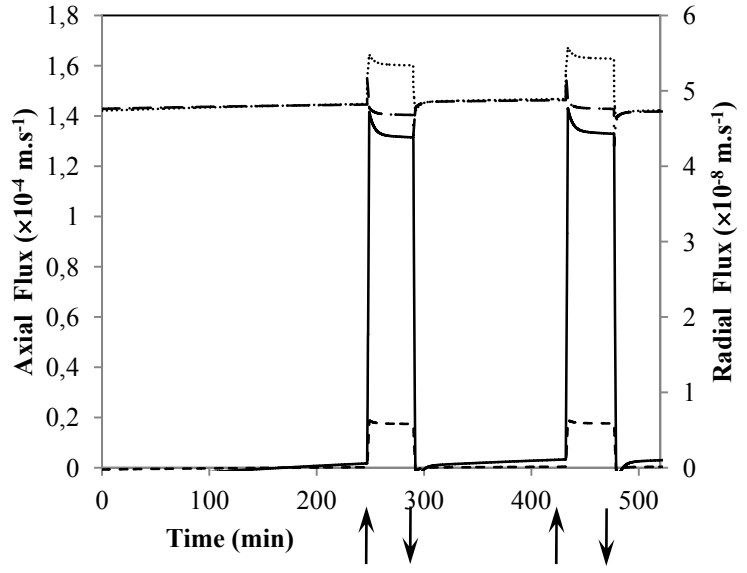

Figure 6.25 – Axial: (·····) j_{in}; (· –) j_{out} and radial: (—) j_{12}; (----)·j_{23} fluxes for the sucrose treatments presented in Fig. 6.21.

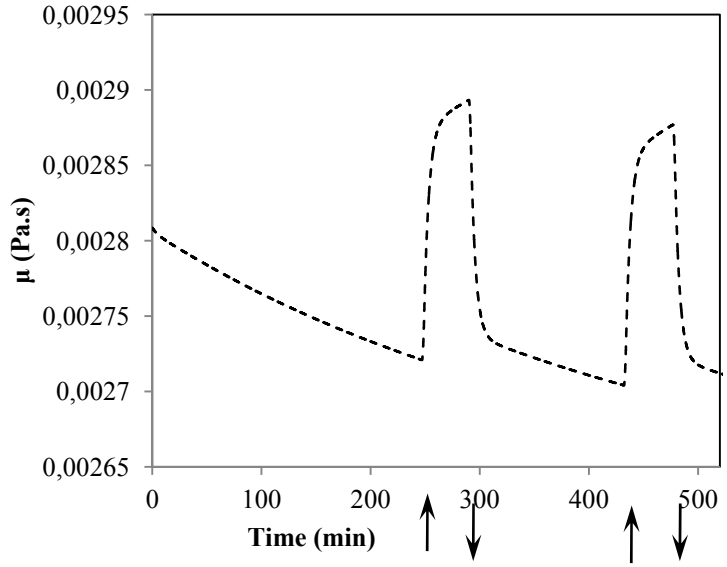

Figure 6.26 – Viscosity in compartment 1 (----) for the sucrose treatments presented in Fig. 6.21. Treatment times are indicated by arrows.

6.4.4 Effects of Mannitol on ^{11}C Translocation in Squash

The model predictions for mannitol treatments were very similar to the sucrose effects previously described, namely in terms of pressure (Fig. 6.28), concentration (Figs. 6.29, 6.30), axial and radial fluxes (Fig. 6.31) and solution viscosity (Fig. 6.32). From the similarity of the effects caused by sucrose and by mannitol perfusions we believe that, like sucrose, mannitol is also taken up by the plant. For the same reasons described before, a very good agreement with experimental data is found when p_{out} is specified to decrease during treatment (as in Table 6.4). A big difference between sucrose and mannitol occurs at 500 mM. As Figs. 6.27 and 6.33 show, not only the effect of mannitol perfusion is different than sucrose for the same concentration but it is also different from the effect observed at 300 mM. Similarly to sucrose there is also mannitol uptake into the plant tissue as suggested by the values of transfer coefficients different than nought which gave the best model fit and are equal to the to the transfer coefficients for the endogenous solutes. However, no good fit was obtained for the second treatment, 500 mM mannitol. The cause for this big discrepancy during the 500 8mmM mannitol treatment is the phloem

stoppage observed as an immediate effect of perfusion of 500 mM mannitol, which is not fully predictable by the model (Fig. 6.33).

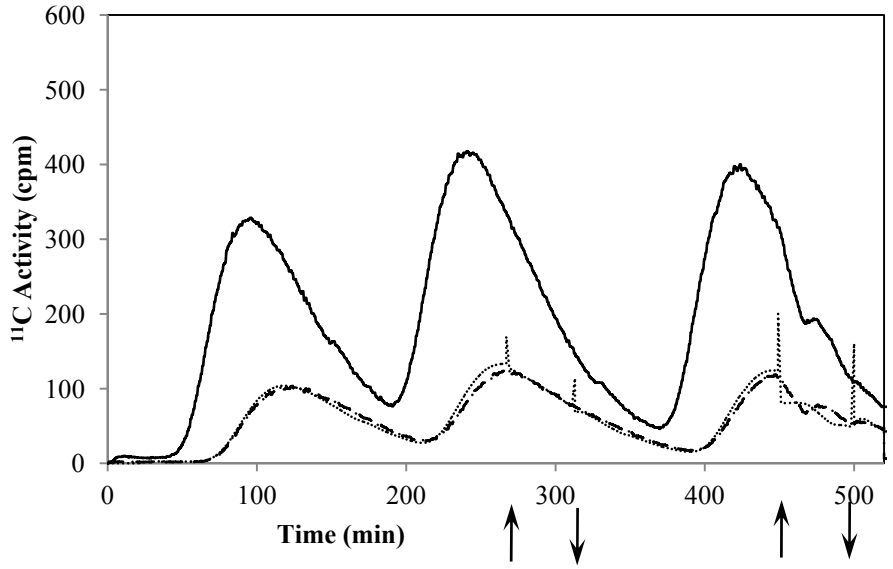

Figure 6.27 – Experimental data of input activity (–) and output activity (· –) for the perfused internode and model prediction for the output activity (····) for an experiement with two mannitol treatments of 300 and 500 mM with variable p_{out} (Fig. 6.28A) giving variable Δp (Table 6.4): k_{12} = 1.58×10^{-3} s^{-1}, k_{21} = 6.0×10^{-5} s^{-1}; k_{23} = 5.0×10^{-6} s^{-1}; k_{12t} = 1.58×10^{-3} s^{-1}; k_{21t} = 6×10^{-5} s^{-1}; k_{23t} = k_{32t} = 5×10^{-6} s^{-1}; σ_{12} = σ_{21} = σ_{12t} = σ_{21t} = 0.5; k = 0.55×10^{-11} m^2; all other parameters the same as in Fig. 6.6. Treatment times are indicated by arrows.

Table 6.4 – Values of the pressure difference Δp for the experiment of Fig.6.21.

	Before Treatment	**During 1st Treatment**	**After 1st Treatment**	**During 2nd Treatment**	**After 2nd Treatment**
Δp (MPa)	0.0100	0.0106	0.00995	0.01070	0.00970

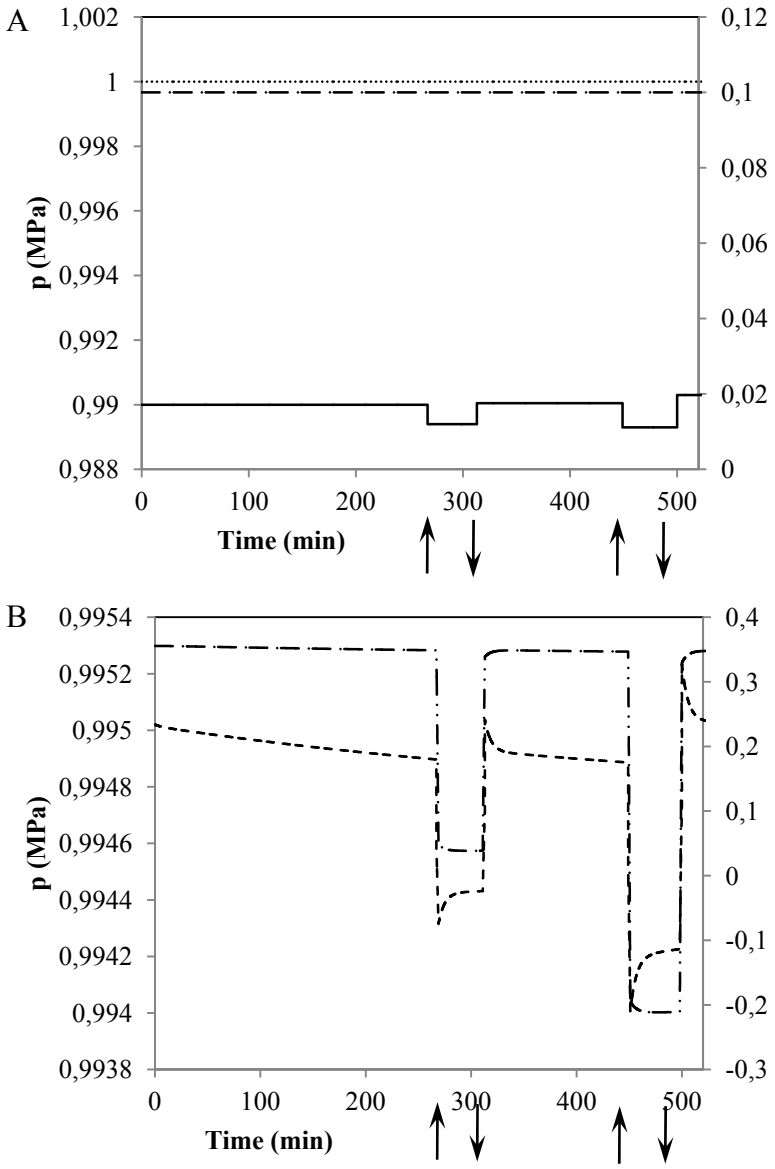

Figure 6.28 – Pressure values for the mannitol treatments presented in Fig. 6.27: A – (·····) p_{in}; (—) p_{out}; (· –) p_3 referenced to the right hand side axis; B – (----)·p_1; (· · –) p_2 referenced to the right hand side axis.

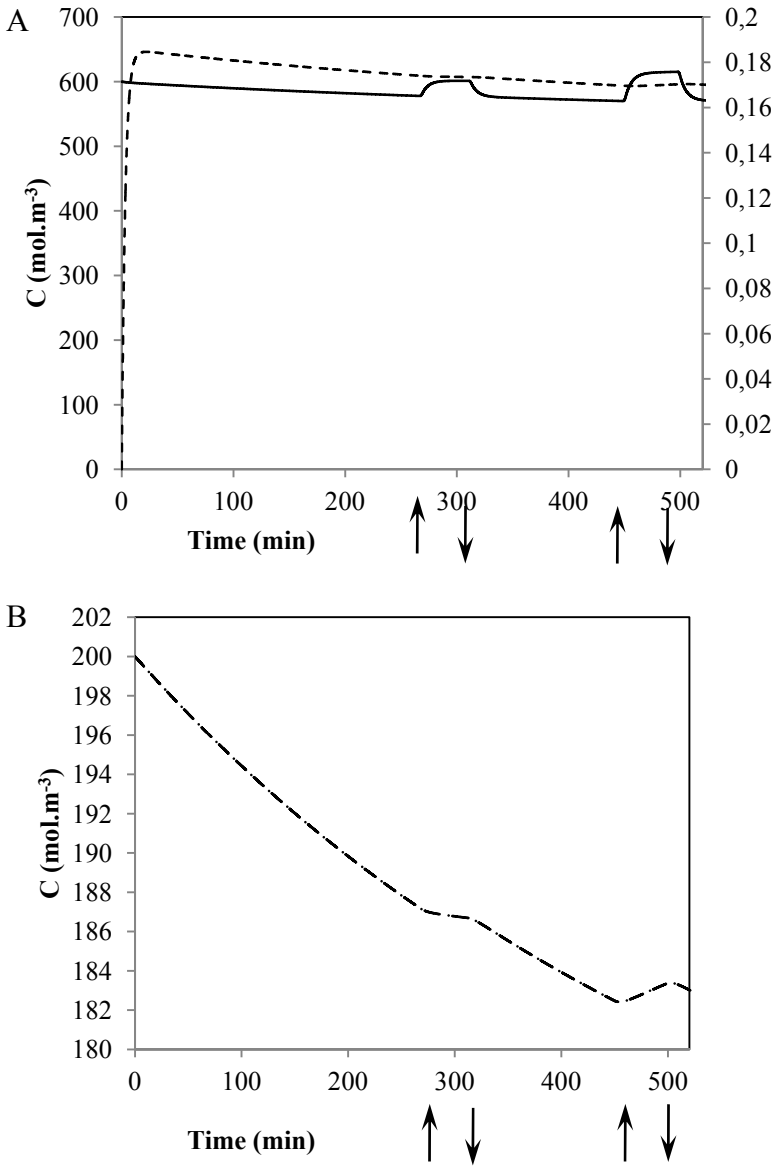

Figure 6.29 – Solute concentration for the mannitol treatments presented in Fig. 6.27: A – (—) C_1; (----) C_3, which is referenced to right hand side axis; B – (· –)C_2. Treatment times are indicated by arrows.

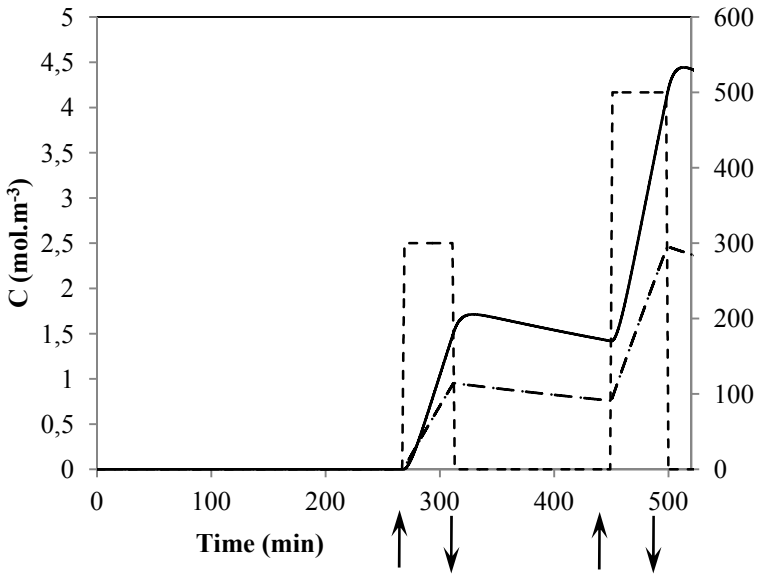

Figure 6.30 – Mannitol concentration within the model for the mannitol treatments presented in Fig. 6.27: (—) compartment 1, (· –)compartment 2; (----) concentration in compartment 3, C_3, is referenced to the right hand side axis.

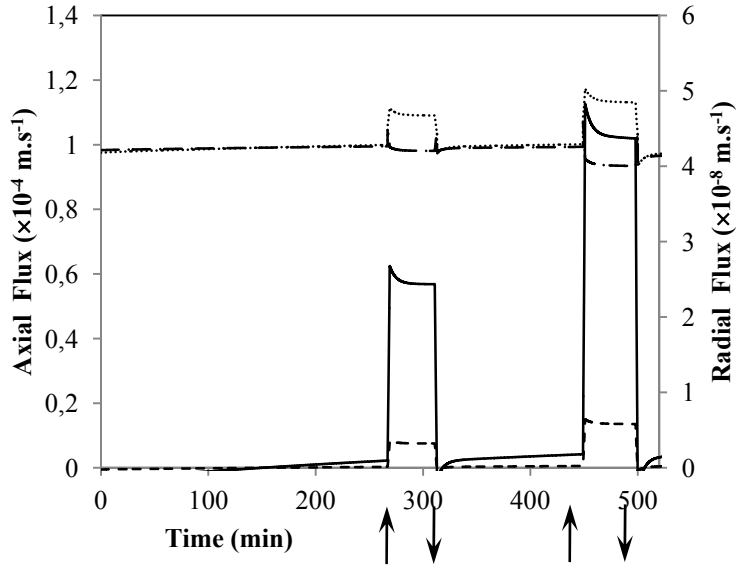

Figure 6.31 – Axial: (·····) j_{in}; (· –) j_{out} and radial: (—) j_{12}; (----)·j_{23} fluxes for the mannitol treatments presented in Fig. 6.27. Treatment times are indicated by arrows.

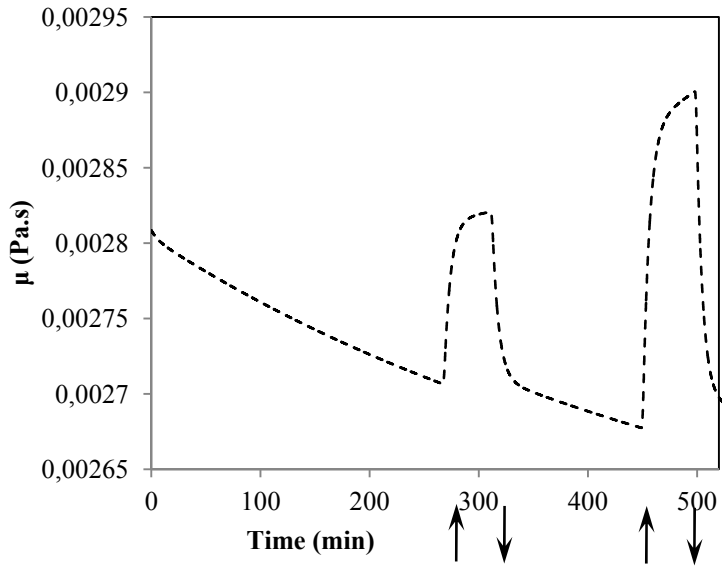

Figure 6.32 – Viscosity in compartment 1 (·····) for the mannitol treatments presented in Fig. 6.27. Treatment times are indicated by arrows.

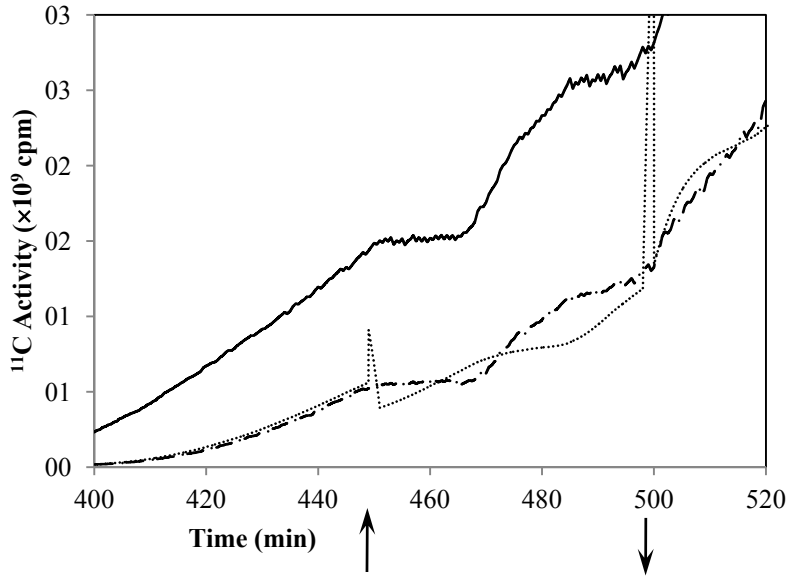

Figure 6.33 – Experimental decay-corrected data of input activity (–) and output activity (· –) for the perfused internode and model prediction for the output activity (····) for the mannitol treatments presented in Fig. 6.27.

7. Discussion

This study was mainly focused on radial water and solute exchanges between the phloem and the surrounding tissue in plant stems and how they affect pressure, concentration and velocity within sieve tubes. Both theoretical and experimental methods were used and in the following sections we discuss their main results and implications for phloem transport.

7.1 Effect of Radial Water Exchange

Radial water exchange across the sieve tube membrane causes a deviation from laminar flow described by Hagen-Poiseuille equation (2.3). The combined effects of a "higher viscosity" and an increase in the velocity due to radial water inflow cause greater increases in the pressure gradient, $\frac{dp}{dz}$, in the direction of flow (3.119). As both pressure and solute concentration decrease in the direction of flow so does the radial water inflow across the sieve tube membrane and the increase in the flow velocity is attenuated (Fig. 3.4A). Horwitz (1958) concluded, from the low Reynolds number estimated, that the flow in sieve tubes would be laminar, even with sieve plates separating sieve tube elements. In this situation, viscous effects should far outweigh accelerative effects and the dissipation of pressure inside sieve tubes would still be proportional to the first power of the average flow velocity (2.4). However, Horwitz (1958) showed that there is acceleration of flow due the entrance or exit of water through the sieve tube membrane which invalidates to use the Hagen–Poiseuille equation (2.3), since it is only applicable to tubes limited by a rigid impermeable wall. Lang (1973) showed experimentally the effects of radial water exchange on both pressure and solute concentration on his experimental setup simulating sieve tube transport. Lang (1973) observed an increasing pressure gradient and simultaneous decreasing concentration gradient in the direction of flow as predicted by Horwitz (1958) when there is water inflow along the pathway (Fig. 2.2).

These results were also reproduced theoretically by assuming, as opposed to Horwitz (1958), that phloem transport is described by Hagen–Poiseuille equation (2.3)

coupled with radial water exchange across the sieve tube membrane, given by Starling's equation (2.6) (e.g. Tyree, Christy & Ferrier, 1974). With these assumptions Tyree, Christy & Ferrier (1974) found that average axial velocity increased non-linearly with distance, and towards the end of the sieve tube to unrealistic values, not only non-expected to occur in plants but also hard to conciliate with phloem physiology. Tyree, Christy & Ferrier (1974) called this increase in average axial velocity a "runaway phenomenon" and observed that changing the sieve tube hydraulic membrane conductivity, L_p, did not change the overall behaviour of the model. The runaway phenomenon was still there but with different values. They also showed that the runaway phenomenon was not an artefact caused by their numerical method. Hence, these facts suggest that the cause the runaway phenomenon lies in the governing equations and boundary conditions used. The runaway velocity occurred in the pathway region where there was radial water exchange. This result, together with Horwitz (1958) remarks and Tyree, Christy & Ferrier (1974) comments on the limitations of using Hagen–Poiseuille equation, did not prevent authors using this equation for describing phloem flow. In fact, Goeschl & Magnuson (1986) suggested that Tyree, Christy & Ferrier (1974) model could be improved by considering explicit functions of loading or unloading processes at source and sink regions respectively. However, they still obtained the same "runaway phenomenon", for which they gave no explanation (Fig. 2.3).

More recently, Thompson & Holbrook (2003a) used Horwitz' arguments wrongly to justify what they called the "local" use of Hagen–Poiseuille equation obtaining again the pronounced increased in average axial velocity at the end of the pathway region. Contrary to what Thompson & Holbrook (2003a) suggested, neglecting the inertial terms in the Navier–Stokes equation (3.3) does not necessarily imply the direct applicability of the Hagen–Poiseuille equation (2.3), but in the steady state actually gives Stokes equation (2.13) (Phillips & Dungan, 1993; Rand & Cooke, 1978). So far, all the models based on Hagen–Poiseuille equation (2.3) exhibited this runaway behaviour on the axial velocity and none gave any explanation for its origin and of its likelihood in plants.

In our steady state model of phloem transport, obtained from solving Navier–Stokes equation (3.3), we did not observe this runaway phenomenon and the changes in the average axial velocity were more pronounced at the beginning of the system (Fig. 3.4A) where radial water inflow was bigger (Fig. 3.4B) as the pressure and concentration differences across the sieve tube membrane were also bigger (Figs. 3.3, 3.5). In our case, we carefully chose the boundary conditions to reflect known physiological conditions of

the phloem (Table 3.1). Constraining model parameters to be within the physiological range (§ 3.6), we found that the shapes of velocity, pressure and concentration curves are quite similar for different parameter values used and the runaway phenomenon was never observed. In fact, the failure to choose proper boundary conditions led Phillips & Dungan (1993) to obtain unrealistic values for concentration, pressure and average axial velocity, specifically at the end of the pathway (Fig. 2.4) where the average axial velocity varied from 15 to almost 50 times the initial value (Fig. 2.4A). In the steady state model presented in our study the average axial velocity at the end of the system was only about 1.5 times the initial value (Fig. 3.4A), with smaller increases towards the end in contrast to the increasing gradient observed with the runaway phenomenon (e.g. Tyree, Christy & Ferrier, 1974). Phillips & Dungan (1993) used values for the apoplast pressure, p_{out}, higher than what is observed in plants and they also assumed in some examples $p_{out} > p$, the turgor pressure inside the sieve tube, which is totally unrealistic. In addition, they also used wrong values for parameter $\widehat{H}$ (3.52).

Our steady state model confirms Horwitz (1958) remarks against the use of Hagen–Poiseuille equation by showing that radial water exchanges, although small in magnitude ($\approx 10^{-10}$ m.s^{-1}), affect the pressure gradient in the direction of flow. Also, the radial water exchange predicted in our steady state model is about 10 times smaller than the values reported by the models based on Hagen-Poiseuille equation (e.g. Thompson & Holbrook, 2003a; Tyree, Christy & Ferrier, 1974) which supports the idea that the origin of the runaway behaviour in the axial velocity lies in the governing equations used. In order to examine this hypothesis we note that the average axial velocity is given by (3.115):

$$\overline{v_z}(z) = U - \frac{2}{R}\frac{d\boldsymbol{q}}{dz} - \frac{2}{L}\frac{d\boldsymbol{s}}{dz} - \frac{3UR\beta\boldsymbol{v}(0)}{2\nu} \tag{7.1}$$

As long as there is radial water inflow, described by both zeroth $\boldsymbol{v}\left(\hat{z}\right)$ (3.66) and first $\boldsymbol{u}\left(\hat{z}\right)$ (3.99) order functions, by definition (3.71) and (3.104), both $\frac{d\boldsymbol{q}}{dz}$ and $\frac{d\boldsymbol{s}}{dz}$ will be negative, thus increasing the average velocity with distance. However, as flow proceeds and the water potential difference across the sieve tube membrane decreases with distance

so do functions $\frac{d\boldsymbol{q}}{dz}$ and $\frac{d\boldsymbol{s}}{dz}$; less water will flow in. Hence, the increase in the axial velocity will be less than it was at the beginning. The runaway phenomenon described is not observed.

The pressure gradient relates to the average axial velocity, as given by (3.119):

$$\frac{d\mathrm{p}}{dz}(z) = -\frac{8\mu}{\beta R^2}\overline{\mathrm{v}_z}(z) - \frac{6\rho}{R^2}\boldsymbol{v}(z)\left(2\int_0^{z'}\boldsymbol{v}(z)\,dz' - UR\right) \tag{7.2}$$

where the radial water flow is described by the zeroth order function $\boldsymbol{v}\left(\hat{z}\right)$ (3.66). The first term of the right hand side of equation (7.2), $-\frac{8\mu}{\beta R^2}\overline{\mathrm{v}_z}(z)$, is the so-called "local" Hagen-Poiseuille equation (2.3) used by other models (e.g. Thompson & Holbrook, 2003a). Hence, the pressure gradient (7.2) has extra terms that depend on the radial water flow both explicitly by the zeroth order function $\boldsymbol{v}\left(\hat{z}\right)$ (3.66) and implicitly through the average axial velocity $\overline{\mathrm{v}_z}(z)$ (7.1). The balance between these two contributions, and specifically $\boldsymbol{v}\left(\hat{z}\right)$, which is negative for water inflow, contribute to a lesser increase of the pressure gradient, and consequently the average axial velocity, with distance, thus preventing the runaway phenomenon from happening.

In contrast, from the governing equations of the model presented by Thompson & Holbrook (2003a) we have that in the steady state:

$$\frac{d\mathrm{p}}{dz} \propto \frac{1}{\mathrm{C}(z)} \tag{7.3}$$

which means that the dilution of the sieve tube solute concentration due to water inflow will cause an increase of the magnitude of the pressure gradient, thereby causing the increase in speed, which is predicted by Hagen-Poiseuille equation (2.3). This is what we believe to be the cause of the runaway phenomenon described in previous models. In our case there is no explicit and simple inverse relation between the pressure gradient and solute concentration as equation (7.2) shows and as plotted in Fig. 7.1. The dependence in solute concentration is implicit through the radial water flow, which is represented by

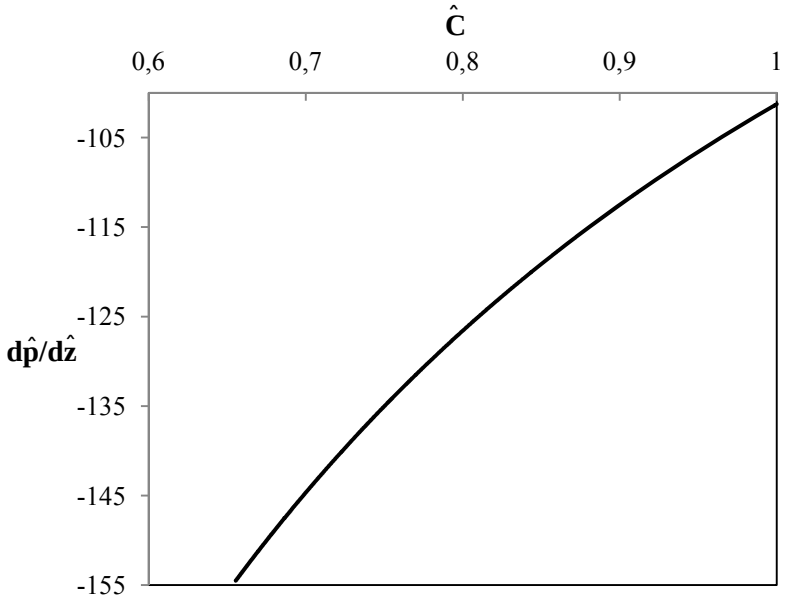

Figure 7.1 – Pressure gradient versus concentration for a flow within a sieve tube limited by a semipermeable membrane ($\sigma = 1$) and with sieve plates present.

$v\left(\hat{z}\right)$ (3.66) and consequently and also implicitly by the average velocity (7.1). The relation between the pressure gradient and solute concentration described by (7.2) prevents average axial velocity from increasing with distance, in contrast to the models based on the Hagen-Poiseuille equation. In fact, due to dilution of the sieve tube solute concentration and concomitant decrease in pressure, radial water inflow will decrease with distance thus decreasing the changes in pressure gradient (7.2) and increasing less the velocity (Fig. 7.1).

We also observed that flow within the sieve tube is similar to Hagen-Poiseuille flow only for sieve tube membrane hydraulic conductivity, L_p, in the order of 10^{-20} $m.s^{-1}.Pa^{-1}$; meaning that curves c and d of Fig. 3.3A will be identical and equation (3.154) will be close to an identity. Not only this value for the sieve tube membrane hydraulic conductivity, L_p, is much lower than the values reported for phloem tissue (§ 3.6.4) but also it represents such a small radial water exchange so that concentration, pressure and velocity would hardly change with distance. This situation seems unlikely to happen in the phloem. Our steady state model presents a more realistic picture of phloem transport than other previous models (e.g. Phillips & Dungan, 1993) in that the predicted turgor

pressure gradient, between –0.25 and –0.39 MPa.m^{-1} (Fig. 3.3B), and the sieve tube osmotic pressure gradient, from –3.7 to –0.4 MPa.m^{-1}, agree with experimental measurements (Hammel, 1968; Hocking, 1980; Kaufman & Kramer, 1967; Rogers & Peel, 1975).

7.2 Effect of Sieve Plates and Other Intracellular Structures

Rand & Cooke (1978) showed that any estimate of the hydraulic conductivity of sieve tube lumen and sieve plate pores derived from Hagen–Poiseuille equation (2.3) is likely to be high. However, the fact that from Hagen–Poiseuille equation it is possible to derive expressions of the sieve tube axial conductivity from dimensional data of cell lumen and sieve plate pores, (2.7) and (2.14), is probably the main reason for authors to use it. In this way, these expressions not only provide a direct way of linking anatomy to physiology, confirming the plausibility of pressure driven laminar flow in sieve tubes, but also show how important anatomy data can be for mathematical modelling of phloem transport (Mullendore *et al*., 2010; Sheehy *et al*., 1995; Thompson & Hoolbrook, 2003b). This link between anatomy and physiology to mathematical modelling is not so direct using Horwitz' (1958) equation (2.4), that we admit.

However, our steady state model shows that anatomy and physiology data can still be used while solving Navier–Stokes equation (3.3) given the proper boundary and initial conditions as the expressions for velocity (3.114, 3.115, 3.116) and pressure (3.117, 3.118, 3.119) show, as being dependent of the radial water exchange across the sieve tube membrane, which is in its turn dependent on the membrane properties, as well as cell dimensions. Our choice of ε (3.32), dependent solely on sieve tube dimensions, as the parameter used in the perturbation expansion (§ 3.3, 3.4) allow us to determine the accuracy of our results by the relative contribution of higher order terms. For narrower and longer sieve tubes (with smaller values of ε) higher order terms are less important so that pressure, velocity and concentration can be given by zeroth order terms only. These are obtained from solving the coupled equations (3.128) and (3.130) only. Wider sieve tubes, with bigger radius, thus bigger ε, will have a greater lateral area which means that more water will flow across the sieve tube membrane. Hence, more evident will be the effects of water radial exchange on pressure, axial velocity and concentration described

above. Therefore, the deviation from Hagen–Poiseuille flow will be more pronounced with an increased non-linearity of both pressure and concentration with distance. The resistance imposed by sub cellular structures, i.e. cytoplasmic components, phloem proteins (P–protein), and their relation to sieve plates could be added to the sieve plate impedance factor β affecting the sieve tube resistance only, and described by the viscous term of the Navier–Stokes equation (3.3). The effects observed in our model would thus be enhanced, i.e. the pressure changes due to viscous losses. Hence, the problem turns out to be how to best describe the influence of those sub cellular structures on the overall resistance of the pathway. It would also be helpful to compare these results with the effect of different sieve tube element structure, e.g. inclined sieve plates.

7.3 Effect of Radial Solute Exchange

Solute exchange across sieve tube membranes in the pathway region between sources and sinks has not been properly studied in mathematical modelling of phloem transport. This study presents the first mathematical model of phloem transport that includes flux of solutes across the sieve tube membrane along the pathway between source and sink regions. Radial solute exchange, in this case passive, is described as a sum of diffusive and convective fluxes across the sieve tube membrane (3.22). This fact is more relevant as our steady state model is the first model to use diffuse solute flux described by the irreversible thermodynamics formalism which defines the membrane permeability to solutes, P_s, as a function of the membrane properties; i. e. the membrane hydraulic conductivity, L_p, and the solute reflection coefficient, σ (3.151) (Kedem & Katchalksy, 1958). The steady state model predictions showed that the effects of radial water flow in modifying the Poiseuille flow (as just discussed above) were weakened (Figs. 3.6, 3.7) for the more realistic case of a permeable sieve tube membrane ($\sigma < 1$).

In simulations of phloem transport, only Tyree, Christy & Ferrier (1974) have considered the pathway region to be limited by a permeable membrane. However, it was only for the special case of a 15 m long path, where solute flux across the sieve tube membrane was constant throughout the whole length. Hence, it neglected any effect of concentration difference across the sieve tube membrane on radial solute flux and thus phloem flow. The Tyree, Christy & Ferrier (1974) model, as in all other models presented so far, considered the pathway region to be limited by a semipermeable membrane where

only water radial exchange occurs ($\sigma = 1$). We believe that the reason for that assumption is mostly the lack of anatomy and physiology data on phloem transport in the pathway region. Not only radial fluxes, but also transport parameters such as membrane permeability to solutes were not known. In this study we present a way of including the radial solute flux which is known to happen in the pathway region, in order to give a more realistic perspective on phloem transport. Considering metabolism and storage processes that occur throughout the stem of plants, especially in big specimens like trees, radial solute fluxes are very likely to occur and far from being neglected.

Our steady state model results showed that the water influx, dependent on the water potential difference across the sieve tube membrane, which is highly influenced by the concentration difference across the sieve tube membrane, is decreased and even reversed for leakier membranes (Fig. 3.7B). The sieve tube membrane permeability to solutes, P_s, (in this case sugars) (3.151) lies in the bottom range of the values reported for plant cells, 10^{-10} to 10^{-6} $m.s^{-1}$, and it is smaller than the values reported for non-charged solutes (Diamond & Wright, 1969; Nobel, 1999). This smaller sieve tube membrane permeability to solutes reflects the efficient specialization of sieve tube elements to bulk flow, as it minimizes the diffusive solute loss favoured by the concentration difference across the sieve tube membrane. Hence, we have a more efficient system of carbon transport along the plant body that is built to keep solute losses at minimum. Such an efficient transport system is of most convenience for big specimens where source and sink regions may be far apart. In the case of *cucurbitaceae*, the combination of a small solute sieve tube membrane permeability to sugars, e.g sucrose, with the fact that they transport oligosaccharides that exist in the phloem only and seem not to leave it diffusively (Schaffer *et al.*, 1996; Webb & Gorham, 1964, 1965), further illustrates the specialization of sieve tubes to a more efficient system for solute transport bulk flow.

In this study we present a more comprehensive and integrative way of using anatomy and physiology data on mathematical modelling of phloem transport. Application of the Navier–Stokes equation (3.3) with the boundary conditions that describe both water and solutes radial fluxes allow us to understand better the dynamics of phloem transport and how pressure, velocity and solute concentration are affected by the plant physiological status. Reloading of solutes through active processes could be added to the boundary condition (3.22). Whether described by the product of another transport coefficient, presumably constant, by the apoplast solute concentration or by

Michaelis–Menten kinetics, the effect of solute reloading on phloem flow would be mainly to counteract the passive solute loss, thus keeping a concentration difference across the sieve tube membrane that would draw less water into the sieve tube (Fig. 3.7B). Consequently the changes of turgor pressure, velocity and concentration with axial distance would be less then observed with passive solute loss only. Also, it would further illustrate the efficiency of sieve tubes to bulk flow on minimizing radial solute loss. Thus the decrease seen in both the axial velocity and axial solute flux would be attenuated and their profiles would be closer to those for less permeable membranes (Figs. 3.7A, 3.9A).

The results presented in this study point that a compromise must be achieved by sieve tubes between promoting an efficient delivery throughout the plant body and minimizing the passive solute loss to the apoplast. Hence it would also be elucidating to include reloading mechanisms and to see its efficiency with different sieve tube element structure, e.g. sieve plate configuration. These studies would certainly give a better understanding on sieve tube specialization and how cell structure contributes to that. Equation (7.2) clearly demonstrates the deviation from the linear relationship of Poiseuille flow, commonly used in mathematical models of phloem transport, and its dependence on the radial exchange of both water and solutes. In addition, it also allows relating it with the anatomical and physiological parameters that describe the sieve tube membranes, i.e. L_p, P_s and sieve tube structure and dimensions (7.1, 7.2). Hence, we have a better understanding of all the underlying processes that contribute and affect phloem flow.

7.4 Sieve Tubes are in Water Potential Equilibrium with the Apoplast

The assumption that sieve tubes are in water potential equilibrium with their surrounding apoplast in plant stems is generally used when measuring indirectly turgor pressure gradients in sieve tubes (Kaufman & Kramer, 1967; Sovonick-Dunford *et al*., 1981; Wright & Fisher, 1980). In our steady state model (Fig. 3.4B) the water potential difference, $\Delta\Psi$, across the semipermeable sieve tube membrane varies with distance, between –0.5 and –0.1 MPa, being less if sieve plates are neglected. For a more realistic case of the permeable sieve tube membrane, the water potential difference across it is even less, as the results from Fig. 3.7B suggest, as the radial water inflow decreases for

$0.7 < \sigma < 1$, e.g. for $\sigma = 0.8$, $\Delta\Psi$ varies between –0.16 to –0.02 MPa with distance. Notwithstanding, these results refer to an idealized sieve tube, submitted to both initial and boundary conditions that may not reflect the overall phloem physiological conditions, e.g. active solute transport has not been considered, they confirm Lang's (1974) conclusions: $\Delta\Psi$ is negligible when compared with the sieve tube turgor pressure so that sieve tubes are basically in water potential equilibrium. Murphy (1989b) extended Lang's (1974) analysis showing that symplastic connectivity between sieve tubes and the surrounding tissue would not affect the radial water potential equilibrium assumption in sieve tubes greatly. However, we conclude that this common assumption of radial water potential equilibrium between sieve tubes and their surrounding apoplast is more realistic in phloem transport modelling if a sieve tube permeable membrane is considered, as the value of $\Delta\Psi$ is smaller when compared with a semipermeable membrane (Fig. 3.7B). Thus closer to $\Delta\Psi \approx 0$. Assuming this *quasi* radial water potential equilibrium, from $\Delta\Psi = \Psi - \Psi_{out}$ we have that the sieve tube axial turgor pressure gradient is simply given by the sum of both the axial external water potential gradient and the osmotic pressure gradient within sieve tubes (2.10):

$$\frac{dp}{dz} \cong \frac{d\Psi_{out}}{dz} + \frac{d\Pi}{dz} \tag{7.4}$$

Ignoring $\Delta\Psi$ between sieve tubes and the apoplast, equation (7.4) should yield good estimates of phloem turgor pressure and turgor pressure gradients specifically in pathway regions, as in stems.

7.5 Translocation Speed

From the early stages of using radioactive isotope labelling for studying phloem transport, translocation speed was one of the main parameters of interest. It could be used to validate or abolish different theories and models of phloem transport or simply to best describe and quantify mass transport within the phloem. Here we compare and discuss different methods to determine translocation speed. As experimental and data collecting techniques evolved and *in vivo* studies became possible, a more realistic picture was obtained. However, there are several factors to consider if one wants to quantify

radioisotope movement within the phloem. The half-width of a ^{11}C pulse moving in the plant usually increases. This is most probably the result of a combination of factors. For example, the movement of carbon into and out of the sieve tubes would change the activity of the carbon in transit and hence the amount of carbon arriving at a given point. In addition, different speeds of translocation within the pulse of tracer moving in the phloem would have contributed to the increase in half-width. It was pointed out by Evans *et al*. (1963) that the different speeds are more likely to reflect variations in the resistance to transport through different sieve tubes, than from expected parabolic gradients in speed due to laminar flow across single sieve tubes. Any variations in the cross-sectional area of sieve tubes, or their number, would alter the resistance to transport and hence might be expected to produce a range of speeds. On the other hand, different speeds are also plausible due to different turgor pressure gradients in adjacent sieve tubes in larger plant species with wider stem cross sections, such as in tree species (Hammel, 1968). A range of speeds emphasizes the limitations of the concept of a single translocation speed value and the necessity of defining the methods used in the estimation. Any measurement of the bulk flow speed based on the amount of labelled material moving through a given part of the plant will be underestimated, giving a speed value smaller than the real bulk flow as more tracer leaks out. Tracer will seem to arrive more slowly as a lesser amount will be detected at a given point after some time interval. For this reason and when workings with isotopes, authors prefer to define tracer translocation speed. While this will give an idea of the order of magnitude of the phloem flow rate, it is not the same in concept. So, in order to best determine the tracer translocation speed that approximates to the real phloem flow speed, minimizing the effects of leakage of the ^{11}C, the time of half-maximum activity at each position has been used (Ferrieri *et al*., 2005; Moorby *et al*., 1974; Troughton & Currie, 1977; Troughton *et al*, 1974). At this point tracer leakage will be least in the period soon after arrival of the pulse at any one position at that time; the vast majority of labelled material arriving at that location will surpass the fraction of tracer that is leaking out because the phloem translocation rate is much higher than the lateral efflux rate. An alternative estimate of a mean value is to use the time of maximum rate of change in half life corrected activity (Fig. 5.6) as an indication of a position within the ^{11}C pulse. This corresponds to the point of inflection for the half life corrected data (Fig. 5.5) and the front of the pulse is almost symmetrical about the point of inflexion (Troughton *et al*., 1974). Therefore, this method provides a reasonable estimate of a typical speed. In all

cases, a transit time depends on two detection points from which we get the representative tracer translocation speed value.

The values of tracer translocation speed for species studied in this work, wheat and squash, (Figs. 5.7 and 5.8) are similar and fall well within the order of magnitude observed for translocation in sieve tubes. Also, we conclude that transfer function analysis is also a good method for estimating translocation speed, as the estimated values agree very well with estimates from half-life corrected data (compare data from Figs. 5.7B, and 5.8B with data from Figs. 5.7A and 5.8A). Both wheat (Fig. 5.7) and squash (Fig. 5.8), whether being perfused or not, showed tracer translocation speed values ranging from 0.6 to 1.8 $cm.min^{-1}$, being faster in wheat than in squash. The tracer translocation speed for wheat presented in this study agrees well with previous works of Wardlaw (1965) who observed values from 0.65 to 1.8 $cm.min^{-1}$ using ^{14}C labeling. From ^{11}C labeling on wheat plants, values of 0.65 $cm.min^{-1}$ (Roeb & Fisher, 1991) and 1.0 to 1.3 $cm.min^{-1}$ (Roeb & Britz, 1991) were observed. ^{11}C labeling has also been used previously on *cucurbitaceae*, namely on *Cucumis melo* for which a rate of transport of 0.96 $cm.min^{-1}$ was measured (Schaffer *et al*., 1996) which is within the range of the values reported in this work as well as in the range of 0.66 to 2.14 $cm.min^{-1}$ of the first transport rate measurements obtained from phloem exudation rates done by Crafts (1931, 1932) on *Cucurbita pepo* and *Cucumis sativus* L. *In vivo* studies using ^{11}C labeling showed values ranging from 2.8 to 4.9 $cm.min^{-1}$ in *Zea mays* leaves (Throughton *et al*., 1974; Throughton & Currie, 1977) and from 1.3 to 3.5 $cm.min^{-1}$ in rice (*Oryza sativa* L.) (Troughton *et al*., 1974). Pickard *et al*. (1978a, b) measured values up to 3 $cm.min^{-1}$ in moonflower (*Ipomoea alba* L.). Moorby *et al*. (1974) observed values between 0.9 and 1.1 $cm.min^{-1}$ in tomato (*Lycopersicon esculentum*). Jahnke *et al*. (1998) have determined translocation to occur in young tree stems of *Fraxinus excelsior* and *Sorbus aucuparia* from 0.4 to 1.0 and from 0.5 to 0.9 $cm.min^{-1}$ respectively, also using ^{11}C labelling. More recently, Peuke *et al.* (2001) used NMR flow imaging to determine phloem flow velocities of 1.5 $cm.min^{-1}$ in castor bean (*Ricinus comunis*). In the same way as the species studied in the present work (Fig. 5.7 and 5.8) Peuke *et al.* (2001) observed that the flow speed did not change much during the day, which suggests that phloem transport occurs almost steadily. Windt *et al*. (2006) obtained values ranging between 1.5 and 2.6 $cm.min^{-1}$ for grey poplar (*Populus tremula* × *Populus alba*), *Ricinus comunis*, *Lycopersicon esculentum* and tobacco (*Nicotiana tabacum*). Using the same technique, Mullendore, Windt & Knoblauch (2010) have measured an average phloem flow speed in

Cucurbita maxima of 1.2 cm.min^{-1} in very good agreement with the values reported in this work for the same species (Fig. 5.8).

7.6 Perfusion by ABS Does Not Affect Phloem Transport

Perfusion of the stem as a way of modifying the stem apoplast is not usually done while studying phloem transport and as a treatment one could think as affecting phloem transport. However, perfusion of the stem by an apoplastic bathing solution, ABS, showed that the plant remains stable in both water uptake and phloem transport. Thus, perfusion by ABS can serve as a reference state to compare with when other solutes are also perfused. Under the radial water potential equilibrium assumption (7.4), we can write the sieve tube average axial velocity (7.1) as:

$$\overline{v_z}(z) \simeq -\frac{\beta R^2}{8\mu}\left(\frac{d\Psi_{out}}{dz}+\frac{d\Pi}{dz}\right) \qquad (7.5)$$

Perfusion of a stem internode with ABS will make that part of the plant a secondary source of water for the whole plant, as the results in wheat (§ 5.8) and squash (§ 5.9) suggest. Thus, we will have a local increase in the apoplastic water potential Ψ_{out} of that perfused region (becoming less negative and closer to $\Psi_{ABS} \approx \Psi$ of pure water), due to the low resistance (high hydraulic conductivity) of plant cell walls to water movement (Nobel, 1999). Consequently, the apoplastic water potential gradient $\frac{d\Psi_{out}}{dz}$ in the perfused region becomes practically null as the whole apoplast in that region will be at the same water potential.

However, as the steady state model results show, changes in the apoplastic water potential gradient affect mainly the radial water exchange (Fig. 3.11B). The effects seen in the axial velocity are very small (Fig. 3.11A) and even less in the sieve tube pressure (Fig. 3.10). Hence, according to these steady state model predictions, no significant differences in the axial velocity should be expected in the perfused region between ABS perfused and non-perfused plants. Our experimental results confirm this prediction as there is no significant differences in the translocation of tracer in the perfused region on both perfused and non-perfused plants (Figs. 5.7, 5.8).

As in the perfused internode, there was also no difference in the translocation speed in the immediate downstream internode between perfused and non-perfused plants (Fig. 5.8). There are two possible reasons for no difference. First, due to its close proximity it is likely that the apoplast water potential of the downstream internode is not that different from the perfused internode in non-perfused plants. This is even more so as all the leaves located downstream of the load node were removed (§ 4.4), leaving very few small young leaves at the apex as a sink for xylem flow to supply transpiration and tissue growth, that could maintain a strong apoplastic water potential gradient along the growing stem (Cavalieri & Boyer, 1982). Hence, the apoplast water potential gradient in the downstream internode is likely to be similar in magnitude to the perfused internode in non-perfused plants. Perfusion by ABS increases the apoplast water potential in the perfused internode and by that it may locally increase the apoplast water potential gradient in the downstream internode. However, according to our steady state model results even doubling the apoplast water potential gradient does not affect sieve tube turgor pressure (Fig 3.10) and consequently axial average speed (Fig. 3.11A), although it increases water radial flow (Fig. 3.11B). As described before, the small radial water flow reflects the water potential difference across the sieve tube membrane, $\Delta\Psi$, which is also small. Thus the changes in radial water flow (Fig. 3.11B) are still small and insufficient to change sieve tube turgor pressure and average velocity (Fig. 3.10, 3.11A). It is quite likely that perfusion by ABS caused smaller changes in the apoplast water potential gradient of downstream internode to the case shown in Figs. 3.10 and 3.11, thus its effects are even smaller. Second, based on the turgor pressure regulating mechanism suggested by Lang (1983), Thorpe *et al*. (1983) and Thompson & Holbrook (2003b), the turgor pressure gradient will not be affected. The very small changes seen in the sieve tube pressure, in our steady state model, due to changes in the apoplastic water potential agree with a turgor pressure regulating mechanism existing in sieve tubes (Fig. 3.10).

Therefore, any increase in the perfused internode sieve tubes water potential, and consequently in sieve tubes turgor pressure, due to perfusion by ABS, will be readily transmitted to all adjacent sieve tubes, not changing the flow in the immediate adjacent downstream internode. The plant had adapted, converging to a similar steady state after perfusion started. That is the typical response to a perturbation, and it may include responses in many places (e.g. loading). Had we measured speed further and closer to the apex, probably some more significant effect on translocation speed would have been

noticeable due to perfusion by ABS. However, most likely these differences would not be large, due to specific experimental setup conditions, namely the removing of all the leaves between the load node and the apex.

Once perfused with ABS, and due to the consequent local increase in Ψ_{out} in the perfused internode, the apoplastic water potential difference between the upstream regions and the perfused region will decrease when compared to non-perfused plants, according to the negative axial water potential gradient along the stem (Cavalieri & Boyer, 1982). Thus, according to equation (7.5), a smaller apoplastic water potential gradient $\frac{d\Psi_{out}}{dz}$ between the perfused internode and the upstream regions due to ABS perfusion will cause a decrease in the translocation flow rate compared with non-perfused plants in the load node region as shown in Fig. 5.8.

Note that the changes in $\frac{d\Psi_{out}}{dz}$ in the load node internode are probably more severe than the examples shown in the steady state model (§ 3.7.3) as there are mature leaves transpiring close to this region. The differences in translocation speed between the load node region and its downstream internodes are most probably a result of the special experimental setup conditions rather than an indication of a supposedly normal situation in real plants. Since all the internodes located downstream of load node were made leafless therefore no big differences in Ψ_o would have occurred once the plant had adapted to defoliation (e.g. one day after leaves removal). On the other hand, upstream the load node leaves were kept, allowing transpiration to be a process of maintaining $\frac{d\Psi_{out}}{dz}$ in those regions. Accordingly, it is reasonable to expect bigger $\frac{d\Psi_{out}}{dz}$ between the source regions and the perfused region than within the perfused internode and between this and its immediate downstream internodes. Hence translocation speed will be higher in the upstream regions than in the downstream regions according to equation (7.5), and shown in Fig. 5.8 for non perfused plants (squash in this case).

7.7 Tracer Loss

The importance of radial solute exchange in phloem transport along the pathways between source and sink regions can be evaluated by measuring the loss of tracer. Cosgrove & Cleland (1983) observed that the concentration of osmotically active solutes in the cell wall free space of young and growing stem tissues in pea (*Pisum sativum* L.), soybean (*Glycine max* L.) and cucumber (*Cucumis sativus* L.) range from 20 to 70 mOsmolal. It increases from base to apical regions of those tissues and about 75 % of those solutes are organic non-electrolytes. Minchin & Thorpe (1984) found sucrose concentration in the apoplast of bean (*Phaseolus vulgaris* L.) stem ranging from 25 to 60 mM with a negative concentration gradient from basal to apical ends of stems, confirming earlier suggestion (Minchin *et al*., 1983). Thus, in the case of bean the apoplast sucrose concentration gradient lies parallel with the sieve tube sucrose concentration gradient, in the direction of phloem flow. The apparent increase in tracer loss towards the end of the day, most notably in the perfused and downstream internodes is consistent with the existence of sucrose storage processes in the stem of *cucurbitaceae* and can be expected for growth that also occurs in internodes (Schaffer *et al*., 1996). As already discussed, perfusion by ABS is expected to increase Ψ_{out} and the effects on pressure, concentration and axial velocity in the sieve tubes of the perfused internode are negligible. Therefore, we have a very similar phloem translocation state before and during perfusion with ABS. This suggests that phloem unloading should be very similar in both perfused and non-perfused plants in agreement wih the experimental results (Figs. 5.10 and 5.11).

There have been a few quantitative measurements of phloem leakage from the transport pathway. It has been shown that photoassimilates are continuously unloaded from the sieve tubes into the apoplast in leaf petioles of sugar beet (*Beta vulgaris* L.) (Geiger *et al*., 1969), in the stem of soybean (*Glycine max*) (Fisher, 1970), in squash hypocotyl tissue (Hancock, 1977), in the stem of *Vicia faba* (Wolswinkel, 1974, 1978), and in the stem of bean (*Phaseolus vulgaris* L.) (Minchin & Thorpe, 1984; Minchin *et al*, 1984). In addition, sucrose reloading of the sieve tubes occurs from the apoplast of stem and petiole tissues (Hayden *et al*., 1980; Maynard & Lucas, 1982; Minchin & Thorpe, 1984; Minchin *et al*., 1984). Using ^{11}C labelling Minchin & Thorpe (1984) and Minchin *et al*. (1984) showed that, at least in the stems of bean, phloem unloading is a passive and

reloading an active process. Moorby *et al* (1963) estimated a net phloem leakage in soybean stem of about 1 % cm^{-1} based on previous *in vivo* measurement using ^{11}C labelling (Evans *et al*., 1963). Minchin (1978, 1979) and Minchin & Troughton (1980) confirmed theoretically this estimate. Minchin & Thorpe (1987) firstly measured phloem net unloading rate in the immature stem of bean up to 4 % cm^{-1} using ^{11}C labelling. These studies have contributed to the current picture of the phloem pathway between source and sinks regions as a leaky system with passive unloading of sugars into the apoplast being linearly related with sieve tubes sugar concentration (Patrick, 1990). Both wheat and squash also show tracer unloading, most likely in the form of sugar. Particularly in squash the values of tracer unloading, from 3 to 5 $\%.cm^{-1}$, agree with the values presented by Minchin & Thorpe (1987) for bean. The low tracer loss, about 0.3 $\%.cm^{-1}$, observed in the wheat peduncle is most likely related not only with the almost mature state of the peduncle but also with the grain filling stage in the ear that makes it a strong sink at the time of experiments. The leakage of tracer from the phloem pathway is also shown by the detection of tracer in the perfusion solution (Table 5.2, Fig. 5.34), albeit a very small amount that was about 10^4 times smaller than the loss of tracer into the tissue surrounding the phloem pathway (Fig. 5.11). The existence of tracer unloading is further supported by observing that the experimental tracer activity profiles could be very well simulated by the compartmental model that included radial exchange of both water and solutes (Figs. 6.6 and 6.12).

7.8 Effects of Phloem/Apoplast Water Exchange on Phloem Translocation

The importance of tissue water status and specifically water exchange alone for phloem translocation is illustrated by the effects of squash internode perfusion by PEG. Polyethyelene glycol (PEG) is commonly used as osmoticum for plant water studies because it is not taken up by plant tissues (Carpita *et al*., 1979; Oertli, 1986). Thus only water flux is involved in response to water potential differences between the perfused tissue and the PEG solution. The water potential of the PEG solutions used is lower than the ABS water potential of the normally perfused internode. Therefore more concentrated PEG solutions will have lower water potentials than the tissue water potential and less water will be taken by the plant than from ABS alone. As confirmed experimentally, the

plant water uptake rate decreased as PEG concentration increased from 100 to 500 mOsmol (Figs. 5.28 to 5.30). Consequently due a decrease in plant water uptake as ABS pefursion is replaced by PEG perfusion the water potential of the perfused internode will be more negative than in its previous ABS perfusion status ($\Psi_{ABS} \cong 0.01$ MPa). As PEG is impermeant to cell membranes it seems likely that PEG did not invade the squash internode tissues and therefore had its major effect on the pressure, p_{out}, rather than on the osmotic component of Ψ_{out}. So it can be expected that the reduction in the apoplastic water potential surrounding the perfused internode sieve tubes causes a reduction in pressure within those sieve tubes, with a concomitant water efflux from them into the surrounding apoplast. The more negative the apoplastic water potential the more water is removed from sieve tubes. This is very well illustrated in the compartmental model simulations of the squash perfused internode (Fig. 6.19).

Due to the decrease in pressure in compartment 1 (sieve tubes), as a result of perfusion with PEG the turgor pressure gradient between that compartment and upstream regions increases (Fig. 6.17B). Hence, according to equation (7.2) this increase in the turgor pressure gradient results in a greater translocation flow rate and an increased influx of photoassimilates into the perfused region (Fig. 6.19). The decrease in tracer loss in the load node region (upstream of the perfused internode) is a consequence, with more tracer leaving this region (Figs. 5.14, 5.17 and 5.19). Therefore the tracer loss changes in the load node region are not the consequence of changes in sugar concentration in that region, as seen in the perfused internode, but rather they are due to changes on flow speed. The increase in translocation flow rate into sink regions, with lowered water potential, was observed before using PEG as an osmoticum for bathing bean root (*Phaseolus vulgaris* L.) (Lang & Thorpe, 1987). Also, Minchin & Thorpe (1987b) observed reduction in the translocation flow into a sink (upper shoot of young *Phaseolus vulgaris* L. plants) subjected to an increased local atmospheric pressure. The same phenomenon was observed by Schurr & Jahnke (1991) upon increasing the pressure on the roots of ^{11}C labelled castor bean plants (*Ricinus communis*), while the reverse situation, an increase in tracer flux, was observed when the roots were submitted to a decrease in pressure, when their water potential was also decreased. Previously, Swanson *et al*. (1976) found, in *Phaseolus* plants, coupling between the translocation rate into a sink and its transpiration rate.

The increased photoassimilate influx into the perfused internode observed at higher PEG concentrations (Fig. 6.19), contributes to increased rate of influx of ^{11}C (Figs. 5.18 and 5.22). In this way, a local increase of solutes (Fig. 6.18A) and labelled photosynthate within the perfused internode sieve tubes and a higher concentration gradient of sucrose across the sieve tube plasmalemma are thus enhanced. As a result there will be an increase in tracer leakage across the sieve tube membrane, simultaneously increasing the accumulation of tracer in the stem apoplast (Minchin *et al*, 1984; Minchin & Thorpe, 1987). This can be easily seen in the compartmental model simulations of PEG perfusion (Fig. 6.18B). Also, this accumulation of tracer in the stem apoplast is reflected by the increase observed in tracer loss in the perfused internode as shown in Figs. 5.14, 5.17 and 5.19. Therefore the combined effects of increased translocation speed into the perfused internode, and increased sieve tube concentration, explain both the increased tracer influx rates into the perfused internode (Figs. 5.18, 5.22), and the increased tracer loss in that same region, when perfused by PEG (Figs. 5.14, 5.17 and 5.19).

In the downstream internode, beyond the perfused internode, there will be a sum of the simultaneous changes occurring upstream. First, there will be a decrease in turgor pressure gradient between the perfused internode and the downstream internode. This is caused by lowering the sieve tubes turgor pressure as a result of PEG perfusion, which will result in a decrease in transport speed (7.2) into the downstream internode as compared with ABS perfusion only. Second and simultaneously occurring due to an increased photoassimlate influx into the perfused internode and to an increase in sugar concentration in the perfused internode sieve tubes, there will be also an increase in sieve tube concentration in the downstream internode. This in turn will lead to an increase in tracer leakage similar to what occurs at the same time in the perfused internode as shown by Figs. 5.14, 5.17 and 5.19. Due to this combination of effects we see an increase in tracer influx in the downstream internode, a consequence of changes on the axial sieve tube concentration gradient (Figs. 5.18 and 5.22). These results confirm the importance of water status upon phloem translocation and show the relevance of transient changes in the apoplastic water potential gradient $\frac{d\Psi_{out}}{dz}$ on phloem transport, which is often assumed as negligible in comparison with the sieve tubes osmotic gradient $\frac{d\Pi}{dz}$.

7.9 Raffinose is Not Loaded Into the Phloem

Raffinose is one of the main sugars transported in the phloem of *cucurbitaceae* (Richardson & Baker, 1982, 1984; Schaffer *et al*., 1996) and specifically in the model plant species of this work *Cucurbita maxima* (Fiehn, 2003). However, cell membrane transporters of raffinose have only been identified in chloroplasts so far (Schneider & Keller, 2009). We wanted to test the likelihood of raffinose uptake into the phloem in the stem of squash. But due to its limited solubility in water solutions, up to 15 % (m/v) at 22 ºC – the temperature of the experiments in this work – raffinose could only be used up to a maximum of approximately 200 mM concentration. Raffinose, stachyose and verbascose and all the oligosaccharides detected so far exist in the sieve tubes and associated intermediary cells and companion cells mainly (Beebe & Turgeon, 1996; Haritatos *et al*., 1996, 2000; Holthaus & Schmitz, 1991; Madore & Webb, 1981a; Oparka & Turgeon, 1999; Webb & Gorham, 1964). This shows that, while never leaving the phloem, serving only as way of transporting carbon, oligosaccharides at the same time provide a very efficient way of preventing passive leakage from sieve tubes.

Hence, due to their relative larger size than sucrose and mannitol molecules, as a treatment raffinose will behave as an osmoticum in the same way as PEG and not enter plant cells although it may penetrate into the perfused internode tissue. This is consistent with the similar effects in tracer loss (Figs. 5.14) and in tracer flux (Fig. 5.15) of perfusion by 100 mM raffinose and of an osmotically equivalent PEG solution. In the same way, the reduction in water uptake in the perfused internode when perfused with raffinose 100 mM is not significantly different from when it was perfused with an osmotically equivalent PEG solution, being less severe than the decrease cuased by both sucrose and mannitol at the same concentration (Fig. 5.28). These results suggest that raffinose is not loaded into the phloem and most likely if penetrating the tissue it will be not far apart from the pith cavity bordering cells.

7.10 Sucrose Uptake into the SECC in Squash Internodes

Sucrose is the most common sugar species transported in the phloem, being almost universal (Zimmerman & Ziegler, 1975), and is also one of the main sugars

transported in the phloem of *cucurbitaceae* (Richardson & Baker, 1982, 1984; Schaffer *et al*., 1996). These facts suggested the hypothesis that sucrose could also be loaded in squash internodes. Perfusing the squash internode pith cavity with a sucrose solution both the increased tracer loss (Figs. 5.14, 5.17 and 5.19) and the axial tracer influx rate into the perfused internode (Figs. 5.15, 5.18, and 5.22) were dependent on the sucrose concentration of the perfusion solution. At the same time, water uptake into the perfused internode decreased with the increasing sucrose concentration in the internode pith cavity bathing solution (Figs. 5.28 to 5.30), and was even reversed for sucrose concentration of 500 mM (Fig. 5.30). Qualitatively these results are similar to those when PEG was the osmoticum, but sucrose had the much more dramatic effect on ^{11}C transport, yet during perfusion by PEG plant water uptake was never reversed. This suggests that water exchanges between the sieve tubes and the surrounding apoplast did also occur in sucrose perfusion treatments, similar to the previously described mechanism when PEG was the osmoticum. However, the higher tracer loss and tracer influx rate observed, together with the more severe decreases in water uptake caused when sucrose was used compared with PEG, suggest that, unlike PEG, sucrose is taken up by the perfused internodes sieve tubes. As mentioned before, sucrose is found in the apoplast and is one of the sugars transported in the phloem of squash (Fiehn, 2003; Hendrix, 1982; Richardson & Baker, 1982, 1984). Hence, in perfusing the squash internode pith cavity with a sucrose solution it is possible that not only due to its smaller molecular size but also due to its role and nature in plants, sucrose will be taken up by the sieve tube elements. This is also supported by the fit to experimental tracer activity profile obtained with our compartmental model if there was sucrose uptake into sieve tubes (Fig. 6.21). As the sucrose concentrations used as treatments were most likely higher than apoplastic sucrose (Minchin & Thorpe, 1984), sucrose concentration in the apoplast in the perfused internode would have been increased. Consequently less labelled sucrose will be reloaded actively into sieve tubes after leakage (as more binding sites are being occupied by unlabelled sucrose). In this way, the ^{11}C labelled sucrose will increase in the perfused internode apoplast, i.e. tracer loss will increase. Indeed, this "trapping" of labelled sucrose occurred for more concentrated sucrose perfusion solutions (Figs. 5.14, 5.17 and 5.19). Axial flow would have been promoted by the combined effects of i) tracer accumulation in the apoplast due to sucrose trapping mechanism and ii) the increase in flow into the perfused internode. The latter is caused by the lowered apoplastic water potential gradient between the upstream regions and the perfused internode, as described before for PEG perfusion.

These combined effects explain the increase on the influx of tracer into the perfused internode, more evident for higher sucrose concentrations (Figs. 5.18 and 5.22). Simultaneously, since sucrose levels are raised in the apoplast when compared with PEG effects, sucrose perfusion will cause more dramatic changes in apoplastic water potential, lowering it more than an osmotically equivalent PEG perfusion. Both components of the apoplastic water potential will be affected. Combined with the water exchange occurring simultaneously between sieve tubes and the apoplast, a more dramatic change in sieve tube pressure and sieve tube concentration would have occurred leading to the observed differences, in tracer loss and in rate of tracer influx, between sucrose and PEG perfusions. The combined effect of solute and water exchanges between the perfusion solution and the perfused internode tissue would lead to higher reductions in plant water uptake, and even their reversal, when perfused at higher sucrose concentrations.

The effect of further lowering the apoplastic water potential in the perfused region by the sucrose treatment would have caused an increase in the axial apoplastic water potential gradient between the upstream regions and the pertfused internode, which led to an increase in flow into the perfused internode. Although, the sieve tube osmotic gradient between upstream regions and the perfused internode might have been decreased due to water removal and consequent increase in sieve tube concentration in the perfused internode and possibly also to sucrose uptake from the perfused internode apoplast. However, since the effects in tracer loss in the load node region for both sucrose and PEG perfusions (Figs. 5.17 and 5.19) were similar, it is likely that the concentration gradient changes caused by perfusion of both solutes, which do not contribute to an influx increase into the perfused internode, are not enough to compensate for the more severe decrease in apoplastic water potential gradient between upstream regions and the perfused internode. Thus, as with PEG perfusion, the reduced tracer loss in the load node region, when the perfused internode is treated with sucrose (Figs. 5.17 and 5.19), is mostly explained by the changes in translocation flow occurring upstream of the perfused internode and not by changes in tracer loss. In the downstream internode we have the same situation occurring as with PEG treatment, but with sucrose the effect can be expected to be higher than with PEG. The increased influx rate into the perfused region, combined with the increase in concentration due to water removal and uptake of unlabelled sucrose, contributes to an increase in the influx rate and concentration gradient in the downstream regions. This promotes a consequent increase in tracer loss as shown (Figs. 5.17 and 5.19).

The conclusion that sucrose is loaded into phloem in the stem of squash is supported by the knowledge that sucrose is one of the main sugars transported in *cucurbitaceae* (Hendrix, 1973, 1977, 1982; Richardson & Baker, 1982, 1984). In addition, radial movement of sucrose after phloem unloading has also been observed in the stem of *Cucurbita pepo* L. (Webb & Gorham, 1964). Our results of enhanced tracer unloading during sucrose perfusion also agree well with previous observations from Weatherley *et al*. (1959) who observed increased sucrose levels in phloem and xylem effluents while perfusing bark strips from osier (*Salix viminalis*) with sucrose solutions. Weatherley *et al*. (1959) also observed decreased rates of phloem exudation (from aphid stylets) during sucrose perfusion of the bark strips. This decrease agrees with equation (7.3), when the concentration gradient is decreased, provided that all of the sieve tubes are submitted to the similar increased sucrose uptake due to the perfusion treatments imposed. Heyser *et al*. (1976) showed evidence of sucrose uptake and consequent phloem loading in maize leaf strips, observing changes in phloem transport direction when perfusing leaf strips with sucrose solutions using ^{14}C-sucrose which was taken up and loaded into the phloem. Using ^{11}C labelling, Pickard *et al*. (1978b) have also observed an increase of tracer influx rate into downstream regions of a stem segment of moonflower (*Ipomoea alba* L.) perfused with sucrose similar to the results presented in this work, but using much higher sucrose concentrations. Minchin & Thorpe (1984), investigating phloem unloading in the stem of ^{11}C labelled bean plants, perfused peeled stem segments with unlabelled sucrose and observed an increase in labelled material in the bathing solution. They suggested that buffering of changes in sieve tube sucrose concentration probably involves the apoplast. They propose that phloem unloading in bean stem is an unloading of sucrose into the apoplast in which a fairly constant sucrose concentration is maintained by a balance of sucrose uptake into cells. Sucrose is used for growth, maintenance or storage, and reloading into the phloem. Not only is this a generalization of the sucrose retrieval system suggested by Maynard & Lucas (1982), but also the identification of sucrose transporters, in both sieve elements and companion cells within stems and petioles of many species, indicates the existence of retrieval systems for apoplastic sucrose. We conclude that the concurrent unloading and reloading processes along the transport phloem are widespread if not universal in plants (Oparka & Turgeon, 1999; van Bel, 2003b).

7.11 Sucrose Uptake into the SECC of Squash Internodes May Involve an Apoplastic Step

PCMBS is a water-soluble non-permeating sulphydryl-specific reagent which is thought to inhibit sucrose transport across membranes by modifying the carrier proteins (Giaquinta, 1976). The promotion of tracer loss in the presence of PCMBS and its maintenance after treatment removal (Fig. 5.32), suggests there is an apoplastic step in the reloading of tracer that was unloaded in the squash phloem (Minchin *et al*., 1984; Minchin & Thorpe, 1984, 1987). Thus the increase in tracer loss in the perfused internode in the presence of 2 mM PCMBS would be explained by inhibition of an active uptake of tracer. This inhibition would then decrease reloading, and promote tracer loss into the stem apoplast, as observed (Fig. 5.32). From the sucrose trapping mechanism described before and the promotion of tracer loss in the presence of sucrose together with PCMBS (Fig. 32), we conclude that that there is a sucrose-specific system for uptake from the apoplast in the stem of squash (*Cucurbita maxima*), a new observation for this species. The inhibiting of reloading of tracer and of sucrose, caused by PCMBS, and the increased in flow of tracer into the perfused internode during sucrose perfusion both contribute to tracer loss increase (Fig. 5.32). Such evidence of active uptake of sucrose is of interest, since squash, as a member of *cucurbitaceae*, is considered a symplastic phloem loader (Fiehn, 2003; Turgeon & Beebe, 1991). In fact, PCMBS has been tested in *cucurbitaceae*. Thorpe & Minchin (1988) found that phloem loading in abraded *Cucurbita pepo* L. leaves showed a variability of results in response to PCMBS, from no response to a dramatic reduction of transport of labelled photoassimilates from the load region. A possible explanation is that the different PCMBS effects can be explained by the distinctive minor vein structure in that plant family, which suggests that both apoplastic and symplastic loading mechanisms may be present (Turgeon *et al*, 1975). However, their relative contribution to the overall phloem loading is not known. Hence the reduction of transport of labelled photoassimilates from the load region observed in the presence of PCMBS in *Cucurbita pepo* L. leaves would be explained by the inhibiting of the apolastic loading by PCMBS. When there was no response it may be that PCMBS did not penetrate the tissue or that the plant responded by increasing the symplastic loading.

In the stem, there are possibly three sucrose transport systems of interest to the PCMBS-response. First, there is the loss of sucrose from the translocation pathway, where the sucrose concentration will be high, into the stem apoplast. Second, there is the uptake of sucrose from the apoplast into the transport pathway. Third, there is sucrose uptake from the apoplast into other cells of the stem tissue. Uptake of sucrose into slices of *Beta vulgaris* petiole has been shown to obey the same kinetics as phloem loading (Maynard & Lucas, 1982), and to be similarly sensitive to PCMBS. This suggests that phloem loading from the petiole apoplast may be occurring. The same process is thought to happen in plant stems as the results of squash suggest. Comparing the phloem tracer losses in the perfused internode before and during treatments we see that gross unloading of 4.1% cm^{-1} increases to 4.8 $\%.cm^{-1}$ (Fig. 5.32) when perfused with 2 mM PCMBS, suggesting a reloading of tracer per unit length of 0.7 $\%.cm^{-1}$. Also, by comparison of the effects caused by perfusion of 100 mM sucrose with and without PCMBS on the perfused internode gross unloading of tracer goes from 4.8 to 5.3 $\%.cm^{-1}$, respectively (Fig. 5.32). In this case, it gives an apoplastic reloading of tracer per unit length of 0.5 $\%.cm^{-1}$. These values result in retrieval of labelled photoassimilates into the phloem varying from 12 to 17 % of the gross loss of tracer. These results are very similar, and they also agree remarkably with the measurements of reloading and unloading rates in the stem of bean, suggesting that a similar process may be present in both species. Bean is considered an apoplastic loader species, with apoplastic reloading of tracer in the stem (Minchin & Thorpe, 1987; Thorpe & Minchin, 1988).

Tracer loss increase in the downstream internode during perfusion with PCMBS as well as its absent effects in the load node region may be explained in two ways. First, PCMBS is well known to inhibit aquaporins, and thus water transport, in animal cells (Baye & Lazanvecchia, 2000; Naccache & Sha'afi, 1974). However, its effects in plant cells are much more diverse. Wayne & Tazawa (1990) showed that the osmotic water permeability of *Nitellopsis obtusa* was inhibited by the organomercurial sulphydryl-reactive reagent PCMBS, which is also well known to bind to critical cysteine residues of water channels. But PCMBS can also show no blockage of water transport as Schütz & Tyerman (1997) showed on *Chara coralline*. Bowen (1972) observed that PCMBS decreased boron uptake by roots differently in different cultivars of sugarcane, causing inhibition up to 50% in some cultivars, while Wilkinson *et al*. (1994) observed no effect in sorghum root uptake. Boron is taken up by plant roots as undissociated boric acid, which is a non-electrolyte, thus capable of being taken up through aquaporins. Dordas &

Brown (2001) suggest two possible mechanisms of boron uptake: passive diffusion through membrane lipid bilayers and through channel-mediated transport. Dordas & Brown (2001) observed that boron uptake by *Cucurbita pepo* L. roots was strongly reduced by $HgCl_2$ suggesting its sensitivity to mercury similar to what happens in aquaporins. Hence, from Dordas & Brown (2001) results, and noting that in our case we have indeed a reduced water uptake by the plant when perfused with PCMBS with or without sucrose, as shown in Fig. 5.33, we can consider that PCMBS will also affect water exchange, consequently decreasing the tissue water potential. This way, the rate of tracer influx into the perfused internode will increase (Fig. 5.33) by increasing the apoplastic water potential gradient between the upstream regions and the perfused internode, which will lead to an increased flow rate to both the perfusded internode and its downstream internode. The increase in tracer influx into the downstream internode will promote unloading of tracer in that region during PCMBS perfusion. Interestingly, this PCMBS effect is not more pronounced when sucrose is present (Fig. 5.33) as it would be expected if water uptake into the perfused region was strongly reduced.

When PCMBS penetrates into the perfused internode tissue it can also move easily through the xylem and travel to distances far from the perfused internode itself, thus spreading its effects in more regions into the plant (Minchin & Thorpe, 1984, 1987; Thorpe & Minchin, 1988). It can therefore be expected that tracer loss would be increased in regions other than the perfused internode, as indeed occurred downstream (Fig. 5.32). On the other hand, it may well be that such movement would also change the water exchange between sieve tubes and the apoplast in those regions, thus affecting the apoplastic water potential gradient and altering phloem flow into those regions (Fig. 5.33). Although it might be expected that PCMBS in the transpiration stream would affect the load node and the load leaf. But no significant effects were seen in the load node region (Fig. 5.32). This not only suggests the possible dispersion of a very small amount of PCMBS into that region, hence incapable of having visible effects, but also its possible long distribution to regions far from detection. It may well be a more plausible explanation that all these effects will occur simultaneously, making it more difficult to separate their contribution to the results here presented. Or, there was no transport into the xylem at all.

7.12 Mannitol Uptake into the SECC in Squash Internodes

Mannitol, a six carbon polyol, is the most widely distributed sugar alcohol in nature and has been reported in more than 100 species of 70 families of vascular plants (Loescher, 1987; Loescher *et al.*, 1991; Stoop *et al*., 1996). It is also one of the main sugars transported in the phloem, comprising 10 to 60 % of the soluble carbohydrates in the phloem of *apiaceae*, some species of *combretaceae*, *scrophulariaceae* and *rubiaceae* (Bieleski, 1982). It is also typical in the *oleaceae* family along with oligosaccharides (Flora & Madore, 1993). Curiously, sorbitol, which is an epimer of mannitol, is one of the main sugars translocated in *prunoideae*, *maloideae*[1] and some species of *spiraeoideae* (Zimmermann & Ziegler, 1975), and yet they do not transport mannitol. Mannitol is known as a "compatible solute" because its accumulation does not interfere with normal metabolism and at high concentrations can prevent loss of water and compensate for salt accumulation (Conde *et al*., 2007). It has been suggested that sugar alcohols, because of their water-like hydroxyl groups, may mimic the structure of water and maintain an artificial sphere of hydration around macromolecules (Yancey *et al*., 1982). Sugar alcohols have also been postulated as scavengers of activated oxygen species preventing peroxidation of lipids and resulting cell damage, thus conferring more resistance against oxidative stress (Smirnoff & Cumbers, 1989, Williamson *et al*., 1995, Jennings *et al*., 1998). Mannitol synthesis occurs simultaneously with either sucrose synthesis (Rumpho *et al*., 1983) or with oligosaccharide synthesis (Flora & Madore, 1993). To date, no plants have been found that produce mannitol only. Noiraud *et al*. (2001) identified first a mannitol transporter in celery (*Apium graveolens*) phloem and more recently more polyol transporters were also found and characterized in *Prunus cerasus* (Gao *et al*., 2003), *Plantago major* (Ramsperger-Gleixner *et al*., 2004), *Malus domestica* (Watari *et al*., 2004), *Arabidopsis thaliana* (Klepek *et al*., 2005; Schneider *et al*., 2006) and *Oleae europaea* (Conde *et al*, 2007); not surprisingly these results are all for species that transport sugar alcohols through the phloem. In *cucurbitaceae* no evidence exists of any physiological role of mannitol, as it is not present in the phloem sap (Fiehn, 2003; Richardson & Baker, 1982, 1984) and no mannitol carrier has been identified so far, but it

[1] in fact, the name sorbitol comes from the genus *Sorbus* from this family

has been found in the fruits of watermelon (*Citrullus vulgaris*) and squash (*Cucurbita pepo*) (Barker, 1955).

Mannitol is frequently used as osmoticum in transport studies in animal cells as it does not cross animal cell membranes. Based on that and for the same reasons, it has also been used to plasmolyse sieve tubes and parenchyma cells in *Cucurbita pepo* L. callus (Lackney & Sjolund, 1991). Weatherley *et al*. (1959) used mannitol as an osmotic agent to treat isolated bark strips of osier (*Salix viminalis*), and Minchin *et al*. (1984) used sorbitol in osmotic experiments on peeled bean stems. The first intention in this work, on choosing mannitol, was for its role as an osmotic agent. But soon after first experiments were carried out and by comparison with the tracer loss results observed with sucrose and PEG perfusions (Figs. 5.14 to 5.19 and 5.22), together with water uptake rates from the perfused internode (Figs. 5.28 to 5.30), it indicated that there was mannitol uptake into the phloem. Basically, sucrose and mannitol effects only differ for solute concentrations of 500 mM, and most likely higher than that. While, at 100 and 300 mM sucrose and mannitol effects were similar in both tracer loss and water uptake rates during treatments, although the increase in tracer influx into the perfused region and into the downstream internode seemed more prolonged than the increase caused by perfusion of 300 mM sucrose (Fig. 5.18). Comparison of the identical water uptake rates observed during sucrose and mannitol perfusions with the lesser rates observed with PEG perfusion (Fig. 5.28 to 5.30), suggests that penetration of mannitol into the perfused internode tissue was similar to sucrose. This penetration would be favoured by the smaller size of mannitol molecules (about half the size of sucrose molecules) and their non-electrolytic nature, which benefits from the acidic pH of the apoplast and the perfusion solution[2]. In this manner, phloem uptake of mannitol by a similar mechanism to sucrose explains the similarity of their effects (§ 7.10 and 7.11). Whether it is through a specific and different membrane transporter or through the same carrier is not possible to conclude from these results.

[2] mannitol is a weak acid

7.13 Changes in the Pathway Resistance Explain Phloem Stoppage Caused by Mannitol Perfusion

Mannitol effects can also be interpreted by proposing that it is not taken up by the phloem, but does penetrate the plant tissue, unlike PEG. Heyser *et al*. (1976) showed ^{14}C-mannitol uptake in maize leaf strips, it accumulated in the apoplast but was not loaded into the phloem. In this case, the osmotic barrier would be much closer to sieve tubes than with PEG perfusion. Mannitol perfusion would thus affect apoplastic water potential and phloem transport faster than PEG (§ 7.8). Weatherley *et al*. (1959) used mannitol as an osmoticum to perfuse strips of bark of osier (*Salix viminalis*) and they show a simultaneous decrease of phloem exudation rate with increasing sucrose concentration during mannitol perfusion. Their results were explained by water removal from the phloem, raising phloem sugar concentration and viscosity, as inferred for sorbitol perfused bean stems (Minchin *et al* 1984). Minchin *et al* (1984) observed tracer accumulation in both the perfused stem and in the perfusing solution to increase whith sugar concentration in the phloem. The same scenario explained the effects of PEG perfusion (§ 7.8). It is therefore possible that the effects of perfusion by 500 mM mannitol have the same explanation. Thus the temporary phloem stoppage (Figs. 5.20 and 5.22) may be explained by an immediate water removal from sieve tubes, causing rapid local increase in sap viscosity sufficient to temporarily stop flow. In the same way a blockage in a pipe would stop flow everywhere downstream, as we see in Fig. 5.20. The recovery from stoppage with an enhanced influx rate into the perfused region and downstream would come from changes in the sieve tube water relations in order to compensate the decrease in the apoplastic water potential. Since we are not measuring directly sieve tube water uptake it is impossible to tell if this new physiological state of the tissue affected is as stable as the total water uptake suggests (Fig. 5.30). But, transient changes in phloem/apoplast water exchange can be expected to have counterbalanced the decrease in apoplastic water potential, although not measurable by the experiments reported here. Under the turgor pressure gradients expected to drive phloem flow, flow is stopped when the viscous forces outcome the pressure forces necessary to drive flow. The idea of viscosity influence on phloem transport is not new, but the sugar concentration dependence of phloem sap viscosity has been differently treated by different authors

(Ferrier & Christy, 1975, 1977; Goesch *et al*., 1976; Lang, 1978; Murphy, 1989a; Passioura, 1976; Thompson & Holbrook; 2003a). Höltta *et al*. (2005) have shown theoretically that viscosity changes due to increased sugar concentration in the phloem sap could stop phloem flow. However, comparing the effects of perfusion by mannitol and sucrose at 500 mM we see that they both caused the same water uptake reversal and phloem stoppage was only observed during mannitol perfusion. Considering the sucrose uptake into sieve tubes it is hard to think that mannitol could be an enhanced version of the effect caused by perfusion by an equivalent osmotic PEG solution as sucrose would be as close to sieve tubes as mannitol is. The water uptake due to perfusion by 500 mM sucrose or mannitol is similar. Hence the same water removal and consequent viscosity and pressures changes postulated to happen during perfusion by 500 mM mannitol would be expected to occur during perfusion by 500 mM sucrose. Thus phloem stoppage would also be occurring due to perfusion by 500 mM sucrose and probably it would be more severe due to sucrose uptake being an extra factor to increase solute concentration and thus viscosity. But there was no phloem stoppage during perfusion by 500 mM sucrose (Figs. 5.21 and 5.22). Hence we conclude that increase in viscosity due to increased sugar concentration in sieve tubes was not the cause of transient phloem stoppage observed during mannitol perfusion.

The transient phloem stoppage and its subsequent recovery both observed during perfusion by 500 mM mannitol (Fig. 5.20) closely resemble the responses of the same species when 1 cm of the perfused internode was chilled (Fig. 5.36). Both transport stoppages lasted approximately the same time, the plant recovered while still being treated, and with initially higher tracer transport than before treatment in both the perfused internode and the downstream internode during perfusion by 500 mM mannitol. It has long been known that phloem transport stops due sudden decrease in tissue temperature in *cucurbitaceae*, and its behaviour is quite similar to other dicotyledons as being a reversible status (Lang & Minchin, 1986). Also, phloem stoppage in *cucurbitaceae*, as a response to chilling, similar to what has been observed in other species, has been attributed to conformational changes of phloem protein (P-protein), typically found in this family, which changes sap viscosity, by increasing it, and eventually blocks flow (Giaquinta & Geiger, 1973). Protein plugging in *cucurbitaceae* is know to occur upon production of insoluble aggregates of phloem protein 1 (PP1) in response to oxidation (Kleinig *et al*., 1975) or in response to calcium, Ca^{2+}, release into sieve tubes (Furch *et al*., 2010; McEuen *et al*. 1981). From the similarity of the phloem

transport stoppage results in squash observed during perfusion by 500 mM mannitol or chilling treatments and from the fact the different results observed during perfusion by 500 mM mannitol or sucrose we conclude that the cause of the transient flow stoppage may be in attributed to conformational changes of phloem proteins which may be triggered by the presence of mannitol.

7.13.1 Mannitol Catabolism

Alosi *et al*. (1988) suggested that P-proteins undergo conformational changes and gel after titratable groups and sulfhydryl residues are exposed; oxidation of the residues forms the intermolecular disulfide bridges of the gel. Alosi *et al*. (1988) observed that the gelation of diluted phloem exudate from *Cucurbita pepo* fruit is regulated by factors (e.g. oxygen, pH, nicotinamide adenine dinucleotide phosphate (NADPH)) which affect the maintenance of reduced sultfydryl residues. However, they observed that the effects of NADPH on phloem sap gelation were complex as the gelation was only observed for diluted exudates when depleted of NADPH. But, they observed that gelation was also promoted when NADPH concentrations were higher. Mannitol synthesis in higher plants involves a NADPH-dependent mannose-6-phosphate reductase that catalyzes the conversion of mannose-6-phosphate to mannitol-1-phosphate, followed by dephosphorylation by a phosphatase (Fig.7.2) (Loescher *et al*., 1992; Stoop *et al*. 1996). In the non-photosynthetic sink tissue of species that transport mannitol, the conversion of mannitol to mannose is made through a NAD^+-dependent mannitol dehydrogenase (Fig. 7.2). We suggest that upon mannitol uptake into sieve tubes and its subsequent catabolism, possibly involving the reverse reaction where NADPH-dependent mannose-6-phosphate reductase participates (Fig. 7.2), there is an increase in NADPH cytosolic concentration. Note that because mannitol is a weak acid its uptake would be favoured by the alkaline pH of sieve tube sap so that mannitol dissociation is promoted. Hence, accumulation of mannitol in SE/CC could lead to high concentrations of NADPH, which in its turn could trigger P-protein gelation, and stop phloem transport. This situation could be transient as the plant adapts to this new condition of dealing with mannitol catabolism. This fact would explain the absence of phloem transport stoppage during perfusion by sucrose 500 mM, as sucrose is not involved directly in any reaction that would increase NADPH levels in the sieve tubes cytosol. The same scenario is possible if mannitol

conversion to mannose, as it happens in sink tissues, involves a $NADP^+$-dependent mannitol dehydrogenase, thus producing NADPH upon mannitol oxidation. One way of testing this hypothesis would be to analyze phloem sap exudates when phloem stoppage occurs during perfusion by mannitol, for changes in the protein content and NADPH levels. Also some microscopy would be necessary to observe protein plugging during high concentration mannitol perfusion.

7.13.2 Ca^{2+}-dependent P-protein Gelation

Furch *et al*. (2010) observed proteinaceous occlusion in *Cucurbita maxima* sieve tubes after damage. They observed a dramatic drop in soluble sieve element proteins levels and a simultaneous coagulation of sieve element proteins shortly after the burning

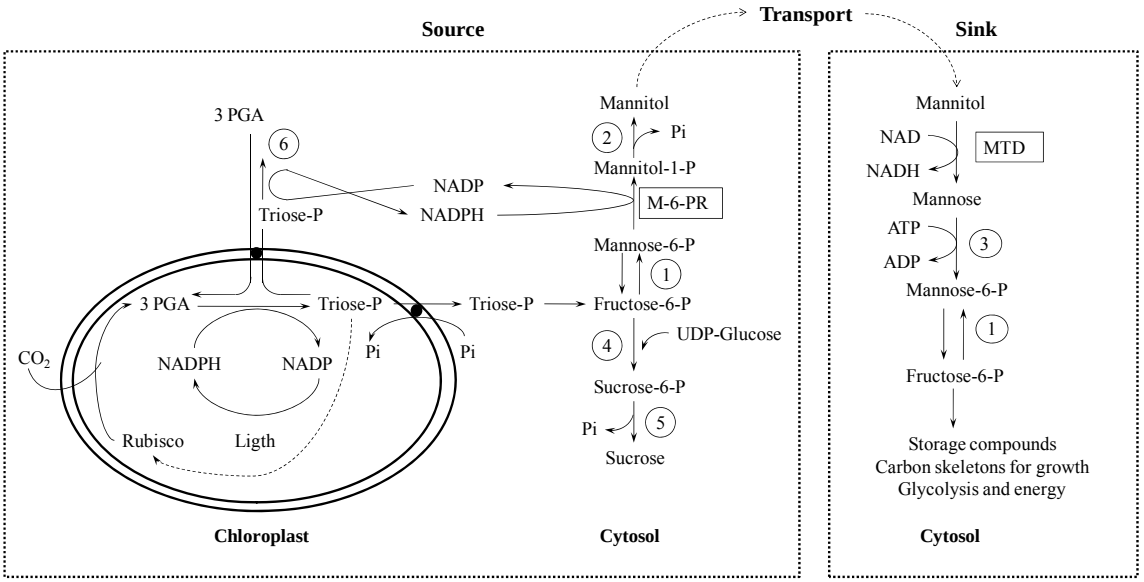

Figure 7.2 –Synthesis, transport and catabolism of mannitol in plants. Enzymes involved are: (M-6-PR) mannose-6-phosphate reductase; (MTD) mannitol dehydrogenase; (1) phosphomannose isomerase; (2) mannose-1-phosphate phosphatase; (3) hexokinase; (4) sucrose-6-phosphate synthase; (5) sucrose-6-phosphate phosphatase; and (6) non-reversible triose-phosphate dehydrogenase. The chloroplast outer membrane is represented (adapted from in Stoop *et al*., 1996).

stimulus which stopped phloem transport. They suggested stop of mass flow by Ca^{2+}-dependent occlusion mechanisms attributed to Ca^{2+} influx into the sieve tubes during the

passage of damage-induced electropotential waves (EPW) and the reversibility of the occlusion was explained by removal of Ca^{2+} ions. Given the potential Ca^{2+}-biding sites on the phloem protein (PP1) (McEuen *et al*., 1981) Furch *et al*. (2010) suggest PP1 as the main candidate for proteinaceous occlusion prior to callose occlusion after sieve tube damage in *Cucurbita maxima*. The expansion of forisomes (protein bodies) in sieve tube element protoplasts of broad bean (*Vicia faba*) in response to osmotic shock or suction and the absence of forisome expansion when Ca^{2+} influx was inhibited, by Gd^{3+} or EGTA, suggested the presence of mechano-sensitive Ca^{2+} channels in the sieve tube element plasma membrane (Hafke *et al*., 2007). Mechano-sensitive Ca^{2+} channels have been identified in plant cells (Kaneko *et al*., 2009). With this in mind, and as an alternative to mannitol catabolism induced gelation hypothesis, it is possible that water efflux from sieve tubes and concomitant pressure decrease causes a Ca^{2+} release into sieve tubes that triggers PP1 polymerization in response to a sudden turgor pressure change. Its transient nature would then be explained as an adaptation by the plant to its new local water status. However, against this second hypothesis we note that sucrose perfusion always caused similar water uptake changes to mannitol perfusion (Figs. 5.28, 5.29 and 5.30), and its effects on tracer loss and tracer influx were only different from mannitol perfusion at 500 mM (Fig. 5.22). Hence, it is unlikely that mannitol and sucrose perfusion, and at higher concentrations in particular, would cause different pressure changes due to changes in water uptake. Yet phloem stoppage never occurred with perfusion by 500 mM sucrose. Thus, with similar pressure changes in sieve tubes, it is hard to explain why only with mannitol such a mechano-sensitive mechanism was operating. We emphasize that both these hypothesis are not possible to confirm based in the data we present. However, given the circumstantial evidence presented the first hypothesis seems the more likely. Protein polymerization triggered by mechano-sensitive Ca^{2+} channels may well occur in the sieve tube element plasma membrane of squash (*Cucurbita maxima*), but it seems unlikely to have occurred in the experimental conditions of this study. Protein polymerization triggered by mechano-sensitive Ca^{2+} channels could be tested by observing the effects of Gd^{3+} and EGTA on phloem stoppage during high concentration mannitol perfusion and compared with the evidence for the mannitol catabolism hypothesis.

7.14 Differences in the Physiological State in Wheat Explain Phloem Transport Results Diversity

Wheat was initially chosen as the model plant due to the apparent ease of access to its vascular system by perfusing its peduncle's pith cavity (Fig. 5.1). Soon after the first experiments were performed and perfusion treatments were done, it showed a remarkable diversity of responses as shown in Figs. 5.12, 5.13 and 5.31, which makes interpretation difficult. The reason for these multiple responses from similarly grown plants might be in the particular physiological development typical of this species. In wheat plants grown under our experimental conditions, ear emergence, i.e. when the ear fully appears at the flag leaf ligule, occurs between 5 to 6 weeks after sowing (Roeb & Britz, 1991; Roeb & Dautzenberg, unpublished data), after which the plant is in full reproductive stage of development. At that age the wheat peduncle continues to develop and extend, reaching its full length at about 7 to 8 weeks of age. Before the first week after ear emergence, the amount of ^{11}C-labelled photoassimilates being accumulated in the ear is very small compared to the amount of labelled photoassimlates accumulated in the roots and lower internodes below the flag leaf node (Roeb & Jahnke, 2007). However, the partition of labelled carbon between the ear and the rest of the plant, specifically the roots, changes dramatically within 2 to 3 weeks after ear emergence, thus 7 to 9 weeks after sowing. During this period the ear shows an increased accumulation of assimilates at the expense of the rest of the plant and grain filling initiates. Simultaneously, there is a dramatic decrease in the carbon accumulation in the vegetative part of the wheat plant (lower internodes and roots).

During this grain filing period there are diel fluctuations in the movement of labelled assimilates towards the ear and towards lower internodes and roots below the flag leaf node (Roeb *et al*., 1986; Roeb & Britz, 1991; Roeb & Jahnke, 2007). Both oscillations patterns of the ear and of the lower vegetative part of the plant are approximately 180^{o} out of phase, and the oscillations of carbon transport towards the ear occur with periods of 65 to 82 min. The grain filling stage continues as indicated by increasing in tracer accumulation in the ear, but after 3 weeks after ear emergence, or 9 weeks of age, the oscillations stop or become more spaced in time and a second shift in carbon partition happens. After this time, at about 4 weeks after ear emergence, the

labelled assimilate accumulation in the ear decreases dramatically while it increases again in the vegetative part (Roeb *et al*., 1986; Roeb & Britz, 1991; Roeb & Jahnke, 2007). At about this time the ear and peduncle start to dry as the flag leaf shows its signs of aging. Most of the ear carbon supply comes from the flag leaf while the lower leaves supply mainly the roots and lower internodes (Roeb & Jahnke, 2007). Thus during reproductive growth the wheat ear becomes the dominating sink organ with very little carbon being accumulated in the peduncle, as ^{14}C labelling results showed (Roeb & Jahnke, 2007). This is also suggested by the big differences in ^{11}C partition between the ear and the rest of the plant (Fig. 5.9) and the small tracer loss values observed in the wheat peduncle (Fig. 5.10), less than 0.5 % cm^{-1}, smaller than the values for squash (Fig. 5.11) and the 4 % cm^{-1} for bean (Minchin & Thorpe, 1987a). The smaller tracer partition of recent assimilate observed in the vegetative part of wheat as shown in Fig. 5.9 agrees well with the observations of Roeb & Jahnke (2007) of the strong dominance of the ear as a sink and that the main export from the flag leaf goes predominantly to the ear. Roeb & Jahnke (2007) were also able to show that the majority of recent assimilate exported from labelling one of the lower leaves would go towards the roots, but in the long term the ear would be revealed as the main sink in the reproductive stage of plant development in wheat, accumulating the majority of the available carbon supply. Thus, the ear and the roots are the main sink organs in wheat while the peduncle seems to be just a pathway organ in which there is very little accumulation of recent fixed assimilates, specifically in the reproductive stage of plant development.

All these findings together with the small tracer loss results shown in Fig. 5.10 show that despite the good access to the vascular system and the apoplast surrounding it, the wheat peduncle is not a good system to use if one wants to study phloem/apoplast interactions. First, the small tracer loss observed shows that the majority of recently fixed labelled assimilates is in transit and almost nothing is unloaded in the peduncle. Second, as the sucrose and mannitol perfusions show (Figs. 5.12 and 5.13), tracer loss changes very little in both the peduncle and the vegetative part, even at very high sugar concentrations and with different responses from similarly treated plants. This agrees with the strong dominance of the ear as a very strong sink which might limit the unloading of assimilates in the peduncle, namely when these come from its main source of supply – the flag leaf. On the other hand, the oscillations in carbon transport to both the ear and the vegetative part, in a less developed plant, could explain the different responses observed from sucrose and mannitol perfusions namely between having an effect and not having

any effect at all. When the transport to the ear was reduced and shifted to the vegetative part, in the down part of the ear oscillation, allowing for some possible solute exchange in the peduncle, changes in tracer loss can be expected to occur. The diversity of PCMBS results could be explained in the same way.

With only daily three pulse application of ^{11}C it was impossible to establish whether the plants are in the daily oscillations cycle, and to relate that information with the treatment applications. The observed daily carbon transport oscillations cycle in the grain filling period are only possible using continuous ^{11}C labelling (Roeb *et al*., 1986, Roeb & Britz, 1991; Roeb & Jahnke, 2007). The diverse responses to solute perfusion could also result from limited solute penetration into the plant tissue. However, the microscopy showing penetration of fluorescein (Fig. 5.1) and the peduncle water uptake (Figs. 5.25 and 5.26) show that there was solute uptake into the wheat tissue. This is also supported by the hydraulic coupling observed between root water uptake and peduncle water uptake (Figs. 5.26 and 5.27), which shows an increase in root water uptake as a result of a decreased apoplastic water potential in the peduncle due to solute and water exchange caused by perfusions of 700 mM mannitol and sucrose.

Due its particular development, we conclude that the wheat plant it is not a good model species if one wants to study phloem/apoplast interactions through perfusion treatments together with ^{11}C labelling. As these results show, there is very little tracer loss compared with other species which somehow limits the likelihood of changing it in a detectable way. This is even more limited by the strong dominance of the ear as a sink. In addition, the wheat peduncle can only be perfused after ear emergence when is extending. Before that it is enclosed in flag leaf sheath with the ear and it is a very young and soft tissue making impossible to perfuse successfully it the way showed here in these experiments (§ 4.4). At that particular time, as shown by Roeb & Britz (1991), very little recently fixed labelled assimilates goes to the peduncle and to the ear which complicates its usefulness in ^{11}C labelling studies at that period. Unfortunately when the peduncle is suitable to be perfused, in the way presented in this study, it is also the time that the ear reveals its strong dominance and possibly causes all the diverse results reported here. Finally, when grain filling ends so does the carbon movement towards the ear and through the peduncle, making it again unsuitable for short-lived tracer studies, apart from the fact that it also starts to dry and aging effects manifest strongly. Basically, the use of the wheat is very limited not only by time but also by the peculiar physiological state of the plant. Perfusion of the lower internodes could be an alternative possibility and

anatomically they are not very different from the ear peduncle (Patrick, 1972). However, this study has not addressed that possibility. Not only they are much shorter than the peduncle, being mostly enclosed by the lower leaves, but also most of carbon accumulation happens in the roots and at the ear. The recently published findings on fructan metabolism and the accumulation known to happen in the peduncle suggests that it could be a good system to use instead (Gebbing, 2003). Castor bean (*Ricinus communis*) was tested as an alternative model plant to wheat as it also has a hollow stem. However, it was not possible to assure a good sealing between the needles and stem epidermis thus compromising the perfusion of solutions. Although it could be maintained for some time, eventually solution leakage was observed to occur.

7.15 Compartmental Model Analysis of Phloem Transport

The dynamics of ^{11}C labelled photoassimilates observed within squash internodes could be explained by the compartmental model of the perfused squash internode, in which there was radial exchange of water and solutes between the sieve tubes and the surrounding tissue that was described by transfer coefficients. The proposed compartmental model suggests that phloem transport in squash stem occurs with very small changes in the turgor pressure gradient (Figs. 6.8, 6.13) that drives sieve tubes sap flow and consequently in its speed (Figs. 6.10, 6.15). This same result is suggested by the measurements of translocation speed, which also varies very little, although the translocation speed was only indirectly determined on the three daily pulse applications (Fig. 5.8). The same behaviour was seen on wheat (Fig. 5.7), where the translocation speed changes very little throughout the day. The model showed that net loss was almost constant, as with translocation speed and turgor pressure gradient. As observed experimentally, tracer loss into the internode pith cavity perfusion solution ($\approx 4\times10^{-4}$ $\%.cm^{-1}$) was very small compared with tracer loss from the pathway (3 to 5 $\%.cm^{-1}$) (Table 5.2, Fig. 5.11). Consistent with this ratio, and very well illustrated in all model simulations, the endogenous solute concentration in the pith cavity, C_3, was about 10^{-4} of the sieve tube concentration, C_1 (e.g. Fig. 6.9).

Due to sucrose uptake from the perfusion solution into the perfused squash internode tissue as indicated by its non-zero transfer coefficients, there is phloem loading of sucrose (Fig. 6.24). However, due to the relative insensitivity of the model to changes

in the other tracer transfer coefficients, we must assume they are constant. But, as net loss of tracer is a combination of both unloading and reloading processes, which experimental evidence suggests as occurring through different mechanisms, any change in the passive unloading of tracer, simulated as being a consequence of sucrose uptake from the apoplast, will certainly change the net loss of tracer.

As Figs. 6.33 shows, the effects of mannitol perfusion on phloem transport of tracer are beyond the model capabilities of simulation. The model does not distinguish between chemically different solutes. The transfer of tracer and solutes between compartments is empirically described by coefficients not explicitly related to the chemical or structural nature of the solutes in question. Therefore, it is not that surprising that both simulations for sucrose and mannitol revealed good fitting with experimental data using similar transfer coefficients. The transfer coefficients values estimated for the two solute treatments are not significantly different, and they fall within the range of the values found for the transfer coefficients of endogenous solutes. We can conclude that both solutes entered the tissue and the sieve tube elements. That was of course already suggested by the similarity of experimental results. However, mannitol had a very different effect from sucrose at concentrations of 500 mM, stopping phloem transport, which of course is not predicted with this model (Fig. 6.33). Clearly there were changes in the pathway resistance to flow, not considered in this model. Viscosity is one factor that does cause resistance to change, and in this compartmental model viscosity is a function of sugar concentration only (6.38). But, as is very well known, *cucurbitaceae* phloem sap has a high protein content, which must influence viscosity not only due to concentration changes, but also due to structural changes related to protein molecular configuration. This affects phloem flow, which behaves physically closer to a colloidal suspension flow. No dependence of phloem sap viscosity on protein concentration or molecular structure was considered in this compartmental model. In addition, no sub cellular structures which also affect sieve tube resistance are considered in this model. Specifically, the sieve tube axial conductivity, k, in the compartmental model is taken as function of cell geometry and structural factors only. However, sieve tube axial conductivity might change if any blockage occurs due for example to callose accumulation in sieve plate pores, which is typically considered as a defence mechanism against mechanical damage. As the nature of the phloem stoppage observed during perfusion by 500 mM mannitol is not known, we cannot distinguish between the possible contributions that change the sieve tube axial conductivity, k, which was taken as constant

for every simulation but being different for different plants, and in the phloem sap viscosity.

Another model limitation is the fixing of both input and output turgor pressures, of which their difference defines phloem sap flow. Any natural changes on sieve tube turgor pressure, both upstream and downstream of the perfused internode, that result from changes in water exchange within compartment 1 are not represented in the model. The same applies within the perfused internode. Consequently the model does not simulate changes in speed or in tracer influx and efflux as the experimental results suggest. On the other hand and in the absence of any treatment a constant turgor pressure gradient across compartment 1 gave good model simulations, suggesting that any turgor pressure changes outside compartment 1 were not important, and the turgor pressure gradient was not affected.

Finally, considering xylem flow would increase the number of variables and model parameters to fit. However, it would make the model more accurate and closer to reality. Although structurally both xylem and phloem systems in squash are physically very close (Figs. 5.2 and 5.3), which suggest their interaction is likely, in fact very little is known at that level. Basically the inclusion of xylem stream, using Darcy's equation (2.15), would require adding more compartments in which radial loading and unloading of water and solutes would be described again by empirical transfer coefficients, but also the conductivity of xylem vessels, similar to what was done with the phloem. Alternatively, although there are no measurements done on transpiration, making it difficult to analyse any model simulations of that process, its inclusion would possibly help to better understand and even simulate water exchanges between the plant and perfusion solution (§ 5.9). Thus, unrealistic simulations giving negative pressures in compartment 2 would be avoided. This absence of xylem flow also complicates the interpretation of the model predictions regarding compartment 2, as it assumes very good mixing and solute uniform distribution within a compartment that in reality represents very different types of cells.

7.16 Future Work

On the theoretical level, a time-dependent model based on Navier–Stokes and convection-diffusion equations to simulate the transient phenomenon observed during perfusion treatments would give a very important contribution to a better understanding of phloem transport, namely changes in water and solute exchange and phloem stoppage, and their implications on pressure and speed profiles. This could be supplemented by testing other solute exchange mechanisms (e.g. active solute loading) and the dependence of phloem sap viscosity on phloem protein polymerization could be studied as the cause of phloem stoppage. In addition, and dealing with a time dependent model tracer conservation equations could also be incorporated.

On the experimental level further clarification is needed regarding the nature of phloem stoppage in squash sieve tubes due to osmotic shock, as observed during perfusion by 500 mM mannitol. Testing the effects of PCMBS could thus help to better support mannitol uptake and elucidate about an apoplastic step involvement. On the other hand, testing Ca^{2+} channels inhibitors (e.g. Gd^{3+}) or calcium chelators (e.g. EGTA) would clarify not only the existence of Ca^{2+}-dependent phloem protein polymerization behind phloem stoppage observed during mannitol perfusion but also its nature.

8. Conclusions

A steady state model of phloem transport, developed using Navier-Stokes equation and convection-diffusion equation with allowance for water and solute exchange along the pathway, showed that radial water exchange affects the pressure gradient. Passive solute exchange, dependent on the sieve tube membrane permeability to solutes, P_s, also affects the pressure gradient by modifying water exchange. This result is significantly different from Hagen-Poiseuille flow which has been used so far in most mechanistic descriptions of phloem transport, not considering solute radial exchange. The predicted values for the solute sieve tube membrane permeability, P_s, are well bellow the range expected for plant cells and reflect the efficient specialization of sieve tubes for long-distance transport on minimizing solute passive loss.

The simultaneous use of ^{11}C labelling and solution perfusion of plant stem internodes proved to be a successful and useful method to study the dynamics and rapid changes in phloem transport in squash and wheat that occurred upon manipulation of the local plant apoplastic environment surrounding the vascular systems. It has been established that the ^{11}C method is non-invasive and physiologically harmless due to the short half-life of the tracer. Complementing this technique with perfusion of the stem internodes makes it suitable for repeated measurements of the same plant specimen.

It was shown that there is an apoplastic step involved in phloem reloading in squash stem internodes. Sucrose is one of the main sugar species involved, which not only confirms the more general idea that it may be an almost universal condition in plants but also is a new finding regarding *cucurbitaceae* species. No work as been published so far showing sucrose retrieval processes in the stem internodes of *cucurbitaceae* species.

It was shown that solute and water exchange between the phloem and the apoplast can induce pathway resistance changes, due to changes in phloem sap viscosity. This explains transient phloem stoppage observed during perfusion at high mannitol concentrations. From this study it is not possible to conclude if those changes in viscosity are due solely to water removal from sieve tubes or due to changes in protein

configuration triggered by changes in sieve tube turgor pressure caused by water removal. It is not possible to conclude if mannitol is taken up by the phloem as happens with sucrose. Future work is needed concerning mannitol uptake, involvement of proteins in changes on the phloem pathway resistance. These facts could throw light on phloem stoppage caused by osmotic treatments and chilling. Neither aspect has yet been properly studied in *cucubitaceae* species. The use of ^{11}C labelling and perfusion of stem internodes offers a good way of doing so.

We found that wheat is not a good species for combined studies of ^{11}C labelling and stem perfusion for studying phloem transport in the peduncle. Its particular seasonal physiological state revealed that by the time the peduncle is suitable for perfusion, the ear is the dominant sink organ in the plant. Therefore very little unloading occurs in the stem, leaving very few chances for a successful manipulation of that same process in the perfused peduncle. Possibly younger plants could be used when only vegetative growth occurs. However, at that stage stem internodes are small, soft and are mostly enclosed by the leaves, complicating a successful perfusion.

The dynamics of ^{11}C labelled photoassimilates within the perfused squash internode can be explained by compartmental model analysis. The proposed compartmental model suggests that phloem transport in squash stem occurs in a *quasi* steady state situation with passive unloading of photoassimilates. There are very small changes in the tracer loss, in the turgor pressure gradient that drives sieve tubes sap flow, and consequently its speed. Solute and water exchanges are also very well simulated by the proposed compartmental model. Xylem flow as sub-cellular structures and protein content could be considered on future developments of the compartmental model. Both the experimental work and the theoretical models presented in this monograph illustrate the importance of considering solute and water exchanges in pathway regions between sources and sinks. It offers a way of using mathematical modelling of phloem transport as a very useful tool for studying phloem physiology.

Bibliography:

Aikman, D. P. (1980) – Contractile proteins and hypotheses concerning their role in phloem transport, *Can. J. Bot.* **58**: 761-772

Aikman, D. P., Anderson, W. P. (1971) – A Quantitative Investigation of Peristaltic Model for Phloem Translocation, *Ann. Bot*. **35**: 826-832

Aloni, B., Wyse, R. E., Griffith, S. (1986) – Sucrose Transport and Phloem Unloading in Stem of *Vicia faba*: Possible Involvement of a Sucrose Carrier and Osmotic Regulation, *Plant Physiol*. **81**: 482-486

Alosi M.C., Melroy D.L., Park R.B. (1988) – The Regulation of Gelation of Phloem Exudates from Cucurbita Fruit by Dilution, Glutathione, and Glutathione Reductase, *Plant Physiol*. **86**: 1089–1094

Amin, M. (1983) – A Mechanism of Translocation based on High Proton Mobility and K^+ Counterflux at Negatively Charged Surfaces in Sieve Elements, *J. Biol. Physics* **11**: 111-116

Anderson, W. P. (1976) – Physico-chemical Assessment of Plasmodesmatal Transport, In *Intercellular Communication in Plants: Studies on Plasmodesmata*, ed. Gunning, B. E. S. & Robards, A. W., Springer-Verlag, Berlin, pp. 107-20

Andrew, J., Smith, C., Milburn, J. A. (1980) – Osmoregulation and the Control of Phloem Sap Composition in *Ricinus communis* L., *Planta* **148**: 28-34

Applegate, H. G. (1960) – Freezing-Point Depression of Hoagland's "Carbowax" Systems, *Nature* **186**: 232-233

Arthur, J. C. (1880) – The Stem of Pumpkin for Illustrating Plant Hystology, *Botanical Gazette* **5**: 133-135

Ayre, B. G., Keller, F. Turgeon, R. (2003) – Symplastic Continuity between Companion Cells and the Translocation Stream: Long-Distance Transport is Controlled by Retention and Retrieval Mechanisms in the Phloem, *Plant Physiolgy* **131**: 1518-1528

Bancal, P., Soltani, F. (2002) – Source-sink Partitioning. Do We Need Münch?, *J. Exp. Botany*, **53**: 1919-1928

Barker, S.A. (1955) – Acyclic Sugar Alcohols, in Modern Methods of Plant Analysis (Vol. 2) (Paech, K. and Tracey, M.V., eds), pp. 55-63, Springer

Baye, A., Lanzavecchia, A. (2000) – The Role of Aquaporins in Dendritic Cell Macropinocytosis, *J. Exp. Med.* **191**: 743–747

Beebe, D.U., Turgeon, R. (1992) – Localization of Galactinol, Raffinose,and Stachyose Synthesis in *Cucurbita pepo* Leaves, *Planta* **188**: 354-361.

Beitler, G. A., Hendrix, J. E. (1974) – Stachyose: an Early Product of Photosynthesis in Squash Leaves, *Plant Physiol*. **53**: 674-676

Benedek, G. B., Villars, F. M. H. (2000) – Physics With Illustrative Examples From Medicine and Biology, 2nd ed, Springer–Verlag, New York, USA

Biddulph, O., Cory, R. (1957) – An Analysis of Translocation in the Phloem of the Bean Plant using THO, P^{32}, and C^{14}, *Plant Physiol*. **32**: 608-619

Bieleski, R. L. (1982) – Sugar alcohols, In *Encyclopedia of Plant Physiology, New Series*, Vol 13A, Loewus, F. A., Tanner, W., eds, Springer-Verlag, New York, USA, pp 158-192

Boersma, L., Lindstrom, F. T., Childs, S. W. (1991) – Model for Steady State Coupled Transport in Xylem and Phloem, *Agron. J*. **83**: 401-408

Bouchard, C., Grandjean, B. P. A. (1995) – A Neural Network Correlation for the Variation of Viscosity of Sucrose Aqueous Solutions with Temperature and Concentration, *Food Science & Technology – Lebensmittel-Wissenschat & Technologie 28*:157-159

Bowen, J. E. (1972) – Effect of Environmental Factors on Water Utilization and Boron Accumulation and Translocation in Sugar Cane, *Plant Cell Physiology* **13**: 703-14

Buttery, B. R., Boatman, S. G. (1964) – Turgor Pressures in Phloem: Measurements on Hevea Latex, *Science* **145**: 285-286

Braun, W., Leman, A., Taubert, H. (1999) – Pflanzenanatomisches Praktikum I, Spectrum Akademischer Verlag, Germany

Cadzow, J. A. (1973) – Discrete-Time Systems. An Introduction with Interdisciplinary Applications, Prentice-Hall Inc, New Jersey USA

Canny, M. J. (1973) – Phloem Translocation, Cambridge University Press, UK

Canny, M. J. (1977) – Flow and Transport in Plants, *Ann. Rev. Fluid Mechanics* **9**: 275-296

Canny, M. J., Phillips, O. M. (1963) – Quantitative Aspects of a Theory of Translocation, *Ann. Bot*. **27**: 379-402

Carpita, N, Salubarse, D., Montezinos, D., Delmer, D. P. (1979) – Determination of the Pore Size of Cell Walls of Living Plant Cells, *Science* **205**: 1144-1147

Castro, M. A. (1986) – Vessel-Parenchyma Pit Membranes in *Cucurbita Maxima* Duch., *IAWA Bulletin* **7**:251-254

Cataldo, D. A., Christy, A. L., Coulson, C. L., Ferrier, J. M. (1972) – Solution Flow in the Phloem I: Theoretical Considerations, *Plant Physiol*. **49**: 685-689

Cataldo, D. A., Christy, A. L., Coulson, C. L. (1972) – Solution Flow in the Phloem II: Phloem Transport of THO in *Beta Vulgaris*, *Plant Physiol*. **49**: 690-695

Cavalieri, A. J., Boyer, J. S. (1982) – Water Potentials Induced by Growth in Soybean Hypocotyls, *Plant Physiol*. **69**: 492-496

Chirife J., Buera, M.P. (1997) – A Simple Model for Predicting the Viscosity of Sugar and Oligosaccharide Solutions, *J. Food Eng.* **33**: 221-226

Choné, X., van Leeuwen, C., Dubourdieu, D., Gaudillère, J. P. (2001) – Stem Water Potential is a Sensitive Indicator of Grapevine Water Status, *Ann. Bot*. **87**: 477-483

Christy, A. L., Ferrier, J. M. (1973) – A Mathematical Treatment of Münch's Pressure-Flow Hypothesis of Phloem Translocation, *Plant Physiol*. **52**: 531-538

Christy, A. L., Ferrier, J. M. (1975) – Time-dependent Behaviour of a Mathematical Model for Münch Translocation: Application to Recovery from Cold Inhibition, *Plant Physiol*. **55**: 511-514

Clauss, H., Mortimer, D. C., Gorham, P. R. (1964) – Time-course Study of Translocation of Products of Photosynthesis in Soybean Plants, *Plant Physiol*. **39**: 269-273

Conde, C., Silva, P., Agasse, A., Lemoine, R., Delrot, S., Tavares, R., Geros, H. (2007) – Utilization and Transport of Mannitol in *Olea europaea* and Implications for Salt Stress Tolerance, *Plant Cell Physiol*. **48**: 42-53

Connor, D. J., Legge, N. J., Turner, N. C. (1977) – Water Relations of Mountain Ash (*Eucalyptus regnans* F. Muell.) Forests, *Aust. J. Plant Physiol.* **4**: 753-762

Cosgrove, D. J., Cleland, R. E. (1983) – Solutes in the Free Space of Growing Stem Tissues, *Plant Physiol*. **72**: 326-331

Crafts, A. (1931) – Movement of Organic Materials in Plants, *Plant Physiol*. **6**: 1-41

Crafts, A. (1932) – Phloem Anatomy, Exudation, and Transport of Organic Nutrients in Cucurbits, *Plant Physiol*. **7**: 183-225

Cronshaw, J. (1981) – Phloem Structure and Function, *Ann. Rev. Plant Physiol*. **32**: 465-484

Cronshaw, J., Esau, K. (1968a) – P-Protein in the Phloem of *Cucurbita* I. The Development of P-Protein Bodies, *The Journal of Cell Biology* **38**: 25-39

Cronshaw, J., Esau, K. (1968b) – P-Protein in the Phloem of *Cucurbita* II. The P-Protein of Mature Sieve Elements, *The Journal of Cell Biology* **38**: 292-303

Currier, H. B. (1957) – Callose Substance in Plant Cells, *American Journal of Botany* **44**: 478-488

Cutler, D. F., Botha, T., Stevenson, D. W. (2008) – Plant Anatomy an Applied Approach, Blackwell Publishing, UK

Dagan, Z., Weinbaum, S., Pfeffer, R. (1982) – An Inifnite-series Solution for the Creeping Motion through an Orifice of Finite Length, *J. Fluid Mech*. **115**: 505-523

Dainty, J. (1976) – Water Relations of Plant Cells, in *Encyclopedia of Plant Physiology*, vol. 2 Part A, ed. U. Lüttge & M. Pitman, Springer-Verlag, New York, USA, pp 12-35

Dainty, J. (1996) – Water Relations in Units, Symbols and Terminology for Plant Physiology, ed. F. B. Salisbury, Oxford University Press, USA, pp 60-63

Daudet, F. A., Lacointe, A., Gaudillère, J. P., Cruiziat, P. (2002) – Generalized Münch Coupling between Sugar and Water Fluxes for Modelling Carbon Allocation as Affected by Water Stress, *J. Theor. Biol*., **214**: 481-498

Diamond, J.M., Wright, E. M. (1969) – Biological Membranes: The Physical Basis of Ion and Nonelectrolyte Selectivity, *Ann. Rev. Physiol*., **31**: 581-646

Dixon, H. H., Gibbon, M. W. (1932) – Bast-sap in Plants, *Nature* **130**:661

Dordas, C., Brown, P. H. (2001) – Evidence for Channel Mediated Transport of Boric Acid in Squash (*Cucurbita pepo*), *Plant and Soil* **235**: 95-103

Esau, K. A. (1969) –The Phloem, Encyclopedia of Plant Anatomy, Band V, Teil 2, eds. Zimmerman, W., Ozenda, P. & Wulff, H. D., Gebrüder Borntraeger, Berlin, Germany

Eschrich, W. (1970) – Biochemistry and Fine Structure of Phloem in Relation to Transport, *Ann. Rev. Plant Physiol.* **21**: 193-214

Eschrich, W., Eschrich, B. (1990) - Phloem Transport, *Progress in Botany* **51**: 80-92

Eschrich, W., Evert, R. F., Young, J. H. (1972) – Solution Flow in Tubular Semipermeable Membranes, *Planta* **107**: 279-300

Evans, T.S., Ebert, M., Moorby, J. (1963) – A Model for the Translocation of Photosynthate in Soybean, *J. Exp. Botany* **14**: 221-231

Evert, R. F. (1977) – Phloem Structure and Histochemistry, *Ann. Rev. Plant Physiol*. **28**: 199-222

Evert, R. F. , Eichhorn, S. E. (2006) – Esau's Plant Anatomy: Meristems, Cells, and Tissues of the Plant Body: Their Structure, Function and Development, 3rd Ed., Wiley-Liss, pp 357-425

Eszterle, M. (1993) - Molecular Structure and Specific Volume of Pure Sucrose Solutions, *Zuckerind*. **118**: 459-464

Farrar, J. F., Minchin, P. E. H. (1991) – Carbon Partitioning in Split Root Systems of Barley – Relation to Metabolism, *J. Exp. Botany* **42**: 1261-1269

Fensom, D. S., Spanner, D. C. (1969) – Electro-Osmotic and Biopotential Measurements on Phloem Strands of *Nymphoides*, *Planta* **88**: 321-331

Ferrier, J.M. (1975) – Time-Dependent Behaviour of Münch Translocation in Sugar Beet and Trees: Theory vs Experiment in Phloem Transport, ed. Aronoff, S., Dainty, J., Gorham, P. R., Srivastava, L. M., Swanson, C. A., NATO Advanced Study Institutes Series, vol. 4, Plenum Press, USA, pp 531-534

Ferrier, J. M. (1976) – An Approximate Analytical Equation for Sugar Concentration Waves in Münch Phloem Translocation Systems, *Can, J. Bot*. **54**: 2130-2132

Ferrier, J. M. (1978) – Further Theoretical Analysis of Concentration-pressure-flux Waves in Phloem Transport Systems, *Can, J. Bot*. **56**: 1086-1090

Ferrier, J. M., Christy, A.L. (1975) – Time-Dependent Behaviour of a Mathematical for Münch Translocation: Application to Recovery from Cold Inhibition, *Plant Physiol*., **55**: 511-514

Ferrier, J. M., Christy, A.L. (1977) – Role of Concentration-dependent Unloading Mathematical Models of Münch Transport, *Plant Physiol*. **60**: 173-174

Ferrier, J.M., Tyree, M.T., Christy, A.L. (1974) – The Theoretical Time-dependent Behaviour of a Münch Pressure-flow System: The Effect of Sinusoidal Time Variation in Sucrose Loading and Water Potential, *Can. J. Bot.* **53**: 1120-1127

Ferrieri, R. A., Gray, D. W., Babst, B. A., Schueller, M. J., Schlyer, D. J., Thorpe, M. R., Orians, C. M., Lerdau, M. (2005) - Use of Carbon-11 in *Populus* shows that Exogenous Jasmonic Acid Increases Biosynthesis of Isoprene from Recently Fixed Carbon, *Plant Cell and Environment* **25**: 591-602

Fiehn, O. (2003) – Metabolic Networks of Cucurbita maxima phloem, *Phytochemistry* **62**: 875-886

Fisher, D. B. (1970) – Kinetics of C-14 Translocation in Soybean, *Plant Physiol*. **45**: 107-113

Fisher, D. B. (2002) – Long-Distance Transport, in *Biochemistry & Molecular Biology of Plants*, ed. Buchanan, B., Gruissem, W., Jones, R., American Society of Plant Physiologists, USA, pp 730-784

Fisher, D. B., Cash-Clark, C. E. (2000) – Gradients in Water Potential and Turgor Pressure along the Translocation Pathway during Grain Filling in Normally Watered and Water-Stressed Wheat Plants, *Plant Physiol*. **123**: 139-147

Flora, L. L., Madore, M. (1993) – Stachyose and Mannitol Transport in *Olea europea*, *Planta* **189**:484-490

Furch, A. C. U., Zimmermann, M. R., Will, T., Hafke, J. B., van Bel, A. J. E. (2010) – Remote-controlled Stop of Phloem Mass Flow by Byphasic Occlusion in *Cucurbita maxima*, *J. Exp. Botany* **61**: 3697-3708

Gao, Z., Maurousset, L., Lemoine, R., Yoo, S. D., van Nocker, S., Loescher, W. (2003) – Cloning, Expression, and Characterization of Sorbitol Transporters from Developing Sour Cherry Fruit and Leaf Sink Tissues, *Plant Physiol*. **131**: 1566-1575

Garrod, J. E., Herrington, T. M. (1970) – Apparent Molar Volumes and Temperatures of Maximum Density of Dilute Aqueous Sucrose Solutions, *J. Phys. Chem*. **74**: 363-370

Gebbling, T. (2003) – The Enclosed and Exposed Part of the Peduncle of Wheat (*Triticum aestivum*) – Spatial Separation of Fructan Storage, *New Phytologist* **159**: 245-252

Geiger, D. R. (1996) – Phloem Transport in Units, Symbols and Terminology for Plant Physiology, ed. F. B. Salisbury, Oxford University Press, USA, pp 72-74

Geiger, D. R. (1970) – Temporary Inhibition of Translocation Velocity and Mass and Mass Transfer Rate by Petiole Cooling, *Plant Physiol*. **46**: 847-849

Geiger, D. R. (1987) – Understanding Interactions of Source and Sink Regions of Plants, *Plant Physiol*. *Biochemistry* **25**: 659-666

Geiger, D. R., Cataldo, D. A. (1969) – Leaf Structure and Translocation in Sugar Beet, *Plant Physiol*. **44**: 45-54

Geiger, D. R., Saunders, M. A., Cataldo, D. A. (1969) – Translocation and Accumulation of Translocate in the Sugar Beet Petiole, *Plant Physiol*. **44**: 1657-1665

Geiger, D. R., Sovonick, S. A. (1970) – Temporary Inhibition of Translocation Velocity and Mass Transfer Rate by Petiole Cooling, *Plant Physiol*. **46**: 847-849

Geiger, D. R., Sovonick, S. A. (1975) – Effects of Temperature, Anoxia and Other Metabolic Inhibitors on Translocation, in *Encyclopedia of plant physiology (New Series)*, Vol. 1, ed. M. H. Zimmermann & V. A. Milburn, Springer-Verlag, Berlin. Germany, pp. 256-86

Giaquinta, R. T. (1976) – Evidence for Phloem Loading from the Apoplast. Chemical Modification of Membrane Sulfhydryl Groups, *Plant Physiol*. **57**: 872-875

Giaquinta, R. T. (1983) – Phloem Loading of Sucrose, *Ann. Rev. Plant Physiol*. **34**: 347-87

Giaquinta, R. T., Geiger, D. R. (1973) – Mechanism of Inhibition of Translocation by Localized Chilling, *Plant Physiol*. **51**: 372-377

Goeschl, J. D., Magnuson, C. E., DeMichele D. W., Sharpe, P. (1976) – Concentration-dependent Unloading as a Necessary Assumption for a Closed Form Mathematical Model of Osmotically Driven Pressure Flow in Phloem, *Plant Physiol*. **58**: 556-562

Goeschl, J. D., Magnuson, C. E. (1986) – Physiological Implications of the Münch-Horwitz Theory of Phloem Transport: Effects of the Loading Rates, *Plant Cell and Environment* **9**: 95-102

Gould, N., Minchin, P. E. H., Thorpe, M. R. (2004) – Direct Measurements of Sieve Element Hydrostatic Pressure Reveal Strong Regulation after Pathway Blockage, *Functional Plant Biology* **31**: 987-993

Grusak, M. A., Lucas, W. J. (1985) – Cold-inhibited Phloem Translocation in Sugar Beet 2. Characterization and Localization of the Slow-cooling Response, *J. Exp. Botany* **36**: 745-755

Grusak, M. A., Beebe, D. U., Turgeon, R. (1996) – Phloem Loading, in *Photoassimilate Distribution in Plants and Crops, Source-Sink Relationships*, ed. E. Zamski & A. Schaffer), Marcel Dekker Inc., New York, USA, pp 209-227

Gunning, B. E. S., Pate, J. S. (1974) – Transfer cells, in *Dynamic Aspects of Plant Ultrastructwe*, ed. Robards, A. W., McGraw-Hill, London, pp. 441-480

Hafke, J. B., Furch, A. C. U., Reitz, M. U., van Bel, A. J. E. (2007) – Functional Sieve Elements Protoplasts, *Plant Phsyiol*. **145**: 703-711

Hafke, J. B., van Amerongen, J., Kelling, F., Furch, A. C. U., Gaupels, F., van Bel, A. J. E. (2005) – Thermodynamic Battle for Photosynthate Acquisition between Sieve Tubes and Adjoining Parenchyma in Transport Phloem, *Plant Phsyiol*. **138**: 1527-1537

Hall, S. M., Baker, D. A., Milburn, J. A. (1971) – Phloem Transport of ^{14}C-labelled Assimilates in *Ricinus*, *Planta* **100**: 200-207

Hammel, H. T. (1968) – Measurements of Turgor Pressure and its Gradient in the Phloem of Oak, *Plant Phsyiol*. **43**: 1042-1048

Happel, J., Brenner, Brenner, H. (1965) – Low Reynolds Number Hydrodynamics, Prentice-Hall, USA

Haritatos, E., Keller, F., Turgeon, R. (1996) – Raffinose Oligosacharide Concentrations Measured in Individual Cell and Tissue Types in *Cucumis melo* L. Leaves: Implications for Phloem Loading, *Planta* **198**: 614-622

Haritatos, E., Medville, R., Turgeon, R. (2000) – Minor vein structure and sugar transport in Arabidopsis thaliana, *Planta* **211**: 105-111

Hayashi, H., Chino, M. (1986) – Collection of Pure Phloem Sap from Wheat and its Chemical Composition, *Plant Cell Physiol.* **27**: 1387-1393

Hayden, D. B., Fensom, D. S., Thompson, R. G. (1980) – The Extraction of Photosynthate High in [^{11}C]Sucrose and its Translocation in Sunflower Stems, *Can. J. Bot*. **58**: 100-107

Hayes, P. M., Offler, C. E., Patrick, J. W. (1985) – Cellular Structures, Plasma Membrane Surface Areas and Plasmodesmatal Frequencies of the Stem of *Phaseolus vulgaris* L. in Relation to Radial Photosynthate Transfer, *Ann. Bot*. **56**: 125-138

Hendrix, J. E. (1968) – Labelling Pattern of Translocated Stachyose in Squash, *Plant Physiol*. **43**: 1631-1636

Hendrix, J. E. (1973) – Translocation of Sucrose by Squash Plants, *Plant Physiol*. **52**: 688-689

Hendrix, J. E. (1977) – Phloem Loading in Squash, *Plant Physiol*. **60**: 567-569

Hendrix, J. E. (1982) – Sugar Translocation in Two Members of the *Cucurbitaceae*, *Plant Science Letters*. **25**: 1-7

Henton, S. M., Greaves, A. J., Piller, G. J., Minchin, P. E. H. (2002) – Revisiting the Münch Pressure-flow Hypothesis for Long-distance Transport or Carbohydrates: Modelling the Dynamics of Solute Transport inside a Semipermeable Tube, *J. Exp. Botany* **14**: 210-220

Heyser, W., Heyser, R., Eschrich, W., Leonard, O. A., Rautenberg, M. (1976) – The Influence of Externally Applied Organic Substances on Phloem Translocation in Detached Maize Leaves, *Planta* **132**: 269-277

Hoagland, D. R., Arnon, D. I. (1950) – The Water-culture Method for Growing Plants Without Soil, *California Agricultural Experiment Station Circular* **347**:1-32

Hocking, P. J. (1980) – The Composition of Phloem Exudate and Xylem Sap from Tree Tobacco (*Nicotiana glauca* Grah.), Ann. Bot. **45**: 633-643

Holroyd, R. (1924) – Morphology and Physiology of the Axis in *Cucurbitaceae*, *Botanical Gazette* **78**:1-48

Horwitz, L. (1958) – Some Simplified Mathematical Treatments of Translocation in Plants, *Plant Physiol*. **33**: 81-93

Hölttä, T., Mencuccini, M., Nikinmaa, E. (2009) – Linking Phloem Function to Structure: Analysis with a Coupled Xylem–phloem Transport Model, *J. Theor. Biol*. **259**: 325-337

Holthaus, U., Schmitz, K. (1991) – Distribution and Immunolocalization of Stachyose Synthase in *Cucumis melo* L., *Planta* **185**: 479-486

Hölttä, T., Vesala, T., Sevanto, S., Perämäki, M., Nikinmaa, E. (2006) – Modelling Xylem and Phloem Water Flows in Trees according to Cohesion Theory and Münch Hypothesis, *Trees* **20**: 67-78

Hsiang, B., Bush, D. (1992) – Stachyose, Amino Acid and Sucrose Transport in Plasma Membrane Vesicles Isolated from Zucchini, *Plant Physiol*. **99S**: 242

Huber, B. (1941) – Gesichertes und Problematisches in der Wanderung der Assimilate, *Ber. dtsch. Bot. Ges*. **59**: 181-194

Huber, B., Schmidt, E., Jahnel, H. (1937) – Untersuchungen fiber den Assimilatstrom, *Tharandt. Forstl. Jahrb.* **88**: 1017-1050

Jahnke, S., Schlesinger, U., Feiger, G. B., Knust, E. J. (1998) – Transport of Photoassimilates in Young Trees of *Fraxinus* and *Sorbus*: Measurement of Translocation *in vivo*, *Bot. Acta* **111**: 307-315

Jennings, D. B., Ehrenshaft, M., Pharr, D. M.,Williamson, J. D. (1998) – Roles for Mannitol and Mannitol Dehydrogenase in Active Oxygen-mediated Plant Defense. *Proc. Natl Acad. Sci. USA* **95**:15129–15133

Kallarackal, J., Milburn, J. A. (1985) – Respiration and Phloem Translocation in Roots of Chickpea (*Cicer arietinum*), *Ann. Bot*. **56**: 211-218

Kanahama, K., Saito, T (1986) – Vascular System in Cucumber Main Stem, *J. Japan. Soc. Hort. Sci*. **55**:181-186

Kaneko, T., Takahashi, N., Kikuyama, M. (2009) – Membrane Stretching Triggers Mechanosensitive Ca^{2+} Channel Activation in Chara, *J. Membrane Biol.* **228**:33-42

Kargol, A. (1996) – An Integrated Approach to Water Transport in a Plant over Long Distances, *J. Biol. Physics* **22**: 157-173

Kargol, A. (2001) – A Mechanistic Model of Transport Processes in Porous Membranes Generated by Osmotic and Hydrostatic Pressure, *J. Memb. Science* **191**: 61-69

Kargol, A., Kargol, M., Przestalski, S. (1997) – Correlation Relation for the Membrane Transport Parameters L_p, σ, and ω, *J. Biol. Physics* **23**: 233-238

Kargol, M. (1994) – Osmotic, Hydromechanical and Energetic Properties of Modified Münch's Model, *Gen. Physiol. Biophys.* **13**: 3-19

Kargol, M., Kargol, A. (2000) – Membrane Transport Generated by the Osmotic and Hydrostatic Pressure. Correlation Relation for Parameters L_p, σ, and ω, *J. Biol. Physics* **26**: 307-320

Kargol, M., Suchanek, G., Kargol, A. (2001) – Modification and Quantitative Analysis of the Münch Model in the Integrated System of Water Translocation in Plants, *Gen. Physiol. Biophys.* **20**: 191-202

Kargol, M., Suchanek, G., Przestalski, M., Kragol, A. (2003) – Modification of Integrated System of Long-distance Transport of Water in Plants. Where the Plant has its Heart?, *Current Topics in Biophysics* **27**: 3-9

Karmanov, V. G., Meleshchenko, S. N. (1982) – Mechanism of Auto-oscillations of Water Metabolism in Plants, *Biofizika 27*: 144-149

Katchalsky, A., Curran, P. F. (1965) – Nonequilibrium Thermodynamics in Biophysics, Harvard University Press, Cambridge, USA

Kaufman, M. R., Kramer, P. J. (1967) – Phloem Water Relations and Translocation, *Plant Physiol*. **42**: 191-194

Kedem, O., Katchalsky, A. (1958) – Thermodynamic Analysis of the Permeability of Biological Membranes to Non-electrolytes, *Biochimica et Biophysica Acta* **27**: 229-246

Kempers, R., Prior, D. A. M., van Bel, A. J. E., Oparka, K. J. (1993) – Plasmodesmata between Sieve Element and Companion Cell of Extrafascicular Stem Phloem of *Cucurbita maxima* Permit Passage of 3 kDa Fluorescent Probes, *The Plant Journal* **4**: 567-575

Kempers, R., Ammerlaan, A., van Bel, A. J. E. (1998) – Symplasmic Constriction und Ultrastructural Features of the Sieve Element/Companion Cell Complex in the Transport Phloem of Apoplasmically and Symplasmically Phloem-Loading Species, *Plant. Physiol.* **116**: 271-278

Kiyosawa, K. (1991) – Volumetric Properties of Polyols (Ethylene Glycol, Glycerol, Meso-erythritol, Xylitol and Mannitol) in Relation to Their Membrane Permeability: Group Additivity and Estimation of the Maximum Radius of Their Molecules, *Bioch. et Biophs. Acta – Biomembranes* **1064**: 251-255

Kizilova, N. (2008) – Long-distance Liquid Transport in Plants, *Proceedings of the Estonian Academy of Sciences* **57**: 179-203

Kizilova, N. N., Posdniak, L. O. (2005) – Biophysical Mechanisms of Long-distance Transport fo Liquids and Signaling in High Plants, *Biophys. Bull*. **15**: 99-103

Klepek, Y.S., Geiger, D., Stadler, R., Klebl, F., Landouar-Arsivaud, L., Lemoine, R., Hedrich, R., Sauer, N. (2005) – *Arabidopsis* POLYOL TRANSPORTER5, a New Member of the Monosaccharide Transporter-like Superfamily, mediates H^+-Symport of Numerous Substrates, including myo-Inositol, Glycerol, and Ribose, *Plant Cell* **17**: 204–218

Köckenberger, W., Pope, J. M., Xia, Y., Jeffrey, K. R., Komor, E., Callaghan, P.T. (1997) – A Non-invasive Measurement of Phloem and Xyelm Water Flow in Castor Bean Seedlings by Nuclear Magnetic Resonance Microimaging, *Planta* **201**: 53-63

Komor, E., Orlich, G., Weig, A., Kockenberger, W. (1996) - Phloem loading – not Metaphysical, only Complex: Towards a Unified Model of Phloem Loading, *J. Exp. Bot.* **47**: 1155-1164

Kundu, P. K., Cohen, I. M. (2008) – Fluid Mechnaics, 4th Ed., Academic Press, USA

Kursanov, A. L. (1984) – Assimilate Transport in Plants, 2nd Ed., Elsevier Science, USA

Lacointe, A., Minchin, P. E. H. (2008) – Modelling Phloem and Xylem Transport within a complex Architecture, *Functional Plant Biology* **35**: 772-780

Lackney, V. K., Sjolund, R. D. (1991) – Solute Concentrations of the Phloem and Parenchyma Cells present in Squash Callus, *Plant Cell and Environment* **14**: 213-219

Lagerwerff, J. V., Ogata, G., Eagle, H. E. (1961) – Control of Osmotic Pressure of Culture Solutions with Polyethylene Glycol, *Science* **133**: 1486-1487

Lalonde, S., Tegeder, M., Throne-Holst, M., Frommer, W. B., Patrick, J. W. (2003) – Phloem Loading and Unloading of Sugars and Amino Acids, *Plant Cell and Environment* **26**: 37-56

Lang, A. (1973) – A Working Model of a Sieve Tube, *J. Exp. Botany* **24**: 896-904

Lang, A. (1974) – Tension in the Phloem?, *J. Exp. Botany* **25**: 990-994

Lang, A. (1975) – A New Role for the Sieve Plate, *J. Theor. Biol*. **51**: 303-306

Lang, A. (1978) – A Model of Mass Flow in the Phloem, *Aust. J. Plant Physiol.* **5**: 535-546

Lang, A. (1979) – A Relay Mechanism for Phloem Translocation, *Ann. Bot*. **44**: 141-145

Lang, A. (1983) – Turgor-regulated Translocation, *Plant Cell and Environment* **6**: 683-689

Lang, A., Minchin, P. E. H. (1986) – Phylogenic Distribution and Mechanism of Translocation Inhibition by Chilling, *J. Exp. Botany* **37**: 389-398

Lang, A., Thorpe, M. R. (1986) – Water Potential, Translocation and Assimilate Partitioning, *J. Exp. Botany* **37**: 495-503

Lee, D. R. (1981a) – Elasticity of Phloem Tissues, *J. Exp. Botany* **32**: 251-260

Lee, D. R. (1981b) – Synchronous Pressure-Potential Changes in the Phloem of *Fraxinus americana* L., *Planta* **151**: 304-308

Legge, N. J., Connor, D. J. (1985) – Relating Water Potential Gradients in Mountain Ash (*Eucalyptus regnans* F. Muell.) to Transpiration Rate, *Aust. J. Plant Physiol.* **12**: 89-96

Levitt, D. G. (1975) – General Continuum Analysis of Transport Through Pores I. Proof of Onsager's Reciprocity Postulate for Uniform Pore, *Biophysical J*. **15**: 533-551

Loescher, W. H. (1987) – Physiology and Metabolism of Sugar Alcohols in Higher Plants, *Physiol. Plantarum* **70**: 553-557

Loescher, W. H., Tyson, R. H., Everard, J. D., Redgwell, R. J., Bieleski, R. L. (1992) – Mannitol Synthesis in Higher Plants. Evidence for the Role and Characterization of a NADPH-Dependent Mannose 6-Phosphate Reductase, *Plant Physiol*. **98**:1396-1402

Madore, M., Webb, J. A. (1981) – Stachyose Synthesis in Isolated Mesophyll Cells of Cucurbita pepo, *Can. J. Bot*. **60**: 126-130

Magnuson, C. E., Goeschl, J. D., Fares, Y. (1986) – Experimental Tests of the Münch-Horwitz Theory of Phloem Transport: Effects of the Loading Rates, *Plant Cell and Environment* **9**: 103-109

Magnuson, C. E., Goeschl, J. D., Sharpe, P. J. H., Demichele, D. W. (1979) – Consequences of Insufficient Equations in Models of the Münch Hypothesis of Phloem Transport, *Plant Cell and Environment* **2**: 181-188

Mason, T. G., Maskell, E.J. (1928a) – Studies on the Transport of Carbohydrates in the Cotton Plant I. A Study of Diurnal Variation in the Carbohydrates of Leaf, Bark, and Wood, and off the Effects of Ringing, *Ann. Bot*. **42**: 189-253

Mason, T. G., Maskell, E.J. (1928b) – Studies on the Transport of Carbohydrates in the Cotton Plant II. The Factors Determining the Rate and the Direction of Movement of Sugars, *Ann. Bot*. **42**: 571-636

Maynard, J. W., Lucas, W. L. (1982) – A Reanalysis of the Two-Component Phloem Loading System in Beta vulgaris, *Plant Physiol*. **70**: 1436-1443

McCaskill, A., Turgeon, R. (2007) – Phloem Loading in *Verbascum phoeniceum L.* Depends on the Synthesis of Raffinose-family Oligosaccharides, *PNAS* **104**: 19619-19624

McClendon, J. H. (1981) – The Osmotic Pressure of Concentrated Solutions of Polyethylene Glycol 6000, and its Variation with Temperature, *J. Exp. Botany* **32**: 861-866

McEuen A.R., Hart J.W., Sabnis D.D. (1981) – Calcium-binding protein in sieve tube Exudate, *Planta* **151**: 531-534.

McKinion, J. M., Weaver, R. E. C. (1979) – Simulation of Plant Response to Primary Stress Vectors, *Transactions of the ASAE* **22**: 586-597

Michel, B. E. (1972) – Solute Potentials of Sucrose Solutions, *Plant Physiol*. **50**: 196-198

Michel, B. E. (1983) – Evaluation of the Water Potentials of Solutions of Polyethylene Glycol 8000 both in the Absence and Presence of Other Solutes, *Plant Physiol*. **72**: 66-70

Michel, B. E., Kaufmann, M. R. (1973) – The Osmotic Potential of Polyethylene Glycol 6000, *Plant Physiol*. **51**: 914-916

Michel, B. E., Wiggins, O. K., Outlaw Jr., W. H. (1983) – A Guide to Establishing Water Potential of Two-phase Solutions (Polyethylene Glycol plus Dextran) by Amendment with Mannitol, *Plant Physiol*. **72**: 60-65

Milburn, J. A. (1972) – Phloem Transport in *Ricinus*, *Pestic. Sci.* **3**: 653-665

Milburn, J. A. (1974) – Phloem Transport in *Ricinus*: Concentration Gradients between Source and Sink, *Planta.* **117**: 303-319

Milburn, J. A. (1975) – Pressure Flow, in *Encyclopedia of Plant Physiology*, *Transport in Plants I*, *Phloem Transport*, ed. Zimmermann, M. H., Milburn, J. A., Springer-Verlag, New York, USA, pp 328-353

Milburn, J. A., (1980) – The Measurement of Turgor Pressure in Sieve Tubes, *Ber. Deutsch. Bot. Ges. Bd.* **93**: 153-166

Milburn, J. A., Kallarackal, J. (1984) – Quantitative Determination of Sieve Tube Dimensions in *Ricinus*, *Cucumis* and *Musa*, *New Phytol.* **96**: 383-395

Milburn, J. A., Zimmermann, M. H. (1977) – Preliminary Studies on Sap Flow in *Cocos nucifera* L., *New Phytol*. **79**: 543-558

Minchin, P. E. H. (1978) – Analysis of Tracer Profiles with Applications to Phloem Transport, *J. Exp. Botany* **29**: 1441-1450

Minchin, P. E. H. (1979) – The Relationship between Spatial and Temporal Tracer Profiles in Transport Studies, *J. Exp. Botany* **30**: 1171-1178

Minchin, P. E. H. (1986) – Why Use Short-lived Isotopes? in *Short-lived isotopes in Biology*, Proceedings of an International Workshop, 26-30 August, ed. P. E. M. Minchin, DSIR Bull. 238, Lower Hutt, New Zealand, pp. 3-5.

Minchin, P. E. H., Lang, A., Thorpe, M. R. (1983) – Dynamics of Cold Induced Inhibition of Phloem Transport, *J. Exp. Botany* **34**: 156-162

Minchin, P. E. H., Ryan, K. G., Thorpe, M. R. (1984) – Further Evidence of Apoplastic Unloading into the Stem of Bean: Identification of a Phloem Buffering Pool, *J. Exp. Botany* **35**: 1744-1753

Minchin, P. E. H., Thorpe, M. R. (1982) – Evidence for a Flow of Water into Sieve Tubes Associated with Phloem Loading, *J. Exp. Botany* **33**: 233-240

Minchin, P. E. H., Thorpe, M. R. (1984) – Apoplastic Phloem Unloading in the Stem of Bean, *J. Exp. Botany* **35**: 538-550

Minchin, P. E. H., Thorpe, M. R. (1987a) – Measurement of Unloading and Reloading of Photo-assimilate within the Stem of Bean, *J. Exp. Botany* **38**: 211-220

Minchin, P. E. H., Thorpe, M. R. (1987b) – Is Phloem Transport due a Hydrostatic Pressure Gradient? Supporting Evidence from Pressure Chamber Experiments, *Aus. J. Plant Physiol.* **14**: 397-402

Minchin, P. E. H., Thorpe, M. R. (1993) – Sink Strength: a misnomer, and best forgotten, *Plant Cell and Environment* **16**: 1039-1040

Minchin, P. E. H., Thorpe, M. R. (2003) – Using Short-lived Isotope ^{11}C in Mechanistic Studies of Photosynthate Transport, *Functional Plant Biology* **30**: 831-841

Minchin, P.E. H., Thorpe, M. R., Farrar, J. F. (1993) – A Simple Mechanistic Model of Phloem Transport which Explains Sink Priority, *J. Exp. Botany* **262**: 947-955

Minchin, P. E. H., Troughton, J. H. (1980) – Quantitative Interpretation of Phloem Translocation Data, *Ann. Rev. Plant Physiol*. **31**: 191-215

Moorby, J., Ebert, M., Evans, T.S. (1963) – The Translocation of ^{11}C-labelled Photosynthate in Soybean, *J. Exp. Botany* **14**: 210-220

Moorby, J., Troughton, J. H., Currie, B. G. (1974) – Investigations of Carbon Transport in Plants II. The Effects of Light and Darkness and Sink Activity on Translocation, J. Exp. *Botany* **25**: 937-944

Morison, K. R. (2002) – Viscosity Equations for Sucrose Solutions: Old and New in *Proceedings of APCChE Conference*, 29 Sep-3 Oct 2002, Christchurch, New Zealand

Mullendore, D. L., Windt, C. W., van As, H., Knoblauch, M. (2010) – Sieve Tube Geometry in Relation to Phloem Flow, *Plant Cell* **22**: 579-593

Münch, E. (1926) – Über Dynamik der Saftströmungen, *Ber. Deut. Bot. Ges*. **44**: 68-71

Münch, E. (1927) – Versuche über den Saftkreislauf, *Ber. Deut. Bot. Ges*. **45**: 340-356

Münch, E. (1930) – Die Stoffbewegungen in der Pflanze, Carl Fischer Ed., Jena, Germany

Murphy, R. (1986) – A Reanalysis of Particle Motion in Sieve Tubes of *Heracleum*, *Ann. Bot*. **57**: 667-674

Murphy, R. (1989a) – Water Flow across the Sieve-Tube Boundary: Estimating Turgor and Some Implications for Phloem Loading and Unloading. I. Theory, *Ann. Bot*. **63**: 541-549

Murphy, R. (1989b) – Water Flow across the Sieve-Tube Boundary: Estimating Turgor and Some Implications for Phloem Loading and Unloading. II. Phloem in the Stem, *Ann. Bot*. **63**: 551-559

Murphy, R. (1989c) – Water Flow across the Sieve-Tube Boundary: Estimating Turgor and Some Implications for Phloem Loading and Unloading. III. Phloem in the Leaf, *Ann. Bot*. **63**: 561-570

Murphy, R. (1989d) – Water Flow across the Sieve-Tube Boundary: Estimating Turgor and Some Implications for Phloem Loading and Unloading. IV. Root Tips and Seed Coats, *Ann. Bot*., **63**: 571-579

Murphy, R., Aikman, D. P. (1989) – An Investigation of the Relay Hypothesis of Phloem Transport in Ricinus cumunis L., *J. Exp. Botany* **40**: 1079-1088

Naccache, P., Sha'afi, R. I. (1974) - Effect of PCMBS on Water Transfer across Biological Membranes, *J. Cell Physiol*. **8**: 449-456

Nicole, M., Thouvenel, J. C., Giannotti, J., Chrestin, H., Geiger, J. P., Nandris, D., Rio B. (1991) – The Histology of *Hevea brasiliensis* Phloem Necrosis, *Eur. J. For. Path.* **21**: 27-35

Niklas, K. J. (1992) – Plant Biomechanics, An Engineering Approach to Plant Form and Function, The University of Chicago Press, USA, pp 190-233

Nobel, P. S. (1999) – Physicochemical & Environmental Plant Physiology, 2nd Ed., Academic Press, USA, pp 36-80, 373-384

Noiraud, N., Maurousset, L., Lemoine, R. (2001a) – Identification of a Mannitol Transporter, *AgMaT1*, in Celery Phloem, *Plant Cell* 13: 695-705

Noiraud, N., Maurousset, L., Lemoine, R. (2001b) – Transport of Polyols in Higher Plants, *Plant Physiol. Biochem*. 39: 717-728

Nonweiler, T. R. F. (1975) – Flow of Biological Fluids through Non-ideal Capillaries in *Encyclopedia of Plant Physilogy*, ed. Zimmermann, M. H., Milburn, J. A., vol. 1, part 1, Springer-Verlag, Berlin, pp 474-477

Oertli, J. J. (1969) – Terminology of Plant-Water Energy Relations, *Z. Pflanzenphysiol* **61**: 264-265

Oertli, J. J. (1986) – Negative Turgor Pressures in Plant Cells, *Z. Pflanzenernaehr. Bodenk.* **149**: 60-67

Oparka, K. J., Turgeon, R. (1999) – Sieve Elements and Companion Cells—Traffic Control Centersof the Phloem, *The Plant Cell* **11**: 739-750

Palatt, P. J., Sackin, H., Tanner, R. I. (1974) – A Hydrodynamic Model of a Permeable Tubule, *J. Theor. Biol*. **44**: 287-303

Parthasarathy, M. V. (1975) – Sieve-element Structure, in *Encyclopedia of Plant Physiology, Transport in Plants I, Phloem Transport*, ed. Zimmermann, M. H., Milburn, J. A., Springer-Verlag, New York, USA, pp 3-38

Passioura, J. B. (1976) – Translocation and the Diffusion Equation in *Transport and Transfer Processes in Plants*, ed. Wardlaw, I. F., Passioura, J. B., Academic Press, USA, pp 357-361

Passioura, J. B., Ashford, A. E. (1974) – Rapid Translocation in the Phloem of Wheat Roots, *Austr. J. Plant Physiol.* 1:521-527

Patrick, J. W. (1972) – Vascular System of the Stem of the Wheat Plant, *Aust. J. Bot.* **20**:49-63

Patrick, J. W. (1990) – Sieve Element Unloading: Cellular Pathway, Mechanism and Control, *Physiologia Plantarum* **78**: 298-308

Patrick, J. W. (1994) – Turgor-dependent Unloading of Assimilates from Coats of Developing Legume Seed. Assessment of the Significance of the Phenomenon in the Whole Plant, *Physiologia Plantarum* **90**: 645-654

Patrick, J. W., Zang, W., Tyerman, S. D., Offler, C. E., Walker, N. A. (2001) – Role of Membrane Transport in Phloem Translocation of Assimilates and Water, *Aust. J. Bot.* **28**:695-03

Pedersen, O., Sand-Jensen, K. (1997) – Transpiration Does Not Control Growth and Nutrient Supply in the Amphibious Plant *Mentha aquatica*, *Plant Cell and Environment* **20**: 117-123

Perämäki, M., Nikinmaa, E., Sevanto, S., Ivelsniemi, H., Siivola, E., Hari, P., Vesala, T., (2001) – Tree stem diameter variations and transpiration in Scots pine: ananalysis using a dynamic sap flow model, *Tree Physiology* **21:** 889-897

Peterson, R. L., Peterson, C. A., Melville, L. H. (2008) – Teaching Plant Anatomy through Creative Laboratory Exercises, NRC-CNRC, Canada

Peuke, A.D., Rokitta, M., Zimmermann, U., Schreiber, L., Haase, A. (2001) – Simultaneous Measurement of Water Flow Velocity and Solute Transport in Xylem and Phloem of Adult Plants of *Ricinus communis* over a Daily Time Course by Nuclear Magnetic Resonance Spectrometry, *Plant Cell and Environment* **24**: 491-503

Phillips, R. J., Dungan, S. R. (1993) – Asymptotic Analysis of Flow in Sieve Tubes with Semi-permeable Walls, *J. Theor. Biol.* **162**: 465-485

Pickard, W. F., Abraham-Schrauner, B. (2009) – A "Simplest" Steady-state Münch-like Model of Phloem Translocation, with Source and Pathway and Sink, *Functional Plant Biology*, **36**: 629-644

Pickard, W. F., Minchin, P. E. H., Troughton, J. H. (1978a) – Real Time Studies of Carbon-11 Translocation in Moonflower. I – The Effects of Cold Blocks, *J. Exp. Botany* **29**: 993-1001

Pickard, W. F., Minchin, P. E. H., Troughton, J. H. (1978b) – Real Time Studies of Carbon-11 Translocation in Moonflower. II – The Effects of Metabolic and Photosynthetic Activity and of Water Stress, *J. Exp. Botany* **29**: 1003-1009

Pickard, W. F., Minchin, P. E. H., Troughton, J. H. (1979) – Real Time Studies of Carbon-11 Translocation in Moonflower. III – Further Experiments on the Effects of a Nitrogen Atmosphere, Water Stress, and Chilling: and a Qualitative Theory of Stem Translocation, *J. Exp. Botany* **30**: 307-318

Preston, R. D. (1963) – Ultrastructure and Kinetic Aspects of Solute Translocation in the Stem of Plants, *Prog Biophys Mol Biol.* **13**: 241-60.

Pristupa, N. A. (1983) – Distribution of Ketosugars among Cells of Conducting Bundles of the Cucurbita pepo Leaf, *Soviet Plant Physiol*. **30**: 372-378

Qureshi, F. A., Spanner, D.C. (1973) – Movement of [^{14}C]Sucrose along the Stolon of Saxifraga sarmentosa, *Planta* **110**:145-152

Rand, R. H. (1983) – Fluid Mechanics of Green Plants, *Ann. Rev. Fluid Mechanics* **15**: 29-45

Rand, R. H., Cooke, J.R. (1978) – Fluid Dynamics of Phloem Flow: An Axisymmetric Model, *Transactions of the ASAE* **21**: 898-900,906

Rand, R. H., Upadhayaya, S. K., Cooke, J.R. (1980) – Fluid Dynamics of Phloem Flow: Part II, an Approximate Formula, *Transactions of the ASAE* **23**: 581-584

Regirer, S. A. (1960) – On The Approximate Theory of The Flow of a Viscous Incompressible Liquid in a Tube with Permeable Walls, *Zhurnal Tekhnicheskoi Fiziki*, **30**: 639-643

Reynolds, M. (1932) – Development of the Node in *Ricinus Communis*, *Botanical Gazette* **104**: 167-170

Richardson, P. T., Baker, D. A. (1982) – The Chemical Composition of Cucurbit Vascular Exudates, *J. Exp. Botany* **33**: 1239-1247

Richardson, P. T., Baker, D. A., Ho, L. C. (1984) – Assimilate Transport in Cucurbits, *J. Exp. Botany* **35**: 1575-1581

Roeb, G. W., Britz, S. J. (1991) – Short-term Fluctuations in the Transport of Assimilates to the Ear of Wheat Measured with Steady-state $^{11}CO_2$-labelling of the Flag Leaf, *J. Exp. Botany* **42**: 469-475

Roeb, G. W., Fisher, D. B. (1991) – Some *in vivo* Tracer Techniques for Studying Transport, in *Recent Advances in Phloem Transport and Assimilate Compartmentation*, ed. Bonnemain, J. L., Delrot, S., Lucas, W. J., Dainty, J., Ouest Edt., France, pp 309-316

Roeb, G. W., Jahnke, S. (2007) – Dynamic Carbon Allocation in Wheat Plants in *Sink-source Relantionships and Plant Productivity*, Proceedings of the International Symposium "Sink-source Relationships in Plants", 21-26 May, ed. Ron'zhina, E. S., Kaliningrad, Russia, pp. 200-211

Roeb, G. W., Wieneke, J., Führ, F. (1986a) – A System for Continuously Applying ^{11}C-labelled Carbon Dioxide to Plants Without On-line Connection to the Target Chamber in *Short-lived isotopes in Biology*, Proceedings of an International Workshop, 26-30 August, ed. P. E. M. Minchin, DSIR Bull. 238, Lower Hutt, New Zealand, pp. 41-49

Roeb, G. W., Wieneke, J., Führ, F. (1986b) – Carbon Translocation & Accumulation in Wheat Plants Measured Using ^{11}C-labelled Carbon Dioxide in *Short-lived isotopes in Biology*, Proceedings of an International Workshop, 26-30 August, ed. P. E. M. Minchin, DSIR Bull. 238, Lower Hutt, New Zealand, pp. 72-79

Rogers, S., Peel, A. J. (1975) – Some Evidence for the Existence of Turgor Pressure-Gradients in the Sieve Tubes of Willow, *Planta* **126**: 259-67

Ross, S. M., Tyree, T. (1979) – Mason and Maskell's Diffusion Analogue Reconciled with a Translocation Theory, *Ann. Bot*. **44**: 637-640

Rumpho, M. E., Edwards, G. E., Loescher, W. H. (1983) – A Pathway for Photosynthetic Carbon Flow to Mannitol in Celery Leaves, *Plant Physiol* **73**: 869-873

Salisbury; F., Ross, C. (1992) – Plant Physiology, 4th Ed., Wadsworth Publishing, Belmont, USA, pp 161-187

Sampson, R. A. (1891) – On Stoke's Current Function, *Phil. Trans. R. Soc. Lond. A*, **182**: 449-518

Schaffer, A., Pharr, D. M., Madore, M. (1996) – Cucurbits, in *Photoassimilate Distribution in Plants and Crops, Source-Sink Relationships*, ed. E. Zamski & A. Schaffer, Marcel Dekker Inc., New York, USA, pp 720-757

Schneider, S., Schneidereit, A., Konrad, K. R., Hajirezaei, M. R., Gramann, M., Hedrich, R., Sauer, N. (2006) – *Arabidopsis* INOSITOL TRANSPORTER4 Mediates High Affinity H^+-Symport of *myo*-Inositol across the Plasma Membrane, *Plant Physiol*. **141**: 565-577

Schneider, T., Keller, F. (2009) – Raffinose in Chloroplasts is Synthesized in the Cytosol and Transported across the Chloroplast Envelope, *Plant Cell Physiol*. **50**: 2174-2182

Schulte, P. J., Costa, D. G. (1996) – A Mathematical Description of Water Flow through Plant Tissues, *J. Theor. Biol*. **180**: 61-70

Schultze, E. D. (1991) – Water and Nutrient Interactions with Plant Water Stress, in *Response of Plants to Multiple Schemes*, ed. Mooney, H. A., Winner, W. E., Pell, E. J., Academic, San Diego, CA, pp 89-101

Schulz, A. (1998) – Phloem. Structure Related to Function, *Progress in Botany* **59**: 429-475

Schulz, A., Thompson, G. A. (2001) – Phloem Structure and Function, Encyclopedia of Life Sciences

Schurr, U., Jahnke, S. (1991) – Some in vivo Tracer Techniques for Studying Transport, in *Recent Advances in Phloem Transport and Assimilate Compartmentation*, ed. Bonnemain, J. L., Delrot, S., Lucas, W. J., Dainty, J., Ouest Edt., France, pp 294-300

Schütz, K., Tyerman, S. D. (1997) – Water channels in *Chara coralline, J. Exp. Botany* **48**: 1511-1518

Sdoodee S., Somjun, J. (2008) – Measurement of Stem Water Potential as a Sensitive Indicator of Water Stress in Neck Orange (*Citrus reticulata* Blanco*), J. Sci. Technol.* **30**: 561-564

Sevanto, S., Vesala, T., Perämäki, M., Nikinmaa, E. (2002) – Time lags for xylem and stem diameter variations in a Scots pine tree, *Plant Cell and Environment* **25**: 1071-1077

Sevanto, S., Vesala, T., Perämäki, M., Nikinmaa, E. (2003) – Sugar transport together with environmental conditions controls time lags between xylem and stem diameter changes, *Plant Cell and Environment* **26**: 1257-1265

Sheehy, J. E., Mitchell, P. L., Durand, J-L., Gastal, F., Woodward, F. I. (1995) – Calculation of Translocation Coefficients from Phloem Anatomy for Use in Crop Models, *Ann. Bot*., 76: 263-269

Sheikholeslam, S. N., Currier, H. B. (1977a) – Phloem Pressure Differences and ^{14}C-Assimilate Translocation in *Ecballium elaterium*, *Plant Physiol*. **59**: 376-380

Sheikholeslam, S. N., Currier, H. B. (1977b) – Effects of Water Stress on Turgor Differences and 14C-Assimilate Movement in Phloem of *Ecballium elaterium*, *Plant Physiol*. **59**: 381-383

Smirnoff, N., Cumbers, Q. (1989) – Hydroxyl Radical Scavenging Activity of Compatible Solutes, *Phytochemistry* **28**: 1057-1060

Smith, K. C., Magnuson, C. E., Goeschl, J.D., DeMichele, D. W. (1980) – A Time-dependent Mathematical Expression of the Münch Hypothesis of Phloem Transport, *J. Theor. Biol*. **86**: 493-505

Smith, J. A. C., Milburn, J. A. (1980) – Osmoregulation and the Control of Phloem Sap Composition in *Ricinus comunis* L., *Planta* 1**28**: 28-34

Sovonick-Dunford, S. (1986) – Water Relations Parameters of White Ash Sieve Tubes. in *Phloem Transport*, ed. Cronshaw, W. J. Lucas and R. T. Giaquinta, Alan R. Liss, Inc., New York, pp. 187-91

Sovonick-Dunford, S., Ferrier, J.M., Dainty, J. (1982) – Water Relations Parameters of the Phloem. Determinations of Volumetric Elastic Modulus and Membrane Conductivity using an Applied Force Method and Shrinkage and Swelling of Tissues in Solutions at Differing Osmotic Pressure, *Ann. Bot*. **51**: 27-37

Sovonick-Dunford, S., Lee, R. D., Zimmermann, M. H. (1981) – Direct and Indirect Measurements of Phloem Turgor Pressure in White Ash, *Plant Physiol*. **68**: 121-126

Spanner, D. C., Prebble, J. N. (1962) – The Movement of Tracers along the Petiole of *Nymphoides peltatum* I. A Preliminary Study with ^{137}Cs, *J. Exp. Botany* **13**: 294-306

Stoop, J.M.H., Williamson, J.D., Pharr, D.M. (1996) – Mannitol Metabolism in Plants: a Method for Coping with Stress, *Trends Plant Sci*. **5**: 139-144

Streeter, V. L., Wylie, E. B., Bedford, K. W. (1998) – Fluid Mechanics, McGraw-Hill

Swanson, C. A., Hoddinott, J., Su, J. W. (1976) – The Effect of Selected Sink Leaf Parameters or Translocation Rates, in *Transport and Transfer Processes in Plants,* ed. I. F. Wardlow and J. B. Passioura, Academic Press, USA, pp. 347-56

Taiz, L., Zeiger, E. (2001) – Plant Physiology, 3rd Ed., pg 193-221, SinauerAssociates Inc. Sunderland, USA

Taiz, L., Zeiger, E. (1998) – Plant Physiology, 2nd Ed., pg 61-101, SinauerAssociates Inc. Sunderland, USA

Tammes, P. M. L., van Die, J., Ie, T. S. (1971) – Studies on Phloem Exudation from Yucca flaccida Haw. VIII. Fluid Mechanics and Exudation, *Acta Bot. Neerl*. **20**: 245-252

Tanner, W., Beevers, H. (1990) – Does transpiration have an essential function in long-distance ion transport in plants?, *Plant Cell Environ.* **13:** 745-750

Tanner, W., Beevers, H. (2001) – Transpiration, a Prerequisite for Long-Distance Transport of Minerals in Plants?, *PNAS* **98**: 9443-9447

Thompson, M. V. (2005) – Scaling Phloem Transport: Elasticity and Pressure-Concentration Waves, *J. Theor. Biol*. **236**: 229-241

Thompson, M. V. (2006) – Phloem: The Long and the Short of it, *Trends in Plant Science* **11**: 26-32

Thompson, M. V., Holbrook, N. M. (2003a) – Application of a Single-solute Non-steady-state Phloem Model to the Study of Long-distance Assimilate Transport, *J. Theor. Biol*. **220**: 419-455

Thompson, M. V., Holbrook, N. M. (2003b) – Scaling Phloem Transport: Water Potential Equilibrium and Osmoregulatory Flow, *Plant Cell and Environment* **26**: 1561-1577

Thompson, M. V., Holbrook, N. M. (2004) – Scaling Phloem Transport: Information Transmission, *Plant Cell and Environment* **27**: 509-519

Thompson, R. G., Fensom, D.S., Anderson, R. R., Drouin, R., Leiper W. (1979) – Translocation of ^{11}C from leaves of *Helianthus*, *Heracleum*, *Nymphoides*, *Ipomoe*a, *Tropaeolum*, *Zea*, *Fraxinus*, *Ulmus*, *Picea*, and *Pinus*: Comparative Shapes and Some Fine Structure Profiles. *Can. J. Bot.* 57: 845.

Thornley, J. H. M.(1976) – Mathematical Models in Plant Physiology, Academica Press, London, UK, pp 50-73

Thornley, J. H. M. (1987) – The Magnitude of the Temperature-driven Contribution to Within-plant Transport, *Plant, Cell & Environment* **10**: 699-700

Thornley, J. H. M., Johnson, I. R. (2000) – Plant and Crop Modelling, Blackburn Press, USA, pp 105-119

Thorpe, M. R. (1986) – Detection & counting of positron emitting isotopes, in *Short-lived isotopes in Biology*, Proceedings of an International Workshop, 26-30 August, ed. P. E. M. Minchin, DSIR Bull. 238, Lower Hutt, New Zealand, pp. 50-51

Thorpe, M. R., Lang, A., Minchin, P. E. H. (1983) – Short Term Interactions between Flows of Photosynthate, *J. Exp. Botany* **34**: 10-19

Thorpe, M. R., Minchin, P. E. H. (1988) – Phleom Loading and Transport of Endogenously or Exogenously Labelled Photo-Assimilate in Bean, Beet, Maize and Cucurbit, *J. Exp. Botany* **39**: 1709-1721

Thorpe, M. R., Minchin, P. E. H. (1996) – Mechanisms of Long- and Short-Distance Transport from Sources to Sinks, in *Photoassimilate Distribution in Plants and Crops,*

Source-Sink Relationships, ed. E. Zamski & A. Schaffer, Marcel Dekker Inc., New York, USA, pp 261-282

Thorpe, M. R., Minchin, P. E. H., Gould, N., McQueen, J. (2006) – The Stem Apoplast: A Potential Communication Channel in Plant Growth Regulation, in *Vascular Transport in Plants*, ed. Holbrook, M. N. & Zwieniecki, M., Elsevier, U.S.A., pp 201-220

Thorpe, M. R., Minchin, P. E. H., Williams, J. H. H., Farrar, J. F., Tomos, D. (1993) – Carbon Import into Developing Ovules of *Pisum sativum*: The Role of the Water Relations of the Seed Coat, *J. Exp. Botany* **44**: 937-945

Troughton, J. H., Chang, F. H., Currie, B. G. (1974) – Estimates of Mean Speed of Translocation in Leaves of *Oryza sativa* L., *Plant Science Letters* **3**: 49-54

Troughton, J. H., Currie, B. G. (1977) – Relations between Light Level, Sucrose Concentration, and Translocation of Carbon 11 in *Zea mays* Leaves, *Plant Physiol*. **59**: 808-820

Turgeon, R. (1989) – The sink–source transition in leaves, *Ann. Rev. of Plant Physiology & Plant Molecular Biology* **40**: 119-138.

Turgeon, R., Ayre, B. G. (2005) – Pathways and Mechanisms of Phloem Loading, in *Vascular Transport in Plants*, ed. Holbrook, M. N. & Zwieniecki, M., Elsevier, U.S.A., pp 45-67

Turgeon, R., Beebe, D. U. (1991) – The Evidence for Symplastic Phloem Loading, *Plant Physiol.* **96**: 349-354

Turgeon, R., Webb, J. A. (1973) – Leaf Development and Phloem Transport in *Cucurbita Pepo*: Transition from Import to Export *Planta* **113**: 179-191

Turgeon, R., Webb, J. A. (1975) – Leaf Development and Phloem Transport in *Cucurbita Pepo*: Carbon Economy, *Planta* **123**: 53-62

Turgeon, R., Webb, J. A., Evert, R. F. (1975) – Ultrastructure in Minor Veins in *Cucurbita Pepo* Leaves, *Protoplasma* **83**: 217-232

Tyree, M. T. (1970) – The Symplast Concept. A General Theory of Symplastic Transport according to the Thermodynamics of Irreversible Processes, *J. Theor. Biol*. **26**: 181-214

Tyree, M.T. (1974) – Some Inconsistencies that Arise when the Canny-Phyllips Model of Phloem Translocation is Applied to Known ^{14}C-assimilate Profiles in Plant Stems and Petioles, *Can. J. Bot.* **53**: 1128-1131

Tyree, M. T. (1975) – Horwitz-type Models of Tracer Distribution during Unidirectional Translocation, in *Phloem Transport*, ed. Aronoff, S., Dainty, J., Gorham, P. R., Srivastava, L. M., Swanson, C. A., NATO Advanced Study Institutes Series, vol. 4, Plenum Press, USA, pp 475-494

Tyree, M. T. (1975) – Steady State Models of Münch Pressure Flow, in *Phloem Transport*, ed. Aronoff, S., Dainty, J., Gorham, P. R., Srivastava, L. M., Swanson, C. A., NATO Advanced Study Institutes Series, vol. 4, Plenum Press, USA, pp 523-529

Tyree, M. T., Christy, A. L., Ferrier, J. M. (1974) – A Simpler Iterative Steady Sate Solution of Münch Pressure-Flow Systems Applied to Long and Short Translocation Paths, *Plant Physiol*. **54**: 589-600

Tyree, M.T., Dainty, J. (1975) – Theoretical Considerations, in *Encyclopedia of Plant Physiology, Transport in Plants I, Phloem Transport*, ed. Zimmermann, M. H., Milburn, J. A., Springer-Verlag, New York, USA, pp 367-394

van Bel, A. J. E. (1987) –The Apoplast Concept of Phloem Loading has No Universal Validity, *Plant Physiol. Biochem.* **25**: 677-686

van Bel, A. J. E. (1990) – Xylem-Phloem Exchange Via the Rays: The Undervalued Route of Transport, *J. Exp. Botany* **41**: 631-644

van Bel, A. J. E. (1996) – Interaction between Sieve Element and Companion Cell and the Consequences for Photoassimilate Distribution. Two Structural Hardware Frames with Associated Physiological Software Packages in Dicotyledons?, *J. Exp. Botany* **47**: 1129-1140

van Bel, A. J. E. (1998) – The Transport Phloem. Specifics of its Functioning, *Progress in Botany* **54**: 134-150

van Bel, A. J. E. (2003a) – Transport Phloem: Low Profile, High Impact, *Plant Physiol.* **131**: 1509-1510

van Bel, A. J. E. (2003b) – The phloem, a miracle of ingenuity, *Plant, Cell & Environment* **26**: 125-149

van Bel, A. J. E., Ehlers, K., Knoblauch, M. (2002) – Sieve elements caught in the act, *Trends in Plant Science* **7**: 126-132

van Bel, A. J. E., Hafke, J. B. (2005) – Physiochemical Determinants of Phloem Transport in *Vascular Transport in Plants*, ed. Holbrook, M. N. & Zwieniecki, M., Elsevier, U.S.A., pp 19-44

van Bel, A. J. E., Hendriks, J. H. M., Boom, E. J. M. C., Gamalei, Y. V., van de Merwe (1996) – Different Ratios of Sucrose/Raffinose-Induced Membrane Depolarizations in the Mesophyll of Species with Symplasmic (*Catharanthus roseus*, *Ocimum basilicum*) or Apoplasmic (*Impatiens walleriana*, *Vicia faba*) Minor-vein Configurations, *Planta* **199**: 185-192

van Bel, A. J. E., Kempers, R. (1990) – Symplastic Isolation of the Sieve Element–Companion Cell Complex in the Phloem of *Ricinus communis* and *Salix alba*, *Planta* **183**: 69-76

van Bel, A. J. E., Knoblauch, M. (2000) – Sieve Element and Companion Cell: The Story of the Comatose Patient and the Hyperactive Nurse, *Aust. J. Plant Physiol*. **27**: 477-487

van Dyke, M. (1964) – Perturbation Methods in Fluid Mechanics., Academic Press, New York, USA

Vernon, L. P. Aronoff, S. (1952) – Metabolism of Soybean Leaves. IV. Translocation from Soybean Leaves, *Arch. Biochem. Biophys*. **36**: 383-398

Voitsekhovskaja, O. V. (2001) – On the Role of Sugar Compartmentation and Stachyose Synthesis in Symplastic Phloem Loading, PhD Thesis, Georg August University, Göttingen

Vreugdenhil, D. (1985) – Source-to-Sink Gradient of Potassium in the Phloem, *Planta* **163**: 238-240

Vreugdenhil, D., Koot-Gronsveld, E. A. M. (1989) – Measurements of pH, Sucrose and Potassium Ions in the Phloem Sap of Castor Bean (*Ricinus communis*) Plants, *Physiologia Plantarum* **77**: 385-388

Wardlaw, I. F. (1965) – The Velocity and Pattern of Assimilate Translocation in Wheat Plants during Grain Development, *Aust. J. Biol. Sci.* **18**: 269-281

Wardlaw, I. F. (1990) – The Control of Carbon Partitioning in Plants, *New Phytol.* **116**: 341-381

Watari, J., Kobae, Y., Yamaki, S., Yamada, K., Toyofuku, K., Tabuchi, T., Shiratake, K. (2004) – Identification of Sorbitol Transporters expressed in the Phloem of Apple Source Leaves, *Plant Cell Physiol*. **45**:1032-1041

Wayne, R., Tazawa, M. (1990) – Nature of the Water Channels in the Internodal Cells of *Nitellopsis, J. Membrane Biology* **116**: 31-39

Weast, R. C. (1983) – CRC Handbook of Chemistry and Physics, 62nd Ed., CRC Press, USA

Weatherley, P.E. (1972) – Translocation in Sieve Tubes, Some Thoughts on Structure and Mechanism, *Physiol. Vég.* **10 (4)**: 731-742

Weatherley, P.E. (1973) – Solution Flow in Tubular Semi-permeable Membranes, *Planta* **110**: 183-187

Weatherley, P.E., Johnson, R. P. C. (1968) – The Form and Function of the Sieve Tube: A Problem in Reconciliation, *Int. Rev. Cytol.* **24**: 149-192

Weatherley, P.E., Peel, A. J., Hill, G. P. (1959) – The Physiology of the Sieve Tube, Preliminary Experiments using Aphid Mouth Parts, *J. Exp. Botany* **10**: 1-16

Webb, J. A., Gorham, P. R. (1964) – Translocation of Photosynthetically Assimilated ^{14}C in Straight-Necked Squash, *Plant Physiol*. **39**: 663-672

Webb, J. A., Gorham, P. R. (1965) – Radial Movement of C^{14}-Translocates from Squash Phloem, *Canad. J. Botany* **43**: 97-103

Webb, K. L., William, J., Burley, J. W. (1964) – Stachyose Translocation in Plants, *Plant Physiol*. **39**: 973-977

Weir, G. J. (1981) – Analysis of Munch Theory, *Mathematical Biosciences* **56**: 141-152

Whiting, A. G. (1937) – Development and Anatomy of Primary Structure in the Seedling of Cucurbita maxima, *Botanical Gazette* **99**: 497-528

Whittle, C. (1970) – Lateral Movement out of the Sieve Tubes and its Effect on the 14C Translocation Profile in Helianthus Seedlings, *Planta* **95**: 247-263

Wilkinson, R. E., Duncan, R. R., Berry, C. (1994) – Sorghum Seedling Root-tip Elemental Contents after Concomitant Exposure to PCMBS and Mineral Nutrient Solution, *J. Plant Nutrition* **17**: 1393-1397

Williamson, J. D., Stoop, J. M. H., Massel, M. O., Conkling, M. A., Pharr, D. M. (1995) – Sequence Analysis of a Mannitol Dehydrogenase cDNA from Plants Reveals a Function for the Pathogenesis-related Protein ELI3, *Proc. Natl Acad. Sci. USA* **92**: 7148-7152

Willenbrink, J. (2002) – Assimilate Transport in Phloem: Regulation and Mechanism, *Russian Journal of Plant Physiology* **49**: 8-15

Windt, C. W., Vergeldt, F. J., Adrie, Jager, P. A., van As, H. (2006) – MRI of Long-distance Water Transport: a Comparison of the Phloem and Xylem Flow Characteristics and Dynamics in Poplar, Castor Bean, Tomato and Tobacco, *Plant Cell and Environment* **29**: 1715-1729

Wolswinkel, P. (1974) – Enhanced rate of ^{14}C-Solute Release to the Free Space by the Phloem of *Vicia faba* Stems Parasitized by *Cuscuta*, *Acta Bot. Neerl.* **23**: 177-188

Wolswinkel, P. (1978) – Phloem Unloading in Stem Parts Parasitized by *Cuscuta*: the Release of ^{14}C and K^+ to the Free Space at 0°C and 25°C, *Physiologia Pl.* **42**: 167-72

Wright, J. P., Fisher, D. B. (1980) – Direct Measurement of Sieve Tube Turgor Pressure using Severed Aphid Stylets, *Plant Physiol.* **65**: 1133-1135

Wright, J. P., Fisher, D. B. (1983) – Estimation on the Volumetric Elastic Modulus and Membrane Hydraulic Conductivity of Willow Sieve Tubes, *Plant Physiol.* **73**: 1042-1047

Yancey, P. H., Clark, M. E., Hand, S. C., Bowlus, R. D., Somero, G. N. (1982) – Living with Water Stress: Evolution of Osmolyte Systems, *Science* **217**: 1214-1222

Young, J. H, Evert, R. F., Eschrich, W. (1973) – On the Volume-flow in Mechanism of Phloem Transport, *Planta* **113**: 355-366

Zamski, E. (1996) – Anatomical and Physiological Characteristics of Sink Cells, in Photoassimilate Distribution in Plants and Crops, Source-Sink Relationships (eds E. Zamski & A. Schaffer), Marcel Dekker Inc., New York, USA, pp 283-310

Zhang, B. (2005) – Dissection of Phloem Transport in Cucurbitaceae by Metabolomic Analysis, PhD Thesis, Potsdam University

Zhang, B., Tolstikov, V., Turnbull, C., Hicks, L. M., Fiehn, O. (2010) – Divergent metabolome and proteome suggest functional independence of dual phloem transport systems in cucurbits, *PNAS* **107**: 13532-13537

Ziegler, H. (1956) – Untersuchungen Über die Leitung und Sekretion der Assimilate, *Planta* **47**: 447-500

Zimmermann, M. H. (1957) – Translocation of Organic Substances in Trees. II. The Translocation Mechanism in the Phloem of White Ash (*Fraxinus americana* L.), *Plant Physiol*. **32**:399-404

Zimmermann, M. H. (1958) – Translocation of Organic Substances in Trees. III. The Removal of Sugars from the Sieve Tubes in the White Ash (*Fraxinus americana* L.), *Plant Physiol*. **33**:213-217

Zimmermann, M. H. (1969) – Translocation Velocity and Specific Mass Transfer in the Sieve Tubes of *Fraxinus Americana* L., *Planta* **84**: 272-278

Zimmermann, M. H., Brown, C. L. (1971) – Trees, Structure and Function, Springer-Verlag, New York, USA

Zimmermann, M. H., Ziegler, H. (1975) – List of Sugars and Sugar Alcohols in Sieve-tubes Exudates, in *Encyclopedia of Plant Physiology, Transport in Plants I, Phloem Transport*, ed. Zimmermann, M. H., Milburn, J. A., Springer-Verlag, New York, USA, pp 480-503

Abbreviations & Definitions

A	Area
A(t)	Carbon 11 activity at time t
$A_{maximum}$	Carbon 11 maximum activity
ABS	Apoplastic bathing solution
ADP	Adenosine diphosphate
α	Fractional area occupied by sieve plate pores relative to sieve tube lumen cross sectional area
α_T	Fractional net loss of tracer per unit length
ATP	Adenosine triphosphate
β	Sieve plate impedance factor
β^+	Positron
^{11}B	Boron 11
C	Sieve tube solute concentration
C_i	Sieve tube solute concentration at $z = 0$
C_{in}	Input solute concentration
C_m	Solute concentration in the sieve tube membrane
C_{out}	Apoplast solute concentration
^{11}C	Carbon 11
^{14}C	Carbon 14
$^{11}CO_2$	Carbon 11 labelled carbon dioxide
$^{14}CO_2$	Carbon 14 labelled carbon dioxide
^{14}C-sucrose	Carbon 14 labelled sucrose
^{137}Cs	Cesium 137
^{o}C	Celsius degrees
Ca^{2+}	Calcium
$Ca(NO_3)_2$	Calcium nitrate
cmp	Counts per minute
CPJ	Concentration-pressure-flux
$CuSO_4$	Copper sulphate

D	Sieve tube sap solute diffusion coefficient
Δp	Turgor pressure difference
ΔΨ	Water potential difference
EGTA	Ethylene glycol tetraacetic acid
EPW	Electropotential waves
exp	Exponential, *e*
ε	Sieve tube radius/length ratio
f_s	Force per unit volume developed by metabolic processes
Fe-EDTA	Iron ethylenediaminetetraacetate
φ	Azimuth
Φ	Resistance to a pressure driven flow
g	Gravity acceleration
G	System's gain
Gd^{3+}	Gadolinium
Γ	Resistance to a concentration driven flow
h	Height
H_3BO_3	Boric acid
j	Volume flux
j_{in}	Input solution flux
j_{out}	Output solution flux
j_{ls}	Lateral solute flux
j_s	Solute flux
j_{sr}	Radial solute flux
j_{sz}	Axial solute flux
j_W	Water flux
J	Solution flow rate
J_{in}	Input Solution flow rate
J_{out}	Output Solution flow rate
J_s	Solute flow rate
K	Kelvin degrees
K	Bulk modulus
k	Sieve tube axial conductivity (dependent on sieve tube structure only)

k_{lm}	Solute transfer coefficient between compartments *l* and *m*
^{42}K	Potassium 42
K^+	Potassium
KCl	Potassium chloride
KH_2PO_4	Potassium dihydrogen phosphate
K_m	Michaelis–Menten constant
KNO_3	Potassium nitrate
l	Sieve tube element length
l_p	Sieve plate pore length
L	Sieve tube length
L_p	Sieve tube membrane hydraulic conductivity
L_s	Sieve tube axial conductivity
λ	Radioactive decay constant
ln	Natural logarithm
m	Molality
M	Molar
MES	2-(N-morpholino)ethanesulfonic acid
Mev	Mega electronvolt
$MgSO_4$	Magnesium sulphate
$MnSO_4$	Manganese sulphate
min	Minutes
μ	Viscosity
n	Number of samples
N	Number of particles
N_p	Number o sieve plate pores
ν	Kinematic viscosity
$\vec{\nabla}$	Gradient operator
$\vec{\nabla}^2$	Laplacian operator
NAD^+	Nicotinamide adenine dinucleotide (oxidized form)
NADH	Nicotinamide adenine dinucleotide (reduced form)
$NADP^+$	Nicotinamide adenine dinucleotide phosphate (oxidized form)

NADPH	Nicotinamide adenine dinucleotide phosphate (reduced form)
$NaMoO_4$	Sodium molybdate
NaI(Tl)	Sodium iodide activated with thallium
P	Perimeter
$P(x)$	Amount of photoassimilate
^{32}P	Phosphorus 32
p	Turgor pressure
p_{in}	Input turgor pressure
p_{in}	Output turgor pressure
p_{out}	Apoplast pressure
$\mathcal{P}e_r$	Radial flow Péclet number
$\mathcal{P}e_z$	Axial flow Péclet number
P_s	Sieve tube membrane solute permeability
p_3	Turgor pressure within compartment 3
PCMBS	4-(Chloromercuri)benzenesulfonic acid
PEG	Polyethylene glycol
Π	Osmotic pressure
Π_{out}	Apoplast osmotic pressure
Ψ	Water potential
Ψ_{out}	Apoplast water potential
Q	Amount of tracer
ξ	Sieve tube resistance
r	Radial coordinate
R	Sieve tube radius
$\mathcal{R}e$	Reynolds number
R_g	Universal gas constant
r_p	Sieve plate pore radius
ρ	Phloem sap density
ρ_W	Water density
r_s	Sieve plate pore radius
RFO	Raffinose oligosaccharide family of sugars
SE	Standard error
SE/CC	Sieve element companion cell complex

σ	Sieve tube membrane reflection coefficient
ς	Sieve tube resistivity
t	Time
T	Absolute temperature
θ	Systems time delay
THO	Tritiated water
U	Average translocation speed
u_k	Input activity at time k
v	Velocity
v_e	Electron neutrino
v_{max}	Maximum rate of solute flux
v_r	Radial velocity
v_z	Axial velocity
V	Volume
$\bar{V}_S$	Sucrose specific volume
x	Spatial coordinate
x_s	Mole fraction
X	Perfused internode length
y_k	Output activity at time k
Y	Model predicted output activity
z	Axial coordinate
$ZnSO_4$	Zinc sulphate

Appendix

From equation (3.130):

$$\frac{d^2\hat{p}_0}{d\hat{z}^2}\left(\hat{z}\right)=\frac{16\hat{L}_p}{\beta}\left[\hat{p}_0\left(\hat{z}\right)-\hat{p}_{out}\left(0\right)-\frac{d\hat{p}_{out}}{d\hat{z}}\hat{z}-\sigma\hat{H}\left(\hat{C}_0\left(\hat{z}\right)-\hat{C}_{out}\left(0\right)-\frac{d\hat{C}_{out}}{d\hat{z}}\hat{z}\right)\right]$$

we have that:

$$\frac{d^3\hat{p}_0}{d\hat{z}^3}\left(\hat{z}\right)=\frac{16\hat{L}_p}{\beta}\left[\frac{d\hat{p}_0}{d\hat{z}}\left(\hat{z}\right)-\frac{d\hat{p}_{out}}{d\hat{z}}-\sigma\hat{H}\left(\frac{d\hat{C}_0}{d\hat{z}}\left(\hat{z}\right)-\frac{d\hat{C}_{out}}{d\hat{z}}\right)\right] \tag{A.1}$$

and

$$\hat{C}_0\left(\hat{z}\right)=\hat{C}_{out}\left(0\right)+\frac{d\hat{C}_{out}}{d\hat{z}}\hat{z}-\frac{\beta}{16\sigma\hat{H}\hat{L}_p}\frac{d^2\hat{p}_0}{d\hat{z}^2}\left(\hat{z}\right)+\frac{1}{\sigma\hat{H}}\left(\hat{p}_0\left(\hat{z}\right)-\hat{p}_{out}\left(0\right)-\frac{d\hat{p}_{out}}{d\hat{z}}\hat{z}\right) \tag{A.2}$$

Thus:

$$\frac{d\hat{C}_0}{d\hat{z}}\left(\hat{z}\right)=\frac{d\hat{C}_{out}}{d\hat{z}}-\frac{\beta}{16\sigma\hat{H}\hat{L}_p}\frac{d^3\hat{p}_0}{d\hat{z}^3}\left(\hat{z}\right)+\frac{1}{\sigma\hat{H}}\left(\frac{d\hat{p}_0}{d\hat{z}}\left(\hat{z}\right)-\frac{d\hat{p}_{out}}{d\hat{z}}\right) \tag{A.3}$$

Substituting $\frac{d^3\hat{p}_0}{d\hat{z}^3}$ given by (A.1) and $\hat{C}_1\left(1,\hat{z}\right)$ given by (3.136) into equation (3.95) we obtain:

$$\frac{d^2\hat{\mathrm{p}}_1}{d\hat{z}^2}=-\frac{3\mathcal{Re}\beta^2}{64}\left[\frac{d^3\hat{\mathrm{p}}_0}{d\hat{z}^3}\frac{d\hat{\mathrm{p}}_0}{d\hat{z}}+\left(\frac{d^2\hat{\mathrm{p}}_0}{d\hat{z}^2}\right)^2\right]+$$

$$+\frac{16}{\beta}\hat{\mathrm{L}}_\mathrm{p}\left(\hat{\mathrm{p}}_1\left(\hat{z}\right)+\frac{3\sigma\beta\mathcal{Pe}_r\hat{\mathrm{H}}}{64}\frac{d\hat{\mathrm{C}}_0}{d\hat{z}}\frac{d\hat{\mathrm{p}}_0}{d\hat{z}}+\frac{5\sigma\mathcal{Pe}_r\hat{\mathrm{H}}}{24}\frac{d\hat{\mathrm{C}}_0}{d\hat{z}}(0)\right) \tag{A.4}$$

That is

$$\frac{d^2\hat{\mathrm{p}}_1}{d\hat{z}^2}=-\frac{3\mathcal{Re}\beta^2}{64}\left[\frac{16\hat{\mathrm{L}}_\mathrm{p}}{\beta}\left[\frac{d\hat{\mathrm{p}}_0}{d\hat{z}}\left(\hat{z}\right)-\frac{d\hat{\mathrm{p}}_{\mathrm{out}}}{d\hat{z}}-\sigma\hat{\mathrm{H}}\left(\frac{d\hat{\mathrm{C}}_0}{d\hat{z}}\left(\hat{z}\right)-\frac{d\hat{\mathrm{C}}_{\mathrm{out}}}{d\hat{z}}\right)\right]\frac{d\hat{\mathrm{p}}_0}{d\hat{z}}+\left(\frac{d^2\hat{\mathrm{p}}_0}{d\hat{z}^2}\right)^2\right]+$$

$$+\frac{16}{\beta}\hat{\mathrm{L}}_\mathrm{p}\left(\hat{\mathrm{p}}_1\left(\hat{z}\right)+\frac{3\sigma\beta\mathcal{Pe}_r\hat{\mathrm{H}}}{64}\frac{d\hat{\mathrm{C}}_0}{d\hat{z}}\frac{d\hat{\mathrm{p}}_0}{d\hat{z}}+\frac{5\sigma\mathcal{Pe}_r\hat{\mathrm{H}}}{24}\frac{d\hat{\mathrm{C}}_0}{d\hat{z}}(0)\right) \tag{A.5}$$

or

$$\frac{d^2\hat{\mathrm{p}}_1}{d\hat{z}^2}=-\frac{3\beta\mathcal{Re}\hat{\mathrm{L}}_\mathrm{p}}{4}\left(\frac{d\hat{\mathrm{p}}_0}{d\hat{z}}\right)^2+\frac{3\beta\mathcal{Re}\hat{\mathrm{L}}_\mathrm{p}}{4}\frac{d\hat{\mathrm{p}}_0}{d\hat{z}}\frac{d\hat{\mathrm{p}}_{\mathrm{out}}}{d\hat{z}}+\frac{3\sigma\beta\mathcal{Re}\hat{\mathrm{H}}\hat{\mathrm{L}}_\mathrm{p}}{4}\frac{d\hat{\mathrm{p}}_0}{d\hat{z}}\left(\frac{d\hat{\mathrm{C}}_0}{d\hat{z}}-\frac{d\hat{\mathrm{C}}_{\mathrm{out}}}{d\hat{z}}\right)-$$

$$-\frac{3\mathcal{Re}\beta^2}{64}\left(\frac{d^2\hat{\mathrm{p}}_0}{d\hat{z}^2}\right)^2+\frac{16}{\beta}\hat{\mathrm{L}}_\mathrm{p}\left(\hat{\mathrm{p}}_1\left(\hat{z}\right)+\frac{3\sigma\beta\mathcal{Pe}_r\hat{\mathrm{H}}}{64}\frac{d\hat{\mathrm{C}}_0}{d\hat{z}}\frac{d\hat{\mathrm{p}}_0}{d\hat{z}}+\frac{5\sigma\mathcal{Pe}_r\hat{\mathrm{H}}}{24}\frac{d\hat{\mathrm{C}}_0}{d\hat{z}}(0)\right) \tag{A.6}$$

which gives

$$\frac{d^2\hat{\mathrm{p}}_1}{d\hat{z}^2}=-\frac{3\beta\mathcal{Re}\hat{\mathrm{L}}_\mathrm{p}}{4}\left(\frac{d\hat{\mathrm{p}}_0}{d\hat{z}}\right)^2+\frac{3\beta\mathcal{Re}\hat{\mathrm{L}}_\mathrm{p}}{4}\frac{d\hat{\mathrm{p}}_0}{d\hat{z}}\left(\frac{d\hat{\mathrm{p}}_{\mathrm{out}}}{d\hat{z}}-\sigma\hat{\mathrm{H}}\frac{d\hat{\mathrm{C}}_{\mathrm{out}}}{d\hat{z}}\right)-\frac{3\mathcal{Re}\beta^2}{64}\left(\frac{d^2\hat{\mathrm{p}}_0}{d\hat{z}^2}\right)^2+$$

$$+\frac{16}{\beta}\hat{\mathrm{L}}_\mathrm{p}\hat{\mathrm{p}}_1+\left(\beta\mathcal{Re}+\mathcal{Pe}_r\right)\frac{3\sigma\hat{\mathrm{H}}\hat{\mathrm{L}}_\mathrm{p}}{4}\frac{d\hat{\mathrm{p}}_0}{d\hat{z}}\frac{d\hat{\mathrm{C}}_0}{d\hat{z}}+\frac{10\sigma\hat{\mathrm{H}}\hat{\mathrm{L}}_\mathrm{p}\mathcal{Pe}_r}{3\beta}\frac{d\hat{\mathrm{C}}_0}{d\hat{z}}(0) \tag{A.7}$$

where, considering the boundary conditions (3.49), (3.51), (3.52) and equation (3.66), $\frac{d\hat{C}_0}{d\hat{z}}(0)$ is given by equation (3.129):

$$\frac{d\hat{C}_0}{d\hat{z}}(0) = -\hat{L}_p\left[\hat{p}_i - \hat{p}_{out}(0) - \sigma\hat{H}\left(1-\hat{C}_{out}(0)\right)\right]\left[-1-\sigma+(1-\sigma)\hat{C}_{out}(0)\right] \\ -2\hat{P}_s\left(1-\hat{C}_{out}(0)\right) \tag{A.8}$$

Thus the coupled equations we need to solve are (3.128), (3.130) and (A.7), now renumbered as:

$$\frac{\beta}{16}\frac{d\hat{C}_0}{d\hat{z}}\frac{d\hat{p}_0}{d\hat{z}} = \frac{\hat{v}(\hat{z})}{2}\left[-(1+\sigma)\hat{C}_0(\hat{z}) + (1-\sigma)\left(\hat{C}_{out}(0) + \frac{d\hat{C}_{out}}{d\hat{z}}\hat{z}\right)\right] + \\ +\hat{P}_s\left(\hat{C}_0(\hat{z}) - \hat{C}_{out}(0) - \frac{d\hat{C}_{out}}{d\hat{z}}\hat{z}\right) \tag{A.9}$$

$$\frac{d^2\hat{p}_0}{d\hat{z}^2}(\hat{z}) = \frac{16\hat{v}(\hat{z})}{\beta} = \frac{16\hat{L}_p}{\beta}\left[\hat{p}_0(\hat{z}) - \hat{p}_{out}(0) - \frac{d\hat{p}_{out}}{d\hat{z}}\hat{z} - \sigma\hat{H}\left(\hat{C}_0(\hat{z}) - \hat{C}_{out}(0) - \frac{d\hat{C}_{out}}{d\hat{z}}\hat{z}\right)\right] \tag{A.10}$$

$$\frac{d^2\hat{p}_1}{d\hat{z}^2}(\hat{z}) = -\frac{3\beta\mathcal{R}e\hat{L}_p}{4}\left(\frac{d\hat{p}_0}{d\hat{z}}\right)^2 + \frac{3\beta\mathcal{R}e\hat{L}_p}{4}\frac{d\hat{p}_0}{d\hat{z}}\left(\frac{d\hat{p}_{out}}{d\hat{z}} - \sigma\hat{H}\frac{d\hat{C}_{out}}{d\hat{z}}\right) - \frac{3\mathcal{R}e\beta^2}{64}\left(\frac{d^2\hat{p}_0}{d\hat{z}^2}\right)^2 + \\ +\frac{16}{\beta}\hat{L}_p\hat{p}_1 + (\beta\mathcal{R}e + \mathcal{P}e_r)\frac{3\sigma\hat{H}\hat{L}_p}{4}\frac{d\hat{p}_0}{d\hat{z}}\frac{d\hat{C}_0}{d\hat{z}} + \frac{10\sigma\hat{H}\hat{L}_p\mathcal{P}e_r}{3\beta}\frac{d\hat{C}_0}{d\hat{z}}(0) \tag{A.11}$$

from which we obtain the dependent variables $\hat{C}_0$, $\hat{p}_0$ and $\hat{p}_1$. Taking:

$$\mathrm{Y}_0 = \hat{\mathrm{C}}_0\,,\quad \mathrm{Y}_1 = \hat{\mathrm{p}}_0\,,\quad \mathrm{Y}_2 = \hat{\mathrm{p}}_1\,,\quad \mathrm{Y}_3 = \frac{d\hat{\mathrm{p}}_0}{d\hat{z}} = \frac{d\mathrm{Y}_1}{d\hat{z}} \quad \text{and} \quad \mathrm{Y}_4 = \frac{d\hat{\mathrm{p}}_1}{d\hat{z}} = \frac{d\mathrm{Y}_2}{d\hat{z}} \qquad \text{(A.12)}$$

The three coupled equations above can be written as a system of first order differential equations that is easier to solve than the original system of coupled equations (A.9) to (A.11):

$$\frac{d\mathrm{Y}_0}{d\hat{z}} = \frac{8\hat{\mathrm{L}}_\mathrm{p}}{\beta \mathrm{Y}_3}\left[\mathrm{Y}_1 - \hat{\mathrm{p}}_\mathrm{out}(0) - \frac{d\hat{\mathrm{p}}_\mathrm{out}}{d\hat{z}}\hat{z} - \sigma\hat{\mathrm{H}}\left(\mathrm{Y}_0 - \hat{\mathrm{C}}_\mathrm{out}(0) - \frac{d\hat{\mathrm{C}}_\mathrm{out}}{d\hat{z}}\hat{z}\right)\right]\times$$

$$\times\left[-(1+\sigma)\mathrm{Y}_0 + (1-\sigma)\left(\hat{\mathrm{C}}_\mathrm{out}(0) + \frac{d\hat{\mathrm{C}}_\mathrm{out}}{d\hat{z}}\hat{z}\right)\right] + \frac{16\hat{\mathrm{P}}_\mathrm{s}}{\beta \mathrm{Y}_3}\left(\mathrm{Y}_0 - \hat{\mathrm{C}}_\mathrm{out}(0) - \frac{d\hat{\mathrm{C}}_\mathrm{out}}{d\hat{z}}\hat{z}\right) \qquad \text{(A.13)}$$

$$\frac{d\mathrm{Y}_3}{d\hat{z}} = \frac{16\hat{\mathrm{L}}_\mathrm{p}}{\beta}\left[\mathrm{Y}_1 - \hat{\mathrm{p}}_\mathrm{out}(0) - \frac{d\hat{\mathrm{p}}_\mathrm{out}}{d\hat{z}}\hat{z} - \sigma\hat{\mathrm{H}}\left(\mathrm{Y}_0 - \hat{\mathrm{C}}_\mathrm{out}(0) - \frac{d\hat{\mathrm{C}}_\mathrm{out}}{d\hat{z}}\hat{z}\right)\right] \qquad \text{(A.14)}$$

$$\frac{d\mathrm{Y}_4}{d\hat{z}} = -\frac{3\beta\mathcal{Re}\hat{\mathrm{L}}_\mathrm{p}}{4}\mathrm{Y}_3^2 + \frac{3\beta\mathcal{Re}\hat{\mathrm{L}}_\mathrm{p}}{4}\mathrm{Y}_3\left(\frac{d\hat{\mathrm{p}}_\mathrm{out}}{d\hat{z}} - \sigma\hat{\mathrm{H}}\frac{d\hat{\mathrm{C}}_\mathrm{out}}{d\hat{z}}\right) - \frac{3\mathcal{Re}\beta^2}{64}\left(\frac{d\mathrm{Y}_3}{d\hat{z}}\right)^2 +$$

$$+\frac{16}{\beta}\hat{\mathrm{L}}_\mathrm{p}\mathrm{Y}_2 + \left(\beta\mathcal{Re} + \mathcal{Pe}_r\right)\frac{3\sigma\hat{\mathrm{H}}\hat{\mathrm{L}}_\mathrm{p}}{4}\mathrm{Y}_3\frac{d\mathrm{Y}_0}{d\hat{z}} -$$

$$+\frac{10\sigma\hat{\mathrm{H}}\hat{\mathrm{L}}_\mathrm{p}\mathcal{Pe}_r}{3\beta}\left\{\hat{\mathrm{L}}_\mathrm{p}\left[\hat{\mathrm{p}}_\mathrm{i} - \hat{\mathrm{p}}_\mathrm{out}(0) - \sigma\hat{\mathrm{H}}\left(1 - \hat{\mathrm{C}}_\mathrm{out}(0)\right)\right]\left[-1-\sigma+(1-\sigma)\hat{\mathrm{C}}_\mathrm{out}(0)\right] +\right.$$

$$\left.+2\hat{\mathrm{P}}_\mathrm{s}\left(1 - \hat{\mathrm{C}}_\mathrm{out}(0)\right)\right\} \qquad \text{(A.15)}$$